DOCTOR OF PHILOSOPHY

Interactions, particle size and surface effects in magnetic nanoparticle systems.

Blanco-Mantecon, Mireia

Award date:
2000

Awarding institution:
Bangor University

Interactions, particle size and surface effects in magnetic nanoparticle systems

by

Mireia Blanco-Mantecón

Thesis submitted to the University of Wales, Bangor, in candidature for the degree of

Doctor of Philosophy

School of Electronic Engineering and Computer Systems,

University of Wales, Bangor

Bangor,

Gwynedd,

February, 2000

" To all my friends, visible and invisible,
that have put their hope, their heart and their energy
so that the seeds contained in this work,
could germinate in good soil "

The first thanks go to all my family, for giving me all the grounding for all the future tasks that awaited (and still await) for me in this life. Thanks for the strength, the education, the trust and all above all, the love they have given me. They planted many little seeds in me, that slowly grew with the years and the experience, and are still growing, strong roots. Thanks.

I will always be grateful to the people that helped me at the beginning of this academic journey: Ana Ruiz de Gopegui, Federico Cebollada y Puerto Morales. First just teachers, now friends and still great teachers. I will never have enough words of gratefulness. Special thanks for the support they showed in the last hours of this writing up. It is most appreciated and valued. Thanks.

Thanks to all the people I shared the space and the experiences with: Andy, Evi Dova, Leslie Pritchard, Gwynn, Lee and Justine, with whom I had some interesting chats, healthy fights and competitions, and lots and lots of experiences together, group therapy, collective psychoanalysis..... Special thanks to JC (John Cambrige), without whom I bet nothing would have been done, if left to my own devices. Thanks John.

Thank you to the guys in Liverpool (specially Gabi Milford and Dominic Dickson) for the Mössbauer measurements, and very good moments of fun. Thanks to Andy Davies for the excellent TEM micrographs. Thanks to M. Puerto Morales for the X-ray spectra. Thanks to Nick Walsmley for some of the subroutines used in this work, as well as some wise advice in computational matters; but above all, thanks for always supporting and believing in me. Thanks to Steve Wells and V.J. in Liquids Research for all their time and good advice.

Thanks to Matthew Wenger for all the growth that we have experienced together. Thanks for your teachings, your support and your faith in me. Special thanks to Andy Goodman,

who has always had time to talk about physics, constantly contributing with illuminating conversations and good ideas. Thanks for your insight in the problems and your time as a friend. Huge thanks to Consuelo, Pieter, Ana(s), Vivi, Barbara, Simon, Martin, Rich, Marcus, Steve, Vicky, Spud, for being my friends and companions, and sharing with me conversations, laughs, life, moments...

More thanks to another very special friend, Moose (Christopher Hancock), also for lots of hours of psychoanalysis, and lots and lots of support and love. By his side, I must mention again the endless help and support of M. Puerto Morales, now recently mum, for believing in me, and always be there for me. She is a wise and incredibly efficient worker and an invaluable friend. I wish her the greatest happiness in her life.

Thanks to all the 'fine particle' visitors, specially Montse Garcia del Muro, Maribel Montero and Victor Franco, with whom I had long and constructive talks about magnetism and life, because ... *everything is interwoven* to an incredible extent.

I would also like to thank Oscar Iglesias, Montse Garcia del Muro P. Jund, D. Kechrakos, M. Hanson, Dominic Dickson, Mohammad El-Hilo and Roy Chantrell for their help and encouragement, drawing some light on their work while I was studying it and trying to use it for the results of this thesis.

Almost at the end, but not the last thanks to Kevin O'Grady for introducing me in the immense and still fairly unknown oceans of magnetism and psychoanalysis. Thanks for taking me on board and setting me off, almost unknowingly, in this my new path now.

And finally, the biggest thanks to all those that have been my friends, my confessors, my lovers, my support, my life ... for helping me to learn, to live, to love.

ENDLESS and PROFOUND THANKS.

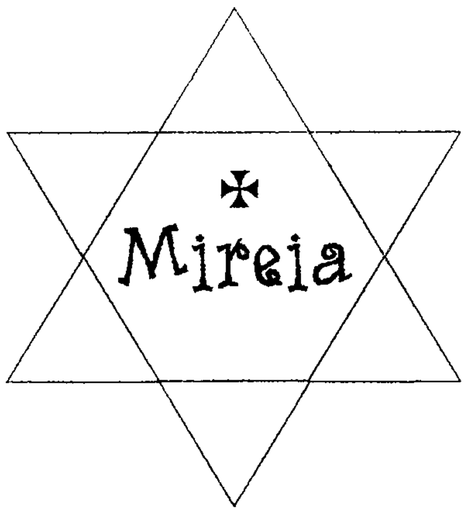

Table of contents

List of symbols

✣ = Section

A = atomic weight

α_i = direction cosines of M_s relative to the crystal axis

$\alpha = \mu H / kT$

$L(\alpha)$ = Langevin function

$cc = cm^3$

χ = susceptibility

χ_i = initial susceptibility

$\overline{\chi_i}$ = normalised susceptibility, χ_i / M_s

χ_{irr} = irreversible susceptibility

D = particle diameter

D_p = physical median diameter

D_{vp} = diameter corresponding to the median physical volume

D_{vm} = diameter corresponding to the median magnetic volume

DCD = dc-demagnetisation magnetisation

ΔE = energy barrier

ΔE_{eff} = effective energy barrier

ΔM = delta M plot

Δf_0 = error of f_0

$\langle d_1 \rangle$ = average inter-particle separation

(d_1, ψ_1) = location of the first neighbours

δ_D = domain wall thickness

δ = surfactant length

e = ellipticity of a particle

E_{anis} = anisotropy energy

E_{dip} = dipolar energy

E_{exch} = exchange energy

E_{field} = energy of a magnetic moment in a field

E_{mag} = magnetic energy

E_{ms} = magnetostatic energy

E_{total} = total energy (of a crystal)

E_{wall} = energy of a domain wall

$\varepsilon = M_s / M_{sB}$ = concentration or packing fraction

$f(\Delta E)$ = energy barrier distribution

$f(T_B)$ = distribution of blocking temperatures

$f(T_R)$ = distribution of reduced blocking temperatures

$f(y)$ = lognormal distribution of the variable y

f_0 = attempt frequency ($\tau_0 = f_0^{-1}$)

F = fraction of atoms in the surface of a cluster

FMR = ferromagnetic resonance

FC = field cooled

$FWHM$ = full width at half maximum

g = Landé factor

γ = domain wall energy per unit area of wall

γ_0 = gyromagnetic ratio

Γ = gamma function

$H = H_{app}$ = applied magnetic field

H_c = coercivity or coercive field

H_d = demagnetising field

H_K = anisotropy field

H_{Keff} = effective anisotropy field

$H_{Ki,eff}$ = intrinsic effective anisotropy field

H_m = molecular field

H_r = remanence coercivity

$H_s = H_{sat}$ = saturating field

$HGMS$ = High Gradient Magnetic Separation

IRM = isothermal remanent magnetisation

$J =$ total angular momentum

J_{ex} = exchange integral

$k = k_B$ = Boltzmann constant

K = anisotropy constant

K_{eff} = effective anisotropy constant

$K_s = K_{surf}$ = surface anisotropy constant

K_{shape} = shape anisotropy constant

L = total thickness of a crystal

L_c = critical thickness for SD behaviour

λ = wavelength

M = magnetisation

M_r = remanent magnetisation

M_s = saturation magnetisation

M_{sB} = saturation magnetisation of the bulk

m_i = magnetic moment of particle i

m_z = component of the magnetisation in the magnetic field direction

mCi = mili-Curie

μ = magnetic moment per particle or atom and permeability

μ_B = Bohr magneton

μ_{eff} = effective magnetic moment of the atom

μ_H = maximum momentum of each atom in the direction of the applied magnetic field

M = magnetisation

M_s = saturation magnetisation

M_{sB} = bulk saturation magnetisation

$\overline{M}_d(H)$ = reduced DCD remanent magnetisation

$\overline{M}_r(H)$ = reduced IRM remanent magnetisation

$M_r(\infty)$ = remanent magnetisation at saturation

$M_r(t)$ = remanent magnetisation at time t

M_r / M_s = remanence to saturation ratio

MHS = magnetohydrostatic separation

MQT = macroscopic quantum tunnelling

n = number of particles per unit volume and number of atoms per cluster

N = Avogadro's number

N_d = demagnetising factor

N_x, N_y, N_z = demagnetising factors in the x, y and z directions

n_s = number of absorbed molecules per unit area

$\langle n_1 \rangle$ = mean number of first neighbours

ν_{res} = resonant frequency

ω_s = surface anisotropy density

p = concentration of magnetic material

r = distance between magnetic moments or particles

ρ = density

ρ_i = number density of atoms/molecules in particle i

S = coefficient of magnetic viscosity

SD = single domain

SFD = switching field distribution

σ = standard deviation of the distribution of lnD

σ_v = standard deviation of the distribution of lnV

s_i = spin or magnetic moment of particle i

t = measurement time

T = temperature

T_B = blocking temperature

T_{Beff} = effective blocking temperature

T_{Bm} = median blocking temperature

T_m = maximum temperature of the ZFC curve

T_{0tot} = total ordering temperature

T_{0Bi} = blocking contribution to T_{0tot}

T_{0i} = interaction contribution to T_{0tot}

$T_R = T / T_{Bm}$ = reduced blocking temperature

TEM = Transmission Electron Microscopy

TDR = temperature decay of remanence

T^* = crossover temperature for MQT

τ = relaxation time

θ = Curie-Weiss temperature

U_s = entropic repulsion energy

V = particle volume

VSM = vibrating sample magnetometer

V_m = median volume

V_p = critical volume for superparamagnetic behaviour

ξ = angle between the hard axis in the surface axes system and the tangent to the ellipse

ξ_1 = interaction parameter

$y = V / V_m = T / T_B$ = reduced variable

$y = V / V_p$ = reduced critical diameter for superparamagnetic behaviour

ZFC = zero field cooled

Summary

This work has involved the study of the magnetic behaviour of small magnetic nanoparticle systems. Due to the reduced size of magnetic nanoparticles they present distinctive properties, such as size and surface effects, that have been analysed in this work, as well as the effect of interactions in such systems. The samples chosen for the study were magnetite particles in the form of a ferrofluid and Co nanoclusters in a non-magnetic matrix of Cu. Both systems present very narrow particle size distributions, which facilitates the interpretation of the data.

The samples have been subjected to basic characterisation, which includes the determination of the distribution of magnetic particle sizes using the magnetisation curves at room temperatures, TEM microscopy and X-ray diffraction, in the case of the ferrofluid samples. For the nanoclusters, a time of flight spectrometer has been used to obtain the number of atoms per cluster. Many of the measurements have been performed at low temperatures, where thermal effects are minimised. For such measurements the samples have been frozen in a zero applied field, so that they have a random distribution of magnetic moments prior to the measurement. The energy barrier distributions have been calculated via the temperature decay of remanence (TDR). From this study, an effective anisotropy constant has been calculated. For the study of the interactions, surface and size effects, magnetisation, susceptibility (ZFC), remanence and delta-M curves, as well as the time dependence of magnetisation have been studied. The attempt frequency of the different particle size systems has been calculated using different techniques.

The basic magnetic behaviour can be explained on the basis of the Néel blocking model. It has been found that the systems with the smaller particles have significant surface effects, which are enhanced at lower temperatures. Interactions, which are weak due to the low concentration of magnetic material in the samples (<10%), have been found to be overall demagnetising and the evolution of the magnetic properties with dilution has been explained. As is the case for the surface effects, interaction effects are stronger at low temperatures due the reduction of thermal effects. The experimental results have been compared with calculations from a Montecarlo model for fine particles, which includes the effects of concentration, anisotropy, particle size and temperature.

" By mind I understand

that power of the soul

which thinks and develops concepts ".

Aristotle, 384-322 B.C.

When darkness surrounds you, say:
"This darkness is the dawn that hasn't yet been born,
and although the action of the night feels heavy on me,
dawn will be born in me again, as it is born on the mountains".

Khalil Gibran, *The Garden of the Prophet*

1. Introduction

Present day recording technology demands smaller sizes for each generation of products as miniaturisation is becoming of prime importance. In fact it is not only the recording industry which demands systems with increasing higher densities and more sensitive recording and reading heads; many other devices require miniaturisation, for example in applications for the aerospace and telecommunications industry, and thus smaller and smaller systems are designed, produced and studied. Also, exciting new physics and applications stem from small particle systems. In particular, the understanding of the transition from atomic to bulk behaviour is of fundamental importance in solid state physics. Thus, a good understanding of these small particle systems is vital. Such systems are normally referred to as nanoparticles, or more generally, nanostructures, as the particle sizes involved lie in the nanometer range. The work presented in this thesis has been developed to study the magnetic properties of magnetic nanoparticle systems, an area of study which has traditionally been known as fine particle magnetism.

The systems under study in this thesis are magnetite (Fe_3O_4) particles in the form of a ferrofluid and Co/Cu nanoclusters. Both systems were supplied with different particle sizes. The advantage of the ferrofluid system is that it is possible to change the concentration of the samples without varying the particle size distribution, which facilitates the study of interactions. Furthermore, the control of the particle size in

ferrofluids has been extensively documented, and it is relatively easy to synthesise particles with very small particle sizes (<100Å) and narrow distributions. Similarly, for the nanocluster systems, the size of the clusters (number of atoms per cluster) is controlled by a magnetron cluster source, which produces atomic clusters. These systems, as well as the ferrofluids, have very narrow size distributions. Due to the weak interactions ($\varepsilon \leq 10\%$, where ε is the concentration of magnetic material) and the narrow distribution of particle sizes, ferrofluid and nanocluster systems are very close to idealised systems of monodispersed particles. These idealised systems are fundamental to test theoretical models and to study properties of nanostructured systems.

The experimental data has been compared with the results from a theoretical Montecarlo model developed by El-Hilo et al. [1998] for fine particles. In this model the effect of thermal fluctuations, interactions, applied magnetic field and size effects are included. The relaxation of the magnetic moment caused by thermal activation over the energy barrier [Néel (1949 *a*)] can be studied. The parameters obtained from the basic characterisation of the samples, such as particle size, concentration, anisotropy constant, etc. have been used to generate the theoretical curves. Besides the testing of the Montecarlo model just described, the main aim of this work is the study of particle size, interactions and surface effects on the behaviour of magnetic nanoparticles.

The basic theoretical concepts of small magnetic particle systems are associated with thermal activation over anisotropy energy barriers. Such systems, composed by single domain (SD) particles with sizes smaller than 100Å, are superparamagnetic at room temperatures although the distribution of sizes gives rise to mixed complex behaviour.

The systems that have been studied in more depth are the magnetite particles. Samples with three different particle sizes, were diluted to different degrees for the study of interactions. Magnetisation curves at room temperatures have been measured, in order to calculate the magnetic size distribution of the systems. Assuming a lognormal distribution of particle sizes, and a Langevin behaviour of the systems, a median magnetic diameter and standard deviation of the distribution of magnetic sizes are calculated using the method of Chantrell et al. [1978] and a best fit subroutine. Also, from the room temperature measurements some interaction and surface effects have been observed. The samples have been subjected to transmission electron microscopy (TEM) and X-ray diffraction in order to characterise the physical and crystalline particle size, respectively. The use of the lognormal distribution function of particle sizes is justified at the light of

the TEM results, as is the case for the majority of fine particle systems [Granqvist and Buhrman (1976)].

The temperature decay of remanence (TDR), which is the relaxation of the remanent magnetisation with temperature, has been used to calculate the distribution of energy barriers in the systems as well as an effective anisotropy constant. Particle concentration has been found not to affect the values of the remanence to saturation ratio.

Once the distribution of particle sizes and energy barriers is known for the different systems, various magnetic studies are performed at low temperatures, so as to minimise thermal effects and be able to study interaction and size effects more clearly. For all the low temperature measurements, the ferrofluid has been frozen in a zero applied field, so that a random configuration of magnetic moments can be achieved. Initial susceptibility measurements have been widely used to characterise interactions in fine particle magnetism [O'Grady et al. (1983), Dormann et al. (1988, 1996, 1998 *a*, *b*), El-Hilo et al. (1988, 1992 *b*, *c*), Mørup et al. (1995)]. The peak of the susceptibility curves has been found to depend on particle size and concentration, so that it appears at higher temperatures for larger particles and more concentrated systems. This is because in both cases, higher particle volumes or stronger interactions, the energy barrier for reversal is increased. The effect of the applied field on the susceptibility curves for different dilutions, has also been assessed. The presence of a small applied field when the samples are being frozen, previous to the measurement of the susceptibility curves, induces a small texture in the systems which affects the main characteristics of the curves. Thus care must be taken to freeze the samples in an absolute zero field.

Traditionally it has been accepted [Néel (1947 *b*), Wohlfarth (1955)] that dipolar interactions lower the coercivity of the systems. To test this prediction, the magnetisation curves at low temperatures have been measured and the coercivity recorded, for different concentrations. The opposite behaviour to that predicted has been observed for the ferrofluid systems, possibly due to the weak dipolar interactions present in these systems. The remanence to saturation ratio has also been calculated from the magnetisation curves and it has been found to decrease for higher concentrations, as predicted by different theoretical models [El-Hilo et al. (1998), Kechrakos and Trohidou (1998)].

The study of the remanence curves versus applied field is also an interesting method to study the energy barriers of the system. In this case, unlike in the case of the magnetisation

curves, the component of the magnetisation that is recorded is due to irreversible changes of magnetisation. The moments that contribute to the remanence curves are those which have not been able to overcome the energy barrier for reversal. Thus the study of these curves will give an insight of how the energy barriers are affected by concentration, and possibly by particle size, as it has been observed. The derivative of the remanence curves gives the distribution of anisotropy fields of the system [O'Grady and Chantrell (1992)] which is also affected by interactions.

Delta-M (ΔM) plots are widely used in the characterisation of interactions in magnetic media [Kelly et al. (1989)], and they have been used in this work to assess the type of interactions in the systems, which have been found to be predominantly demagnetising for all the ferrofluid samples.

Time dependence relaxation of the magnetisation has been studied at low temperatures. A linear dependence of the relaxation of magnetisation with ln(t) has been found. The results show clearly the effects of particle size, where the smaller particle size systems relax faster than the larger particle sizes, as it would be expected from the smaller energy barriers present. How interactions affect the relaxation of the magnetisation in the systems, however, is not clear.

With the ever increasing demand in data rates and densities, it is of prime importance to study the natural attempt frequency, f_0, which is the fastest frequency at which a magnetic moment can switch from one direction of magnetisation to another. Different techniques that calculate the attempt frequency in a system of small magnetic particles have been used and compared. The attempt frequency for the different ferrofluid systems is of the order of $\sim 10^9$ Hz. Also, as particle size is reduced it is important to consider the effect of the surface, which becomes fundamental as the surface to volume ratio increases. These effects can lead to properties which differ from those of the bulk materials. It is therefore fundamental to understand the role that the surface plays in nanostructured systems. For this purpose, a section has been dedicated to the study of the surface in the magnetite particles. An estimate of the surface thickness, as well as an approximate value for the surface anisotropy constant for the three ferrofluid systems have been given. The estimated surface anisotropy is higher for the smaller particle size samples, as expected from their larger surface to volume ratio.

In general, it has been observed that the effects of interactions, particle size and surface anisotropy are significantly enhanced at low temperatures, due to the fact that thermal effects are diminished. Overall, the interactions have been found to be demagnetising, and weaker for the smaller particle sizes, which, on the other hand, present much stronger surface effects.

The Co/Cu nanoclusters were produced at the CLRC Daresbury Laboratory using a magnetron cluster source. Two samples have been studied with particles of approximately 30 and 50 Å in diameter, respectively, and different concentrations of 5, 10% and 50%. For the characterisation of the samples, some of the experimental techniques used for the characterisation of the ferrofluid samples have been used, namely magnetisation curves at room and low temperatures, and temperature decay of remanence. The physical particle size distribution has been calculated using a time of flight spectrometer.

Although the lower concentration clusters are superparamagnetic at room temperatures, it is not clear that the differences with concentration observed in the curves are solely due to the presence of purely dipolar interactions or if some exchange is also present in the systems. Furthermore, it does not seem to be the case that different concentration samples have exactly the same particle size distribution, as is the case in ferrofluids, making the correct interpretation of the data obtained difficult, both at room and at low temperatures. A clear understanding of the microstructure of these systems is required if any further progress is to be made. Values for the effective anisotropy constants in these materials have been obtained from the temperature decay of remanence data. The calculation of these anisotropy constants is an important result due to the lack in the bibliography of such data for small Co particles.

In the essence of the darkness is
'to call into existence from non-existence that we are searching for' .
Joseph Rael, from *Being and Vibration*'

The mistery of the metaphor is the art of listening to life
in the activity of work, of allowing yourself to be living harmony.
Metaphors give a way to become more inside our universe.
If we can name, or identify our world,
we know better to fit in harmony with it.
Harmony is the warmth of the heart slipping through a slice of light.
By becoming more attuned to the vibrations of life,
we come closer to our natural state.
We clear our blocks and our resistances.
We discover the power to be.
(Joseph Rael, from *Being and Vibration*)

2.Theory of fine particle magnetism

2.1. Single-Domain particles

To define a single-domain particle is fundamental, as all the work in this thesis deals with this type of particles. As the name indicates, they are not formed by domains, or, in other words, they only contain one domain. Thus, all the magnetic moments in the particle point in the same direction.

2.1.1. Magnetostatic energy

The magnetostatic or self-energy is the driving force that leads to the formation of domains in a magnetic system. It is created by the particle's own magnetic field. When the magnetic field lines radiate out from the north to the south pole, due to the Coulomb interaction between magnetic free poles, they produce a field inside the magnetic sample that tends to demagnetise (H_d) the sample. These magnetic free poles are so called because they are not compensated by other poles of opposite sign in the immediate neighbourhood. H_d is proportional and opposite to the magnetisation, M, that produces it. Hence, it can be expressed as,

$$\boldsymbol{H}_d = -N_d \boldsymbol{H} \qquad \text{(Eq. 2.1)}$$

where N_d is the demagnetising factor of the particle which depends on its shape.

When a body is magnetised it stores magnetostatic energy, E_{ms},

$$E_{ms} = -\frac{1}{2}\boldsymbol{H}_d \cdot \boldsymbol{M} \qquad \text{(Eq. 2.2)}$$

Thus, the energy of a magnet in its own field is of the same form as the potential energy per unit volume (erg/cc) of a magnet in an applied field H_{app}, namely

$$E_p = -\boldsymbol{H}_{app} \cdot \boldsymbol{M} \qquad \text{(Eq. 2.3)}$$

the only difference being the factor $1/2$. Substituting the value of H_d in Eq. 2.2, the magnetostatic energy can be expressed by,

$$E_{ms} = \frac{1}{2} N_d M^2 \qquad \text{(Eq. 2.4)}$$

Different shape objects will have different demagnetising fields along different directions; thus the magnetisation vector will prefer to lie along the direction where the demagnetising field is smaller. This gives rise to an anisotropy, that due to its origin is called shape anisotropy (✣2.2.2). Also, the dipole-dipole interaction (✣2.5.1.1.a) is of magnetostatic origin. In this case the magnetic field produced by a particle affects not only itself but also neighbouring particles.

It is important to remember that the magnetisation of most magnetised bodies is not uniform. The field lines diverge towards the ends, so that in this region, the flux density is less than in the centre. That means that H_d is stronger near the poles. This observation needs to be made when effects of corners, surfaces, contours or any other kind of interface are evaluated. In these situations, the more intensive demagnetising fields in those specific areas of the sample are of prime importance.

2.1.2. Formation of Single-Domains (SD)

The formation of domain walls will be promoted to decrease the magnetostatic energy of the system. As shown in Fig. 2-1, if the sample splits into two domains the magnetostatic energy can be reduced, because the division brings north and south poles closer together, decreasing the spatial extent of the demagnetising field, H_d. If the sample splits into four domains, the magnetostatic energy will decrease again [Cullity (1972)]. However, the formation of domain walls is a process energetically 'expensive'. The formation of a wall

increases the exchange energy (✣2.5.1.1.b) between the magnetisation vectors of different domains.

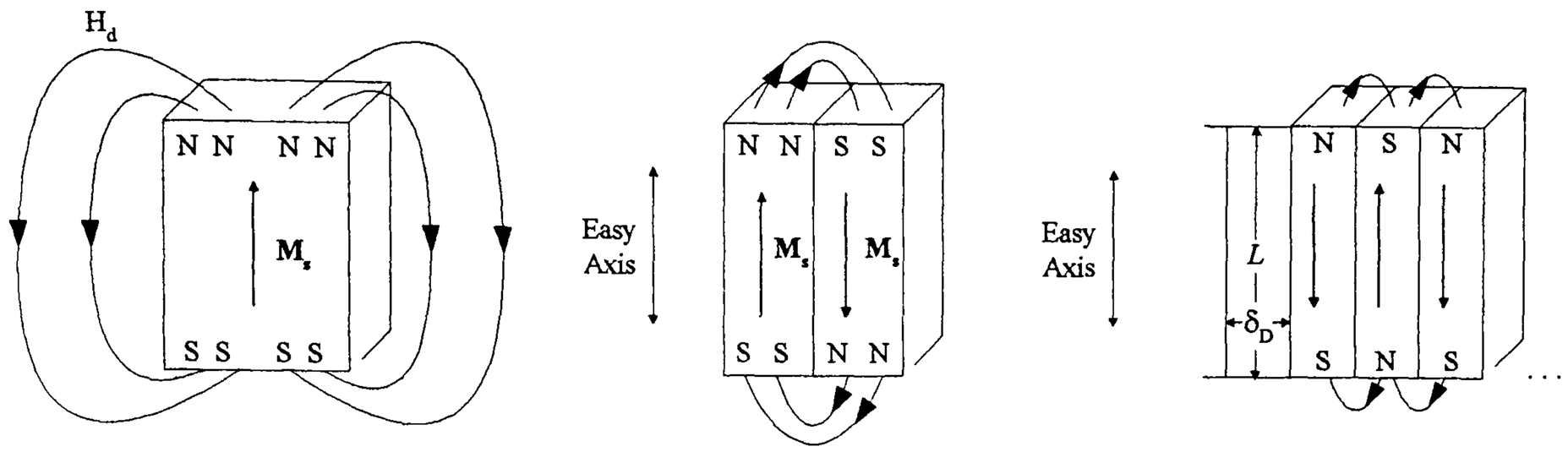

Figure 2-1

Domain wall formation in a single crystal.

A single crystal with uniaxial anisotropy has total energy which can be expressed as,

$$E_{total} = E_{ms} + E_{wall} \qquad \text{(Eq. 2.5)}$$

For a multi-domain crystal, E_{ms} per unit area of the top surface is [Chikazumi (1964)],

$$E_{ms} = 1.7 M_s{}^2 \delta_D \qquad \text{(Eq. 2.6)}$$

where M_s is the saturation magnetisation and δ_D the wall thickness (Fig. 2-1). The energy necessary for the formation of a wall in a crystal of thickness L, E_{wall}, against the exchange energy is given by,

$$E_{wall} = \gamma \frac{L}{\delta_D} \qquad \text{(Eq. 2.7)}$$

where γ is the domain wall energy per unit area of wall. The energy of a domain wall itself is given by minimising the anisotropy (✣2.2) and exchange energies (✣2.5.1.1.b) in the sample. The exchange energy will tend to increase the thickness of the wall so that the angle between neighbouring spins is the smallest possible, while the anisotropy energy will tend to make the wall the thinnest possible so that less spins lie in non-easy directions. The thickness of a domain wall is given by minimising the total energy of the system, which occurs when the domain wall thickness, δ_D, is

$$D = \sqrt{\frac{\gamma L}{1.7 M_s^{\,2}}} \qquad \text{(Eq. 2.8)}$$

Hence, if a particle has a diameter of the order of or smaller than D, it will certainly be a single domain. The ratio of the energies before and after the division of the sample into domains is also an interesting quantity, given by

$$\frac{E(\text{single}-\text{domain})}{E(\text{multi}-\text{domain})} = 2.4\sqrt{\frac{M_s^{\,2} L}{\gamma}} \qquad \text{(Eq. 2.9)}$$

There is a critical size, L_c, below which the single-domain structure has lower energy than a multi-domain configuration. For the Fe_3O_4 samples studied in this thesis, assuming $M_s \approx 335\ emu/cc$ as given by the manufacturers, $\gamma \approx 1\ erg/cm^2$ [Néel (1955)], and setting Eq. 2.9 equal to 1, a value of $L_c \approx 154$ Å is obtained.

2.2. Magnetic anisotropy

In general, the energy of a system of magnetic particles has different contributions,

$$E_{mag} = E_{field} + E_{anis} + E_{dip} + E_{exch} \qquad \text{(Eq. 2.10)}$$

Energy of a moment in a magnetic field, $E_{field} = -\boldsymbol{m}\cdot\boldsymbol{H}_{app}$

This energy term is the potential energy of a magnetic particle in the presence of an external magnetic field, H_{app}. In the presence of zero external field, this contribution will be zero.

Anisotropy energy, E_{anis}

Magnetic anisotropy determines a preferred direction for the magnetic moment of the particle to lie, i.e., a direction in which the energy will be minimised. The main contributions to the anisotropy energy, in nanoparticle systems, are the shape of the particles, the symmetry of the crystal structure and their surface. In different systems, there are also other types of anisotropy contributing to the total energy of the system, such as the anisotropies induced by plastic deformation, magnetic annealing, irradiation, and others. However, these are not sources of anisotropy in small particle systems and shall not be included in this thesis.

Exchange energy, $E_{exch} = -2J_{ex}\,\boldsymbol{S}_1 \cdot \boldsymbol{S}_2$

The exchange energy between magnetic moments will contribute to the total energy, depending on the system (see ✣2.5.1.1.b). For a system like a ferrofluid, where the particles are coated with a surfactant, the exchange interaction between particles is negligible, while it will be strong within the particle itself. For a system of nanoclusters of Co embedded in Cu, the exchange energy can be appreciable.

Dipolar Energy, $E_{dip} = -\dfrac{m_1 \cdot m_2}{r^3}\left[2\cos\theta_1 \cos\theta_2 - \sin\theta_1 \sin\theta_2\right]$

(m_1, m_2 = magnetic moment of particles 1 and 2, θ_1, θ_2 = angle between the magnetic moment and the line joining both particles, r = distance between the particles (see Fig. 2-4)).

The dipole-dipole interaction arises due to the field that a magnetic moment creates around itself, thus affecting the rest of the surrounding moments (see ✣2.5.1.1.a.). All the neighbouring magnetic moments will be subjected to the potential energy of this 'dipolar field'. The dipole-dipole is a long-range interaction, which in ferrofluids is predominant and plays a fundamental role in the deviation from ideal behaviour in systems of small magnetic particles.

2.2.1. Crystalline anisotropy

The crystalline or magnetocrystalline anisotropy is the only anisotropy which is intrinsic to the material. It arises due to the spin-orbit interaction within the sample. The electron orbits are linked to the crystallographic structure, and so are the spins associated with them, in such a way that they prefer to align along the well defined crystallographic axis of the crystal. Thus, there are directions in which a given crystal is easier to magnetise than others. This difference can be expressed as a direction-dependent energy term, which has different forms, according to the different crystal symmetries of the samples. When a magnetic field is applied to turn the magnetisation direction away from an easy direction, work needs to be done against the anisotropy force. Therefore, there is some energy stored in a crystal whose magnetisation vector points in a non-easy direction, called magnetocrystalline anisotropy energy.

2.2.1.1. Cubic anisotropy

For a cubic crystal, Akulov showed in 1929 that the energy per unit volume can be expressed in terms of a series expansion of the direction cosines, α_i, of M_s relative to the crystal axis,

$$E = K_0 + K_1\left(\alpha_1^2\alpha_2^2 + \alpha_2^2\alpha_3^2 + \alpha_3^2\alpha_1^2\right) + K_2\left(\alpha_1^2\alpha_2^2\alpha_3^2\right) + \ldots \qquad \text{(Eq. 2.11)}$$

where $K_0, K_1, K_2 \ldots \left(erg/cc\right)$ are constants depending on the material.

In general, K_1 is enough to represent the anisotropy of a system and higher powers are not needed. The first term, K_0, is independent of the angle and hence, usually ignored, because the interest lies in the change in E as M_s rotates from one direction to another. Thus,

- If K_1 is positive, then $E_{100} < E_{110} < E_{111}$ and $\langle 100 \rangle$ is the easy axis. This is the case for iron and ferrites containing cobalt.
- If K_1 is negative, $E_{111} < E_{110} < E_{100}$ and $\langle 111 \rangle$ is now the easy direction of magnetisation. This is the case for nickel and ferrites with no cobalt, such as magnetite.

2.2.1.2. Hexagonal anisotropy

For materials with a single easy axis, e.g., Co or Barium ferrite ($Ba \cdot 6Fe_2O_3$), which have a hexagonal close-packed structure (hcp) structure, the easy direction of magnetisation lies in the c ($\hat{z}$) axis, while any direction in the basal plane is equally hard. Therefore the anisotropy energy depends only on the angle, θ, between the M_s vector and the c axis,

$$E = K_0 + K_1 \sin^2\theta + K_2 \sin^4\theta + \ldots \qquad \text{(Eq. 2.12)}$$

In general, a crystal with a single easy axis, along which the magnetisation can point either up or down is referred to as a *uniaxial crystal*, thus having *uniaxial anisotropy*.

2.2.2. Shape anisotropy

Any magnetised system is subject to a demagnetising field which is proportional to its magnetisation (Eq. 2.1). If the particles in the system are spherical and do not have any other anisotropic contribution, the same applied field will magnetise each of them to the same extent in any direction, i.e. the moment of every particle has no preferred orientation. However, if the particle has a non-spherical shape it will be easier to magnetise it along a

long axis rather than along a short axis, because the demagnetising field along the short axis is stronger than along the long axis.

Thus, shape alone can be a source of magnetic anisotropy. Shape anisotropy has been treated quantitatively for the case of an ellipsoid, which becomes magnetised uniformly throughout its volume. This uniformity is due to the uniformity of the demagnetising field, H_d, in the ellipsoid. Values of the demagnetising factors for different ellipsoids as well as for different shape samples, have been tabulated [Stoner (1945), Bozorth (1951), Morrish (1965), Chen et al. (1991)]. In a prolate spheroid, the long axis of the specimen plays the same role as the easy axis of a uniaxial crystal, with a shape anisotropy constant defined as,

$$K_s = \frac{1}{2}\left(N_a - N_c\right)M_s^2 \qquad \text{(Eq. 2.13)}$$

where N_a and N_c are the demagnetising factors along the short and long axis of the prolate spheroid, respectively. It is interesting to note that a prolate spheroid of saturated cobalt with an axial ratio $c/a = 3.5$ and no crystal anisotropy, would have the same anisotropy as a spherical cobalt crystal with the usual hexagonal crystal anisotropy. For the Fe_3O_4 particles studied in this thesis, with mean axial ratios (c/a) between 1.2 and 1.3, the crystalline anisotropy $(K_1 = 1.1 \times 10^5 erg/cc)$ is dominated by shape effects (see ✣5.11).

2.2.3. Surface anisotropy

The presence of foreign atoms or molecules on a particle's surface can lead to different magnetic behaviour of the moments in the surface from the moments in the core [Berkowitz et al. (1975)]. In the case of ferrofluids, the fact that the surfactant molecules are chemisorbed onto the surface of the particles via weak covalent bonds, leaves the magnetic ions with a deficit of nearest magnetic neighbours, which will alter the exchange coupling between surface spins. This effect will cause a very distinct behaviour of the surface with respect to the core, affecting the reversal mechanism, Langevin behaviour, Mössbauer spectra at high fields and many other magnetic properties.

Hendriksen et al. [1994 *b*] showed that the incomplete alignment of spins in maghemite (90Å) particles in a ferrofluid sample is *not* caused by a large magnetic volume anisotropy, as suggested by Pankurst and Pollard [1991]. This explanation is ruled out because the

observed degree of alignment in the surface in large magnetic fields is independent of the orientations of the easy directions of the samples. The observations by Hendriksen et al. are compatible with the concept of *spin canting* [Coey (1971), Berkowitz et al. (1975), Morrish et al. (1976)]. The majority of spins (core spins) are easily aligned with a relatively small magnetic field, but a fraction of spins are canted and remain at an angle to the applied field even in very large fields ($H \sim 4.5\ T$). The fraction of canted spins decreases with temperature, in agreement with earlier experimental findings [Morrish et al. (1976)]. It can be said that the Mössbauer spectra observed by Hendriksen et al. [1994 *b*] in large fields ($H > 0.7\ T$) consists of two components: one component accounting for the majority of spins that are fully aligned with the applied field, and a component accounting for the canted spins.

Only a few authors have tried to give an analytical description of this surface effect. Brown [1963 *b*] considered a surface anisotropy density of the form,

$$\omega = \frac{1}{2} K_s^* (\boldsymbol{n} \cdot \boldsymbol{m})^2 \qquad \text{(Eq. 2.14)}$$

where K_s^* is a constant, $\boldsymbol{n}$ is the normal to the surface and $\boldsymbol{m}$ is the unit vector parallel to the magnetisation. This is a surface anisotropy which depends only on the shape of the surface, and where the energy minimum is attained when the moment at the surface lies tangential to this surface. However this problem was never solved, because of the lack of a satisfactory numerical value for K_s^*.

The particular case of a sphere has been studied by Aharoni [1987, 1997], where he incorporates a non-zero surface anisotropy density,

$$\omega_s = K_s\left(1 - m_z\right)^2 \qquad \text{(Eq. 2.15)}$$

K_s being a constant and m_z the component of the unit magnetisation vector along the easy axis, $\hat{z}$, of the particle. He uses this form of surface anisotropy to calculate its effect on the reversal mechanism of a sphere (see ✣2.3.1).

Finally, Dormann et al. [1997] derived another expression for the same problem of the surface anisotropy, for an ellipsoid of revolution,

$$E_s = K_s S\left[\frac{1}{2} + F(e)\cos^2\xi\right]\sin^2\theta \qquad \text{(Eq. 2.16)}$$

where K_s is the surface anisotropy constant, S the surface area, θ is the angle between the magnetisation vector and the easy axis of the ellipsoid, ξ is the angle between the hard axis in the axis system of the surface and the tangent to the ellipse, and $F(e)$ is defined as,

$$F(e) = \frac{1}{2}\frac{\left(4 - 3/e^2\right)\arcsin e + \left(3/e^2 - 2\right)e\sqrt{1-e^2}}{\arcsin e + e\sqrt{1-e^2}} \qquad \text{(Eq. 2.17)}$$

where e is the ellipticity of the particle, with $e^2 = 1 - b^2/a^2$ ($2a$ and $2b$ the major and minor axis, respectively), and is approximated by $F(e) \cong 4/15e^2 + 32/315e^4$ for small ellipticities. Both terms in Eq. 2.16 have uniaxial symmetry, but while the first one vanishes for a perfect sphere, the second term does not. In fact the second term occurs in surfaces of low symmetry and simple imperfections on the particle surface will lead to this low symmetry.

It is not yet clear which expression is most appropriate to characterise the surface anisotropy in small particle systems. The surface anisotropy in small particles may be uniaxial or pseudo-uniaxial, as suggested by Aharoni [1987, 1997] or Dormann et al. [1997] or, alternatively, the moments on the surface may be distributed almost isotropically around the core of the particle and tangential to the surface as proposed by Brown [1963 *b*]. Dormann et al. [1997] added surface anisotropy to other anisotropies present in particle systems, and showed the expected behaviour of such systems (see ✣2.2.4).

2.2.4. Predominant anisotropy in different media

To distinguish among different kinds of anisotropies in a sample is difficult, unless one dominates. In the case of two uniaxial anisotropies of different origin, if both anisotropies are along the same easy axis, they add. When the anisotropy easy axes are at right angles to each other, then M_s will lie along the easy axis whose anisotropy constant is higher; if both anisotropies have equal strength they cancel each other and the system has no anisotropy. When the anisotropies are not at right angles, M_s will lie along an axis between the easy axis of the two anisotropies.

In Dormann et al. [1997, p.300] several cases of combined anisotropies are treated, and results for the total anisotropy energy term are given. Dormann et al. considered the case of a surface anisotropy with a uniaxial component (Eq. 2.16) together with the effect of

both shape and/or crystalline anisotropies. For the case of surface plus one of the uniaxial anisotropies, the results indicate that for particles below a critical volume the surface anisotropy will be dominant and above this value it will be the volume anisotropy which dominates. When the three types of anisotropy, surface, shape and crystalline, are included, the situation is more complex.

2.3. Mechanisms of reversal of magnetisation in single-domain particles

2.3.1. Rotation 'in unison' or coherent rotation

This mode of reversal was first suggested by Stoner and Wohlfarth [1948] as a model for single domain, non-interacting particles. They postulated a precise structure in space for the magnetisation vector, at $T = 0K$. During a coherent rotation, all the spins within the particle remain strongly exchanged coupled and behave as a single magnetic moment, rotating at the same time, when a high enough field is applied in the direction opposite to that of the saturating field. In fact, this reversal mode is a minimum of Brown's differential equations, which were derived later [Brown (1957)] to describe the evolution of the magnetisation when a small deviation from saturation is considered. These equations of motion are derived from the minimisation of the total energy of the system, which includes the anisotropy, exchange and magnetostatic energies, as well as the interaction with the applied magnetic field. The main predictions from the Stoner-Wohlfarth model for a system of non-interacting particles, with their easy axis randomly oriented, are a remanence to saturation ratio of 0.5 and a coercivity $H_c = 0.48H_K$, where H_K is the anisotropy field ($2K / M_s$).

The coherent rotation mode is the one that takes place for ellipsoids below a certain size [Aharoni (1959, 1986)]. For the case of surface anisotropy, very little has been done to calculate the influence of this anisotropy on the reversal mechanisms of small particles. A particular case of a sphere has been studied by Aharoni [1987, 1997], in which he contemplates the existence of a non-zero surface anisotropy density, $\omega_S = K_S\left(1-m_z\right)^2$ (Eq. 2.15), as shown in ✣2.2.3. The results show that the reversal mechanism is the buckling mode [Frei et al. (1957), Aharoni (1996)] even for rather low values of K_S. However, as already stated in ✣2.2.4, it is not clear how realistic the functional form of Eq. 2.15 is.

2.3.2. Curling

This mode, described by Frei et al. [1957], is another eigenfunction of Brown's equations. Frei et al. presented curling as a model for reversal of magnetisation (see Fig. 2-2), initially for the cases of a sphere and an infinite cylinder, and compared the energies of the system with that of other models. Curling is a mode of *incoherent* reversal.

In the extreme case of an infinite cylinder (axial ratio, $c/a \rightarrow \infty$), the spins are always parallel to the surface during a curling reversal. In this case, no free poles are formed and no magnetostatic energy is involved in the rotation. The energy barrier to a curling reversal is, therefore, entirely due to exchange energy. However, for finite values of c/a there will be some magnetostatic energy involved and the coercivity will depend on packing fraction. The model also predicted that the coercivity depends strongly on the size of the particles, varying as $1/D^2$, where D is the particle diameter. Results of the variation of coercivity with particle size were given by Luborsky and Morelock [1964] for iron whiskers, which the authors claimed confirmed the existence of curling.

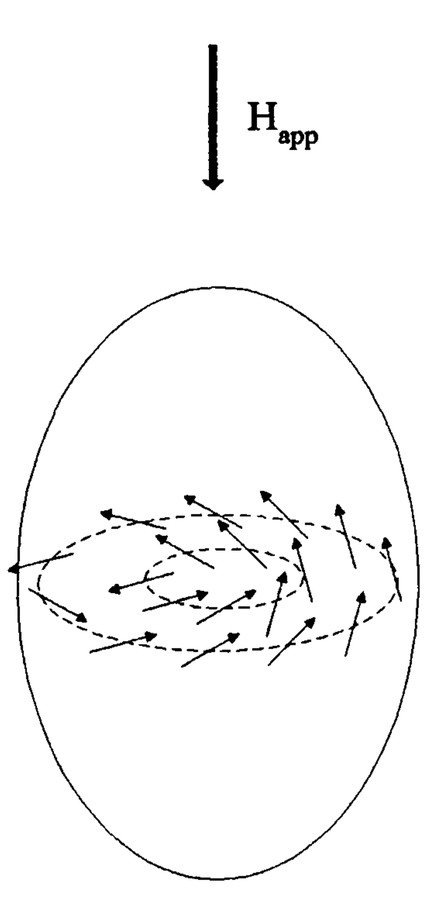

Figure 2-2

Curling mode in a prolate ellipsoid

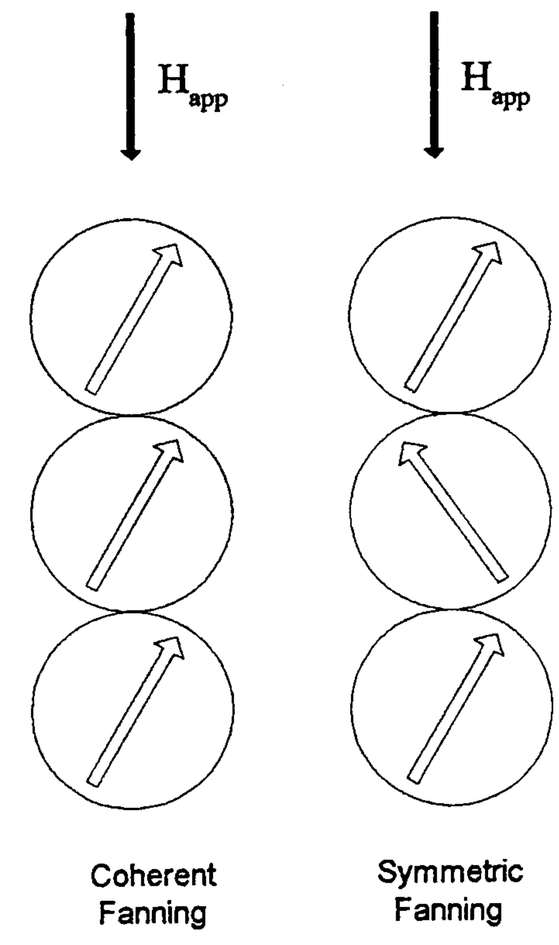

Figure 2-3

Fanning mode in a chain of spheres

2.3.3. Fanning (symmetric and non-symmetric)

This mode was suggested by Jacobs and Bean [1955] due to the shape of electrodeposited iron particles observed with the electron microscope. These particles appeared as a chain of spheres. According to Jacobs and Bean, particles with this geometry can rotate either coherently (all the moments in all the spheres are always parallel) or by 'fanning', in

which the M_s vectors of successive spheres 'fan out' in a plane by rotating in alternative directions in consecutive spheres (see Fig. 2-3).

The model assumes a linear chain of spheres with a coherent rotation of the magnetisation in each sphere, but not at the same angle for all the spheres. If the magnetisation reverses by fanning it always has a transverse circumferencial component. This model was called *non-symmetric* fanning. However, to simplify the calculations, most of the study was made for an approximation called *symmetric* fanning, in which half of the spheres rotate a certain angle and the other half at minus the same angle. It was found that the energy barrier for reversal by symmetric fanning is a third of the energy barrier for reversal by coherent rotation. It must be stressed that the non-symmetric fanning is easier than symmetric fanning, because the energy is minimised over more parameters.

2.4. Superparamagnetism

The theoretical explanation of paramagnets was first given by Langevin [1905]. He assumed a paramagnet to consist of atoms or molecules, each of which has the same magnetic moment, μ. In the absence of an applied field, these atomic moments point at random and cancel one another, so that the magnetisation of the specimen is zero. When a field is applied there is a tendency for each atomic moment to align in the field direction. However, thermal agitation of the atoms opposes this tendency and tends to keep the atomic moments pointing at random. The result is partial alignment in the field direction, and therefore a small positive magnetisation.

The magnetisation of a system of paramagnetic particles is described by,

$$M = n\mu L(\alpha) \qquad \text{(Eq. 2.18)}$$

where $L(\alpha)$ is the Langevin function, $L(\alpha) = \coth \alpha - 1/\alpha$, and $\alpha = \mu H/kT$, being μ the magnetic moment per particle, H the magnetic field, k Boltzmann constant, T the absolute temperature and n the number of particles per unit volume of the assembly. The product $n\mu$ is the maximum moment that the material can have, i.e. the saturation magnetisation, M_s. Hence Eq. 2.18 can be also expressed as $M / M_s = L(\alpha)$.

The Langevin function describes the evolution of magnetisation of a system classically, i.e. when each individual atomic moment can point in any arbitrary direction, which is

normally the case for high temperatures and relatively low fields. However, in solids the spin can only take discrete orientations, due to the spatial quantization of the angular momentum. In this case, the expression for the magnetisation is modified to give the Brillouin function [1927],

$$\frac{M}{M_s} = \frac{2J+1}{2J}\coth\left(\frac{2J+1}{2J}\right)\alpha' - \frac{1}{2J}\coth\frac{\alpha'}{2J}, \qquad \text{(Eq. 2.19)}$$

where g is the Landé factor, J the total angular momentum per atom, $\alpha' = gJ\mu_B H/kT = \mu_H H/kT$, μ_H being the maximum moment of each atom in the field direction and μ_B the Bohr magneton.

Superparamagnetism occurs in particles of magnetically ordered material, which become so small that the energy barrier to changes in the direction of their magnetisation can be overcome by thermal energy. In this situation, relaxation between different easy directions of magnetisation is very rapid compared with the time of the measurement, and the particles behave as the atoms in a paramagnetic substance. Using the classical probability of jumping over an energy barrier, ΔE, the relaxation time follows an Arrhenius law [1889], expressed by [Néel (1949 *a*)] as,

$$\tau = {f_0}^{-1} e^{\frac{\Delta E}{k_B T}} \text{ where } \Delta E = KV \text{ for } H = 0, \qquad \text{(Eq. 2.20)}$$

where K and V are the anisotropy (uniaxial) constant and the volume of the particle, respectively. Hence the relaxation time of the particle, due solely to thermal effects, i.e., when no magnetic field is applied to the system, is of the order of $\tau = e \cdot {f_0}^{-1} \approx 2.7 \cdot 10^{-9}$ sec, considering $f_0 \approx 10^9 s^{-1}$ (see ✣5.10.1). A particle will be superparamagnetic when the measurement time, t, is higher than the relaxation time of the particle, i.e., $KV < \ln(t.f_0)kT \approx 25kT$ ($f_0 \approx 10^9 s^{-1}$, for the particles in this thesis).

Thus, at room temperatures, a system of superparamagnetic particles will have zero magnetisation unless a magnetic field is applied that aligns the magnetic moments in the field direction. If a system is said to exhibit superparamagnetism, there are also two other conditions that need to be fulfilled:

- There is no hysteresis, i.e., both the remanence and coercivity are zero.
- Magnetisation curves measured at different temperatures superimpose when M is plotted as a function of H/T.

The term *superparamagnetism* was first coined by Bean and Livingston [1959], although its existence was first predicted by Néel [1949 *b*]. It was so called because the moments of superparamagnetic particles are orders of magnitude larger than those involved in paramagnetism, as they consist of several thousand atoms. For example, a spherical particle of iron, 50 Å in diameter, contains 5560 atoms thus having a magnetic moment of $(5560)\cdot(2.2) = 12000\ \mu_B$, large compared with the magnetic moment per atom of a normal paramagnet, normally of a few Bohr magnetons.

Validity of the Langevin approach

For small particle systems, the Langevin approach is valid always when there is no anisotropic contribution to the energy of the system. This is normally the case for particles in a fluid, which are free to rotate, thus the anisotropy energy does not affect the magnetisation of the ferrofluid. Chantrell [1977] described the magnetisation of a solid dispersion of particles with randomly distributed easy axis in the presence of a *uniaxial anisotropy*. For the case of $KV << 25kT$ the expression he obtained for the magnetisation reduces to the Langevin function, and hence H/T superposition will be obtained. Excellent superposition was obtained by Becker [1957] in Co-Cu alloys, Bean and Jacobs [1956] in iron particles suspended in frozen mercury and Williams et al. [1993 *b*] in ferrofluid systems over a certain range of temperatures. For particles with $KV \geq 25kT$ the behaviour of the magnetisation will not follow the Langevin equation, due to the contribution of the anisotropy energy, $KV\sin^2\theta$. The superparamagnetic behaviour disappears, and H/T superposition is not expected anymore. These theoretical predictions were confirmed by Williams et al. [1993 *b*] and Hanson and co-workers [1993].

2.4.1. Superparamagnetic vs blocked particles

In a real system, due to the spread in particle sizes, one is always confronted with the existence of two types of particles: *blocked* and *superparamagnetic*. Superparamagnetic particles have been extensively described in the previous section. A particle is blocked when, in the time and at the temperature of the measurement, thermal effects are not enough for it to overcome its energy barrier for reversal. Therefore, in a system with distributed properties (volumes or/and anisotropies), for a constant temperature, there will be a mixture of blocked and superparamagnetic particles.

There are some relevant definitions when working with superparamagnetic/blocked particles, in the absence of an applied field ($H_{app} = 0\ Oe$), namely,

1. The *critical volume* below which the particles are superparamagnetic,

$$V_p = \frac{\ln(\tau . f_0)kT}{K}, \qquad \text{(Eq. 2.21)}$$

where $\ln(\tau . f_0) \approx 25$ for a *100 sec* measurement and $f_0 \approx 10^9 s^{-1}$ (✣5.10.1) in the absence of applied field. Above this volume, and at temperature T, the particles become blocked.

2. The *blocking temperature*, which is the temperature below which the particle, with volume V and anisotropy K is blocked,

$$T_B = \frac{KV}{\ln(\tau . f_0)k} \qquad \text{(Eq. 2.22)}$$

Considering an attempt frequency $f_0 = 7.7 \cdot 10^9 s^{-1}(Hz)$ (✣5.10.1), an effective anisotropy constant of $K = 4.6 \cdot 10^5 (erg/cc)$ (✣5.4.5), and a median diameter of 59 Å (✣5.5.1.1), the critical diameter and the blocking temperature for sample F028 are going to be calculated, assuming spherical particles and the absence of magnetic field. According to these values, $D_P(T = 297K) = 167$ Å, $D_P(T = 4K) = 40$ Å. Because the probability of finding a particle larger than 167 Å is 10^{-6}% (see ✣5.3.1), at room temperature, it can be said that all the particles in sample F028 are superparamagnetic, while at *4K*, the particles with diameters above 40 Å will be blocked. For the same sample, the value of the median blocking temperature is $T_{Bm} = 13\ K$. Thus for $T > 13\ K$ a particle with a diameter of 59 Å is superparamagnetic, while it will be blocked below this temperature. It is also very interesting to know if the particles are blocked or superparamagnetic in the temperature range in which the initial susceptibility $\overline{\chi}_i$ is studied (✣5.6). For the same parameters used previously, $D_P(T = 100K) = 116$ Å and $D_P(T = 180K) = 141$ Å for sample F028. The probability of finding a particle larger than 116 Å is 10^{-4}%. Hence, between 100 and 180K practically all the particles in sample F028 are superparamagnetic. Equally, for sample F024 ($D_{vm} = 77$ Å), $D_P(T = 100K) = 126$ Å and $D_P(T = 180K) = 156$ Å ; since the probability of finding a particle larger than 130 Å is 0.03%, at 100K there would be some large particles

contributing to $\overline{\chi}_i$. However, this contribution only represents 1% of the total susceptibility of the system at 100K and it becomes zero for higher temperatures.

2.5. Interaction effects

2.5.1. Type of interactions in nanoparticles

In a ferrofluid-type system there are magnetic and non-magnetic forces or interactions in play. Among the non-magnetic forces the most relevant are the Van der Waals (✣4.1.4). These interactions, however, are minimised by the presence of the surfactant which gives rise to a steric hindrance and, in any case, the magnetic dipole-dipole energy is approximately 10 times larger than the non-magnetic energy for particles with mean diameters of 100 Å [Jund et al. (1995 *b*)] at a separation of 100 Å. In other fine particle systems, such as magnetic metals and alloys of magnetic materials in a non-magnetic matrix, both dipolar and exchange coupling may be present.

2.5.1.1. Magnetic interactions

2.5.1.1.a. Dipolar interaction

In Fig. 2-4 the geometrical configuration of two interacting magnetic dipoles, m_1 and m_2, is presented schematically. The mutual potential energy between them is,

$$E_p = -\frac{m_1 \cdot m_2}{r^3}\left[2\cos\theta_1 \cos\theta_2 - \sin\theta_1 \sin\theta_2\right] \qquad \text{(Eq. 2.23)}$$

Dipolar interactions have a double role. Firstly, they influence the colloidal properties of ferrofluids (✣4.1.5). Secondly, they have an important effect on the magnetic properties of a fine particle system.

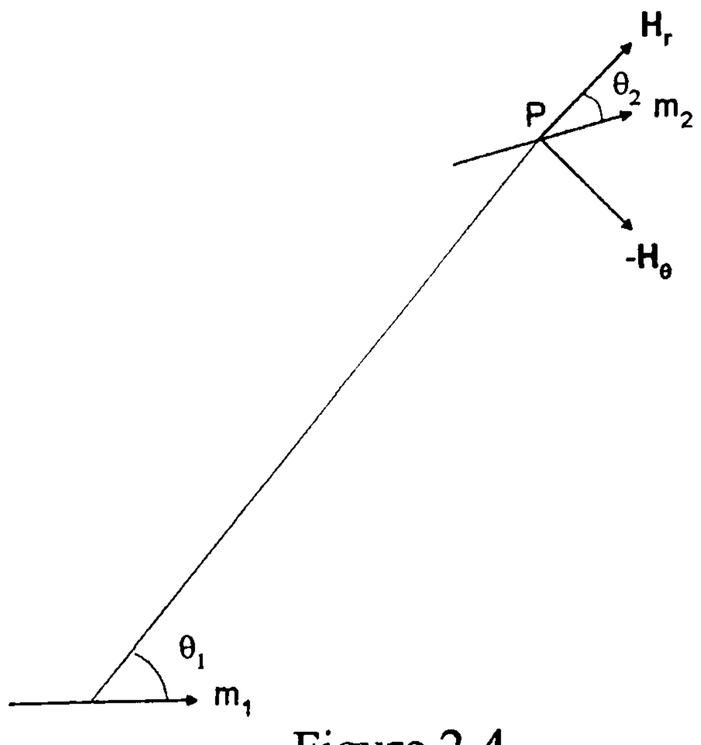

Figure 2-4

Dipolar interaction between 2 magnetic dipoles, m_1 and m_2.

In a two particle system and in a group of particles, dipolar interactions differ for different geometries. If the particles are aligned forming a chain-like structure, the configuration of minimum energy will be that where both moments are pointing in the same direction, and the interactions are magnetising for both particles [Cullity (1972)]. For larger systems, the overall effects are generally demagnetising to minimise the total magnetostatic energy. This is why closed loop structures are commonly observed in dipolar interacting systems [Hess and Parker (1966)].

In real systems, the particles in a fluid tend to form aggregates of a few particles in zero applied field, due to poorly coated particles. They have been observed by TEM and detected in kerosene-based magnetic fluids via viscosity and diffusion coefficient measurements [Buzmakov (1994)]. The formation of these aggregates was attributed to Van der Waals forces. Depending on the number of particles in the aggregates, their size, the temperature and the field applied to the system, different stable geometrical configurations are attained (see Appendix IV). Early studies by Menear et al. [1983, 1984] investigated the degree of spatial ordering within a 2D system of small magnetic particles in the form of a colloidal suspension concluding that, in zero applied field, only dimers and trimers are present in the system. When a field is applied to the system, it aligns the magnetic moments in these small aggregates, increasing the attractive interaction energy between particles. Using a 3D Montecarlo model, Martin et al. [1987, 1992] confirmed Menear results, also showing the presence of some closed loop structures and larger aggregates as the temperature of the system was lowered.

Jund et al. [1995 *a*, *b*] studied the minimum energy configurations (equilibrium geometry) in a ferrofluid, where small groups ($4 < N < 15$) of 100Å magnetic particles are present (see Appendix IV). For the calculations, molecular dynamics simulations and Monte Carlo techniques were used. The energy of the system includes the dipole-dipole term and a non-magnetic Lennard-Jones type potential: repulsive at short distances and attractive at long ones, due to both intrinsic and surfactant-induced effects. 2D ring structures were predicted to be the fundamental state in the absence of an external magnetic field at low temperatures of a few degrees Kelvin. Such structures have been reported for example by Hess and Parker [1966].

In a recent work, Tománek et al. [1997] extended the previous study by Jund et al. The small agglomerates of particles form stable structures of rings or chains, depending on the field and temperatures applied (see Appendix IV). Similar studies have been

published recently by other authors [Satoh et al. (1998)]. An interesting work by Chantrell et al [1996] showed how the remanence ($T = 77\ K$) of a system of small particles, decreases if a realistic initial configuration of the particles is considered, instead of a totally random configuration.

The nature of the interaction problem in the presence of an applied field, and its relation to the geometrical configuration of the system, is presented schematically in Fig. 2-5, for elongated single-domain particles. In Fig. 2-5 (a) part of the external field of particle A is sketched and this field acts in the $+z$ direction on particle B below it, but in the $-z$ direction on particle C beside it. Thus the interaction field depends not only on the separation of the two particles but also on their positions relative to the magnetisation direction of the particle considered as the source of the field [Cullity (1972)].

Suppose now that the M_s vectors of these particles (Fig. 2-5, a) have all been turned upward by a strong field in the $+z$ direction. This field is then reduced to zero and increased in the opposite direction $-z$. The field of A at C now aids the applied field, and C will reverse its magnetisation at a lower applied field than if A was absent. The coercivity will therefore be lowered. The opposite conclusion applies if the particles A and B are considered, and the coercivity will increase.

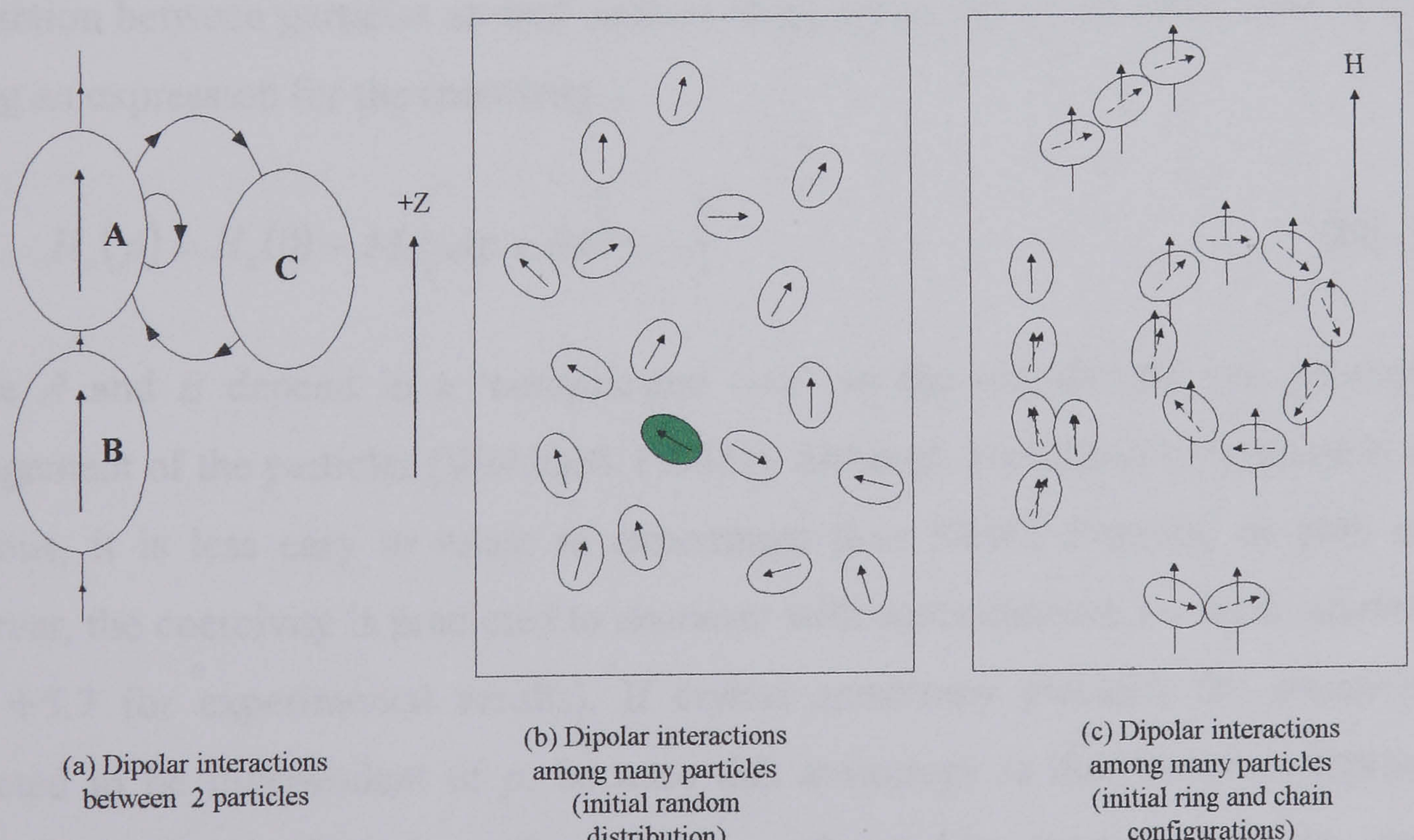

(a) Dipolar interactions between 2 particles

(b) Dipolar interactions among many particles (initial random distribution)

(c) Dipolar interactions among many particles (initial ring and chain configurations)

Figure 2-5

The problem sketched in Fig. 2-5 (a) seems relatively easy; however, a quantitative study of the interactions in a three particle system is very difficult, and an analytical solution for the many-body problem shown in Fig. 2-5 (b and c) is virtually impossible; to

compute the coercivity or any other magnetic property, it is necessary to know the field at the interior of the shaded particle due to all the other particles, both at the start and during the reversal.

Variation of the coercivity with dipolar interactions

Considering only uniaxial anisotropy, Néel [1947 *b*] gave an expression for the coercivity of a system of spherical particles isotropically distributed, as a function of the concentration, p,

$$H_c(p) = H_c(0)(1-p) \qquad \text{(Eq. 2.24)}$$

where $H_c(0)$ is the coercivity of an isolated particle. For $p=1$, the particles are everywhere in contact and the coercivity becomes zero, in the absence of another anisotropy. However, although this relationship has been approximately verified in some cases [Weil (1951)], it is by no means generally applicable. Wohlfarth [1955] criticised Néel's simplistic approach due to its reliance on an effective field, i.e. pM_0, which is inconsistent with a system of significant aggregation, since aggregates can take many different forms, such as rings, chains, etc. In Wohlfarth's calculations the actual forces of interaction between particles as well as their shape anisotropies are considered in detail, giving an expression for the coercivity,

$$H_c(p) = H_c(0) - M_0\left(Ap + Bp^{\frac{5}{3}} + \ldots.\right) \qquad \text{(Eq. 2.25)}$$

where A and B depend in a 'complicated way' on the orientations and geometrical arrangement of the particles [Wohlfarth (1955)]. Although Wohlfarth's treatment is more rigorous, it is less easy to relate to experiment than Néel's formula; in both cases, however, the coercivity is predicted to *decrease* with concentration, i.e. with interactions (see ✣5.7 for experimental results). If crystal anisotropy prevails, the coercivity is expected to be independent of p, because this anisotropy is due to forces (spin-orbit coupling) that are internal to the particle, and not like shape anisotropy, due to magnetostatic fields external to the particle.

In figure 2-5 (c), a realistic initial configuration of the particles is displayed. In this figure the initial ($H=0$) geometrical configuration of the particles is presented, which is not altered by the presence of an applied magnetic field, as in the case of a frozen ferrofluid.

In the absence of a field, the spins would align along their easy axis directions (dotted arrows, in Fig. 2-5, *c*), in different structures such as rings or chains. When a high enough field is applied, each of these particles will align in the field direction, shown by the continuous arrows. Still a many body problem, the knowledge of system's geometry can give a better understanding of how interactions behave in this kind of systems, especially if the experimental magnetic data, e.g., magnetisation curves, ZFC-FC, TDR, time dependence, are compared for different particle concentrations, in the light of these initial configurations.

Traditionally, dipolar interactions have been considered to be demagnetising; however, recent theoretical results predict magnetising dipolar interactions in some especial cases. A Montecarlo model by Kechrakos et a. [1998] predicts magnetising effects for systems with concentrations $\varepsilon < 16\%$, when dipolar interactions dominate the anisotropy term in the system. Using this model, the coercivity decreases upon sample dilution for systems with low anisotropy. Also recent results by Walmsley et al. [to be published in J. Appl. Phys. (2000)] show magnetising interactions in thin films with weak dipolar interactions.

2.5.1.1.b. Exchange interaction

Solid *ferromagnets* have a nonvanishing magnetic moment or spontaneous magnetisation in the presence of zero applied magnetic field. This phenomena is due to magnetic interactions of a different nature than the dipolar interactions. In other solids, known as *antiferromagnets*, although there is no net total moment in the absence of a field, there is a far from random spatial distribution of the individual moments, due again to a magnetic interaction favouring antiparallel orientation of magnetic moments. When a material contains two lattices of different magnetic moments, coupled antiferromagnetically, it presents a total magnetic moment resulting from the uncompensated spins. This type of material is known as a *ferrimagnet*.

The origin of the exchange interaction lies in the ever present Coulombic forces and the indistinguishability of the electrons. Some transition metal atoms have a net magnetic moment that goes from $2.2\mu_B$ in Fe to $1.7\mu_B$ in Co and $0.6\mu_B$ for Ni. The spontaneous magnetisation of these systems arises due to the unpaired spins in the 3d and 4s energy levels, which is an energetically stable configuration, because the spins move in different spatial orbits, so as to minimise the Coulomb repulsion. It was Heisenberg in 1926, the first to explain the phenomena of exchange coupling in the He atom.

The exchange interaction for a pair of atoms with spins s_1 and s_2 is given as,

$$E_{ex} = -J_{ex}\,\mathbf{s}_1 \cdot \mathbf{s}_2 \qquad \text{(Eq. 2.26)}$$

where J_{ex} is the exchange integral, being $J_{ex} > 0$ for a ferromagnet and $J_{ex} < 0$ for an antiferromagnet. The dependence of this energy, more precisely, of the exchange integral, J_{ex}, with interatomic distance, is plotted in the Bethe-Slater curve (Fig. 2-6) for atoms with their electrons in the 3d orbit.

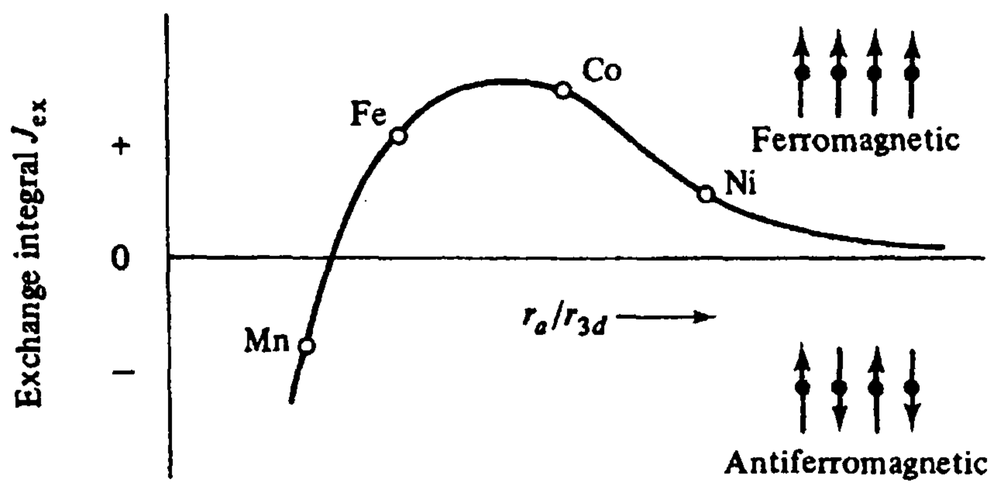

Figure 2-6

Bethe-Slater curve for atoms with their electrons in the 3d orbit, where r_a is the atom radius and r_{3d} the radius of the 3d orbit.

The magnetic interaction described by Eq. 2.26 is known as *direct exchange*, because it arises from the direct Coulomb interaction among electrons of the two ions or atoms. It often happens that two magnetic ions are separated by non-magnetic ions. It is then possible for the magnetic ions to have a magnetic interaction mediated by the electrons in their common non-magnetic neighbours, which may be more important than the direct exchange. This type of magnetic interaction is called *superexchange*. It occurs in the spinel structures like magnetite, through the oxygen atoms. Yet another source of magnetic interaction can occur between electrons in the partially filled *f*-shells in rare earth metals. In addition to their direct exchange coupling, the *f*-electrons are coupled through their interactions with the conduction electrons. This mechanism, in a sense the metallic analogue of superexchange in insulators, is known as *indirect exchange*. It can be stronger than direct exchange coupling, since the *f*-shells generally overlap very little. There are also important exchange interactions in metals among the conduction electrons themselves, often referred to as *itinerant exchange*.

Normally, exchange interactions are magnetising-type interactions, as revealed in the delta *M* plots of many thin film media which are strongly exchanged coupled systems. However, sometimes, and depending on the magnetic state of the system, may this be

generated for example by the applied field [Dova et al. (1997)] or differences in interparticle distance [El-Hilo et al. (1993 *a*)], these interactions may manifest as demagnetising. The actual geometrical disposition of the magnetic material in the system is fundamental for the effects of interactions as previously commented; in the work by Batlle et al. [1997 *a*] this seems to be the reason for the shift from magnetising to demagnetising interactions. Also it must be born in mind that exchange interactions can oscillate from ferro to antiferromagnetic, depending on the spacing between magnetic layers as is the case in multilayers [Parkin et al. (1990, 1991), Petroff et al. (1991)].

Thus, it is reasonable to say that no definite conclusions can be drawn about the effects of interactions from their origin (exchange/dipolar). The geometry of the magnetic system, as well as the anisotropies involved, the relative strengths of the interactions, the interparticle separations, and the fields applied are of fundamental importance to make a precise evaluation of the nature and effects of interactions in fine particle systems.

2.5.2. Curie-Weiss behaviour

2.5.2.1. Initial susceptibility

The initial susceptibility is defined as the susceptibility of the system in a low magnetic field. If the Langevin function (✣2.4) is used to describe the magnetisation of the system, then the initial susceptibility is given by,

$$\chi_i = \left.\frac{M}{H}\right)_{H\to 0} = \frac{N\mu^2}{3AkT}, \qquad \text{(Eq. 2.27)}$$

where k is the Boltzmann constant, T the absolute temperature, N Avogadro's number and A the atomic weight. Eq. 2.27 is the well-known 'Curie law'. The use of the Langevin function for the description of the initial susceptibility is justified for particles, especially for the very low fields in which the susceptibility is measured.

In real systems there is invariably a distribution of particle sizes, so that depending on the temperature of the experiment, some of the particles will be blocked while others will be superparamagnetic (✣2.4.1). Considering this fact, Wohlfarth [1979] derived the expressions,

$$\chi_i = \frac{M_{sB}{}^2}{3K}, \text{ for } T<T_B \text{ (a)} \quad \text{and} \quad \chi_i = \frac{M_{sB}{}^2 V}{3kT}, \text{ for } T>T_B \text{ (b)} \qquad \text{(Eq. 2.28)}$$

where M_{sB} is the saturation magnetisation of the bulk material, V the particle volume, T the absolute temperature and K the anisotropy constant. Eq. 2.28 (a) represents the susceptibility of a blocked particle, while the susceptibility of a superparamagnetic particle is given by Eq. 2.28 (b). Both equations need to be modified to account for a distribution of particles volumes, $f(y)$, where y is the reduced volume of the system defined below. Considering a lognormal distribution of particle sizes (see ✣2.6), the total susceptibility, normalised to the saturation magnetisation, $\overline{\chi_i}$, for a non-interacting system is finally expressed as [El-Hilo et al. (1992 *b*)],

$$\overline{\chi_i} = \frac{M_{SB}V_m}{3kT}\int_0^{y_p} yf(y)dy + \frac{M_{SB}}{3K}\int_{y_p}^{\infty} f(y)dy, \quad y = \frac{V}{V_m} \qquad \text{(Eq. 2.29)}$$

where V_m is the median volume of the particles and y_p the reduced critical volume for superparamagnetic behaviour, namely, $y_p = V_p / V_m = 25kT / KV_m$. The first integral represents the contribution of the superparamagnetic particles which dominate the initial susceptibility, while the second integral represents the contribution of the blocked particles, which is very small (~ 4%) and can generally be neglected [Wohlfarth (1979)]. The variation of $\overline{\chi_i}$ with temperature gives rise to a peak at a temperature $T = T_m$; this peak arises due to the increase in the fraction of superparamagnetic particles as temperature increases; after the peak, the value of $\overline{\chi_i}$ decreases again due to thermal agitation. The value of T_m is directly related to the median blocking temperature of the system [Gittleman et al. (1974)],

$$T_m = \beta T_{Bm} \qquad \text{(Eq. 2.30)}$$

where β is a constant dependent on the particle size distribution which becomes unity for a single particle size.

If the variation of $\overline{\chi_i}^{-1}$ with T is examined for $T > T_m$, there appears an apparent negative ordering temperature, T_{0B}, which arises due to progressive blocking of the particles [El-Hilo et al. (1992 *b*)]. If the ordering temperature is calculated in a range of temperatures closer to T_m, T_{0B} will increase in magnitude. Thus it is fundamental to account for this effect before drawing any conclusions about the ordering temperature of the system (✣2.5.2.2). El-Hilo et al. [1992 *b*] derived an analytical expression which

shows explicitly how T_{0B} arises from the blocking effects in the system. Since the variation of $\overline{\chi_i}^{-1}$ with T is usually examined above T_m, i.e., at temperatures $T >> T_{Bm}$ ($V_p >> V$), the second term in Eq. 2.29 can be neglected, and the equation rewritten,

$$\overline{\chi_i} = \frac{M_{SB} V_m}{3kT} b \left(1 - b^{-1} \int_{y_p}^{\infty} y f(y) dy \right) \qquad \text{(Eq. 2.31)}$$

where $b\left(= \int_0^{\infty} y f(y) dy \right)$ is a constant for a given distribution of reduced particle volumes. For a lognormal distribution, this parameter is given by $b = \exp(\sigma_y{}^2 / 2)$.

For $V << V_p$ ($T >> T_{Bm}$), the lognormal distribution function can be substituted by a power law, of the form $f(y) = a.y^{-n}$. In this study, a value of $n = 3$ has been used, since this is the smallest power for which the integral in Eq. 2.31 can be solved analytically. The value of a, as well as the validity range for the substitution (roughly $y \geq 5$), varies depending on the value of the standard deviation, σ_y, of the lognormal distribution. Using this approximation, and integrating Eq. 2.31,

$$\overline{\chi_i}(T) = \frac{bC_0}{T + T_{0B}}, \text{ for } V << V_p \ (T >> T_{Bm}) \qquad \text{(Eq. 2.32)}$$

where $C_0 = M_{sB} V_m / 3k$. Thus a negative ordering temperature is predicted, which is proportional to T_B and is given by,

$$T_{0B} = -\gamma T_{Bm} \qquad \text{(Eq. 2.33)}$$

where $\gamma = \mathrm{a} b^{-1}$, which, for a lognormal distribution of volumes, is $\gamma = a \exp(-\sigma_y{}^2 / 2)$.

2.5.2.2. Origin of the Curie-Weiss behaviour

Early in this century, Weiss [1907] realised that in many paramagnets the dependence of the susceptibility with temperature was of the form,

$$\chi \propto \frac{C}{T - \theta}, \text{ where } C = N \mu^2 / 3Ak \qquad \text{(Eq. 2.34)}$$

In the Langevin theory of paramagnetism, which leads to the simple Curie law, the particles are assumed not to be interacting and only affected by the applied field and

thermal energy. Weiss (and earlier Russian physicist Rósing [1897]), postulated the existence of interactions among the particles, and defined an imaginary magnetic field which he called the 'molecular field', H_m, which was used as a measure of the interactions. This molecular field was considered to be proportional to the magnetisation, $H_m \propto M$. If the effect of this field on the magnetisation is studied, the susceptibility dependence on temperature changes, and it can be described by a Curie-Weiss type law, as shown in Eq. 2.34.

2.5.2.3. Corrections to the ordering temperature T_0, due to blocking and interaction effects

Traditionally the ordering temperature has given information about the type of interactions among the particles in a system. In this way, and considering equation 2.34, when $\theta > 0$ the interactions are magnetising, and if $\theta < 0$ the interactions are demagnetising. El-Hilo et al [1992 *b*] showed theoretically and tested experimentally, that it is necessary to consider two different contributions to the ordering temperature, θ, before drawing any conclusions about interactions. These contributions are the 'blocking contribution', T_{0B} (✣2.5.2.1), and the 'interaction contribution', T_{0i}. In this way, the expression for the susceptibility is generalised in the following manner,

$$\chi \propto \frac{C}{(T + T_{0tot})} \qquad \text{(Eq. 2.35)}$$

$$T_{0tot} = T_{0B} - T_{0i} \qquad \text{(Eq. 2.36)}$$

(the Curie temperature, θ, will be substituted by $-T_{0tot}$ in this section). For the non-interacting case, El-Hilo et al. [1992 *b*] derived the expression 2.31 shown in ✣2.5.2.1 for the susceptibility of a system of fine magnetic particles. The effect of dipolar interactions on the magnetisation was calculated in the same paper. For a weakly interacting system with $\varepsilon = M_S / M_{SB} < 10\%$, as in the systems studied here, the initial susceptibility, $\overline{\chi}_i$, is given,

$$\overline{\chi}_i = \left.\frac{d\overline{M}}{dH}\right|_{H\to 0} \approx \frac{M_{sB}V}{3kT} + \frac{2}{3\times 45}\xi_1 \frac{{M_{sB}}^5 V^3}{(kT)^3}, \qquad \text{(Eq. 2.37)}$$

$$\xi_1 = \frac{\langle n_1 \rangle \left\langle \left(3\cos^2 \psi_1 - 1\right)^2 \right\rangle V_m{}^2}{\langle d_1{}^6 \rangle} \qquad \text{(Eq. 2.38)}$$

where ξ_1 is an interaction parameter, $\langle n_1 \rangle$ the mean number of particles which are first neighbours, (d_1, ψ_1) represents the location of the particle which is a first neighbour and $\langle d_1 \rangle$ is the average inter-particle separation of first neighbours within the cluster. If a distribution *f(y)* of particles sizes is now considered, and for temperatures such that $T >> T_{Beff}$, Eq. 2.37 becomes,

$$\overline{\chi_i} \approx \frac{M_{sB} V_m}{3kT} \int_0^{y_{peff}} y f(y) dy + \frac{2}{3 \times 45} \xi_1 \frac{M_{sB}{}^5 V_m{}^3}{(kT)^3} \int_0^{y_{peff}} y^3 f(y) dy, \quad y_{peff} = \frac{T}{T_{Beff}} \qquad \text{(Eq. 2.39)}$$

where T_{Beff} is the mean effective blocking temperature of the system. When $T >> T_{Beff}$, the lognormal distribution function can again be substituted by a power law, of the type $f(y) = a.y^{-3}$, as it was done in the non-interaction case (✣2.5.2.1), so that the integral in Eq. 2.39 can be analytically solved,

$$\overline{\chi}_i = \frac{C_0 b}{\left(T - \gamma\, T_{Beff} + \frac{2}{5} \xi_1 \frac{M_{sB}{}^2 C_0{}^2 \gamma}{T_{Beff}} \right)^{-1} T}, \qquad \text{(Eq. 2.40)}$$

where $C_0 = M_{sB} V_m / 3k$, $b = \exp(-\sigma^2/2)$ and $\gamma = a \cdot b^{-1}$. The term $\gamma\, T_{Beff} / T$ arises due to *effective blocking* and the term $2\xi_1 M_{sB}{}^2 C_0{}^2 \gamma / 5 T_{Beff} T$ arises due to particle *interactions*. Using the binomial expansion to first order, Eq. 2.40 becomes,

$$\overline{\chi}_i \approx \frac{b C_0}{T + T_{0tot}}, \text{ with } T_{0tot} = T_{0B} - T_{0i} \qquad \text{(Eq. 2.41)}$$

where T_{0B} represents the effective blocking, i.e. $T_{0B} \to \gamma\, T_B$ when $\xi_1 \to 0$ and T_{0i} arises due to interactions. T_{0B} and T_{0i} are given by,

$$T_{0B} = -\gamma\, T_{Beff}, \text{ and} \qquad \text{(Eq. 2.42)}$$

$$T_{0i} = -\frac{2}{5} \gamma \xi_1 \frac{M_{SB}{}^2 C_0{}^2}{T_{Beff}} \qquad \text{(Eq. 2.43)}$$

The total ordering temperature, T_{0tot}, has been obtained for a distributed system of fine particles, in the temperature range $T >> T_{Beff}$, i.e. when the majority of the particles are superparamagnetic. Two distinct contributions, effective blocking and interactions, have been found to contribute to its value. If both contributions are present in a system of particles, i.e. if the distribution of particle sizes is not too narrow and there are interactions in the system, then the sign of T_{0tot} will depend on which contribution dominates in the temperature range under study. A negative T_{0tot} is predicted when T_{0B} is dominant. However, it may be the case that the total ordering temperature is negative, not because the blocking effects are dominant, but because the interactions are indeed demagnetising (✣5.6).

2.5.3. Other magnetic techniques

2.5.3.1. Remanence and Delta M curves

The dependence of the remanent magnetisation on the applied magnetic field (remanence curve) gives information about irreversible magnetisation processes. The basic remanence curves are the isothermal remanence (IRM) curve and the dc demagnetisation (DCD) curve [O'Grady and Chantrell (1992)]. Starting from a demagnetised state, the IRM curve is obtained by applying progressively larger positive fields. After a field is applied, the remanence (H=0 Oe) is recorded. The IRM curve is obtained by plotting the remanent magnetisation against the applied field. For the DCD curve, the initial state is the saturated state. As in the case of the IRM curve increasingly larger fields are applied and the remanence recorded, coming back to the initial saturated state for every field value.

In the absence of interactions, the value of the DCD remanence will be twice that of the IRM remanence, because in the DCD all the particles have a component of the magnetic moment in the direction of the field before the reversal, while for the IRM only half of the initial random distribution of moments will have such a component. This fact is reflected by Wohlfarth's relation [Wohlfarth (1958, 1983)],

$$\overline{M}_d(H) = 1 - 2\overline{M}_r(H) \qquad \text{(Eq. 2.44)}$$

where $\overline{M}_d(H)$ and $\overline{M}_r(H)$ are the IRM and DCD remanences, normalised to the saturation remanence, $M_r(\infty)$, for every field. If for instance there are demagnetising

interactions in the system the absolute value of $\overline{M}_d(H)$ will increase, while $\overline{M}_r(H)$ (always positive) will decrease. Thus, in the presence of interactions Wohlfarth's relation will fail to be true, and any deviation from it will give a measure of the interactions. Henkel [1964] plotted $\overline{M}_d(H)$ against $\overline{M}_r(H)$, and attributed to interactions the deviations from linearity. Later, Kelly et al. [1989] defined a parameter, ΔM, which gives the sign and the magnitude of the interaction qualitatively,

$$\Delta M(H) = \overline{M}_d(H) - \left[1 - 2\overline{M}_r(H)\right] \qquad \text{(Eq. 2.45)}$$

A positive value of ΔM indicates predominantly *magnetising* interactions in the system, and are normally associated with direct exchange coupled systems such as thin films [Mayo et al. (1991)]. Negative ΔM values are due to predominantly *demagnetising* interactions, normally associated with fine particle systems [Fearon and Chantrell (1990)], particulate recording tapes [El-Hilo et al. (1992 *a*)] and Ba ferrite thin films [Li et al. (1996)], which exhibit dipolar coupling. However, it is possible to observe magnetising interactions in systems which exhibit strong dipolar coupling such as Ba ferrite media [Mayo et al. (1990)].

In any case care must be taken when evaluating interaction effects from ΔM plots, as the curve depends strongly on the magnetic state of the system, prior to the measurement [Zhu and Bertram (1988)]. In fact, the initial demagnetised state required for the IRM curve is not easily obtained, even using very slow ac demagnetising techniques. Alternative techniques such as the *generalised* ΔM *plot* have been suggested [Bissell (1994)], that get round the problem of the initial demagnetised state. Theoretical calculations using the Preisach model [Stancu et al. (1998), Della Torre (1965)], reproduced qualitatively the experimental generalised ΔM plots calculated for commercial particulate media.

Finally, it is interesting to note that from the irreversible changes in *M*, the distribution of anisotropy fields can be calculated [Batlle et al. (1993)], and some conclusions can be drawn on the effect of interactions on this distribution (✣5.8.1.1).

2.5.3.2. Variation of coercivity with temperature, $H_c(T)$

An extensive review of the variation of the coercivity with concentration has been made in ✣2.5.1.1.a. From this study, the main conclusion is the difficulty of calculating

analytically the coercivity of the system of small particles when dipolar interactions are predominant.

The variation with temperature of the coercivity of a system of small particles can provide some valuable information. For a system of non-interacting ferro or ferrimagnetic particles, and assuming coherent rotation of the magnetic moments, the coercivity diminishes with the temperature in the following fashion,

$$H_c = H_c(0)\cdot\left(1-\left[\frac{\ln(\tau\cdot f_0)\cdot k}{K\cdot V}\right]^{\alpha}\cdot T^{\alpha}\right) \qquad \text{(Eq. 2.46)}$$

The exponent α is $1/2$ for the case of aligned particles [Bean and Livingston (1959)]. Pfeiffer [1990 *b*] solved the case of a random system of particles, obtaining a value of $\alpha = 0.77$. From equation 2.46, not only the effective anisotropy of the system can be calculated, but also the coercivity at absolute zero, by extrapolation to $T = 0K$ (✣5.7.3).

2.6. Particle size distribution

In all real systems there is always a distribution of particle sizes. This property needs to be accounted for to explain the magnetic behaviour of real systems. It is believed that many small particle systems follow a lognormal distribution of particle sizes [Granqvist and Buhrman (1976)].

2.6.1. The lognormal distribution function.

The dream of any physicist would be an ideal system of identical non-interacting particles. However, in real systems, there is always a distribution of particles sizes. The most widely known distribution in Statistical Mechanics is the Normal or Gaussian distribution function. For granular systems, however, it is generally accepted [Granqvist and Buhrman (1976)] that they follow a lognormal distribution function in most cases.

It was by the turn of last century that the lognormal distribution function (LNDF) was first suggested, by Galton [1879]. The actual derivation of the LNDF was due to Kottler [1950, 1951] and Irani [1959]. The first extensive study, analysing particle size distributions in several different systems was made by Granqvist and Buhrman [1976]. Nowadays, the LNDF is invariably used by many workers in fine particle magnetism.

Essentially, a parameter x is lognormally distributed if its logarithm follows a gaussian distribution function, i.e. if the following relationship is verified [O'Grady and Bradbury (1983)]:

$$f(x)dx = \frac{1}{\sqrt{2\pi}\sigma x} e^{-\frac{\ln x - \mu}{2\sigma^2}} dx \qquad \text{(Eq. 2.47)}$$

where σ is the standard deviation of $\ln x$, and $\mu = \overline{\ln x}$ so that $\bar{x} \approx \exp(\mu)$, where $\bar{x}$ represents the median of x (✣5.2.1.1, ✣5.3.1 and ✣6.2).

2.6.2. Distribution of particle volumes and energy barriers

The distribution of particle sizes gives rise to a distribution of energy barriers to reversal. These characteristics are studied in ✣5.4 together with their influence on the magnetic behaviour of the system.

2.7. Relaxation processes in small particles

Different theories have been proposed in the past for the study of the evolution of magnetisation with time, which are presented in this section. The original theories describe the relaxation of a single magnetic moment. The concept of thermal fluctuations of the magnetic moment of a single-domain particle and its decay toward thermal equilibrium was introduced by Néel [1949 *a*] and further developed by Brown [1963 *a*]. Both assumed a uniform magnetisation and uniaxial anisotropy in order to derive a single relaxation time, the main difference between the results being the pre-exponential factor, f_0 [Jones and Srivastava (1989)]. In fact the problem of the pre-exponential factor is still unresolved [Coffey et al. (1995)]. The majority of theories available nowadays extend the previous results to distributed systems of many particles.

The understanding of the relaxation processes in small particle systems is of fundamental importance in order to understand these processes in more complex systems, such as thin films and bulk materials. Also, the rapidly increasing magnetic storage densities poses the fundamental question of how far the reduction in the bit size can go without inducing significant loss of information.

2.7.1. Mainstream theories

2.7.1.1. Néel's theory

Consider an assembly of particles, small enough to be single-domain (SD). Néel [1949 *a*] considered an ensemble of such particles, which are placed in a large magnetic field. In this situation, all the particle moments will be aligned in the field direction. When the field is switched off the remanent magnetisation decays with time due to thermal effects, the moments relaxing out of the direction of the previously applied field, into their easy axis direction of magnetisation. For a single particle, this decay would follow an exponential law,

$$M_r(t) = M_r(0) \cdot e^{-t/\tau}, \qquad \text{(Eq. 2.48)}$$

where t is the time of the measurement, $M_r(t)$ and $M_r(0)$ the remanent magnetisations at times t and $t = 0\,\text{sec}$, respectively, and τ is the relaxation time. Using the (classical) probability of jumping over an energy barrier, the relaxation time follows an Arrhenius law [1889], which for a system with uniaxial anisotropy was described by Néel [1949 *a*] as,

$$\tau^{-1} = f_0 e^{-\frac{KV}{k_B T}}, \text{ for } H = 0 \qquad \text{(Eq. 2.49)}$$

where KV is the energy barrier for reversal in the absence of a field, K is the anisotropy constant, V the particle's volume, k the Boltzman constant and T the absolute temperature. The pre-exponential factor, f_0, is a constant which was estimated [Néel (1955), Kneller (1964)] to be of the order of $10^9 s^{-1}$. Later, Brown (✣2.7.1.2) defined an expression for f_0 and the value he calculated was practically the same. In recent experimental results for small particle systems different values of f_0 closer to $10^{10} s^{-1} - 10^{12} s^{-1}$ have been reported (ferritin, $\sim 10^{12} s^{-1}$ [Dickson et al. (1993 *a* and *b*)], Fe-C particles, $\sim 2 \cdot 10^{11} s^{-1}$ [Hansen et al. (1998)], α-Fe particles, $\sim 10^{10} s^{-1}$ [Bødker et al. (1998)]). In this thesis (see ✣5.10), different methods have been used to calculate f_0 in the ferrofluid samples, and the results have been discussed. Using the method of Dickson et al. [1993 *a*], the values of f_0 obtained are 3.3±0.7, 5.6±1.3 and $7.7 \pm 1.8 \times 10^9 s^{-1}$ for the F024 ($D_{vm} = 77$ Å), F026 ($D_{vm} = 66$ Å) and F028 ($D_{vm} = 59$ Å) samples, respectively. Recently, Wernsdorfer et al. [1997], measuring the temperature

dependence of the switching field [Kurkijärvi (1972)] in single ellipsoidal fcc Co particles ($D \sim 250$ Å), for very low temperature ranges, $0.15K < T < 6K$, obtained a value of $\tau_0(f_0^{-1}) \approx 4 \times 10^{-9}$ sec ($f_0 \approx 2.5 \cdot 10^8 Hz$). It is important to notice that f_0 is far from constant for systems with cubic anisotropy [Aharoni (1973)] and special care must be taken when studying relaxation data in systems with this kind of anisotropy (see ✣2.7.1.2).

The strong influence of the particle size on the relaxation time is shown below. Assuming spherical particles and the values obtained for the system F028 (Fe_3O_4), $f_0 = 7.7 \cdot 10^9 s^{-1}, K = 4.6 \cdot 10^5 erg/cc$, $T = 300K$, Eq. 2.49 is used to calculate the relaxation times of different particle sizes,

<u>Sphere of Fe_3O_4</u>

Diameter = 152 Å $\Rightarrow$ $\tau = 0.1$sec

Diameter = 168 Å $\Rightarrow$ $\tau = 10^9$ sec

When the particles become very small or the temperature high, the energy barriers for reversal are so small that can be easily overcome by thermal fluctuations. Therefore, the relaxation time is also small and the whole system becomes spontaneously demagnetised after the removal of the field, due solely to thermal effects. This phenomena, as already mentioned before (✣2.4), is called superparamagnetism. Thermal effects will be thus reduced if the temperature of the experiment is lowered so that the relaxation of the magnetisation can be observed in the time of the measurement.

In general, the effect of magnetisation relaxing from the previous 'aligned' positions into the more stable (along the easy axis) 'non-aligned' states, has been observed in many systems and it is known as 'magnetic viscosity'. It will be discussed in more detail in ✣2.7.3.

2.7.1.2. Brown's theory

Brown criticised Néel's approach because he considered it permitted only a single jump of the moment from one energy minima to another, not allowing the spin to spend any time in between these two minima before jumping. Nor does it include the probability for the spin to jump back to the original minimum. Brown [1963 *a*] took these effects into account, deriving a partial differential equation (Gilbert's equation) which described the motion of the magnetic moment of the particle during his random walk from one energy

minimum to another. He considered the magnetisation vector in a particle to 'wiggle' around an energy minimum for a while, then jump to somewhere around the other minimum, also wiggling around this minimum before jumping again. The relaxation time is related simply to the eigenvalue of this differential equation. Brown did not solve the equation but gave an asymptotic solution for the relaxation time identical to that of Eq. 2.49, except for the value of the pre-exponential factor,

$$f_0 = \frac{2K\gamma_0}{M_s}\sqrt{\frac{\alpha}{\pi}}, \text{ for } \alpha >> 1 \qquad \text{(Eq. 2.50)}$$

where γ_0 is the gyromagnetic ratio and $\alpha = KV / kT$. The result given by Brown is valid only for high energy barriers, i.e. $\alpha >> 1$. From his results Brown concluded that for uniaxial anisotropy, the exact solution is not drastically different from what is obtained by considering f_0 constant, which is Néel's approach. The same conclusion can be drawn from the numerical solution of Brown's equations for uniaxial anisotropy, in zero [Aharoni (1964)] and non-zero [Aharoni (1969)] applied fields. Also, Aharoni [1964] calculated numerically the eigenvalues of Brown's equation and stated that Brown's approximation (Eq. 2.50) of the solution for high energy barriers was valid even for rather 'low' energy barriers, say,

$$\alpha = \frac{KV}{k_B T} \geq 1.4 \qquad \text{(Eq. 2.51)}$$

In general, Eq. 2.49 is valid for any other kind of uniaxial anisotropy, if the energy barrier KV is replaced by the energy barrier of that particular case [Aharoni (1993)]. The situation changes completely in the case of cubic anisotropy. Although, at least for $H = 0$, Eq. 2.49 can still be used substituting K by $K_1 / 4$, the assumption of a constant factor, f_0, in front of the exponential is a bad approximation. In a material with cubic anisotropy, there are minima along the x, y and z directions, and very many possibilities for the moment to precess around each one before jumping to one of the others. Evidently, this wealth of possibilities makes a difference in the random walk problem. In fact, the value of τ computed numerically [Aharoni (1973, 1975)] from Brown's equations is quite different from that obtained with the Néel approach.

This difference has been measured by Krop et al. [1974]. In their experiment, the relaxation time is calculated from the line-width of the Mössbauer spectra, for different

sizes and temperatures of a system of $\beta - Co$ superparamagnetic particles, with *fcc* structure, precipitated from a monocrystalline $Cu - 1\%(wt)Co$ solid solution. In Krop's paper the computed solution from Brown's equation [Aharoni (1973)] fits the experimental data quite accurately, while Néel's solution for τ only approaches the experimental data for $\alpha >> 1$, a condition only fulfilled for low temperatures or large particle volumes. Thus, for cubic anisotropy, Brown's solution is much more accurate than Néel's, and they only come together and agree with experiment for quite high energy barriers. Thus, Néel's $\tau \simeq$ Brown's τ only when $(K_1 / 4)V >> kT$. For small particles, where $(K_1 / 4)V \leq kT$, only Brown's solution is realistic. In the case of uniaxial anisotropy, however, both solutions coincide. If a system has a combination of different anisotropies, some of which are not uniaxial, Néel's approach will not be able to describe the evolution of τ, although little work has yet been done on such a system.

A good discussion on Brown's treatment of the relaxation process for small particles with possible surface effects, is given in ✣D.3 of Dormann et al. [1997]. In this work, the authors also give solutions of Brown's equations using different approaches, and for different energy barriers. Particularly interesting are the results for very low energy barriers, which are fundamental for the understanding of the relaxation processes near the natural attempt frequency of the system (f_0), i.e., for very short measurement times, like those attained in Mössbauer and FMR experiments.

2.7.2. Relaxation of the magnetisation in an applied magnetic field

The case of a particle with uniaxial anisotropy, where the magnetic moment of the particle is at an angle ϕ (Fig. 2-7, a) to the easy axis, *z*, and the magnetic field is applied along the easy axis direction, is going to be considered. The total energy of the system is given (Fig. 2-7, b) by,

$$E = KV \sin^2 \theta - \mu H \cos\phi \qquad \text{(Eq. 2.52)}$$

where V is the volume of the particle, K the anisotropy constant, and $\mu = M_{sB}V$. Fig. 2-7 (b) represents a plot of Eq. 2.52 for the values obtained for the ferrofluid samples (✣5.4.5): $D_m = 59\text{Å}$, $K_1 = 4.6 \cdot 10^5 erg/cc$, $K_2 = 2.3 \cdot 10^5 erg/cc$, for different applied fields ($H = 0$, 100 and 1 kOe) as a function of the angle θ.

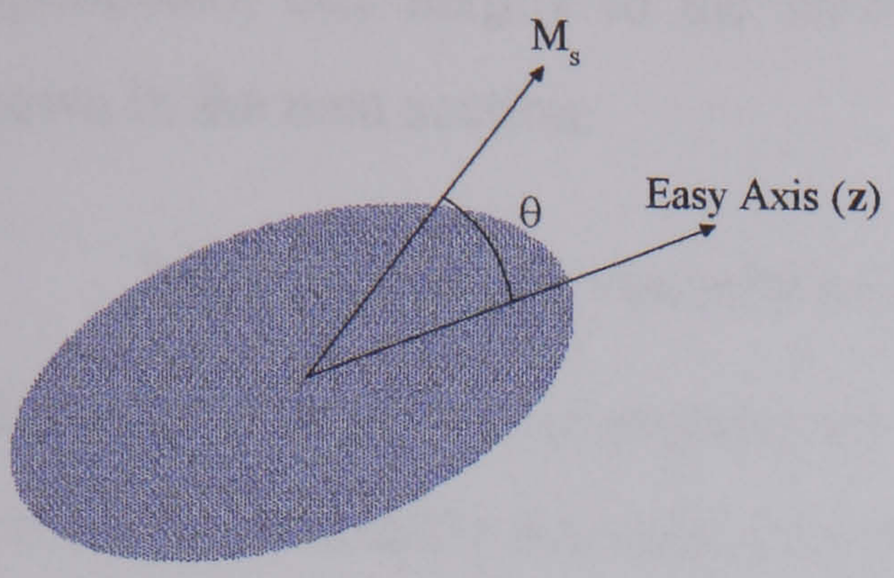

(a)

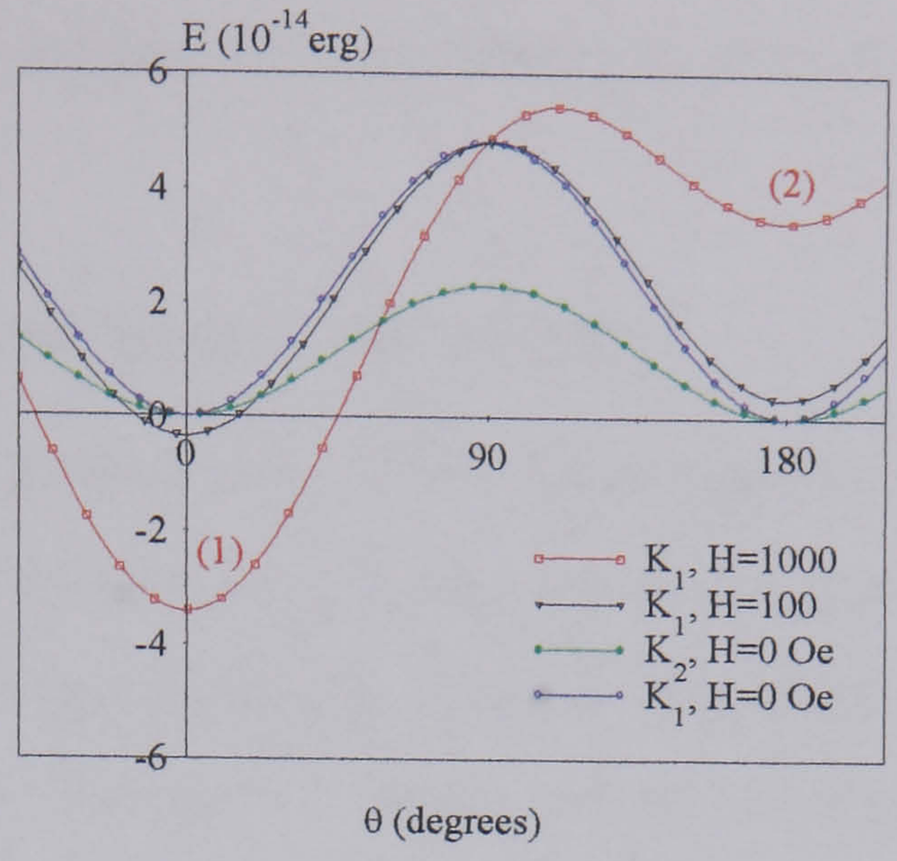

(b)

Figure 2-7

Energy of a uniaxial particle ($D_m = 59$ Å) in the presence of different applied fields. The effect of different anisotropy constants ($K_1 > K_2$) is also shown.

As can be seen from Fig. 2-7 (b) or Eq. 2.52 the system has two energy minima, at $\theta = 0$ and $\theta = \pi$, given by $E_1 = -\mu H$ and $E_1 = +\mu H$, respectively, separated by an energy maximum,

$$E_m = KV + \frac{\mu^2 H^2}{4KV} = KV\left[1 + \left(\frac{HM_s}{2K}\right)^2\right], \qquad \text{(Eq. 2.53)}$$

where $2K / M_s = H_K$ is the anisotropy field. Therefore the energy barrier, $\Delta E = E_m - E_1$, to jump from minimum 1 to minimum 2, is given by,

$$\Delta E_{1\to 2} = K_1 V\left(1 + \frac{H}{H_K}\right)^2, \text{ while } \Delta E_{2\to 1} = K_1 V\left(1 - \frac{H}{H_K}\right)^2, \qquad \text{(Eq. 2.54)}$$

represents the energy barrier to jump from 2 to 1. Therefore the probability for a particle to relax over the energy barrier will be different in both cases,

$$\tau^{-1}{}_{1\to 2} = f_0 e^{-\frac{\Delta E_{1\to 2}}{kT}} \text{ and } \tau^{-1}{}_{2\to 1} = f_0 e^{-\frac{\Delta E_{2\to 1}}{kT}} \qquad \text{(Eq. 2.55)}$$

If the field is zero, the energy barrier to jump from 1 to 2 and vice versa will be identical, and so will be the relaxation time. However it is clear that when a field is applied, Néel's exponential law is not valid to explain the experimental data, and a different energy barrier (due to anisotropy and applied field) needs to be used to explain the relaxation process (see Dormann et al. [1997], ✣D.3.3). In general, magnetic relaxation is rarely

exponential, due mainly to the distributed properties in real magnetic systems, as is shown in the next section.

2.7.3. Magnetic viscosity or time dependence in real systems

Magnetic viscosity is the property of the magnetisation to relax as time elapses, due to reversal via thermally activated processes. If any relaxation is observed in the absence of thermal effects (at zero K), the only possible mechanism is quantum tunnelling of the energy barrier (✣2.7.5). Magnetic viscosity, however, is solely related to thermally activated reversal processes.

In real materials there is always a distribution of particle sizes, $f(V)$, and a distribution of anisotropies, $h(K)$ which leads to a distribution of relaxation times, $g(\tau)$. Therefore the exponential law does not seem the best description for the relaxation of the remanent magnetisation of the whole system. In general, a logarithmic dependence has been observed [Street and Woolley (1949), O'Grady et al. (1981)],

$$M_r(t) = M_r(0) - S \cdot \ln\left(\frac{t}{t_0}\right), \qquad \text{(Eq. 2.56)}$$

where t_0 is a constant and S is the coefficient of magnetic viscosity. In general, t_0 is omitted and absorbed into S, (as is the case in this thesis) which, strictly speaking is invalid, because a logarithm is only defined for a dimensionless number. The logarithmic law makes sense as a sum of exponentials is very close to a logarithmic law. The problem with Eq. 2.56 is that it diverges for very short and very long times. However, between very short and very long measurement times lie almost all the experimental data available. This makes the logarithmic law valid for the analysis of the relaxation processes, at least to a first approximation, although it cannot explain the whole of the relaxation process. There are some cases [Chamberlin et al. (1984), Street et al. (1989)] where the relaxation of the magnetisation does not vary linearly with $\ln(t)$. According to Gaunt [1986], $S = 2M'_s kTf(\Delta E)$ where $f(\Delta E)$ is the distribution of energy barriers at the active region of the sample, i.e. the region which is changing its magnetisation in the field and at the time of the measurement, and M'_s is the spontaneous magnetisation. Thus the slope is proportional to the value of $f(\Delta E)$, which represents the energy barrier that is being overcome. The origin of the non-linear behaviour has been attributed [El-Hilo et al. (1992 *a*), Chantrell and O'Grady (1992)] to the distribution of energy barriers,

the form of which was found to be unimportant. In this situation, according to El-Hilo et al. it was found that a linear $\ln(t)$ law is only valid when $f(\Delta E(t))$ is constant over the range of time examined, while the magnetisation with time will be concave downwards when $f(\Delta E(t))$ is increasing with time and concave upwards when $f(\Delta E(t))$ is decreasing with time.

In the limits of very short times both the exponential and the logarithmic laws are not valid. Recent results by Chantrell et al. [1997, 1998] show that the exponential law for magnetisation relaxation in a *monodispersed* system, breaks down for very small measurement times, i.e., very low energy barriers, which is to be expected [Brown (1979)]. The deviation from the exponential behaviour occurs at the shortest time scales ($t < 1 \cdot 10^{-9}$ sec), where the relaxation is initially very flat; over larger time scales ($t > 2.5 \cdot 10^{-9}$ sec), the relaxation is more closely exponential. The deviation from the exponential behaviour at the shortest time scales reflects the breakdown of the high energy barrier approximation (Eq. 2.49). Brown [1979] gave a different form for the relaxation over small energy barriers. Unfortunately, this asymptotic solution for low energy barriers is only valid for small magnetic fields.

Studies by Wernsdorfer et al. [1995 *b*, 1997] on single magnetic nanoparticles by means of a planar microbridge SQUID, show clear exponential behaviour of the probability of not switching ($p(t) = e^{t/\tau}$) in ferromagnetic particles; for antiferro and ferrimagnetic particles [Wernsdorfer et al. (1995 *b*), Lederman et al. (1993)], *p(t)* was found to be flatter than exponential at low temperatures ($T < 1K$) and steeper at higher temperatures ($T > 4K$). The authors attribute this non-exponential behaviour to the fact that the 'magnetisation reversal of these particles is influenced by spin frustration of noncompensated spins at the interface between the ferromagnetic core and the antiferromagnetic surface layers or at the surface of a ferrimagnetic particle'.

Chantrell et al. [1997, 1998] also presented results for a *distributed* system. In this case the relaxation is most strikingly non-exponential; after an initial slow decay, similar to that of the monodispersed system, it comes a faster decay which slows down considerably at longer times ($t > 3 \times 10^{-9}$ sec). The behaviour of the polydispersed system is close to logarithmic over 1 or 2 decades, due to the spread in relaxation times. When the effects of magnetostatic *interactions* are included, they initially provoke a much faster relaxation; however, at longer times ($t \approx 1 \times 10^{-8}$ sec), the relaxation slows down,

tending to the non-interacting case. Therefore for a distributed system, the relaxation of $M(t)$ for both interacting and non-interacting systems is clearly non-exponential for very short times. It is not linear with $\ln t$ for short time, although for the longer time scales ($t \approx 3 \times 10^{-7}$ sec), the behaviour is more closely logarithmic than exponential, as expected from a system with a distribution of energy barriers, arising from a dispersion in particle size and local fields.

2.7.3.1. Replacing M(t) vs ln(t) for a more physical relation

There have been many attempts to replace Eq. 2.56 for a more physical law, in order to investigate the processes that lead to a distribution of relaxation times, τ, arising from a distribution in energy barriers. One of these attempts was made by Pelcovitz et al. [1983] in spin-glass systems, with their 'one dimensional X-Y model', which leads to the so-called stretched exponentials,

$$M_r = M_0 \exp\left[-C(wt)^{1-n}/(1-n)\right] \qquad \text{(Eq. 2.57)}$$

where M_r, M_0 are the thermoremanent and saturation magnetisation, respectively, C is a constant, w is the relaxation frequency (both temperature independent) and n is the time stretched exponent, which together with M_0 are temperature-dependent constants. This model was successfully used [Chamberlin et al. (1984)] to calculate the time dependence of spin glass systems near the spin glass region. In this case the experiments were made after applying a magnetic field of H=15, 30 Oe in the paramagnetic region, cooling the sample through T_g (glass temperature) to a temperature in the spin-glass region, and measuring the relaxation of magnetisation after the removal of the field.

Another expression for the relaxation time of a magnetic system has been given by Aharoni [1985]. According to Aharoni, the fine details of the distribution of relaxation times have only a second-order effect on the relaxation of the magnetisation, 'which better left to be studied only when the first-order effects have been clarified'; in fact, 'any bell-shaped distribution function is as good as any other'. Thus, the relaxation times are distributed so that the probability, $\mathrm{P}(\tau)$, of having a relaxation time, τ, is taken to be a gamma distribution function. The advantage of this distribution function is that it is easy to integrate analytically. Unfortunately, the expression derived by Aharoni [1985] has only been reported to fit the experimental data in one occasion [Chamberlin et al.

(1984)], for a spin glass system. This expression predicts that the variation of magnetisation with ln(t) is concave downwards. However this is not always the case in many experimental data, such as the non-linear behaviour with ln(t) observed by Street et al. [1989] in aligned NdFeB permanent magnets. These workers, measuring the variation of the magnetisation with time in negative fields after previous saturation in a positive field, observed that the variation of the magnetisation with ln(t) was concave downwards for $H < H_c$ and concave upwards for $H > H_c$. El-Hilo et al. [1992 *a*] predicted this behaviour when a narrow distribution of particles sizes was assumed. Systems with a wide distribution of energy barriers exhibit a small degree of non-linearity and in many cases a linear ln(t) dependence is appropriate, as is the case for a constant distribution of particles sizes [O'Grady et al. (1981)]. It has been shown [El-Hilo et al. (1993 *b*)] that the ln(t) represents a first order approximation to a series expansion which accurately describes the variation of magnetisation with time for a system,

$$\Delta M = \sum_{n=0} S_n \left[\Delta \ln(t)\right]^{n+1} \qquad \text{(Eq. 2.58)}$$

Thus a ln(t) is followed if the distribution of energy barriers, $f(\Delta E)$, is constant during the time of measurement, while for narrow $f(\Delta E)$ non-linear terms of Eq. 2.58 contribute to the variation of M with time.

In any case, none of the techniques available include *interaction* effects, that may either slow down or accelerate the relaxation process depending on the kind of interactions, or even on the time these interactions are measured [Chantrell et al. (1997, 1998)]. A fundamental theory explaining the relaxation mechanisms of a distributed system of spins, that accounts for the effect of interactions has not yet been developed.

2.7.4. T.ln(t/τ_0) scaling

A broad variety of physical systems show time dependent behaviour of some of their physical properties because of the existence of energy barriers separating local minima, corresponding to different equilibrium states of the system. This is the case of small magnetic particle systems, with a volume distribution and random orientation of easy axis, that show blocking phenomena, depending on the experimental time window.

It is interesting to observe the relaxation processes in a large time window to test the theoretical descriptions available. However, the experimental measurement time

available is generally not very long in normal experimental set-ups. A solution would be to use a scaling parameter, that allows the relaxation data obtained at different temperatures, to come together in a unique master curve. Labarta et al. [1993] used the so-called $T\ln(t/\tau_0)$ scaling, where the magnetisation data at different temperatures are plotted together in the same curve. This approach had already been used by Prejean and Souletie [1980] in the study of the magnetic relaxation of spin-glasses and earlier to describe the plasticity of glasses, rubbers and polymers [Rammal (1977), Volkenstein and Ptitsyn (1956)] near their glass transition. This scaling seems a good candidate to achieve large time spans in the relaxation data, fundamental to test the expressions given by some authors (✣2.7.3.1). In this thesis, the $T\ln(t/\tau_0)$ scaling has been used (see ✣5.10.3) to study relaxation data at different temperatures in sample F028, although it does not seem to provide a very good fit to the experimental data.

2.7.5. Quantum tunnelling

At absolute zero, when there are no thermal effects at play, the only way for the magnetisation to jump over an energy barrier is through quantum tunnelling. Thus, to be able to observe macroscopic quantum tunnelling (MQT) of magnetisation, low enough temperatures need to be attained.

MQT, the tunnelling of a microscopic variable through the barriers between two minima of the effective potential of a microscopic system, is an interesting phenomena. It is well known that quantum phenomena can take place at the macroscopic scale, in systems with negligible dissipation, i.e., small interaction of the tunnelling variable with the environment, for example, superconductors, one-dimensional metals and so forth. In a more recent time, it has been predicted that MQT can also be observed in magnetic systems [Chudnowsky and Gunther (1988 *a*, *b*)], such as the tunnelling of the magnetisation vector of a single-domain particle through its anisotropy energy barrier and the tunnelling of a domain wall crossing a larger particle through its pinning energy barrier. These phenomena have been studied both theoretically [Chudnowsky and Gunther (1988), Gunther et al. (1990, 1994), Legget (1986), Klik and Gunther (1990), Barbara et al. (1995 *a*, *b*), Tatara and Fukuyama(1994)] and experimentally [Awschalom et al. (1990, 1992), Paulsen et al. (1992) , Arnaudas et al. (1993), Tejada et al. (1993 *a*, *b*), Barbara et al. (1995)].

The possibility of quantum tunnelling in fine particles was first suggested by Bean and Livingston [1959], as an explanation of Weil's [1954] experimental data, which showed that in single-domain Ni particles the transition between different orientations of the magnetic moments did not disappear completely when decreasing the temperature close to absolute zero. Nowadays, many data, for ferro and antiferromagnetic particles, have been reported [Arnaudas et al. (1993), Paulsen et al. (1992), Awschalom et al. (1990, 1992), Barbara et al. (1995)] which seem to support the existence of MQT of the magnetisation. Chudnowsky and Gunther [1988 *a*, *b*] have calculated the probability of tunneling of the magnetisation of a single-domain particle, through an energy barrier between easy directions, for several forms of magnetic anisotropy.

It has been proposed that there is a characteristic crossover temperature, T^*, below which the escape of the magnetisation from the metastable states is dominated by quantum barrier transitions rather by thermal activation. To make easier the experimental observation of MQT (high T^* and high probability of quantum transition) particles with low magnetisation, small size (radius $< 50\text{Å}$) and no interactions are needed. For example, for $CoFe_2O_4$ ferrofluid particles, with $K = 2 \cdot 10^7 \, erg / cc$ and a radius of 50Å, $T^* \approx 3K$ [Tejada et al. (1993 *a*)]. For more information refer to the book by Dormann et al. [1997, ✣G]. Wernsdorfer et al. [1995 *a*, *b*], making use of a micro-bridge dc-SQUID with a resolution of ~104 μ_B, measured single particles of Co ($\sim 200 \times 100 \times 30$ nm), Ni, CoZrMoNi and TbFe and obtained apparent MQT with $T^* \approx 0.5 - 1.3K$. A scaling plot of $H_c(T, v)$ vs $T.\ln(10^5.T/v)$, where v is the sweep-rate, shows deviation at temperatures lower than 1.5 K from a model based on thermal activation. This new regime was interpreted by the authors [Wernsdorfer et al. (1995 *a*, *b*)] in terms of macroscopic quantum tunnelling of magnetisation.

"Allow ourselves to transcend
that which we have been taught"

(Gregg Marsden, in *Awakening to Zero Point*).

3. Instrumentation

3.1. Vibrating Sample Magnetometer (VSM)

The majority of magnetic measurements included in this thesis were obtained using a Princeton Applied Research (PAR) 455 vibrating sample magnetometer (VSM). In the following section a brief revision of its principle of operation, as well as the noise base characterisation, resolution, the apparatus used for low temperature measurements and screening effects is presented.

3.1.1. Principle of operation

In the VSM, the magnetic sample is centred in a region of uniform magnetic field, supplied by an electromagnet. The maximum field attainable with this electromagnet, in the VSM at Bangor, is 12 kOe. This uniform magnetic field induces a magnetic moment in the sample along the field direction. The sample is mounted at the end of a rod whose other end is connected to a transducer assembly (vibrating head), located above the magnet. The principle of operation is simple: the vibrating head generates a sinusoidal wave which makes the rod vibrate in the vertical direction. This means that the sample will vibrate in a direction perpendicular to that of the field (H_{app}); then, according to Faraday's law, an ac signal (e.m.f.), proportional to the magnitude of the magnetic moment in the

material, will be produced in the detection coils due to the variation of magnetic flux. The pick-up coils are mounted on the inner faces of the electromagnet pole pieces. The induced e.m.f. produced by the rate of change of magnetic flux, is given by,

$$V \propto -\frac{d\Phi}{dt} \propto \frac{dM}{dt} \qquad \text{(Eq. 3.1)}$$

where Φ is the magnetic flux and M is the magnetisation of the sample. The sample has a typical amplitude of vibration of 1mm and is moved at frequency of 82 Hz, so that,

$$V = C(MV) f \sin(2\pi ft) \qquad \text{(Eq. 3.2)}$$

where C is a calibration constant and f is the frequency of the oscillator. The system thus lends itself to phase-sensitive detection (PSD) to improve signal to noise ratio.

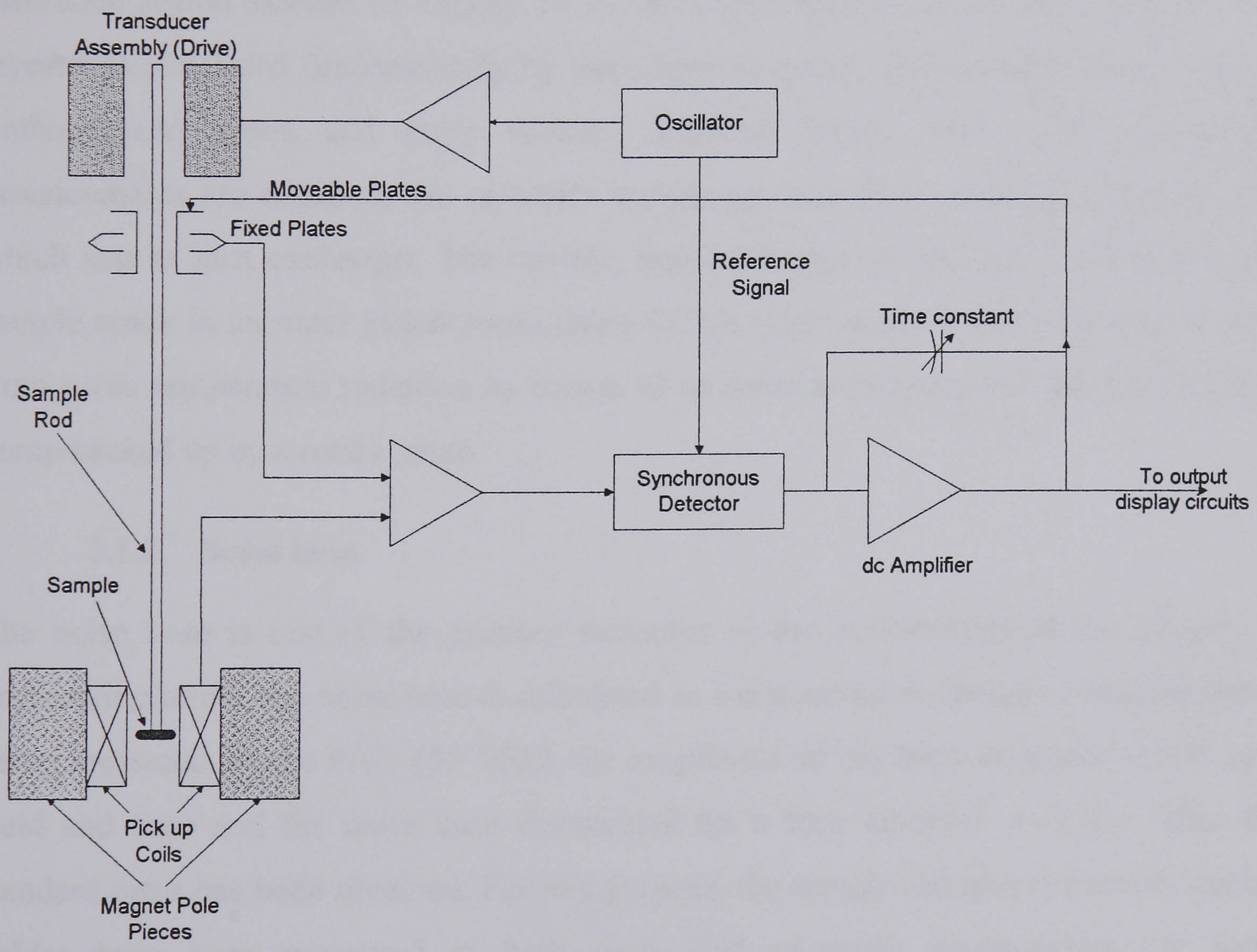

Figure 3-1

Simplified block diagram of the PAR 455 VSM.

Finally, as already outlined in Eq. 3.2, the induced e.m.f. is compared to that of a reference sample (calibration), with a similar shape and size to the one that is being measured, and the magnetic moment of the sample obtained.

3.1.2. Low temperature measurements

For the variation of the sample temperature, the PAR 455 VSM was fitted with an Oxford Instruments CF1200 continuous flow gas cryostat with a transfer gas in the sample space. The coolant is introduced into the cryostat by a vacuum-insulated transfer tube, using a gas flow pump.

An Oxford Instruments 3120 digital controller was used to both measure and control the temperature. The controller uses an AuFe-chromel thermocouple sensor. The base temperature is about $1.8\,K$ and is continuously variable up to $300\,K$ with a temperature stability better than $\pm 0.1\,K$.

The cryostat has a cylindrical sample space which is 7mm in diameter, and the temperature controlled region extends to roughly 10 cm above the bottom of the vacuum space. The cryostat is integrated fundamentally by three layered spaces: inner sample space, coolant (intermediate) space and outer vacuum insulated jacket. When low temperature measurements are required, the cryostat's sample space is filled with gas, normally He, which acts as heat exchanger. The coolant, liquid Nitrogen or Helium, flows around the sample space in an outer jacket surrounding it; this outer jacket is itself vacuum isolated from room temperature radiation by means of an outer case evacuated using a diffusion pump backed up by a rotary pump.

3.1.3. Noise base

The noise base is one of the primary measures of the performance of the system. In engineering terms, the noise base is calculated as the standard deviation of the magnitude being measured. In the PAR 455 VSM, the magnetisation has been measured versus both field and time and the noise base determined for a time constant $\tau = 1\text{sec}$. Also, the standard error has been obtained. For this purpose, the sample rod plus the empty sample holder have been measured at both room and cryogenic temperatures. At room temperatures, in the absence of the cryostat, the noise base is $< 2.5 \cdot 10^{-5}\text{emu}$, while the standard error is $\leq 4.5 \cdot 10^{-6}\text{emu}$. With the cryostat on, at room and at low temperatures (e.g. T=32 K), the noise base is $\leq 6 \cdot 10^{-5}\text{emu}$, while the standard error is $\leq 8 \cdot 10^{-6}\text{emu}$. As it is clearly observed in the previous quantities, the noise base increases with the fitting of the cryostat.

The PAR 455 VSM has an offset in the magnetisation axis, which varies slightly with temperature and the sensitivity the VSM is set at. The magnetic field is stable to $\pm 0.1\ Oe$.

3.1.4. Screening effect in the 1200 CF static cryostat

As observed in Fig. 3-2, the magnetisation signal falls off at low temperatures. The signal screening occurs between the vibrating sample inside the cryostat and the pick up coils. This effect has its origin in the variation of the electrical conductivity with temperature presumably (see ✣3.2.3) of the copper [Blakemore (1985) p. 152] that acts as heat exchanger in the cryostat, around the sample. In this situation the alternating field induced in the vibrating sample generates eddy currents in the Cu plate, which will reduce or screen the signal (voltage) generated by the sample. This effect could be reduced using a slotted radiation shield outside the exchanger. Even though the CF 1200 has this kind of shield, signal screening still takes place.

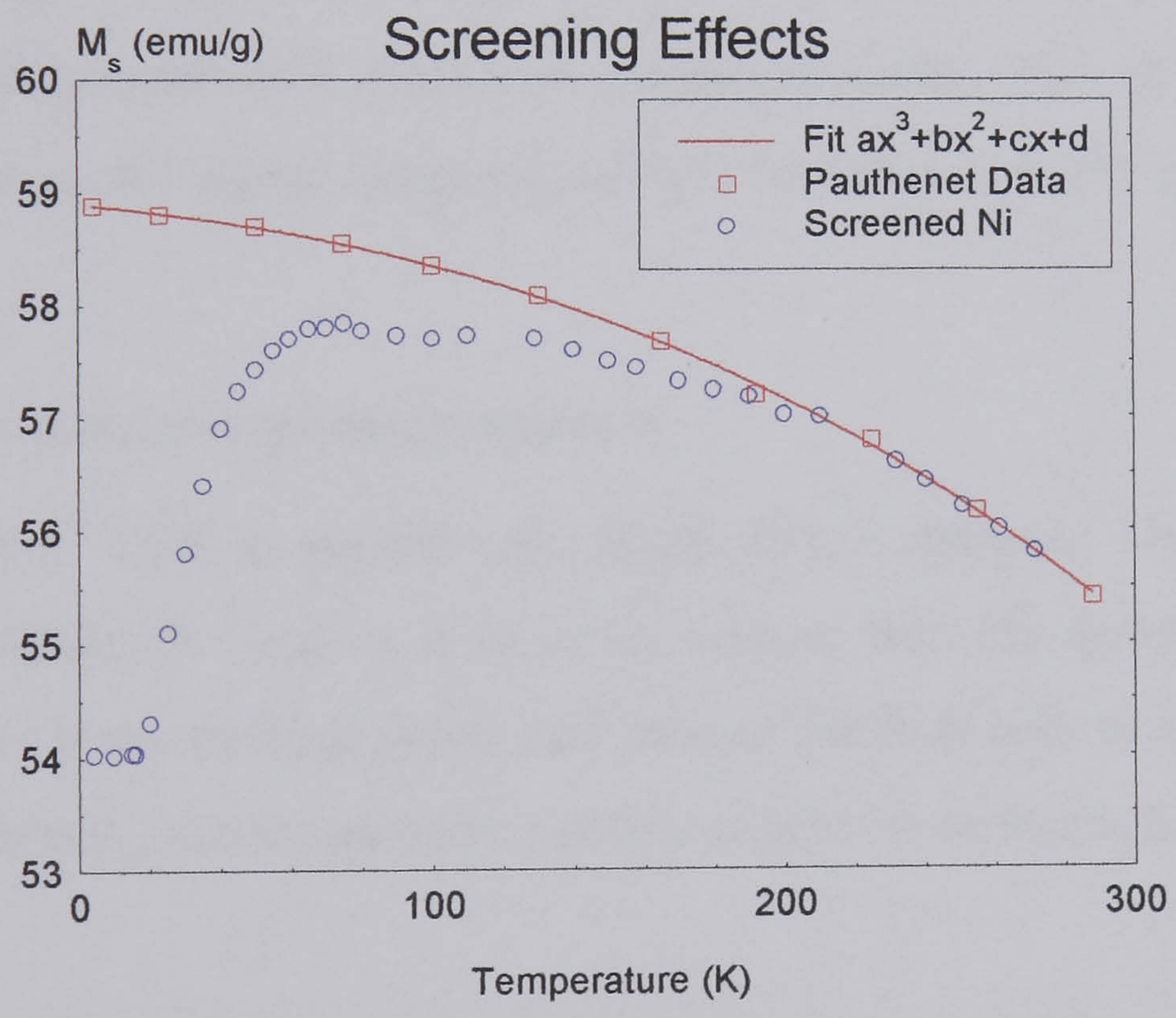

Figure 3-2

Screening effects with temperature observed on the Ni calibration sample when the PAR 455 VSM is fitted with the 1200 static cryostat.

To correct the effect of screening a computer program originally written by El-Hilo [Ph.D. thesis (1990)] and modified for the different measurements performed in this thesis, has been used. The main code of this program is shown in Appendix V.

3.2. Superconducting magnet VSM

The high field magnetic measurements (see ✣5.7.1.2) have been performed in the VSM at Liverpool University, formerly at Bangor University. This VSM, originally developed by Ferguson [1990] at U.C.N.W., is based in the same principle of operation than the PAR 455, with the only difference being that it incorporates an 8 Tesla superconducting magnet. The superconducting magnet generates a magnetic field along the axis of vibration of the sample; hence, in practice, the sample size does not have to be reduced for its insertion in the cryostat as is the case in the PAR 455 VSM. Thus, a larger quantity of sample can be introduced with the consequent improvement of the signal to noise ratio.

3.2.1. Noise base

The noise base measurements were performed measuring the empty holder, with a 15 sec time constant during 10 times this time constant, i.e. 150 sec. The noise base obtained is $\leq 2.1 \cdot 10^{-5}$ emu . Measurements on a thin film sample [Ferguson, Ph.D. thesis, p. 92 (1990)] show that the noise in the signal (magnetisation) is less than $\leq 3 \cdot 10^{-5}$ emu over the full field range.

3.2.2. Low temperature measurements

The superconducting VSM is permanently fitted with a dynamic Oxford Instruments CF1200 cryostat, where the coolant is in direct contact with the sample. This dynamic model provides maximum cooling power and reduces the heat leak to the sample via the sample holder. However, the temperature stability is inferior to that achieved in the static version.

The temperature control unit is an Oxford Instruments ITC4 temperature controller. It is interesting to notice [Ferguson, Ph.D. thesis, p. 80 (1990)] that the error in the temperature is not negligible for high applied fields ($H > 6$ Tesla). For example at 4.2 K and 12 T, the temperature reading was 3.6 K, which yields an absolute error of $\Delta T = \pm 0.6$K, the relative error being $\Delta T/T \sim 14\%$. At 77 K, $\Delta T = \pm 0.9$K and $\Delta T/T \sim 11\%$; and for room temperature measurements, $\Delta T = \pm$ 1.7K and $\Delta T/T \sim 0.06\%$.

3.2.3. Screening effects

Although not as pronounced as in the static model, this cryostat also presents some screening effects that need to be corrected for (see Fig. 3-3). This screening effect seems to

have the same origin as the one observed in the static cryostat, namely the eddy currents induced by the vibrating sample, presumably on the copper radiation shield inside the cryostat, which experiences an increase in conductivity as the temperature is lowered. To minimise this screening effect slots were machined in the Cu radiation shield to break the path of the eddy currents [Ferguson, Ph.D. thesis, p. 83 (1990)]. The effects of screening in this high field VSM are shown in Fig. 3-3, where the 'screened' magnetisation of a Ni calibration sample is compared to the expected values as obtained by Pauthenet [1982]. The correction factors are given in Appendix V.

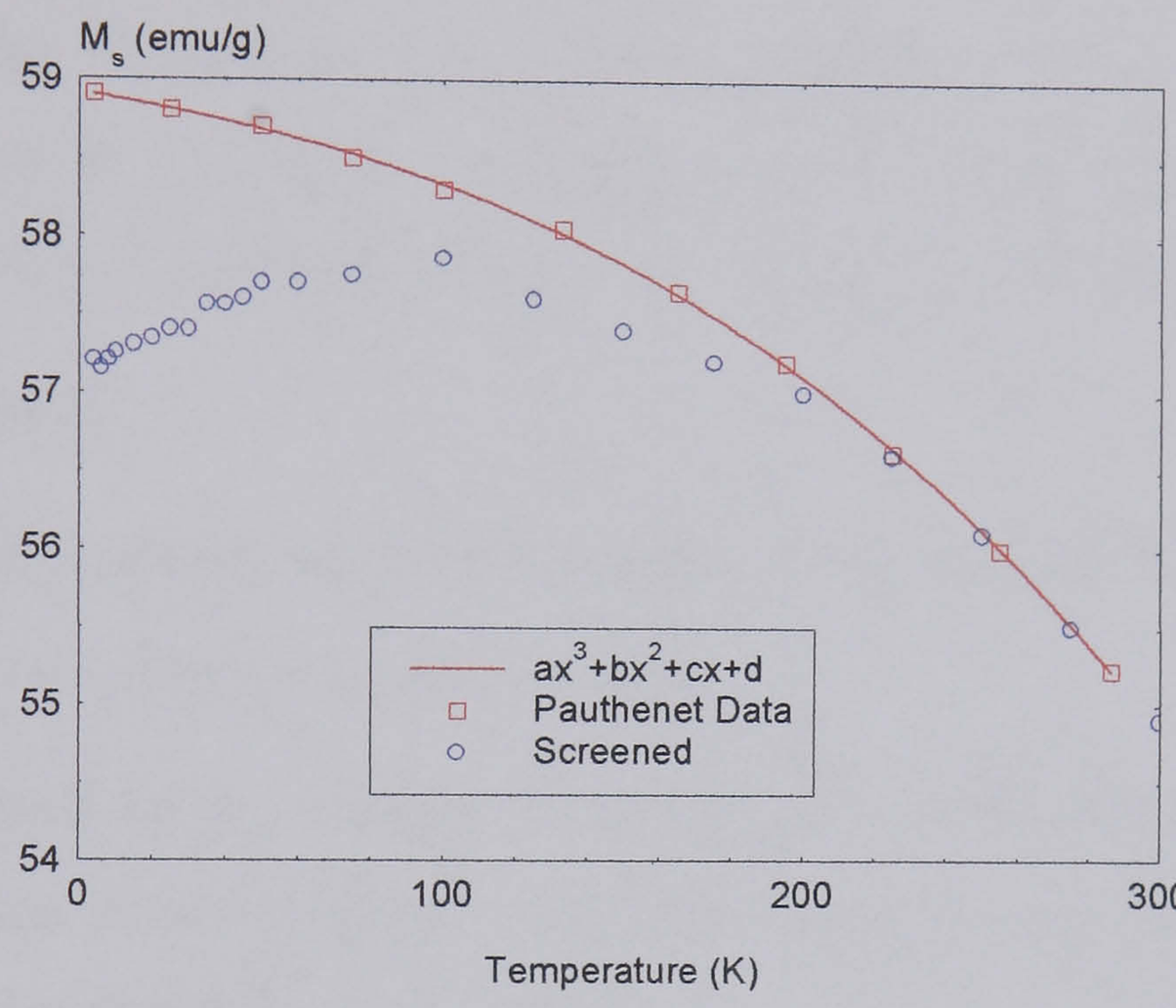

Figure 3-3

Screening effects with temperature observed on the Ni calibration sample in the high field VSM.

In order to pinpoint the exact source of the screening, tests were conducted on a dynamic system modified to operate without the radiation shield and with a fibre-glass OVC (Outer Vacuum Can). Again screening was observed suggesting that the source of the eddy currents must be in the remaining Cu components or perhaps in the stainless-steel sample tube of the cryostat. In fact, there are many metals (not only Cu) such as Zn, Al, Fe, Pb that could be components of the cryostat and which may also experience a considerable increase in the conductivity for T<100K [Blakemore (1985) p. 152].

3.3. Transmission Electron Microscopy (TEM)

Electron micrographs were taken in a HITACHI S-520 Transmission Electron Microscope (TEM), with a 100 keV electron beam. In TEM, the specimen is illuminated by a broad beam of electrons, in this case, of 100 keV, and the image is formed directly by focusing those electrons which pass more or less unscattered through the specimen, i.e., the

transmitted e^-, on a fluorescence screen for direct viewing or on a photographic film for recording. With this technique the morphology and physical size of the particles in ferrofluids can be studied (see ✣5.3). A TEM photograph of sample F024 is shown in Fig. 5-6. To measure the physical size from the micrographs, a Zeiss Analyser, described in ✣3.5, was used.

3.4. X-Ray diffraction

Crystals contain planes separated by a distance *d* (lattice spacing), each plane defined by its Miller indices (hkl). When there is constructive interference from the X-rays scattered by the atomic planes in a crystal, a diffraction peak is observed. The condition of constructive interference from planes with spacing d_{hkl} is given by Bragg's law,

$$n\lambda = n2d_{hkl}\sin\theta_{hkl} \qquad \text{(Eq. 3.3)}$$

where θ_{hkl} is the angle between the atomic planes and the incident X-ray beam, λ is the wavelength of the X-rays, and *n* is a natural number.

The diffractometer used for the analysis of the samples in this thesis is a Philips 1710 model with a graphite monochromator. The diffractograms were taken by Dr. Puerto Morales at the Materials Institute, CSIC, Madrid.

For the analysis of the mean crystallite size of the particles in the samples, $\theta/2\theta$ (or Bragg-Brentano configuration) scans have been performed. In the $\theta/2\theta$ configuration the detector is positioned so that the diffraction angle is $2\theta_{hkl}$, and the crystal is oriented so that the normal to the diffraction plane is coplanar with the incident and the diffracted X-rays. All the measurements were taken with an angular precision of 0.05^0. The radiation employed in this work is the CuKα ($E = 8.04keV$, $\lambda = 1.5418$Å). Once the peak (311) has been fitted to a Lorentzian function, the full width at half maximum (FWHM) is directly related to the structural coherence length, i.e., the size of the crystalline part of the particles (assuming they are spherical, this length would be the sphere's diameter), using the Scherrer's formula (Eq. 5.6, in ✣5.3.2).

3.5. Zeiss particle size analyser

This analyser was constructed in Germany by F. Endter and H. Gebauer, and was marketed in the United States by Carl Zeiss Inc., as the "ZEISS Particle Size Analyser TGZ 3". This

is an extremely valuable piece of equipment capable of generating accurate particle size distributions quickly and at low cost. It was initially design to get information about particle size and particle size distributions in rubber or resin latex. For these materials, as well as for the ones used in this thesis, and many other systems in nature, an accurate description of particle sizes and distributions is of fundamental importance.

For the particle size, analysis a photomicrograph from TEM was used. The image of the particle is compared directly with a circular spot of light, the area of which can be varied by an iris diaphragm, as shown in Fig. 3-4. In this way, the diameter of the particle can be measured and recorded.

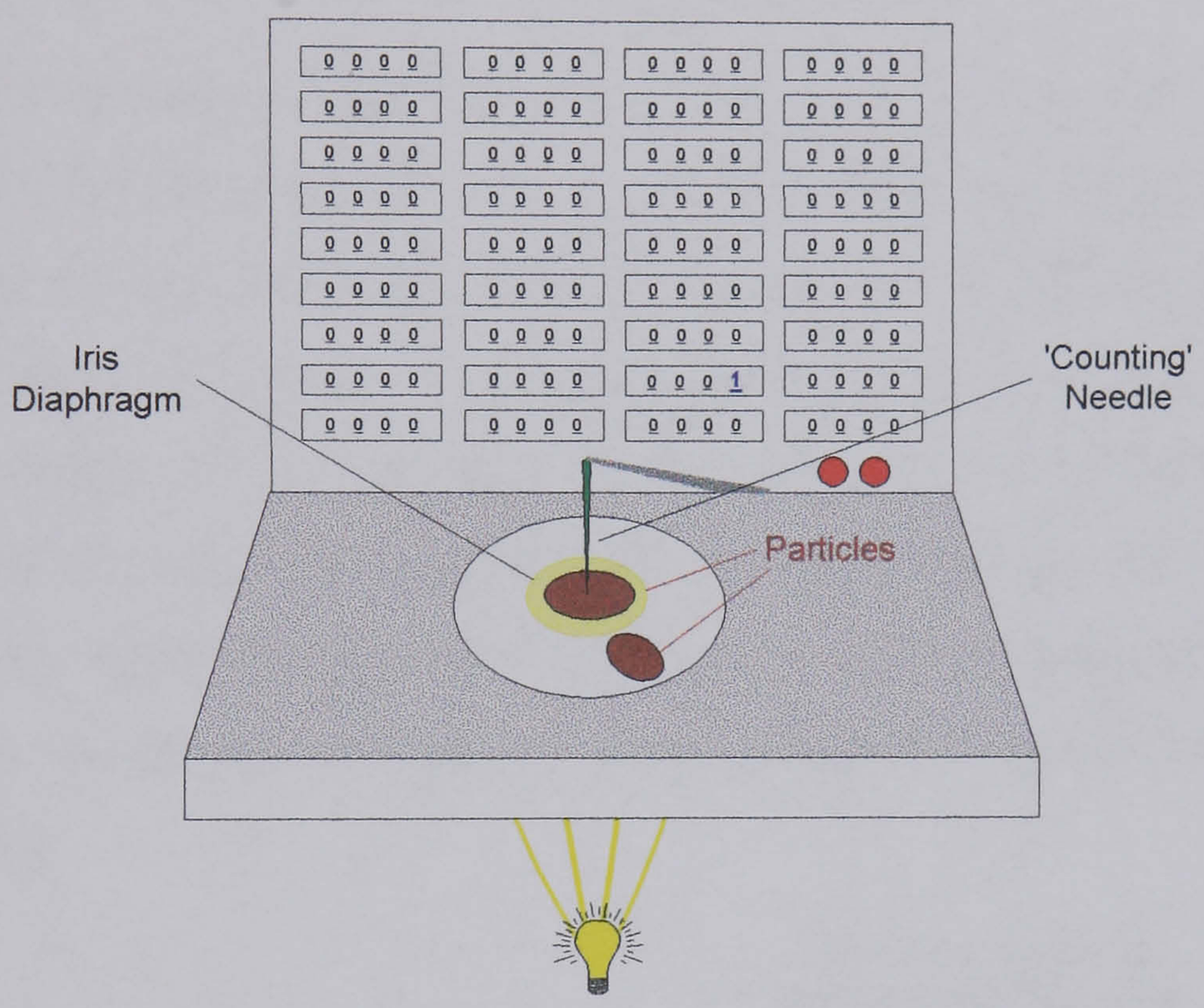

Figure 3-4

Schematic of the Zeiss particle size analyser.

Although the use of the Zeiss Analyser implies a sacrifice in speed due to the rather laborious counting and measuring with respect to the automated techniques, the outcome from this semi-automatic apparatus is highly reliable, since it is the human operator who judges which are individual particles, which are agglomerates (if any) and where the edges of different particles lie. To obtain a realistic distribution with a minimum error, a large number of particles need to be counted. In the case of the ferrofluids in this thesis, 800, 1200 and 1700 particles have been counted for samples F024, F026 and F028, respectively.

To conclude, the Zeiss Particle Size Analyser gives a highly reliable particle size distribution due mainly to the following facts:

1. The analyser marks each particle image as it is measured, so improving the reproducibility of the particle size distribution data.
2. The relatively large number of particle size diameter classes improves the accuracy of the data by giving more detailed histograms.
3. The circular image of the iris diaphragm permits the estimation of the diameter of particles partially obscured by overlapping or agglomeration by the simply matching the curvature of the diaphragm image edge to that of the particle image edge.

3.6. High Gradient Magnetic Separation (HGMS)

The high gradient separation apparatus has been used to filter large particles and aggregates from the ferrofluid samples. For the ferrofluids used in this thesis, the HGMS was performed by the manufacturers, after the production of the samples, at Liquids Research Ltd., Bangor. The process essentially involves generating large magnetic field gradients on the surface of ferromagnetic fibres, which are immersed in a sample of ferrofluid subjected to a large background field. This high magnetic field will produce a high gradient near the fibre's surface, which will result in a strong magnetic attractive force that would attract the largest particles or agglomerates within the ferrofluid system [Oberteuffer (1973)].

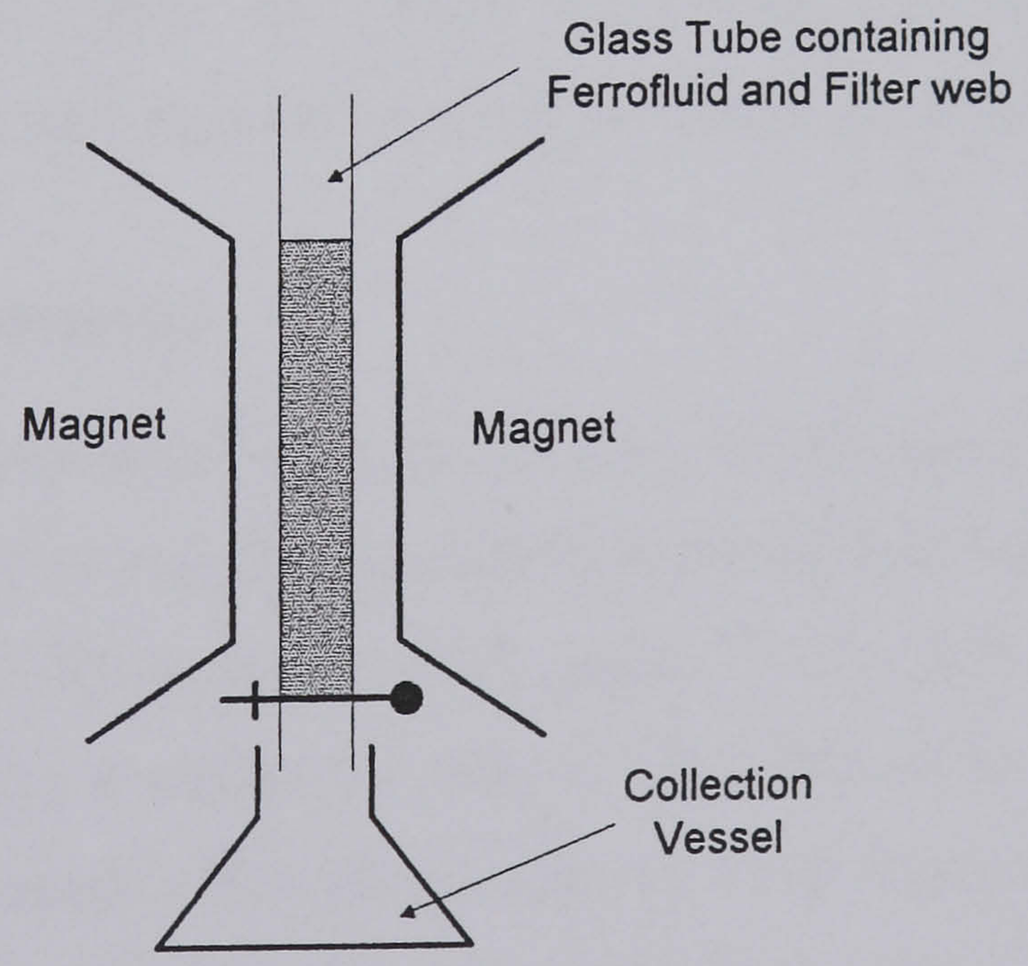

Figure 3-5

Diagram showing the High Gradient Magnetic Separation (HGMS) apparatus.

The design of the HGMS apparatus is relatively simple (see Fig. 3-5); approximately 3cc of the ferrofluid sample are placed in a cylindrical glass column with diameter 0.8 cm. Later, 8μm Nickel fibres are immersed and distributed as uniformly as possible throughout

the liquid. The apparatus is then placed between the pole pieces of an electromagnet, which applies a 2 kOe magnetic field to the system.

The field gradient, ∇H , at the surface of the Ni fibres is approximately equal to,

$$\nabla H = M_f / r_f \approx 10^7 Oe / cm \qquad \text{(Eq. 3.4)}$$

where M_f and r_f are the saturation magnetisation and the radius of the fibre, respectively. Thus the efficiency of the filter is improved as the field gradient is increased. This can be achieved by reducing the radius of the fibres, as shown by Williams [Ph.D. thesis, ✣5.5.4 (1993 *a*].

When the filtering process is complete (around 10 minutes), the tap at the bottom of the column is opened and the 'refined' ferrofluid is recovered by blowing gas under a slight pressure through the open end of the container. In general, the magnetic field is not reduced until the tap has been closed. The effect of reducing the field to increase the ferrofluid yield was revised by Williams [Ph.D. thesis, ✣5.5 (1993 *a*)]. Although the yield of the fluid increases as the applied field is reduced, care must be taken because if the field gradient is reduced too much, the agglomerates and single particles initially captured in the filter will return to the 'filtered' fluid. In his thesis, Williams also studied the influence of the carrier viscosity in the efficiency of the filtering process. As it would be expected, the filtration takes longer the more viscous the carrier liquid. More information about the effect of HGMS on the magnetic and physical properties of ferrofluids is given in ✣4.1.2.

3.7. Mössbauer spectroscopy

The Mössbauer spectroscopy measurements (see ✣5.10.1) where carried out by Gaby Milford and Dominic Dickson at Liverpool University, in a conventional constant velocity spectrometer and a 100 mCi ^{57}CoRh source. The radioactive ^{57}Co undergoes spontaneous electron capture transition to give a metastable state of ^{57}Fe. This in turn decays to the ground state via a gamma ray cascade which includes the 14.4 keV Mössbauer gamma ray (see diagram in Fig. 3-6 (a)). This gives rise to resonant absorption of the ^{57}Fe atoms in the sample to be measured, as shown in Fig. 3-7(b). The effect just described is the so-called *Mössbauer effect* [Mössbauer (1958)]. This effect can only be used for the study of specific materials containing a Mössbauer isotope, in this case Fe, which is very useful for the study of the magnetite particles in the ferrofluid samples of this thesis.

The source of gamma radiation is vibrated to produce a moderate spread in the frequency of the emitted radiation, controlled by the Doppler effect. Mössbauer spectroscopy uses the Doppler-effect-shifted-energy gamma-rays to probe the nuclear energy levels that arise from the interactions between the nucleus and its electronic environment (hyperfine interactions), so as to gain information about the solid state of the sample. In this way, it is possible to probe all the nuclear energy levels of the stationary absorber or sample under inspection. In the case of a Co source, the probe to be studied has to be Fe so as to be able to provide this absorber with a range of frequencies (energies) adequate to excite its different energy levels in order to study its absorption spectra, which would provide information about its magnetic state. The radioactive source is embedded in a solid matrix (Rhodium -Rh-) which provides a recoil-free environment [Mössbauer (1958)] as well as unsplit ground and excited energy levels to simplify the spectrum. Recoilless emission/absorption occurs when the excitation/relaxation between energy levels occurs without the creation of a crystal lattice phonon.

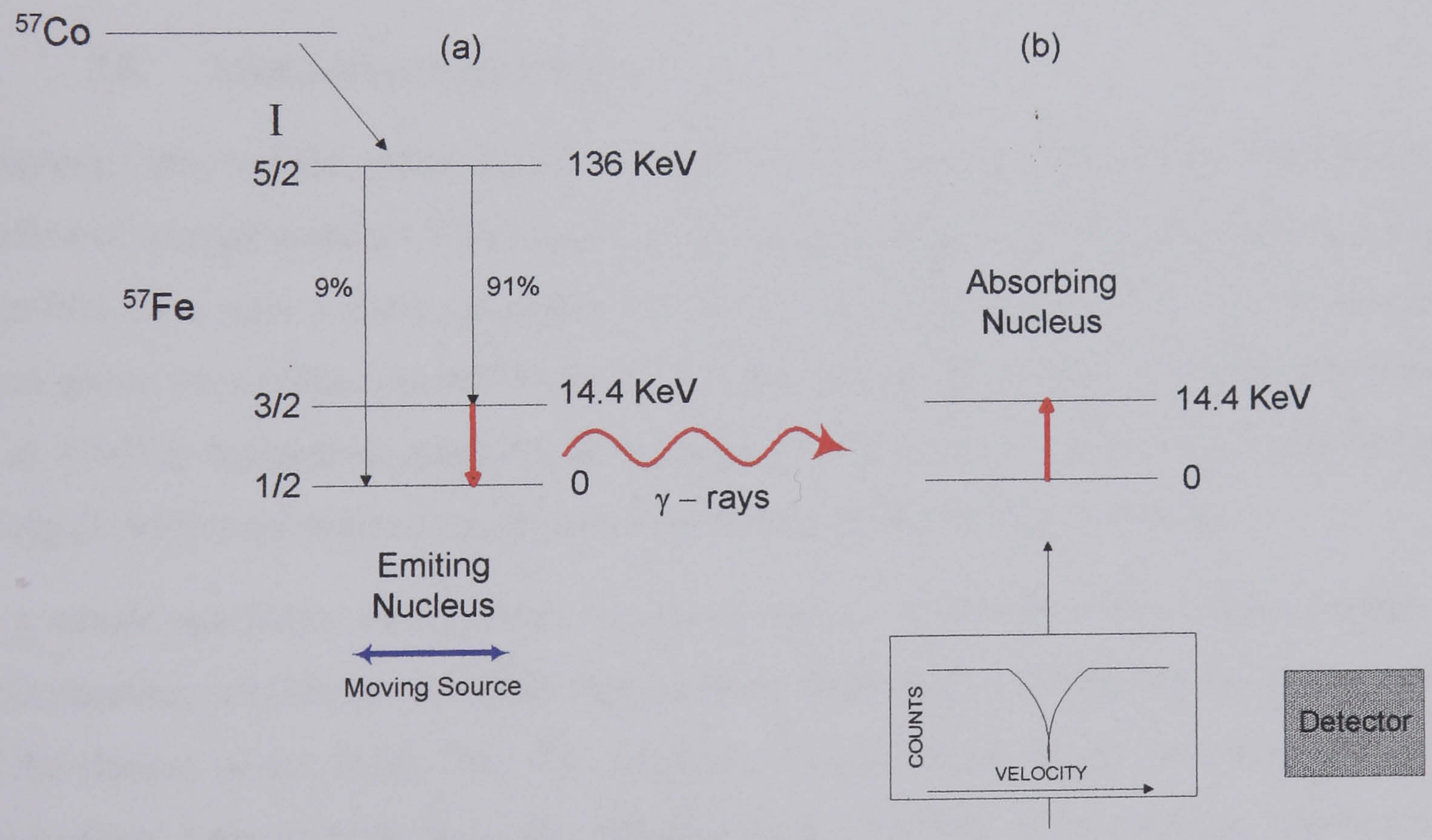

Figure 3-6

Schematic diagram showing a typical Mössbauer set up

The linewidth of the absorption line, Lorentzian in shape, is due to the uncertainty in the energy of the excited state, ΔE, and it is very narrow (~10^{-8}eV for ^{57}Fe) compared with a γ-ray (~10^{4}eV). The velocity (in mm/s) axis, x, is the energy scale (see Fig. 3-6 (b)), and is the change in energy due to the Doppler motion of the source ($1\ mm/s = 4.8 \cdot 10^{-8}\ eV$ for ^{57}Fe). In the y axis, the absorption is expressed in counts. The variable temperatures in the

Mössbauer experiments were obtained with an Oxford Instruments CF500 continuous flow cryostat, with a carbon-glass resistance thermometer for the measurement of the temperature of the sample.

In this thesis Mössbauer spectroscopy has been used to extract very precise information. The spectra is studied to obtain the transition from the (super)paramagnetic to the blocked state. From this transition, it is possible to extract the median blocking temperature of the samples, which is the temperature for which, in the measuring time for the observation of magnetic splitting in the Mössbauer spectra (typically, $t = 5 \times 10^{-9}\, s$), half of the magnetic moments of the sample have relaxed.. From the blocking temperatures via both Mössbauer spectroscopy and TDR (see ✣5.4.1) the attempt frequency of the system, f_0, can be obtained [Dickson et al. (1993 *a*)] (see ✣5.10.1).

An extensive review of the principles of Mössbauer spectroscopy and its applications to the study of magnetic materials was given by Dickson and Berry [1986].

3.8. Magnetron cluster source

Sputtering involves the collisions of ions (usually of an inert gas such as Ar or He) with the surface of a target material, which leads to the ejection of target atoms that are collected in thin-film form onto a stationary substrate. The Co/Cu clusters studied in chapter 6 have been grown on a polyamide substrate, by the technique of magnetron sputtering [Eastham et al. (1997)]. Magnetron sputtering or magnetically assisted sputtering [Wagendisrtel and Wang (1994)] is an enhanced technique with respect to the normal sputtering.

In a simple sputtering arrangement, two electrodes are separated in a vacuum chamber. This chamber is subsequently filled with an inert gas known as the sputter gas (in the case of the clusters of this thesis, He). The substrate is placed at the anode, and the target, i.e. the material being used to form the sputtered layer, is placed at the cathode. Applying a potential difference between the electrodes leads to the ionisation of the inert sputter gas atoms. The resulting ionised gas is known as *plasma*. In this situation, the positively charged sputter gas atoms are accelerated by the electric field into the target at the cathode, where they liberate (or sputter) the target atoms. A proportion of the liberated atoms subsequently condense on the substrate.

Magnetron sputtering (see Fig. 3-7) increases the efficiency of a conventional sputtering system by confining the plasma at the target by means of a magnetic field, normally from

permanent magnets, located near the electrodes. Having the plasma in close proximity to the target causes preferential sputtering of the target which results in an increase in the sputtering rate. Magnetron sputtering has important advantages over conventional sputtering,

a) As the plasma is confined over the target, the ion current density increases, which means that the sputtering can take place at a lower sputtering gas pressure, resulting in a lower contamination of the growing film.

b) The electrons produced in the ionisation of the sputter gas (He) are also confined by the magnetic fields at the target. Hence, substrate heating due to bombardment by electrons is also reduced. This fact together with the fact that the Co and the Cu clusters land at very low speeds in the substrate ensures low coalescence and particle growth due to heating of the substrate.

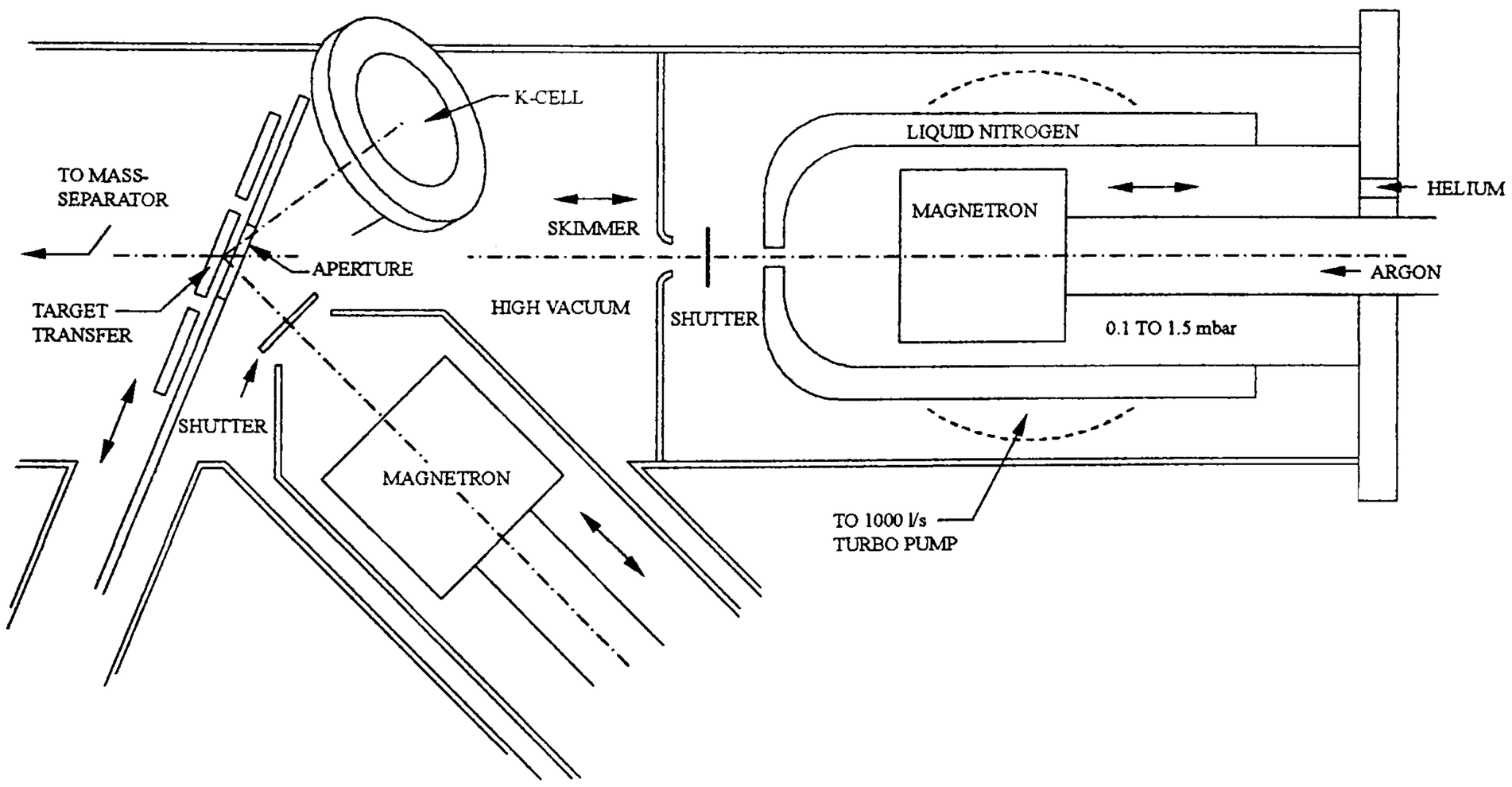

Figure 3-7

Magnetron cluster source and incorporated sputtering device.

The system used for the Co/Cu nanoclusters studied in Chapter 6 uses $SmCo_5$ rare earth permanent magnets and 2 magnetron sputtering heads to produce multilayer films. The base pressure of the system is 1.10-7 mbar and sputtering takes place under a pressure of 3mbar of He. After the Co and Cu clusters had been produced, they were deposited at the same time at very low speeds, to avoid diffusion of atoms or formation of agglomerates.

" Sed espectadores atentos allí donde no podáis ser actores "

(Be eager spectators, there where you cannot be actors)

J.E. Rodó

4. Sample Description

4.1. Ferrofluids

The production of the ferrofluids is a multi-stage process; once the particles have been synthesised, they are coated with a surfactant. Then, the particles are dispersed in a compatible carrier liquid. Ferrofluids are suitable systems for the study of interactions because the particle size distribution in the samples remains constant upon dilution, being interparticle separation the only variable that may account for the different observations. Also, the control of particle size and stabilisation of small magnetic particles in a ferrofluid are well known processes that facilitates the manufacture and understanding of the samples.

4.1.1. Manufacture of the ferrofluid

The colloidal particles studied in this thesis were prepared by Liquid Research Ltd. via co-precipitation of two metallic salts from aqueous solution. For the manufacture of magnetite ($Fe_3 0_4$) two aqueous solutions of ferrous (Fe II) and ferric (Fe III) salts are added to an excess of alkali. The reaction is described by,

$$8\,[M]OH + Fe^{3+} + Fe^{2+} \rightarrow Fe_3O_4 + 8\,[M]^{+} + 4H_2O \qquad \text{(Eq. 4.1)}$$

where $[M]^+$ is the metallic ion, which can be K^+, Na^+ or $(NH_4)^+$ -non metallic-, depending on the desired size of the particles. The reaction described by Eq. 4.1 has been extensively investigated by several workers e.g. Khallafalla and Reimers [1980], Gribanov et al. [1990] and Williams [1990]. The production of ultrafine particles in this way depends not only upon the chemical composition of the salts but also on the conditions that exist at the time of the formation of the precipitate; for example, the particle size is influenced by different experimental variables such as the solubility of the precipitate in the medium in which is being formed, the nature of the alkali, the precipitating temperature, the concentration of the reactants and the rate at which they are mixed.

Experimental variables that minimise the particle size include low temperature, which decreases the solubility of the precipitate in the solution. Also, the size of the particle varies depending on the alkali used for the reaction; in this way, increasing particle sizes are obtained following the series KOH, $NaOH$ and $(NH_4)OH$. This was the method used to obtain the three different particle sizes of the ferrofluids in this thesis. For more details see Gribanov et al. [1980]. Williams [1993 *a*] studied the effect of adding different concentrations of the Fe (II and III) salts, at different rates and precipitation temperatures, and the effect of stirring them vigorously or stirring slowly or not at all. Although a systematic study into the experimental control of particle size was not undertaken, it was observed that the higher the precipitating temperature, the larger the particles; equally, a slow addition of the salts leads to larger particles when compared to those obtained by a fast addition of these salts.

Once the magnetic particles are synthesised, the surfactant is added. After the addition of the surfactant, which ultimately stabilises the particles in the carrier liquid by an entropic mechanism (see ✣4.1.4.3), the particles are separated from solution, filtered and washed in water to remove all salts. Then they are washed in acetone to remove any unbound or physisorbed surfactant. A hydrocarbon carrier liquid (isopar-M) is then added, in which the particles are dispersed. The solution is gently heated to evaporate residual acetone. Finally, the sample is centrifuged to remove any large aggregates ($> 1\mu m$) [Kaiser and Miskolczy (1970)]. Any aggregates that may have remained are removed by the more fine filtering technique called HGMS (further details about this technique are given in the next section, ✣4.1.2).

There are many other methods to obtain fine magnetic particles. For example, Bandow et al. [1987] reported the preparation of ultrafine colloidal magnetite particles in water pools in water/oil microemulsions. In this case the size of the particles is controlled by the size of the pools. Other techniques are grinding [Papell (1965), Kaiser and Milkolczy (1970), Khalafalla and Reimers (1973)], evaporation [Granqvist and Buhrman (1976), Nakatani et al. (1987)], electrodeposition [Luborsky and Paine (1960), Hoon (1980)] and precipitation from non-aqueous solution [Smith (1981), O'Grady (1982), Nakatani et al. (1993), Lambrick et al. (1987)]. Fine particles can also be prepared by the sol-gel technique, sputtering, thermal evaporation, laser ablation, etc. A very comprehensive revision of the different techniques available for obtaining nanoparticles is found in Hadjipanayis and Siegel [1993] and Edelstein and Cammarata [1996].

4.1.2. Ferrofluid refinement by High Gradient Magnetic Separation (HGMS)

As prepared, ferrofluids invariably contain a degree of aggregation: the particles in these 'primary' aggregates are irreversibly bonded together, either before the surfactant coating is applied or when the surfactant coating is complete. Thus these aggregates behave as single particles with relatively high magnetic moments in the presence of an applied field. In order to increase the long-term stability of ferrofluids and minimise the interactions within the system, as well as obtaining narrow distribution of particles sizes, these aggregates need to be removed.

One of the methods employed to eliminate large aggregates from the ferrofluids is the so-called High Gradient Magnetic Separation (HGMS) (see ✣3.6). This technique was initially developed in mineral processing, making it possible to efficiently separate weakly (para)magnetic particles for which conventional magnetic devices, such as belt and drum separators, were ineffective [Gerber (1982)]. HGMS has been used in other industrial applications such as desulphurisation of coal, the removal of corrosion products from water in thermal power plants and kaolin purification for paper manufacture. Effluent water may be treated by 'seeded' HGMS, whereby non-magnetic pollutants are bonded to magnetic particles and removed by magnetic filtration. HGMS has also been applied in the isolation of red blood cells (containing paramagnetic haemoglobin) from whole blood [Roath et al. (1990)] and in the purification of high-Tc superconducting materials [Labroo et al. (1992)]. An extensive revision of the early theory and applications of HGMS is given

by Gerber and Birss [1983]. O'Grady et al. [1986] adapted the technique for ferrofluid refinement.

The principle of the HGMS was explained in ✣3.6. It is interesting to show the studies of Parker et al. [1982] who considered the contribution of particle interactions to the force acting on a particle when it is subjected to HGMS. The authors concluded that for very small values of the particle radii ($r < 10\text{Å}$), the build-up of particles on the magnetised fibre (stainless steel fillings) is negligible due to thermal diffusion. Thus particles smaller than this size cannot be filtered. The repulsive interactions (see ✣4.1.4) between particles dominate for $10\text{Å} < r < 50\text{Å}$, tending to reduce the amount of build-up that is predicted in the absence of particle interactions. For large particles, $r > 50\text{Å}$, the interparticle dipolar attraction forces tend to increase the build-up.

Williams [Ph.D. thesis, ✣5.5 (1993)] arrived at very interesting results with respect to magnetic filtering of ferrofluids. The variation of the field gradient has a strong bearing on the final particle size distribution. According to Williams, large aggregates are removed in relatively small applied fields ($H \approx 200Oe$) which is reflected in the initial reduction of the mean particle size of the system. However, as the field gradient is increased, due to a higher applied field ($H < 1800Oe$) it seems as though even single particles are removed, with the corresponding fall in the width of the particle size distribution, while the mean particle size remains constant. The removal of single particles seems to be also more efficient the larger the particles in the system, as observed by Williams when comparing TEM images of three ferrofluids with different particle sizes ($D_{vm} = 51$, 78 and 101 Å), before and after HGMS.

According to O'Grady et al. [1986], although the magnetic and physical sizes do not seem notably altered after HGMS, the stability of the ferrofluid to field gradients is greatly enhanced due to the reduction of agglomerates in the fluid. Similar results have been obtained by Buzmakov [1995], who studied the microstructure and sedimentation stability of kerosene-based magnetite colloids exposed to a magnetic field with a homogeneous vertical gradient of the magnetic field strength. The concentration distribution was studied photometrically, measuring the attenuation of the light beam passing through the layer of liquid. For the non-filtered sample, after removal from the magnetic field, there appear spherical drop aggregates with radii of several microns. The dissolution of the aggregates and the restoration of the equilibrium concentration was accomplished in one to two days.

Unlike the non-HGMS samples, the filtered ferrofluids exhibited no drop aggregates. In this case, the switching off of the field was followed by a rapid dissolution of the deposit, which was composed by colloidal particles undetectable in the optical microscope. In the light of these results, the authors concluded that magnetic separation, which removes coarse particles with large magnetic moments from the liquid is an efficient method of increasing the stability of ferrocolloids with respect to aggregation. Also, filtered ferrocolloids present higher sedimentation stability, i.e., less amount of sediments upon removal of the field gradient. Further dilution of the filtered sample with pure kerosene produced no decrease in the sedimentation stability, only modifying the microstructure of the sediment, in which some drop aggregates could be seen.

O'Grady et al. [1986] also studied the variation of the normalised susceptibility, $\overline{\chi}_i$, with filtering time, t_f. The authors obtained some interesting results. After a certain filtering time, the saturation magnetisation diminishes with time, while the $\overline{\chi}_i$ remains constant. This is a clear evidence that for a long enough filtering time, it is not only the big particles which are being removed but a uniform part of the distribution of particles sizes. Thus, the size distribution remains constant ($\overline{\chi}_i \sim$ constant) and it is only the number of particles present in solution which diminishes. Also, the more diluted samples take less time to be filtered.

Other interesting studies of the effect of HGMS on the particle size, magnetic properties, and fluid stability have been performed by several authors [e.g. Watson (1973), Blums and Chukhrov (1993)].

4.1.3. Chemical composition

4.1.3.1. Properties of the non-magnetic components

4.1.3.1.a. The surfactant

Once the magnetic particles have been synthesised [Khalafalla and Reimers (1980)], the particles surface needs to be treated in order to prevent aggregation. The surfactant is a species that adsorbs at the interface between the solute (or magnetic precipitate) and solvent (or carrier liquid) phases.

All surfactant molecules have two very well defined regions:

1. Lyophobic region, which has very little attraction for the solvent, and

2. Lyophilic region, which has a strong attraction for the solvent.

When a surfactant molecule is dissolved in a solvent, the presence of the lyophobic group causes a distortion of the solvent liquid structure, increasing the free energy of the system. It then involves less work to bring a surfactant to an interface (particle surface) than it is to bring it to a solvent molecule. Thus the surfactant concentrates naturally at this interface. Also, the lyophilic group prevents the surfactant from being expelled out of the carrier liquid as a separate phase. This would produce the disolvatation(*) of the lyophilic groups from the magnetite particles and the coating would be destroyed.

Consequently, the molecules of surfactant orientate themselves with the lyophobic portion of the molecule out of the solvent, congregating at the interface. The surface tension between the two media (solvent or carrier liquid and solute or magnetite particles) is then determined by the surfactant molecules rather than by the solvent molecules. The surfactant decreases the work needed to create a unit area of interface, which results in a reduction of the interfacial (or surface) tension [Gibbs (1929)].

The lyophobic group is a long-chain hydrocarbon and the lyophilic group is an ionic or highly polar group. Depending on the distribution of electric charge of the constituent molecules, there are four kinds of surfactants: anionic, cationic, amphoteric or non-ionic; thus, depending on the polar-head group, the hydrocarbon chains carry, in a polar solution (e.g. aqueous solution), a negative, a positive, both positive and negative, or no charge at all, respectively. Anionic and cationic surfactants are totally incompatible with each other, while amphoteric and non-ionic are compatible with all others [Rosen (1978)]. For the ferrofluids utilised in this thesis an anionic surfactant has been used, namely, oleic acid, $CH_3(CH_2)_7CH=CH(CH_2)_7COO^-H^+$.

Colloidal particles dispersed in polar solutions have a net electric charge concentrated at the surface, and these charged units attract oppositely-charged ionic particles. The inner shell of charge and the outer atmosphere is called the electric double layer, which will be studied in ✣4.1.4.2. Khalafalla and Reimers [1980] investigated the relative stability of water-based ferrofluids containing magnetite particles coated with anionic and cationic surfactants. These workers concluded that the former were more effective stabilisers:

(*) Solvation is a process which involves the attachment of molecules of solvent to ions.

adsorption of anionic surfactants onto the particle surface occurs by chemical bonding to the tightly-held negatively charged inner portion of the electric double layer, whereas cationic surfactants can only bond to the positive diffuse layer; expansion of the double layer by dilution can then detach the cationic surfactants from the particles.

The surfactant has also an important role in preventing the oxidation of the magnetite cores of the particles in the fluid, providing a chemical barrier to oxidation as a consequence of the nature of its bonding to the particle surface [Rocchiccioli-Deltcheff et al. (1987)].

4.1.3.1.b. The carrier liquid

The main property of the carrier liquid is its chemical compatibility with the surfactant molecules coating the magnetic particles. Assuming this compatibility, the desirable properties for the carrier liquid are: low evaporation, low viscosity and chemical inertness. In the case of the ferrofluids in this work the carrier liquid chosen was ISOPAR V, which meets all the requirements.

4.1.3.2. Magnetic particles

As already commented, the particles utilised for the magnetic studies in this thesis are magnetite, Fe_3O_4. Ferrimagnetic in nature, they have an inverse spinel structure as is the case of many other ferrites [Cullity, p. 184 (1972)]. Each particle has a net magnetic moment and due to the small sizes present, they will exhibit superparamagnetic behaviour (see ✣2.4 and ✣5.2) at room temperatures.

The bulk material presents a saturation magnetisation of 480 emu/cc. However, during the precipitation reaction it was observed that the saturation magnetisation was reduced to 335 emu/cc (reported by the manufactures, Liquids Research Ltd.). This is the value that has been used in this thesis wherever necessary.

4.1.4. Non-magnetic interactions

4.1.4.1. Van der Waals attraction

Van der Waals (or London) forces are weak attractive forces between atoms or molecules which vary inversely as the sixth power of the interatomic or intermolecular distance. They

are due to momentary(*) dipoles of opposite sign caused by fluctuations in the electronic configuration of the atoms or molecules when they approach each other; i.e., they are forces arising from the mutual perturbations of the electron clouds of two atoms or molecules.

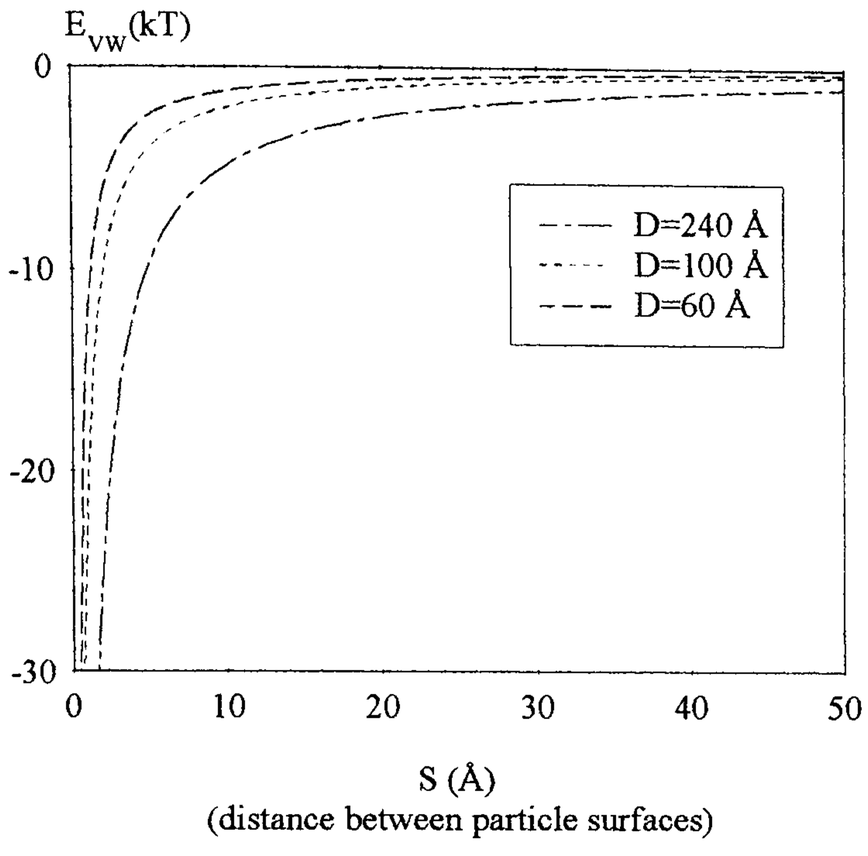

Figure 4-1

Van der Waals energy between two spheres with the same radius, in units of kT.

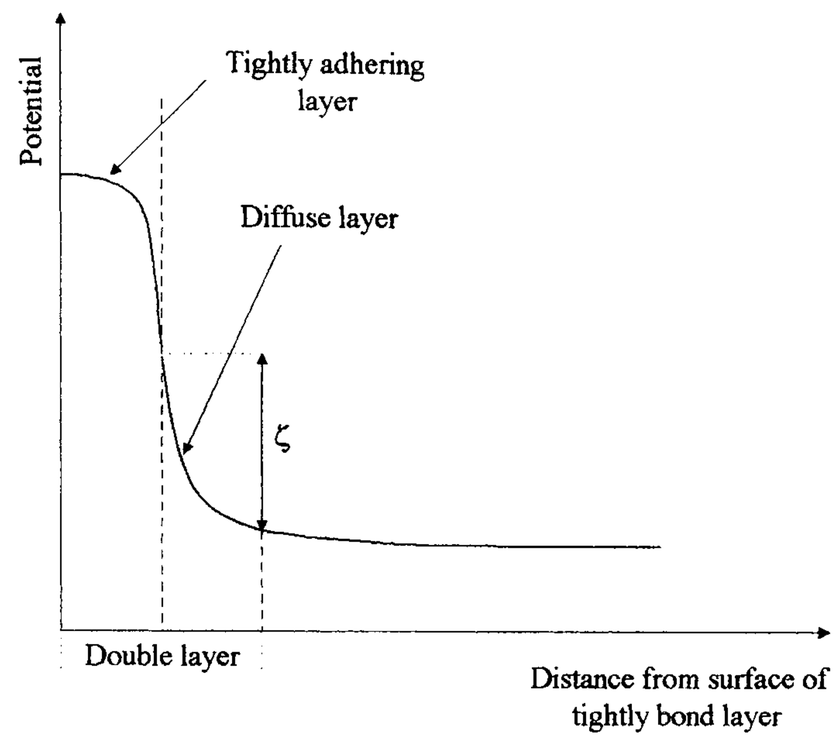

Figure 4-2

Electric potential vs distance from the surface of the particle [Jirgensons et al (1954)].

For the case of two interacting spherical particles with radii r_1 and r_2, and surface separation S, the attraction energy between them is given by Hamaker [1936],

$$E_{VW} = -A_{VW}\frac{r_1 \cdot r_2}{6S(r_1 + r_2)} \qquad for \quad r_1, r_2 >> S$$
$$E_{VW} = -16A_{VW}\frac{r_1 \cdot r_2}{9S^6} \qquad for \quad r_1, r_2 << S \qquad \text{(Eq. 4.2)}$$

where A_{VW} is the so-called Hamaker constant defined by,

$$A_{VW} = \pi^2 \rho_1 \rho_2 C_{12} \qquad \text{(Eq. 4.3)}$$

where ρ_1, ρ_2 is the number density of atoms/molecules in particle 1 and 2, respectively, and C_{12} is a constant that incorporates a characteristic ionisation energy and the polarisability of the material. Rosensweig [1979] assigns a value of $A_{vw} \approx 10^{-12}$ erg for iron particles dispersed in a hydrocarbon.

(*) The time averaged dipole moment is zero but it always has an instantaneous value.

For particles with $D < 100$ Å, the Van der Waals attraction becomes less important, as it can be seen in Fig. 4-1. For an interparticle distance of 20Å (length of surfactant tail) it is of the order of $\approx 1 - 2kT$, i.e. easily overcome by thermal effects.

4.1.4.2. Electrostatic repulsion

Colloidal particles dispersed in a polar medium can acquire electric charge by (i) surface dissociation, where ions leave dissociable groups on the particle surface, (ii) adsorption of ions from polar solutions, e.g., H_3O^+ and OH^- from water, (iii) adsorption of ions from substances dissolved in the solution, e.g. an ionic surfactant such as sodium oleate, or (iv) from crystal lattice defects.

The net charge on colloidal particles gives rise to an *electric double layer*. The first layer, close to the particles, contains the tightly bonded species, which may include ions; then, there is a diffuse outer layer integrated by oppositely charged material, which maintains the charge neutrality. The variation of the electrostatic potential within the electric double layer is shown schematically in Fig. 4-2. The ζ potential is the potential measured from the surface of the tightly bound layer. It is this potential which gives rise to particle transport phenomena in an applied electric field. This behaviour was observed by Bibik et al. [1973] in a ferrofluid. Thus, electrostatic repulsion is very common between particles dispersed in polar liquids and is caused by the Coulombic repulsion of the immobile layers of ions stuck tightly to the surfaces of the particles. The radius of the 'sphere' that captures this rigid layer is called *radius of shear*.

Apart from playing an important role in several preparative methods, the electrostatic repulsion mechanism has been used to disperse ferrofluid particles [e.g. Massart (1981)]. In some cases, the presence of the electric double layer enables ferrofluids and other colloids to be stabilised without the addition of surfactants [Jackson (1965)]. In the majority of cases, however, a surfactant is added to the system which can adhere to parts of the double layer, and although the addition of these ionised molecules reduces the net charge of the particle, it provides additional stability via entropic and enthalpic repulsion as shown in the following sections, 4.1.4.3 and 4.1.4.4.

4.1.4.3. Entropic repulsion

The entropic, or steric repulsion, arises between the 'tails' of the long hydrocarbon molecules adsorbed onto the particles surface. The effect of these molecules is to prevent

the cores of two colloidal particles from coming into contact when they approach each other. This process is known as *steric hindrance*. The polar groups of the adsorbed species associate with the particle surface either physically or chemically, whilst the tails are chosen with properties similar to those of the surrounding liquid. These surfactant molecules can be simply linear groups with an anchor group at one end (e.g. oleic acid) or long polymers with many anchor groups along the chain, so that they can adsorb at more than one site (multiple anchoring). When two particles approach each other closely they will tend to compress the surface-adsorbed layers surrounding each particle, which act as elastic bumpers. Thermodynamically, the repulsion is due to the decrease in the number of possible configurations of the adsorbed chains when the two particles approach one another, which results in a reduction in entropy and the corresponding increase in the free energy; hence at short range, an effective repulsive force between the particles is produced, which prevents the cores of the particles from coming together.

The calculation of the entropic repulsion is not simple and differs for each surfactant and carrier. Mackor [1951] considered the steric repulsion in terms of a rigid tail-rod attached to a universal head-hinge, this attached itself to a flat surface. He used a statistical analysis, treating the surfactant molecules as rigid rods with a universal coupling constant. A more rigorous treatment by Scholten [1978] provides an order of magnitude for the entropic repulsion energy, U_S (the sub-index S stands for entropy),

$$U_S = \frac{2}{3}\pi n_S kT\left(\delta - \frac{S}{2}\right)^2\left(1.5D + 2\delta + \frac{S}{2}\right)\frac{1}{\delta}, \qquad \text{if } S < 2\delta$$
$$U_S = 0, \qquad \text{if } S \geq 2\delta \qquad \text{(Eq. 4.4)}$$

where n_S is the number of adsorbed molecules per unit area ($n_S \approx 10^{14}\, molecules / cm^2$), δ is the length of the surfactant molecule, S is the particle separation, and D the particle diameter. For $S \approx \delta$ and $D = 50\text{Å}$, the entropic energy has a value of $U_S \approx 15kT$, which is more than adequate for the stabilisation of the particles against aggregation, due to magnetic and Van der Waals forces (see ✣4.1.6).

Steric stabilisation is widely exploited in ferrofluid manufacture because it offers several distinct advantages over electrostatic repulsion, namely, it is equally effective in polar and non-polar dispersion media, at high and low volume fraction of particles, and is practically insensitive to the presence of electrolytes.

4.1.4.4. Enthalpic repulsion

When the surfactant molecules have a strong affinity for their binding molecules, the approach of two coated particles also involves the distortion of these surfactant-solvent bonds. This process is energetically endothermic and therefore constitutes a repulsive force. The analysis of this enthalpic repulsion is specific to each system but a generalised analysis by Bagchi [1972] on non-aqueous systems implies that it is at least an order of magnitude less than the entropic term.

4.1.4.5. Born repulsion

Born repulsion is a Coulombic interaction which arises when the electron clouds of particles or atoms are very close, repelling each other. The force is negligible at large distances but increases very rapidly as the atoms approach one another closely. Born suggested that this repulsive energy could be expressed by,

$$E_B = k/r^m \qquad \text{(Eq. 4.5)}$$

where k is a constant and the power m, obtained from compressibility data, increases with increasing atomic size ($m \approx 5$ for He, $m \approx 12$ for Xe). The value of m in colloidal systems is very difficult to estimate because it is much more sensitive to surface structural details than the double layer repulsion and the Van der Waals attraction [Overbeek (1952)].

Although this is a very short range repulsion, it also helps to prevent irreversible coagulation of particles brought together by Van der Waals or magnetic forces.

4.1.4.6. Hydrodynamic interactions

According to the well-known formula of Stokes, the resistance experienced by a spherical particle with radius r moving in a non-flowing liquid of viscosity η_0 is given by,

$$F_H = 6\pi r \eta_0 v_p \qquad \text{(Eq. 4.6)}$$

where v_p is the velocity of the particle. The velocity of the liquid in the neighbourhood of the particle decreases very slowly with increasing distance from the particle and, at distance R from its centre, the velocity is of the order of $vr/2R$ [Hermans (1949)]. Thus, if a second particle is moving at a distance R from the first particle, its velocity will be increased by an amount of this order.

Although these type of interactions do not play an important role in the stability of the ferrofluid (as is the case of the other interactions), they need to be considered when studying the dynamic behaviour of particles in the fluid, for example in the presence of an applied magnetic or electric field, or under the effect of gravity.

4.1.5. Magnetic interactions

The magnetic interactions present in the ferrofluid sample are the dipolar interactions, extensively described in ✣2.5.1.1.a. They seem to be the dominant interactions, as calculated by Jund et al. [1995 *b*]. These authors gave an order of magnitude of the dipole-dipole energy for a particle with a mean diameter of 100 Å: it is approximately 10 times larger than the maximum well depth of the non-magnetic energy.

4.1.6. The balance of forces

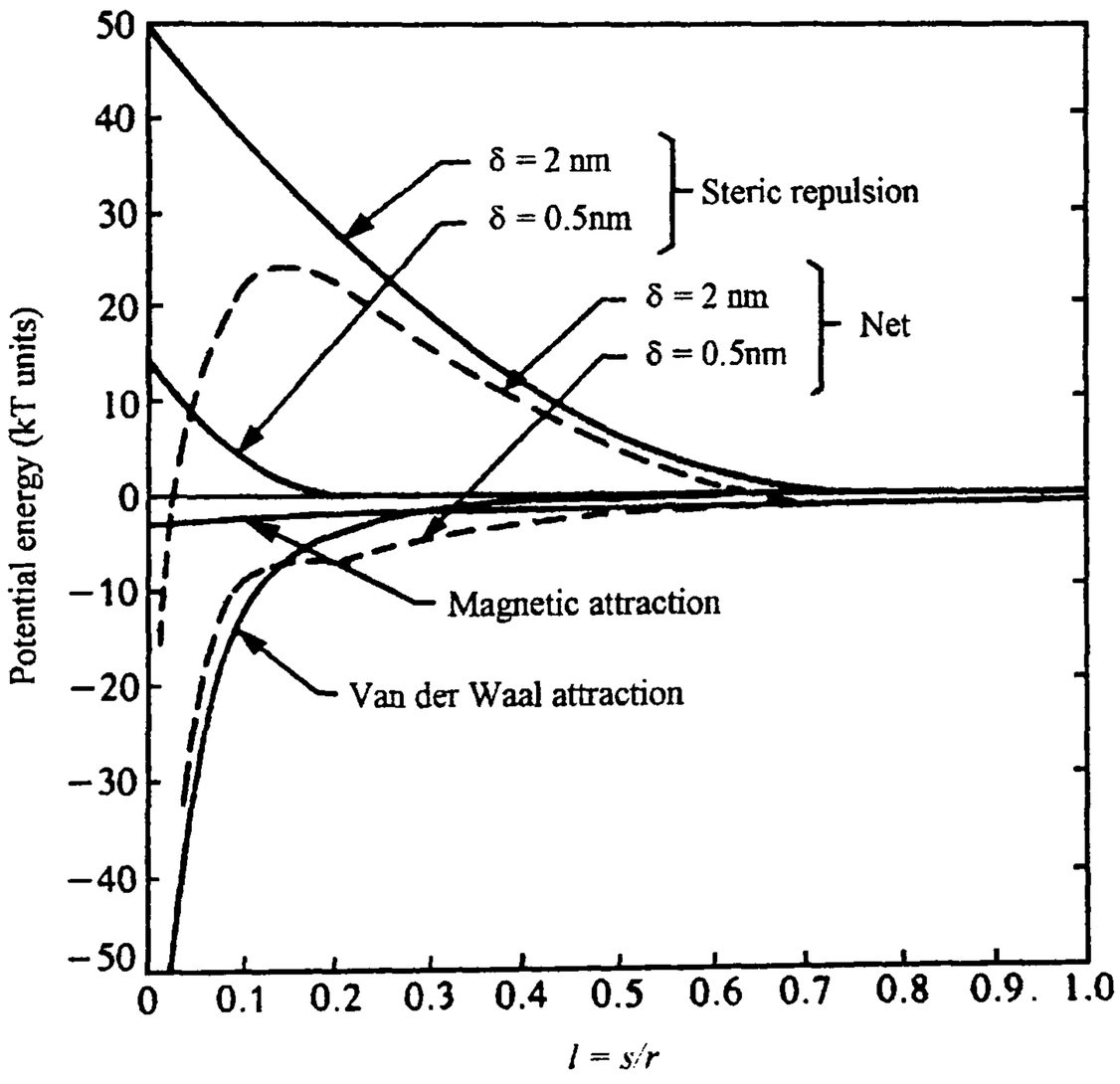

Figure 4-3

Potential energy plotted as a function of surface-to-surface separation (in units of the particle radii) for surfactant-coated Fe_3O_4 particles, with a mean diameter D_m = 100 Å, and n_s=10^{14} molecules/cm^2 (after Rosensweig [1985]).

Whether surfactant-coated ferrofluid particles remain monodispersed or not is determined by the sum of the Van der Waals energy, the magnetic attractive energy and the steric repulsion. In Fig. 4-3 below the net interaction is shown for a fluid containing 100 Å magnetite particles with a surface coverage of $n_s = 10^{14}$ molecules/cm^2 (approximately,

50% coverage of oleic acid molecules). As it can be observed from the figure, an adsorbed layer with a typical length $\delta = 20\,\text{Å}$ produces a net potential curve representing an energy barrier of more than $20k_BT$; because this barrier exceeds the average thermal energy by an order of magnitude, statistically only a few particles will cross the barrier and the rate of particle aggregation is negligible. On the contrary, if the adsorbed layer has a length $\delta = 5\,\text{Å}$, it cannot prevent aggregation. Scholten [1978] calculated that whilst thermal motion keeps ferrite particles with $D = 100\,\text{Å}$ and $\delta = 10\,\text{Å}$ evenly distributed in the absence of a magnetic field, the net curve, in the presence of an aligning field, displays a minimum at about $D = 40\,\text{Å}$, which is expected to lead to particle aggregation.

4.1.7. Properties of ferrofluids

The systems under study in Chapter 5 are colloidal suspensions of magnetic particles in a carrier liquid. Colloidal solutions differ from substances that form true solutions in that they do not obey the solution laws: the alterations of the boiling and freezing points are inappreciable, and the osmotic pressures very small.

Another characteristic of ferrofluids is the change in their rheological properties with the magnetic field; in this sense, an applied magnetic field will induce an anisotropic viscosity in a ferrofluid, where the viscosity parallel to the applied field is significantly greater than that perpendicular to the field [Rosensweig et al. (1969), Schliomis (1972)].

In some cases, due to the electric double layer on the particles surface in a ferrofluid, the particles can move in the presence of an applied electric field. This phenomena is known as *electrophoresis*. Electrophoretic techniques are used mainly to study the electric double layer. Bibik et al. [1973] observed electrophoretic behaviour in a water-base ferrofluid; however, for the case of the particles used in this work, which are dispersed in a non-polar medium, there will be no net charge on the particle surface and electrophoretic effects will not be observed. A good review of electric effects in colloids is given in Smith [1969].

As is the case for electrophoresis, depending on the carrier, the ferrofluid will present high conductivities (like in water-base colloids) or very low or no electrical conductivity (for a non-polar medium) due to the insulating nature of the carrier liquid. The conductivity of a ferrofluid with a non-polar carrier liquid can be increased by including a highly conductive compound as a surfactant [Chagnon (1990)]. Ferrofluids also present *magnetodielectric effect*, which is a field-induced anisotropy in the relative dielectric constant of the fluid

[Colteu (1983)]. The thermal conductivity of a ferrofluid, however, is not affected by the presence of an applied field [Popplewell et al. (1982)].

It is well known [Neuringer and Rosensweig (1964)] that a body immersed in a ferrofluid is subjected to a magnetic pressure gradient when the fluid is under the effect of an applied field. In the parts of the fluid where the field is stronger, there will be an increase in the magnetic pressure; hence, a non-magnetic body immersed in a ferrofluid experiences a force along the direction of decreasing field intensity, and in extreme cases the pressure gradient can be sufficiently large so as to expel the body from the ferrofluid. This property is known as *magnetic buoyancy* or *self-levitation.*

Under the influence of a magnetic field gradient the surface of a ferrofluid can be observed to display a number of well defined liquid spikes. This unusual phenomena is known as *surface instability* [Cowley et al. (1967)].

Depending on the rotation mechanism (Neél or Brown) of the ferrofluid particles, they can remain stationary under the presence of an applied field (Neél rotation) or they can physically rotate (in the case of Brownian rotation) moving with them the surfactant molecules together with the entrained molecules of the carrier liquid. This effect was first observed by Moskowitz and Rosensweig [1967].

Brown and Hosnell [1969] studied a suspension of micron-sized magnetic particles in the presence of a rotating field and observed that the particles rotated in the direction opposite to the rotating field. Although the phenomenon has not yet been satisfactorily explained, Rosensweig et al. [1990] concluded that it is associated with the non-equilibrium states of the magnetic torque and viscous stress arising due to the particles having insufficient time to respond to a continually changing orientation of the applied field. It was observed by Popplewell et al. [1990] that when non-magnetic particles are included in a ferrofluid, the initial low-frequency rotation is in the same sense as the field, whilst at higher frequencies the rotation is in the opposite sense. In this case the torque, T_d, on the non-magnetic particles arising from the applied field and the induced diamagnetic moment opposes the torque due to the viscous stress, T_s, at the fluid/particle interface. Hence the particles rotate counter to the applied field direction when $T_s > T_d$ or in the same direction when $T_s < T_d$.

When ferrofluids are subjected to a magnetic field they become optically anisotropic, i.e., light with its electric vector parallel to the magnetic field is found to be absorbed more than light with its electric vector perpendicular to the field. This effect is known as *positive*

dichroism and has been observed by many workers (e.g. Martinet [1974]). Ferrofluids also present (positive) *birefringence*. In this effect the light with its electric vector parallel to the field experiences a higher refractive index than light perpendicular to the field. For more information on this effect, see Scholten [1980], Hartmann and Mende [1984], Popplewell et al. [1987] and Sakhnini and Popplewell [1993].

4.1.8. Applications of ferrofluids

Ferrofluids are widely used in many applications. Some of the applications utilise the property that a ferrofluid is attracted and positioned using magnetic fields. The ferrofluid seal is the most developed application of ferrofluids. In seal applications [Rosensweig (1982)], the ferrofluid is attracted to the gap between a toroidal permanent magnet and a rotating shaft, forming a liquid O-ring; that is, the ferrofluid creates an impermeable ring around the shaft while allowing it to rotate with negligible friction. Also, any heat generated is dissipated through the liquid so that high rotation rates are possible (up to $5 \cdot 10^4$ rpm in a high vacuum of 10^{-8} Torr).

Magnetic inks are another less widespread application of magnetic liquids. Two different technologies have been developed in ink-jet printers: the electrostatic and the magnetic ink methods. In the former, the fluid is ejected from a nozzle in the form of charged droplets and deflected using an electric field. The interaction of the charged droplets and the use of high voltage electronics, however, pose considerable technological problems. In the magnetic ink systems, a uniform stream of ferrofluid droplets is formed by introducing periodic disturbances along a flowing fluid jet; these are then deflected on passing through the magnetic field gradient of a transducer coil [Fan and Toupin (1975), Sambuceti (1980), Maruno et al. (1983)]. The fluid inks based on ferrofluids contain particles that are predominantly superparamagnetic in the dried-ink state. Chandrasekhar et al. [1987] and Charles et al. [1988] studied magnetic inks containing Co ferrite particles for their use in character recognition work.

There are also several applications based on the magnetic buoyancy or levitation force induced on bodies immersed in a ferrofluid. One of these applications is magnetohydrostatic separation (MHS), which is based on the variable density of a ferrofluid when subjected to an applied field, which is used on an industrial scale to sort materials, such as waste metals and precious stones, that differ in density [Kaiser and Kurtiss (1976)]. The passive levitation of a non-magnetic body is also applied in the

grinding and polishing processes for metals, ceramics and plastics [Umehara and Kato (1987)], where they observed a removal rate three times larger than that in traditional mechanical surface-finishing methods.

The ferrofluids are also very often used as dampers; in this case they have a dual function: firstly, the buoyancy force on the magnetic or non-magnetic body enables the moving mass to be positioned without any solid contact; secondly, the colloid is able to dissipate the kinetic energy of unwanted motion or oscillations. Furthermore, a ferrofluid offers the advantage over conventional viscous media that it can be held in position by a magnetic field and does not need a closed vessel with its consequent sealing problems to contain the liquid. The most common damping application of ferrofluids is in the moving-coil or conventional loudspeaker.

Another group of applications is based on the thermomagnetic convection properties of ferrofluids and the magnetic buoyant force exerted on the bubbles that are formed on boiling. One of these applications is the magnetocaloric pump; since the temperature is a measure of the disorder in a system, a sample of material that is thermally insulated from its surroundings must become cooler when it is magnetised (ordered). Shustrov [1992] has monitored this temperature change on application of a field as a function of the initial fluid temperature. Resler and Rosensweig [1964] proposed a device for the direct conversion of thermal energy to energy of fluid motion based on the change of magnetisation with temperature in a ferrofluid. Many industrial devices rely on thermal convection for the transfer of heat. Convection takes place whenever a fluid is heated non-uniformly; this is usually the case when the fluid is heated at the bottom and cooled at the top. The heated lower layers become less dense than the cooler upper layers, which is an unstable configuration; when the temperature difference between the bottom and the top exceeds a critical value, an organised pattern of fluid circulation develops as the heavier and lighter regions of the fluid respond to gravity. When the working fluid is replaced by a ferrofluid and a magnetic field applied at the bottom of the heating section, the circulation is driven by changes in the magnetisation of the ferrofluid with temperature rather than by changes in density. Furthermore, any bubbles formed are quickly removed from the fluid pool by magnetic levitation effect, resulting in an increase of latent heat transfer. This effect could be applied in the cooling of motors, loudspeaker and other equipment where a magnetic field is already present [Takahashi et al. (1992)].

One of the possible applications of ferrofluids is to use it to probe the local environments of other materials; for example, ferrofluid particles may be incorporated into biological cells, and the response of the sample to an alternating magnetic field can provide information about the local viscosity. Investigators at Perth University are currently developing a technique by which very small magnetite particles in a ferrofluid are introduced in a cancerous liver. By applying high frequency magnetic fields, heat is generated which will act locally, killing only the cancerous cells. A temperature increase of 5-6 ^{0}C is sufficient to eliminate the cells. Many other bio-medical applications of magnetic nanoparticles in different carriers were the object of the Second International Conference on the Scientific and Clinical Applications of Magnetic Carriers (http://www.ccf.org/cc.radonc/conferences, Cleveland, Ohio, U.S.A., May 28-30, 1998)

Recently, Tománek et al. [1997] suggested the use of ferrofluids in high density memory system. According to their calculations, small ($D_m \approx 100\,\text{Å}$) particles in a ferrofluid form aggregates of a few particles ($N \sim 4-15$ particles), which can change from a chain to a ring structure, under the influence of a very small and localized field. In this memory systems, the field would be produced by a sharp tip of soft magnetic material, like the ones used in the Atomic Force Microscope (AFM). The tip can both modify the equilibrium structure (ring-chain or chain-ring) of the system by changing the field and temperature ('assembly of nanostructures'), as well as being able to distinguish magnetically between the different isomers ('detection of nanostructures'). The detection or reading of information is made, as in the AFM, by the different attraction that different isomers exert on the probe. In this manner memory units can be stored in the form of small chains and/or rings, detected and deleted, by the application different applied fields and/or temperatures.

4.2. Nanoclusters (Co/Cu)

The manufacture of the Co/Cu nanoclusters studied in Chapter 6 was reviewed in ✣3.8. In the following sections, the different possibilities for cluster deposition are shortly revised. Some physical and chemical properties, as well as some of the magnetic characteristics of magnetic nanoclusters are discussed. Finally, a review of the applications and possible future applications of these nanostructured materials is presented.

As well as ferrofluids, cluster systems represent ideal media for the study of interactions with concentration and particle size. While the particles in a ferrofluid would present

solely weak dipolar interactions, the nanocluster systems are expected to present more complex interactions, dipolar as well as exchange, which are intended to be explained.

4.2.1. Cluster assemblage

In general, cluster beams can be used to deposit material on substrates. Once the clusters have been produced in a magnetron cluster source (see ✣3.8), the deposition falls into two classes:

a) deposition in which the clusters are ionised and accelerated so that they have energies of the order of keV before they reach the substrate, and

b) deposition of low-energy neutral clusters.

If high energy cluster beams are used, the clusters fragment on the substrate, thus creating additional nucleation sites and enhancing diffusion. Using high-energy cluster beams, Yamada et al. [1984] were able to obtain an epitaxial coating of Al on Si (111) surfaces. If low-energy cluster beams are used, then the clusters do not fragment on striking the substrate and nanostructured thin films are produced. This is the case of the nanoclusters in this thesis (see chapter 6).

Although with the low-energy beams the clusters do not fragment, they can diffuse on the surface. If two clusters meet by diffusion, they can 'touch' but still remain separate entities. The other possibility is that they fuse into a larger cluster. By fusing they decrease their surface free energy. There appears to be an energy for coalescence which increases with cluster size. Thus, if both clusters are large, no coalescence will occur.

Metallic clusters containing approximately 1000 atoms seem to present reduced melting temperatures [Edelstein and Cammarata (1997)]. If the reduced melting temperature is comparable to the substrate temperature, then the clusters are liquid-like and there is no barrier to fusion. In this case, coalescence will be unhindered until the melting temperature of the fused clusters is larger than the substrate temperature. Fusion of clusters of refractory and covalently bonded materials is sufficiently hindered so that the average cluster size in these materials on the substrate is likely to be similar to the average cluster size of the incident cluster beam. The subject of cluster assembled materials has been reviewed by Melinon et al. [1995].

The clusters used in this work were prepared by Derek Eastham at Daresbury Laboratories by low energy co-deposition of Co clusters with an atomic beam of Cu from a magnetron cluster source, in a high vacuum deposition chamber. From room temperature magnetisation curves, it can be observed that the nanoclusters have a magnetic size similar to the physical size expected for clusters with their number of atoms, i.e., 1000 and 8000 atoms, respectively (see ✣6.2).

4.2.2. Physical and chemical properties of clusters

The study of the physical and chemical properties of clusters is an area of great interest since it provides new ways to explore the gradual transition from atomic or molecular to condensed matter systems. Clusters provide unique systems for understanding certain complicated condensed phase phenomena such as nucleation, solvation, adsorption and phase transitions. It is not unusual for the properties of clusters to be different from those of the bulk material with the same composition. This is not too surprising in small clusters in which the atomic structure is different from that of the bulk material; however, even clusters large enough that their atomic structure is the same as the bulk structure can have these modified properties. Several books as well as review articles have been devoted to detailed investigations of cluster properties [Sugano et al. (1987), Jena et al. (1987), Moskovitz (1986), Johnson (1980), Russell (1989), Jena et al. (1992), and the entire issues of J. Phys. Chem. 91, 10 (1987, 1986), Chem. Rev. 86, 3 (1986, 1987), Z. Phys. D. 3, 2-3 (1986, 1988), Z. Phys. D. 26, 1-4 (1993, 1991)]. In this section, some important properties of clusters are briefly described, with an emphasis on metal clusters.

An interesting property of small clusters is the presence of 'magic numbers'. Similar to the stability of atoms with full atomic shells, clusters whose total number of valence electrons fill an electronic shell are specially stable. For example, for Na_n clusters the magic numbers are observed as peaks in the abundance spectra where n=8, 20, 40, 58, 92) which correspond to major electronic shell closings. The abundance spectra drops sharply above these magic numbers.

For clusters of noble gas atoms and generally for large clusters ($n > 100$), the magic numbers are determined by geometric considerations and not by the filling of electronic shells. As suggested by Mackay [1962], the magic numbers of inert gas clusters containing from 13 to 923 atoms arise from the closing of shells and sub-shells of icosahedral structures [Echt et al. (1981), Farges et al. (1986), Northby (1987), Lethbrigde and Stace

(1989), Schriver et al. (1989)]. For example, Martin et al. [1990] explained the magic numbers observed in the mass spectra of Na_n with $1500 < n < 22000$ by the completion of icosahedral or cuboctahedral shells of atoms. In some other metal clusters, such as Pb_n, the stability is also dominated by geometric considerations [LaiHing et al. (1987), Farley et al. (1989)] and the strong magic numbers observed correlate with the icosahedral structures. The subject of icosahedral shells of atoms in inert gas clusters has a long and interesting story. For a review, see *Proc. Faraday Symp. on Large Gas Phase Clusters* [1990].

Another interesting feature of clusters is the surface to volume ratio. Using a liquid drop model [Jortner (1992)], the volume V and surface area S of a cluster containing n atoms can be expressed as,

$$V = \frac{4}{3}\pi R_0^{\,3} n \qquad \text{and} \qquad S = 4\pi R_0^{\,2} n^{2/3} \qquad \text{(Eq. 4.7)}$$

where R_0 is the radius of a single atom. The fraction of the atoms that are surface atoms, $F = n_s / n$ is given by,

$$F = 4 / n^{1/3} \qquad \text{(Eq. 4.8)}$$

In clusters a large fraction of atoms occupy surface states. For example, $F = 0.4$ for $n = 10^3$, $F = 0.2$ for $n = 10^4$ and $F = 0.04$ for $n = 10^6$. The large surface/volume ratio for clusters is responsible for a variety of electronic and vibrational surface excitations [Jortner (1992)]. Jortner has discussed the physical and chemical consequences of the large surface/volume ratio of clusters and has proposed cluster size equations (CSEs) which describe the gradual transition from the large finite cluster to the infinite bulk system, with increasing cluster size.

Because of the large surface to volume ratio of small clusters, the surface energy plays an important role in determining their properties and even their structure. For example, very small clusters containing fewer than approximately 20 atoms can have structures which are unique to them. Somewhat larger particles have structures which are characteristic of the bulk but with reduced lattice parameters and reduced melting temperatures. The lattice constant decrease has been observed in Al nanoparticles [Woltersdorf et al. (1981)]. It seems to be the case, however, that when the cluster size exceeds approximately 1 nm, the particles usually have either the structure of the bulk materials or metastable structures with bulk values for the lattice constants and melting temperatures.

There are many more interesting properties associated with nanoclusters; unfortunately, their study is out of the scope of this thesis. In this paragraph some references are given for the reader interested in further investigation. For example, ionisation potentials and electron affinities of different metal nanoclusters have been studied by several authors (Al_n [Pellarin et al. (1992)], Fe_n [Yang and Knickelbein (1990)], Li_n [Gohlich et al. (1992), Dugourd et al. (1986)], Au_n [Cheshnovsky et al. (1990), Taylor et al. (1992)] in order to test the electronic shell model. Also the chemical reactivity of clusters has been tested for their application in catalysis and materials processing [Morse et al. (1985)]. Another interesting property of clusters are phase transitions. The most studied phase transition is melting. Studies show that the melting temperature of nanomaterials decreases for clusters smaller than a few hundred angstroms (Goldstein (1992) - Au_n clusters, Peppiatt (1975) - Pb_n clusters].

4.2.3. Magnetic characteristics

The magnetic properties of clusters can, like many other properties, differ from those of corresponding bulk material. For example, clusters of Rh [Reddy et al. (1993), Cox et al. (1993)], Pd, Na, and K [Edelstein and Cammarata(1996)] are ferromagnetic whereas the bulk forms are paramagnetic. Other differences, such as the superparamagnetism of Fe, Co and Ni clusters, are just a consequence of the small size of the clusters. Relatively few investigations have been performed on ferromagnetic clusters [Cox et al. (1985), de Heer et al. (1990)]. The earliest results came from the Exxon group [Cox et al. (1985)] who tried to use depletion in cluster beams to determine magnetic moments. The actual depletion profiles, however, were first observed by de Heer et al. [1990] on Fe_n clusters containing 56-256 atoms. Bucher et al. [1991] performed similar experiments in Co_n clusters. Further experiments on Fe, Co and Ni clusters containing up to 700 atoms at temperatures between 80K and 1000 K have been reported [Billas et al. (1993, 1994)]. Ferromagnetism was observed even in the smaller clusters.

For clusters with fewer than 100-200 atoms the magnetic moments are enhanced and atom-like [Billas et al. (1993, 1994)]. As the size is increased up to 700 atoms, the magnetic moment decreases and approaches the bulk limit, with oscillations possibly caused by the surface induced spin-density waves or structural changes. The magnetism of Ni clusters converges to the bulk limit more rapidly than Co and Fe clusters. In particular, the moment of a Ni cluster with about three layers of atoms (Ni_{150}) is bulk-like, whereas for Co and Fe

about four or five layers are required (Co_{450}, Fe_{550}) before the same bulk-like behaviour is observed.

4.2.4. Present and future applications of nanoclusters

Magnetic properties of nanostructures provide a fertile ground for new discoveries. Thin layers of magnetic materials such as Fe, in conjunction with chalcogenides (group VI B, e.g. S, Se, Te) in intervening layers show evidence of high anisotropies and internal fields perpendicular to the plane instead of the parallel internal fields that usually occur. These materials show a large change in their resistance as the magnetic field is changed (magnetoresistive effect) and appear to be promising for read heads. They also exhibit important properties needed for non-volatile memory devices.

For both particulate and thin film media, the magnetic single domain particles that constitute these systems must become smaller to achieve higher densities with satisfactory signal-to-noise ratios [White (1990)]. However, as particle size decreases, so does the energy barrier to reversal, in such a manner that the magnetisation can be reversed by thermal activation and stable magnetic storage ceases to exist. Higher energy barriers can be achieved by utilising magnetocrystalline anisotropy energy. However, this anisotropy energy often has an unacceptable temperature dependence. One solution may be surface-treated particles and films. In the tape industry, Co has been chemisorbed onto the surface of γ-Fe_2O_3 particles, with a high increase in coercivity (more stable bits). Other surface treatments have also proven effective [Spada et al. (1993)], and it seems appropriate to explore this approach for high densities in both films and particles [Berkowitz and White (1989)]. Write heads can also be considered to fall into the nanostructured category, since the trend is toward utilising thin magnetic films of high-permeability metallic alloys for high recording density [Mee and Daniel (1990)]. The most probable route by which nanostructure research could lead to a successful memory technology would be via nanoelectronics research resulting in the development of an ultrahigh-density very-large-scale-integration (VLSI) integrated circuit (IC) technology. In fact, memory would be an indispensable ingredient in such nanoelectronic technology.

Normal magnetoresistance (MR) heads utilise permalloy ($Ni_{81}Fe_{19}$) films whose resistance changes by about 2% as the recorded bit passes by. Some truly nanocrystalline materials have demonstrated resistance changes more than an order of magnitude larger [Chien et al. (1993), Berkowitz et al. (1993)]. These films consist of magnetic particles less than 10 nm

in diameter dispersed in a non-magnetic matrix. At the moment these materials looked very promising as potential read heads but they were soon discarded due to their wide switching region (distribution of particle sizes) and the large field required to saturate them, due to the presence of such small particles. At present (February 2000) the majority of read heads in the market are made of Giant Magnetoresistance (GMR) materials, in which the signal to noise ratio is superior to that of inductive heads at high data rates [White (1990)]. These GMR heads have a multilayer structure: permalloy (soft or pinned layer), ferromagnet (pinning layer) and antiferromagnet [Nogués and Schuller (1999)]. These materials present a very high change in resistance at very low fields, ideal properties for a good read head.

Magnetotactic bacteria use the earth's magnetic field lines to enable themselves to orientate and move in the direction of nutritional or chemical ingredients. This ability suggests interesting possibilities in order to exploit these properties to develop magnetic sensors and transducer systems. However this is very much for the future as currently it is only in bacteria that the mechanism is fully understood [Dickson et al. (1993 *b*)].

Catalysts have been used for the production of industrially important materials for decades. The importance of small structures in promoting catalytic reaction is well documented [Knözinger (1991)]. Heterogeneous catalysis is highly dependent on two-phase reactions, and is enhanced by increasing the surface area exposed to a chemical reaction. As nanostructures together with the ability to make catalytically active surfaces and the mechanisms involved in catalytic action are understood in greater detail, enhanced capabilities for the production of important and less costly materials should be developed. This field and the related literature are however far too large to address here. Suffice it to say that both the electronic structure and the surface topology are known to be important for catalytic applications.

The generation of the 21st century electronic devices and computers will almost certainly depend on nanometer structures. However, the strongest economic driver is likely to be biomaterials and medicine where the confluence of chemistry, physics, and materials science at the nanometer scale may provide the understanding necessary to start to unravel the processes of life itself.

"If you want to understand the Creator,
you need first to understand its creation"
(Columbanus)

5. Results I. *Ferrofluids*

Introduction

The basic characterisation of the ferrofluid systems as well as a whole range of magnetic and non-magnetic measurements are presented in this chapter. The effects of the different particle sizes, interparticle interactions and surface anisotropy have been studied. The chapter is divided in three sections, 5.A, 5.B, and 5.C. The basic sample characterisation (magnetic and physical) is done in part A; the study of interactions via different magnetic measurements is the object of part B; and the study of time dependence, attempt frequency, f_0, and surface effects, also with some insight into the influence of interactions and particles sizes in such effects, is treated in part C.

The idea of this experimental chapter is to study size, interaction and surface effects using a whole range of magnetic and non-magnetic techniques. In part 5.A, the samples' particle size (physical and magnetic) and energy barrier distributions are determined. In this way, the systems are well characterised enabling the further study of the properties of the materials. For the majority of magnetic measurements, the samples have been frozen initially in a zero magnetic field (ZFC), so that, in all cases, the samples are systems of randomly distributed magnetic moments. Thus given the initial configuration of the systems is the same, the effect of concentration and particle size on remanence to saturation ratio, coercivity, remanence (DCD, IRM) curves, delta M curves and relaxation of magnetisation gives an insight into the way interactions, size and surface effects affect the behaviour of the systems. Interesting is the calculation of the attempt frequency, f_0, using different experimental techniques, for the three particle sizes.

" Only looking at the sky can you find answers to your longings.
Looking at the sky, because looking at it liberates your mind,
not because the answers come from the sky,
but because contemplating infinity we are able to become aware
of the role we play in the Cosmos, that we are connected to it all "
(Translated from *'Inductions. The Geenom Manuscripts'*)

5.A. *Basic characterisation*

5.1. The samples

The materials under study are magnetite (Fe_3O_4) particles, in the form of a ferrofluid (✣4.1). The samples have been supplied (Liquid Research Ltd) with three different particle sizes, 77Å (F024), 66Å (F026) and 59Å (F028). The volume concentration is 10% approximately (see Table 5-1 below). All the samples have been prepared with a surfactant (oleic acid) chemisorbed onto the surface, that coats the particles, preventing agglomeration and reducing dipolar interactions (✣4.1.3). The carrier liquid is a commercial hydrocarbon, called isopar-M. Measurements have been performed in the samples as-prepared, and also in diluted form. The dilutions have been obtained by adding different amounts of isopar-M to the original samples. In this manner, D1 is the sample as given by the manufacturer; D3 contains one part of D1 and three parts of isopar; D4 one part of D1 and four parts of isopar, etc (see Table 5-1).

ε (%)	*D1*	*D3*	*D4*	*D5*	*D6*	*D12*	*D24*
F024	7.1	2.2	1.9	1.4	1.3	0.8	0.4
F028	10.3	3.8	--	2.4	1.7	0.8	0.5

Table 5-1

Volumetric concentration, $\varepsilon = \left(M_s / M_{sB}\right) \times 100$, *of magnetic material for the differently diluted samples.* M_s *and* M_{sB} *are the saturation magnetisation of the ferrofluid and of the bulk material, respectively.*

5.2. Magnetic particle size

The magnetic particle size has been determined using the method by Chantrell et al. [1978] described in Appendix I. According to this analysis, the magnetic particle size is obtained from the initial susceptibility of the sample, χ_i, and the approach of the magnetisation to saturation, characterised via $1/H_0$ (see Appendix I), at room temperature. In ✣5.2.1, three magnetite samples with different particle sizes have been studied. The basic magnetic characterisation is presented in ✣5.2.1.1, and the deviation of the magnetisation curve from a sum of Langevin functions is explained in ✣5.2.1.2. In ✣5.2.2, the effect that particle size bears on the curves is considered. In ✣5.2.3, the influence of the sample concentration on the measurements is discussed.

5.2.1. Magnetisation curves at room temperature

5.2.1.1. Magnetic size parameters

Assuming a lognormal distribution of particle volumes, the magnetisation curves at room temperature ($T = 297K$) are used [Chantrell et al. (1978)] (see Appendix I) to calculate the median diameter, D_{vm}, and standard deviation, σ_v, of the distribution (see Table 5-2). The parameter $1/H_0$ has been obtained considering fields $H > 8.5\,kOe$. The saturation magnetisation of the coated powder was given by the manufacturers as $M_{sB} = 335$ (emu/cc) at room temperature. This value is consistent with the studies by Kaiser et al. [1970] and Berkowitz et al. [1980], who predicted that the saturation magnetisation, M_{sB}, for coated particles is lower than that for the bulk. They found that the average M_{sB} for coated magnetite particles is 68% of the bulk value (485 emu/cc, at room temperature), in close agreement with the value of 335 emu/cc supplied by the manufacturers. The decrease

in the value of M_{sB} was attributed to the adsorption of the surfactant molecules on the particle surface, which causes the moments of the iron atoms close to the surface to be quenched. A reduction in the value of M_{sB} has also been observed more recently by other authors [Tang et al. (1991), Kodama et al. (1996)]. In these studies, the authors attributed this reduction to finite size effects, i.e. the spins in the surface being canted and with reduced exchange coupling.

Using the calculated parameters of the lognormal distribution of sizes (D_{vm} and σ_v) (Table 5-2), theoretical magnetisation curves have been produced (Fig. 5-1, *a* and *b*), assuming a Langevin function for every particle size.

	F024	*F026*	*F028*
D_{vm}(Å) ±2	77	66	59
σ_v ±0.02	0.42	0.41	0.38
M_s(emu/g) ±0.5	20.6	21.7	21.9

Table 5-2

Median diameter and standard deviation of the lognormal distribution of magnetic particle sizes, via the method of Chantrell et al. [1978]

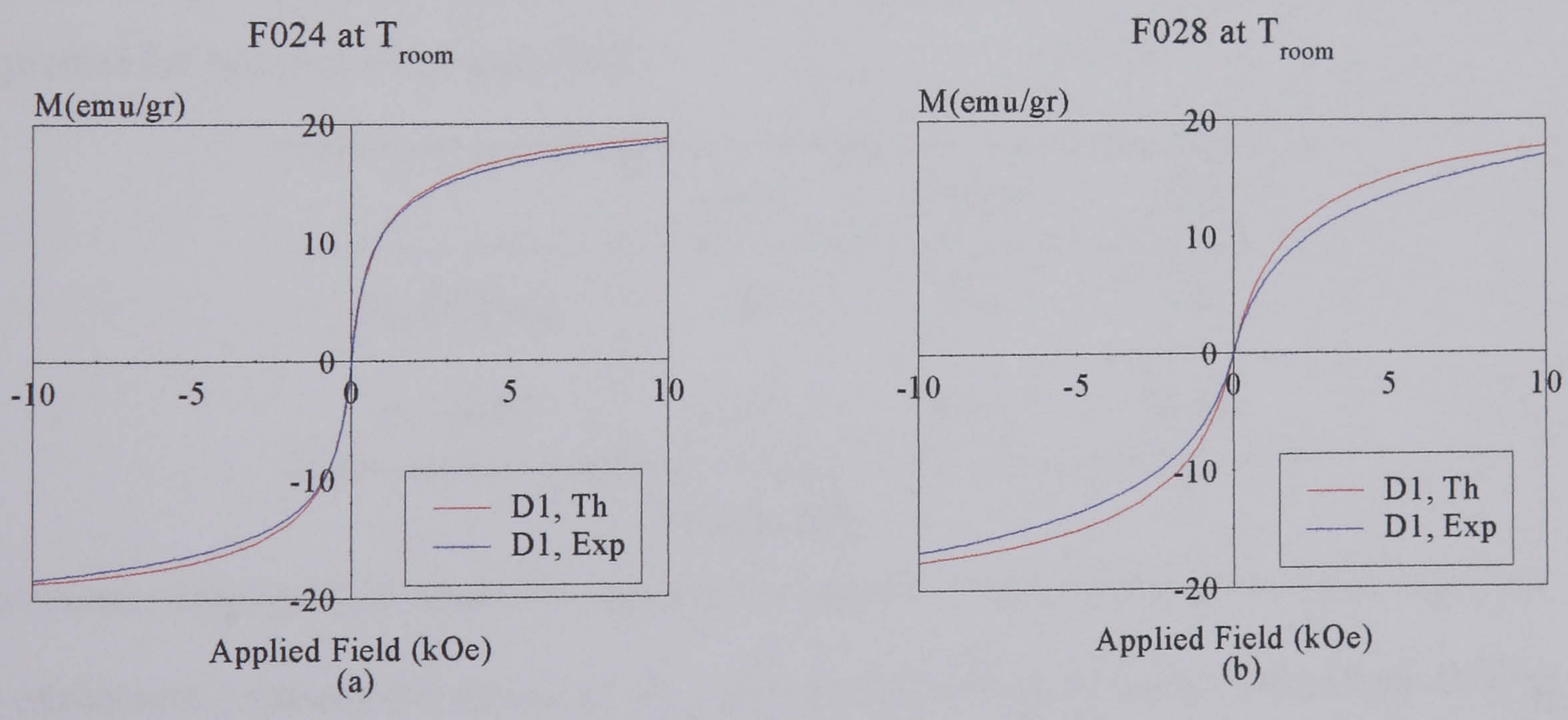

Figure 5-1

Room temperature magnetisation curves (Exp) of samples F024 (a) and F028 (b) fitted to a sum of Langevin functions (Th), using the method of Chantrell et al.[1978]

The results reveal the existence of 3 different particle sizes, which are consistent with the values obtained from the physical analysis via TEM images (✣5.3.1) and the X-ray diffraction data (✣5.3.2). As the particle size decreases, so does the standard deviation of

the correspondent lognormal distribution, probably an artefact due to the definitions of D_{vm} and σ_v in the method of Chantrell et al. rather than to a real narrower spread of particle sizes when the size is diminished. In fact, this trend is not observed in the size characterisation via TEM (Table 5-6).

5.2.1.2. Deviation from the Langevin behaviour

Assuming a sum of Langevin functions (one for each particle size in the distribution), theoretical (*Th*, in Fig. 5-1) magnetisation curves were generated using the parameters obtained by the method of Chantrell et al., displayed in Table 5-2. These curves seem to deviate from the experimental data, the effect being more important as the particle size decreases. The experimental magnetisation curves lie below the theoretical predictions for intermediate and high fields for all samples, and above them for small fields (only visible in F024, see ✣5.2.3). This phenomena may have different origins. One possibility is that the parameters obtained via the method of Chantrell at al. are not realistic; for this purpose a 'best fit' routine has been written, which calculates D_{vm} and σ_v so that the best fit of the experimental data to a sum of Langevin functions is obtained. This approach will also test the validity of Chantrell's method. The characterising parameters calculated for all the materials are presented in Table 5-3. In Fig. 5-2, the best fit and the experimental curves are plotted for samples F024 and F028.

	F024	*F026*	*F028*
D_{vm}(Å) ±2	78	66	58
σ_v ±0.01	0.41	0.41	0.38

Table 5-3

Parameters obtained by the best fit method for all samples, F024, F026 and F028 (see Fig. 5-2)

The agreement between the values of D_{vm} and σ_v calculated by the Langevin best fit (Fig. 5-2) and the method of Chantrell et al. (Fig. 5-1) give a good indication of the applicability of this latter method. The best fit method slightly improves the fit for the F024 sample. However, for sample F028, there is still some deviation of the experimental data with respect to the fitted curve (see Fig. 5-2). A possible reason for the misfit observed in Fig. 5-1 and Fig. 5-2 for F028 is the presence of interactions. However this effect is only

significant for low fields ($H \leq 500\ Oe$) [Bradbury et al. (1985)], and cannot account for the stronger deviations observed at intermediate and high fields. The influence of the interactions on the magnetisation curve will be studied in more detail in ✣5.2.3.

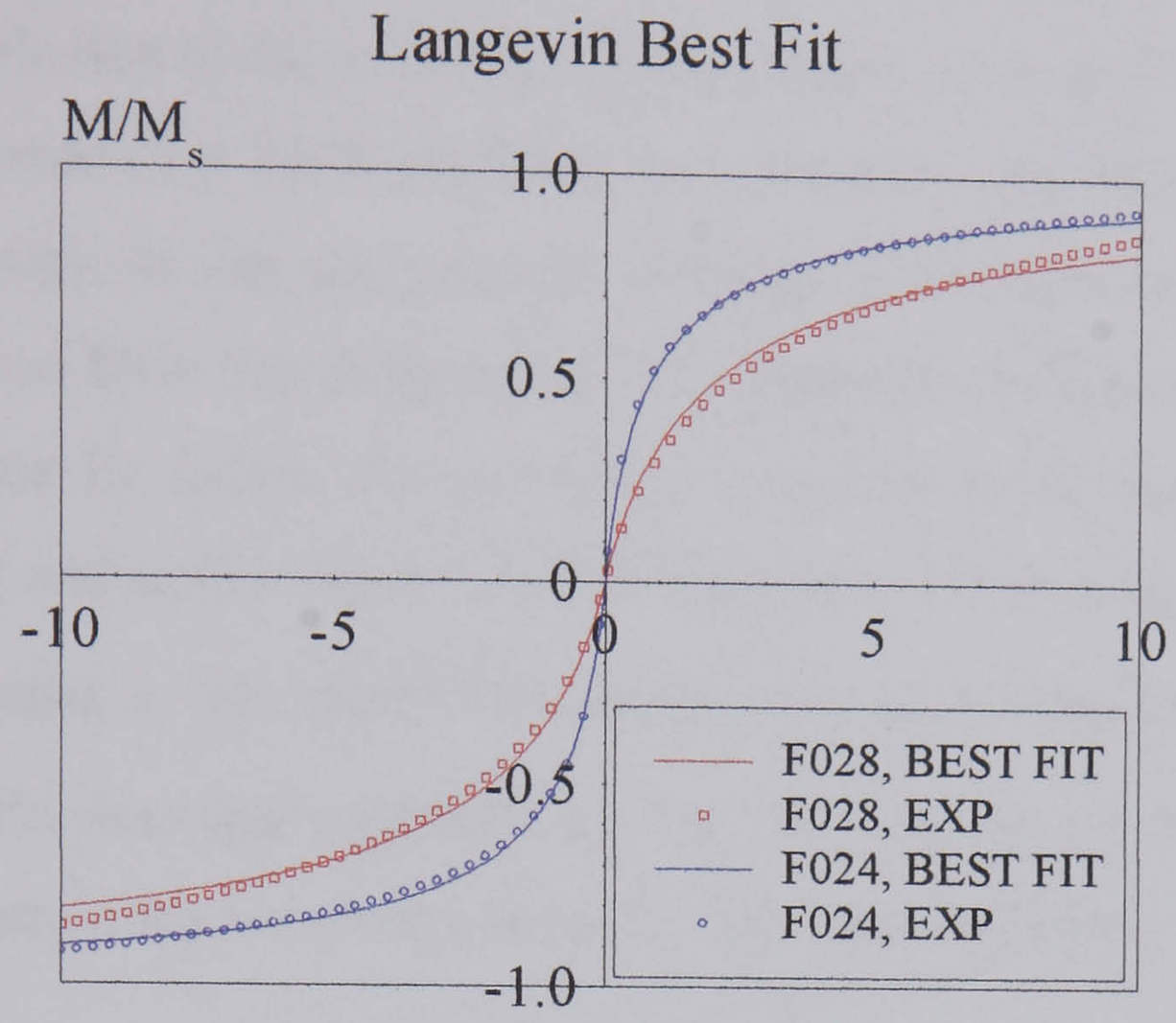

Figure 5-2

Experimental magnetisation curves of samples F024 and F028 fitted *to a sum of Langevin functions*

The more plausible (or at least predominant) explanation for the deviation of the experimental magnetisation curves from the *ideal* Langevin behaviour at high field is the influence of an anisotropic term in the system, as reported by several authors [Hanson et al. (1993), Williams et al. (1993 *b*), Chantrell (1977)]. This anisotropy, in the case of the samples of this thesis, and for room temperature, can only have its origin on the surface of the particles, as the particles are free to rotate in the fluid, and no other anisotropic contribution affects the magnetisation of the systems. As shown in Fig. 5-1, the Langevin fit is poorer for sample F028. Because F028 has a small particle size, and the surface layer is approximately the same for all samples (around 10 Å) (see ✣5.11), the surface to volume ratio is much higher in this last sample. F028 will have a higher proportion of non-aligned (not-so-strongly exchanged coupled) spins, which will be more difficult to 'pin' than the single magnetic cores (exchanged coupled). This would lead to some kind of surface anisotropy. Hence, an extra term (✣2.2.3) that accounts for this effect should be introduced to describe the behaviour of the system. The structure of the magnetic moment in the surface is not completely known, but many authors [e.g. Coey (1971), Morrish et al.

(1976, 1983)] have referred to it, indicating canting of the spins due to the lower coordination number and the geometry of this surface.

Although Hanson et al. [1993] and Chantrell [1977] did their studies to account for an increase of the contribution of the anisotropic terms (shape, stress and/or crystalline) as the temperature was lowered ($T \leq 200K$) in the system, the same idea can be used for the case of any other anisotropy, at any temperature, although some care must be taken in the choice of the analytical form of this term (✣2.2.3). Under the influence of this anisotropy, the experimental data lie below the theoretical Langevin predictions, as observed by Hanson et al. [1993] and in this thesis (Fig.5-1). In Hanson et al. a treatment for a single particle size is presented. In this thesis(*) the method has been extended to account for the distribution of particle sizes (see Appendix II). For this purpose, a best fit subroutine has been written. The form of the anisotropic term that has been included is of the form,

$$E_{an} = K_0' V + K_2' \cos^2 \theta \qquad \textbf{(Eq. 5.1)}$$

where θ is the angle between the easy axis (supposing uniaxial anisotropy) and the direction of the magnetic moment, and K_0' and K_2' are anisotropy constants that depend on the material. A complete description of the method is given in Appendix II.

Preliminary results do not give a satisfactory fit to the experimental magnetisation curves. However, the method is still under development and it will be the object of future work. Special care must be taken in the selection of the mathematical description of this surface anisotropy and in this sense different expressions from $K_2' \cos^2 \theta$ are also being investigated.

This technique is of prime interest as it would provide with a method to obtain a numerical value for the surface anisotropy of small magnetic particles, which has been a very difficult task to date.

(*) During the writing of this thesis, it was observed that in the work by Hanson et al. [1993] there was a double misprint in Eqs. 8 and 9 (see Hanson [1993]). The argument of the bar-modified Bessel functions (Eq. 6) is not $(A \sin \lambda)$ but $(A \sin \lambda \sin \beta)$. Also, there is a sinβ missing in the integrand of both equations (8 and 9). The results, however, are calculated with the correct argument [Hanson (1999), private communication].

5.2.2. Effects of particle size on the magnetisation curve

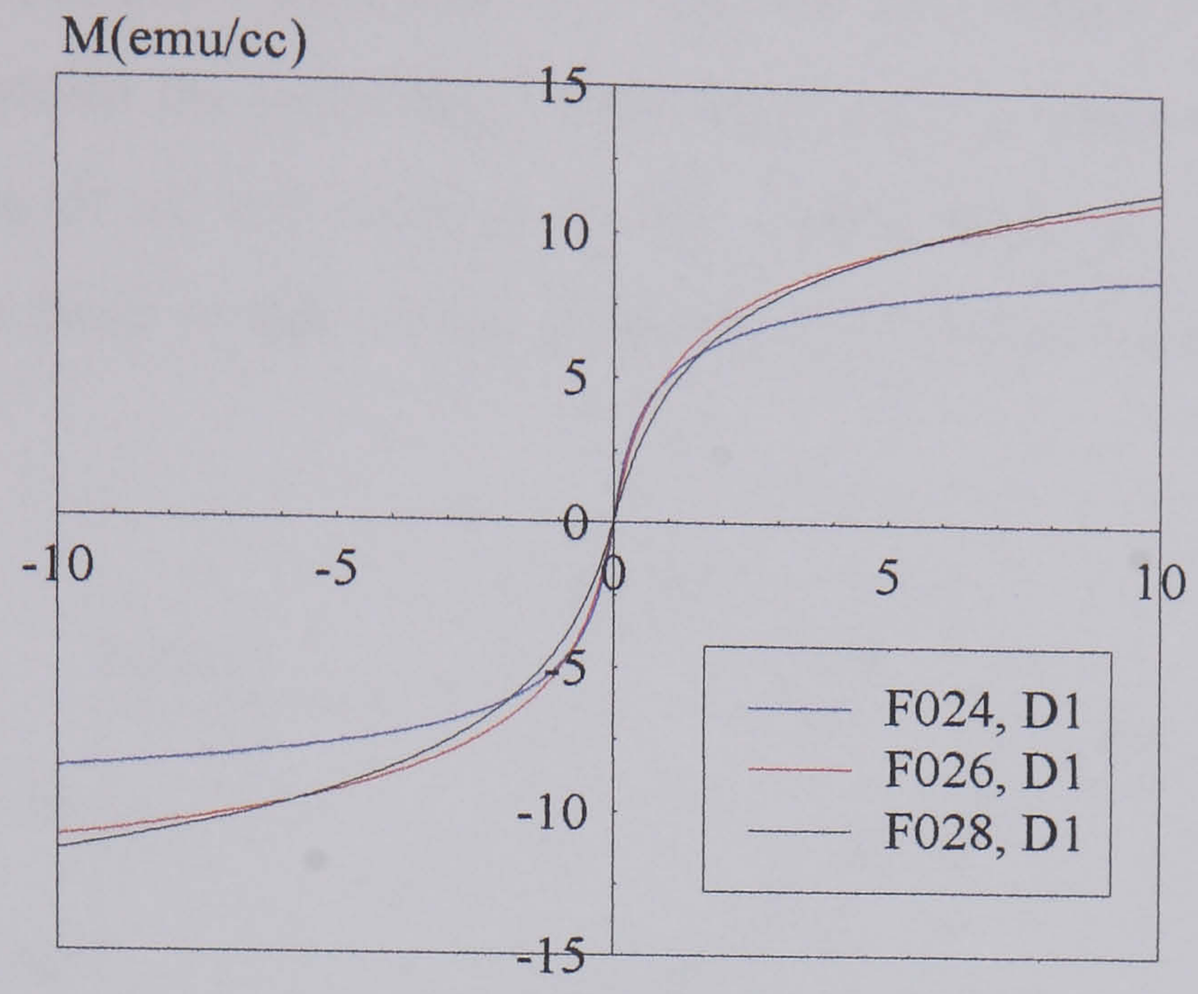

Figure 5-3

Influence of the particle size on the shape of the magnetisation curves.

As particle size decreases, the saturation is much more difficult to approach. This is expected as the randomising effects of temperature will be much more effective for the smaller particles, at a constant temperature. Also, as observed in ✣5.2.1, the smaller particles seem to present a stronger influence of a surface effect, manifest as a steeper slope at high fields in the experimental magnetisation curves, compared to the expected theoretical curves. However, with only the comparison of the magnetisation curves for different particle sizes, nothing can be said about this effect.

5.2.3. Effects of interactions on the magnetisation curve

It has been predicted theoretically and observed experimentally [Bradbury et al. (1985)] for weakly interacting ($\varepsilon < 10\%$) systems that the presence of interactions will deviate the magnetisation of a superparamagnetic sample from its Langevin behaviour. This effect will only be apparent at low fields and in the systems used in this chapter it is only obvious for F024; for the other two samples (F026 and F028), the effect of a strong anisotropy seems to be dominant in all field ranges. Also, as reported by Menear et al. [1983, 1984] and Bradbury et al. [1985], the effects of interactions decrease as particle size is reduced.

According to Bradbury et al. [1985], who studied the effect of interactions in weakly interacting systems ($\varepsilon < 10\%$) using a 2D Montecarlo model, dipolar interactions will

make the experimental data (interacting system) lie *above* the theoretical predictions for relatively low fields ($H \leq 500\ Oe$), which is the case for sample F024 (Fig. 5-4). In a weakly interacting system the long-range order disappears for particle diameters smaller than 100Å (the case of all the samples in this thesis); thus, the enhancement in the magnetisation of the fluid is due to the relatively short range character of the dipolar interaction.

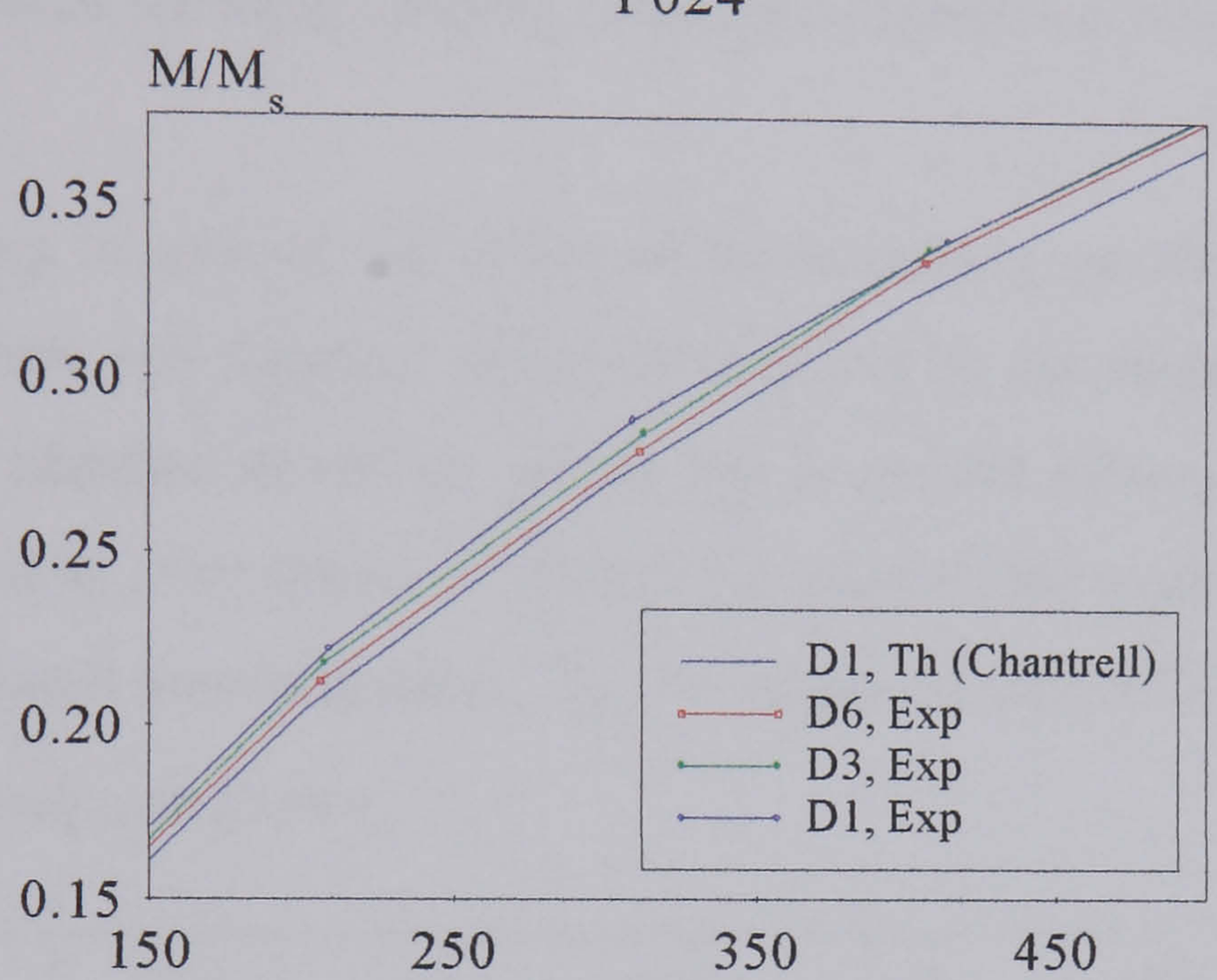

Figure 5-4

Theoretical Langevin curve compared to the experimental data obtained for different dilutions, D1, D3 and D6, of sample F024.

Menear et al. [1983, 1984] investigated the degree of spatial ordering within a system of small magnetic particles in the form of a colloidal suspension via a spatial distribution function (SDF) [Chantrell et al. (1980)] and by evaluating the mean nearest neighbour distances. They concluded that in zero applied field, only dimers and trimers are present in the system, and chains of five or more particles are not. When a field is applied to the system, it aligns the magnetic moments (dimers and trimers) thereby increasing the attractive interaction energy between particles, as shown in ✣2.5.1.1.a. These authors [Menear et al. (1984)] also found evidence of a limited increase in average interaction energy with applied field, the effect being more pronounced for the larger particle sizes ($D_{vm} = 75$ Å). Although large scale field-induced agglomeration has been observed by some authors [Peterson and Krueger (1977), Krueger (1979), Hayes et al. (1975, 1977)] it was not evident in these Montecarlo results, possibly because of the small particle sizes

involved. For higher fields ($H > 500\ Oe$), the effects of interactions are overcome by the effect of the applied field, as observed in these ferrofluids.

Although the enhancement of magnetisation has been observed and explained, the only theoretical model that seems to predict and explain this effect is the one by Bradbury et al. [1985]. The results given by this 2D model were confirmed by Martin [1992] using a 3D replica of the previous model. In any case, these corrections would only account for the low field effect, which for these samples seems less significant than the effect at medium and high fields.

It is also interesting to analyse the effect of concentration on the determination of the magnetic particle size and standard deviation obtained by the method of Chantrell et al., especially, on the standard deviation, which has been said [Menear et al. (1984)] to be particularly affected by interactions. In Tables 5-4 and 5-5, the median diameters, standard deviations and reduced susceptibilities, $\overline{\chi}_i$, for different concentrations of samples F024 and F028, respectively, are shown.

	D1	*D3*	*D4*	*D5*	*D6*	*D12*	*D24*
D_{vm}(Å) ±2	77	77	77	78	76	77	80
σ_v ±0.02	0.42	0.41	0.39	0.38	0.41	0.40	0.39
$(\overline{\chi}_i \pm 0.03)10^{-3}\,\mathrm{Oe}^{-1}$	1.42	1.38	1.30	1.30	1.28	1.35	1.42

Table 5-4

Parameters obtained using the method of Chantrell et al. for different dilutions of sample F024.

	D1	*D3*	*D4*	*D6*	*D12*	*D24*
D_{vm}(Å) ±2	59	58	58	57	58	59
σ_v ±0.02	0.38	0.36	0.35	0.35	0.35	0.36
$(\overline{\chi}_i \pm 0.1)10^{-4}\,\mathrm{Oe}^{-1}$	5.4	5.0	4.8	4.5	4.5	5.0

Table 5-5

Parameters obtained using the method of Chantrell et al. for different dilutions of sample F028.

Although the parameters obtained by the method of Chantrell et al. are somehow modified depending on the concentration of the samples, no definitive conclusions can be drawn about the influence of interactions on these calculations. However, there seems to be an increase of particle diameter for the more diluted samples (D12 and D24 in F24, and D24

in F028). Although it is not significant, it could indicate some agglomeration of the particles caused by a partial loss of surfactant due to the extreme dilution. This seems to be confirmed by the increased values of reduced initial susceptibility, $\overline{\chi}_i$, for D12 and D24(*), as $\overline{\chi}_i$ is dominated by the largest particle sizes [O'Grady et al. (1986), Holmes et al.(1990)].

The initial susceptibility, $\overline{\chi}_i$, seems to decrease as the concentration is lowered (up to D6), which leads to a similar variation in σ_v (see Appendix I). This behaviour is consistent with the local order effects existing in weakly dipolar interacting systems, explained in the previous paragraph. Similar results were predicted by Martin [1992] using a 3D Montecarlo model for a ferrofluid of *Co* particles, in the weakly interacting regime. In his work, Martin finds a decrease in $\overline{\chi}_i$ with decreasing concentration; also, he suggests that there is no evidence of a reduced $\overline{\chi}_i$ due to the formation of flux closure rings.

At lower temperatures, the shape of the magnetisation curve is indeed affected by interactions as is the coercivity and the remanence to saturation ratio, as shown in ✣5.7; however, at these low temperatures, the systems are far from the superparamagnetic state, which is the subject of this section.

5.3. Physical particle size

Samples F024 (D1), F026 (D1) and F028 (D1) have been subjected to physical size analysis. In ✣5.3.1, electron microscope micrographs are presented, which give the physical size of the particles. In ✣5.3.2, X-ray diffraction bears information about the mean crystallite sizes.

5.3.1. Transmission Electron Microscopy (TEM)

The study of the physical particle size has been done analysing TEM images (Fig. 5-6) using a Zeiss analyser, as described in ✣3.5. The particles, in the 3 ferrofluids used for the work, have decreasing particle sizes which follow a lognormal distribution function [O'Grady and Bradbury (1983)], i.e., the logarithm of the diameter follows a normal distribution function,

---

(*)Sedimentometer measurements do not seem to indicate any agglomeration upon dilution; although the agglomerates may well be small enough so as not to sediment in a gravitational field, inducing no change in the sedimentation data.

$$f(D)d(D) = \frac{1}{\sqrt{2\pi}\sigma D} e^{-\frac{(\ln(D)-\mu)^2}{2\sigma^2}} dD \qquad \textbf{(Eq. 5.2)}$$

where D is the diameter of the particle, σ the standard deviation of the logarithm of the diameters and μ is defined as $\mu = \overline{\ln(D)}$.

The values used to obtain the fit described by Eq. 5.2, are not comparable with those obtained from magnetic data, since the parameters $\overline{\ln(D)}$ and σ characterise the distribution of the logarithms of diameters and not the diameters. In this manner,

$$D_p = e^{\mu} \qquad \textbf{(Eq. 5.3)}$$

where D_p is the median diameter of the distribution of particle sizes.

If a volume distribution is required, as is the case for the interpretation of magnetic data, then it can be shown that,

$$\sigma_v = \sigma\,,\; D_{vp} = D_p e^{3\sigma^2} \qquad \textbf{(Eq. 5.4)}$$

where D_{vp} is the diameter associated with the median volume.

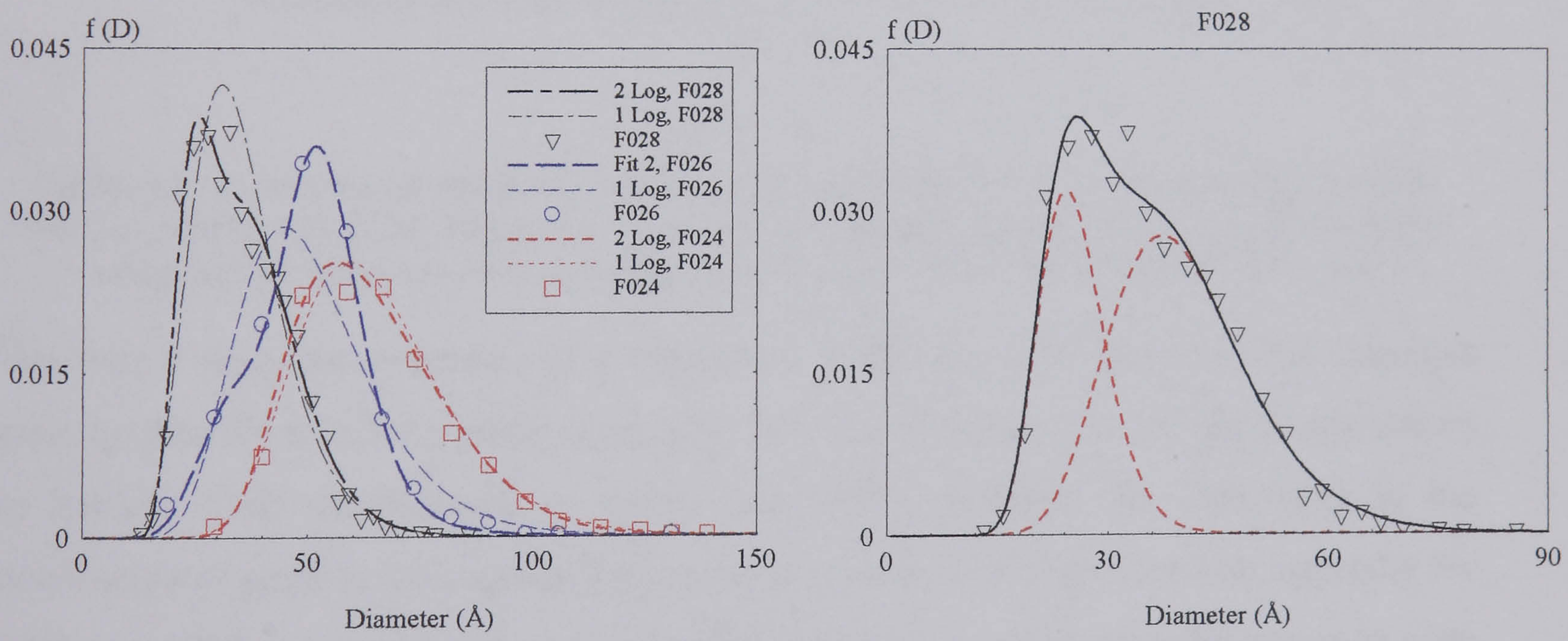

Figure 5-5

Particle size analysis from TEM micrographs for the 3 samples, as a function of the diameter (a). Fig. 5-5 (b) shows the bimodal behaviour in sample F028.

SAMPLE	D_p (Å), σ	D_{p1} (Å), σ_1 , D_{p2} (Å), σ_2 (2 Log)	Percentage (%)
F024	$D_p = 63 \pm 1$ $\sigma = 0.26 \pm 0.01$	$D_{p1} = 75 \pm 1$ $\sigma_1 = 0.20 \pm 0.01$ $D_{p2} = 55 \pm 1$ $\sigma_2 = 0.21 \pm 0.04$	40 % 60 %
F026	$D_p = 49 \pm 1$ $\sigma = 0.30 \pm 0.02$	$D_{p1} = 42 \pm 4$ $\sigma_1 = 0.32 \pm 0.02$ $D_{p2} = 54 \pm 1$ $\sigma_2 = 0.15 \pm 0.02$	47 % 53 %
F028	$D_p = 34 \pm 1$ $\sigma = 0.29 \pm 0.02$	$D_{p1} = 25 \pm 1$ $\sigma_1 = 0.19 \pm 0.04$ $D_{p2} = 40 \pm 3$ $\sigma_2 = 0.24 \pm 0.05$	36 % 74 %

(a)

	Magnetic size	**Physical size**
	D_{vm} (Å) ± 2, $\sigma_v \pm 0.02$	D_{vp} (Å) ± 1, $\sigma_v \pm 0.02$
F024	77, 0.42	77, 0.26
F026	66, 0.41	64, 0.30
F028	59, 0.38	48, 0.29

(b)

Table 5-6

(a) Median diameter and standard deviation of the lognormal distribution of physical particle sizes, as obtained by TEM. Values for single and bimodal distributions are shown. (b) Magnetic and physical diameters corresponding to the median volumes as calculated in Eq. 5.4.

The results show the existence of a *bimodality* in the size distribution, which becomes more evident for smaller particle sizes (Fig. 5-5, b). Although errors in the determination of particle sizes are difficult to assess (see ✣3.5), evidence for bimodality in the distribution of particle sizes arises from the very poor fit to a single function, specially for F026 and F028, as shown in Fig. 5-5. Further evidence for this bimodality seems to arise from the temperature decay of remanence (see ✣5.4.6) studies where a bimodal distribution of energy barriers is observed, presumably due to the bimodality in the physical particle sizes. This effect is particularly evident in sample F028. The data obtained from the particle size analysis are displayed in Table 5-6, with values for a single and a bimodal lognormal distribution functions, for the 3 samples. The reason for the bimodal behaviour is thought to lie in the preparation process of these particles. While the

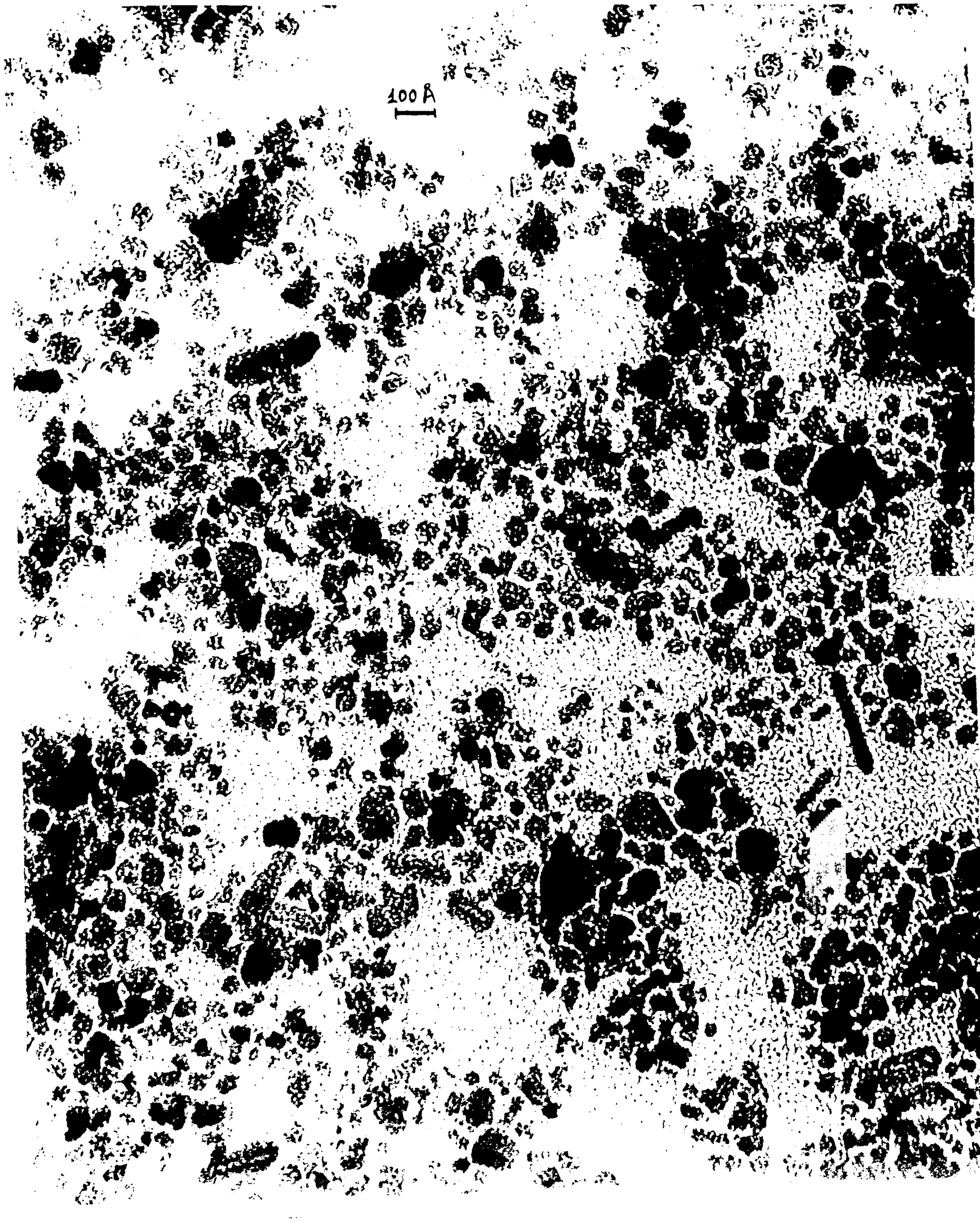

Figure 5-6

TEM micrograph of sample F024

co-precipitation (✣4.1.1) of the two iron salts for the formation of the magnetite particles is taking place, a nucleation process occurs, followed by a growth process possibly including Ostwald ripening, by which the particles grow bigger. While this is happening, surfactant is added to coat the particles, that inhibits the growth process. For the large particle systems (F024), the particles grow to their final sizes almost instantaneously [Davies et al. (1993)], so the addition of the surfactant will not interrupt the growth process, leading to a more uniform single-lognormal distribution of particle sizes, as observed. On the other hand, the smaller particles have a longer growth process, which may have been partially stopped by the introduction of the surfactant. Thus some initial seeds still remain that have not had time to grow, giving way to the bimodality observed. Big agglomerates, which are quite often found in this kind of dispersions, are discarded as having any contribution to the bimodality, as the samples have been filtered using High Gradient Magnetic Separation (HGMS, ✣3.6); in any case the aggregates would have been given a strongest contribution of the larger particles sizes, still not accounting for the 'extra' distribution of smaller sizes.

Particularly for the smaller particles (F026, F028), the bimodal behaviour can be seen quite clearly. In Fig. 5-5, it is shown how 2 lognormal distributions fit the data quite closely, while a single lognormal does not. Following results in other particle systems, different distribution functions (sum of gaussians, lorentzians, gamma...) have also been tried. However the best fit was obtained in all cases with a lognormal or a sum of 2 lognormal distribution functions.

The difference in the magnetic and physical particle sizes (see Table 5-6 *b*), especially for sample F028, is possibly due to an overestimation of the magnetic diameter. This has its origin in the dependency of the magnetic diameter (see Eq. App. 1 in Appendix 1) on two parameters, namely the saturation magnetisation of the sample, M_s, and especially on the parameter $1/H_0$. The fact that due to the small particle size the particles cannot be saturated in a field of 1T gives rise to a erroneously large values $1/H_0$, compared to the values that would be obtained if the systems were near saturation. In the non-saturated system (see Fig. 5-1 *b* and 5-7) the value of $1/H_0$ increases by approximately a factor of 5 compared to the value at saturation, while the value of M_s, in the denominator, increases by approximately a factor of 1.6. Taking both effects into account, and calculating the 6^{th} root (see Eq. App. 1) a value of D_{vm} is obtained which is approximately 1.2 times of the value

expected if the system were be perfectly saturated. This is what is observed for sample F028.

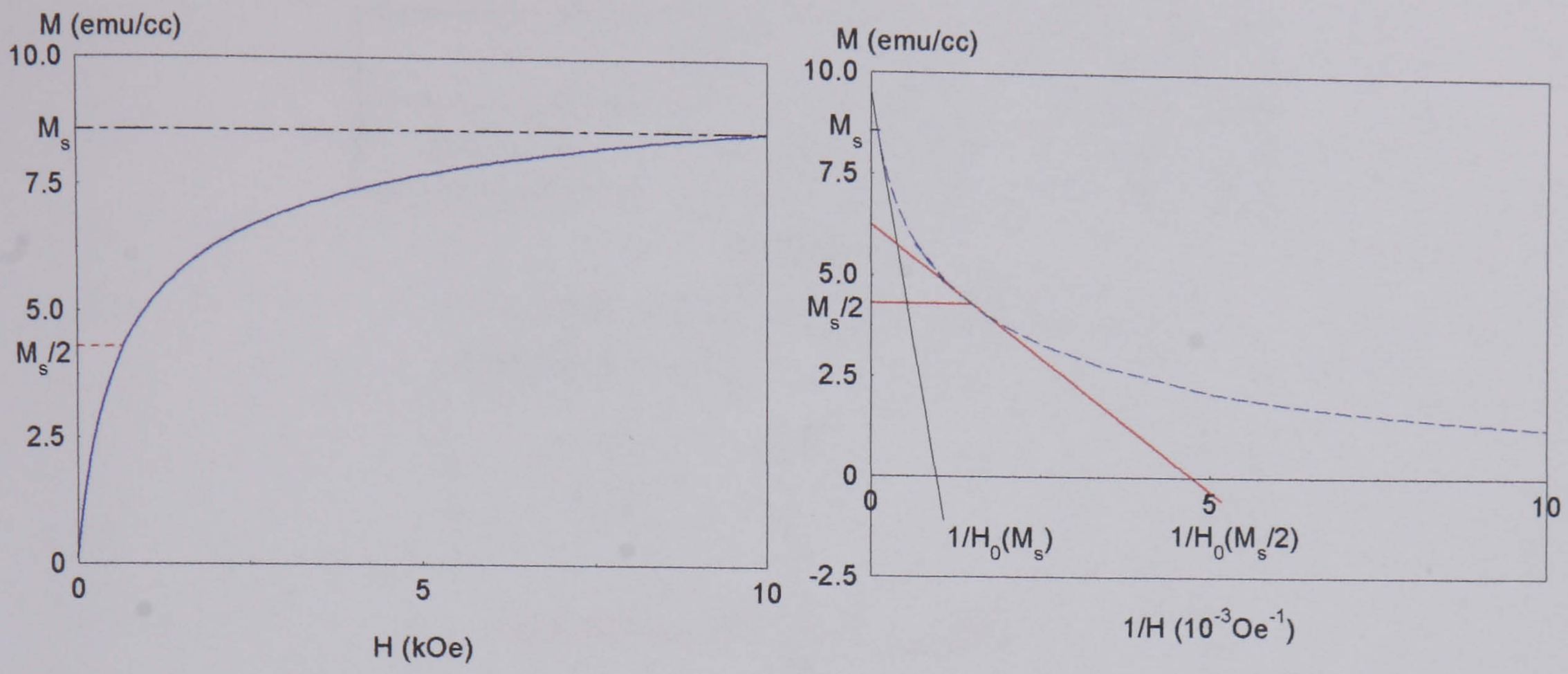

Figure 5-7

(a) Schematic showing the values of the saturation magnetisation, M_s, and $M_s/2$ (far from saturation). Diagram (b) shows how non-saturation ($M_s/2$) has a strong effect in the determination of the parameter $1/H_0$ (Eq. App. 1).

It is interesting to note the presence of some rod-like particles in the F024 samples. These particles are α-FeOOH (goethite) as identified by Sugimoto and Matijevic [1990]. The goethite particles have very little influence on the magnetic measurements performed in this thesis.

5.3.2. X-ray Diffraction

The radiation employed in this work was the CuKα ($E = 8.04keV$, $\lambda = 1.5418$Å). Once the peak (311) has been fitted to a Lorentzian function, the full width at half maximum (FWHM) is directly related to the structural coherence length, i.e., the size of the crystalline part of the particles (assuming them spherical, this length would be the sphere's diameter). The crystal size is obtained from the Scherrer's formula,

$$D = 0.94 \frac{\lambda}{FWHM} \frac{1}{\cos\left(\frac{2\theta}{2}\right)} \qquad \textbf{(Eq. 5.5)}$$

where $\lambda = 1.5418$Å is the incident beam wavelength and 2θ is the angle at the Bragg peak (see ✣3.4). The values for the mean crystallite size in each of the magnetite samples are displayed in Table 5-7 below, which are consistent with the values obtained by TEM

and magnetic size analysis. The X-ray spectra for the different samples are shown in Fig. 5-8.

	F024	**F026**	**F028**
D(Å)	57 ±2	46 ±1	40 ±1

Table 5-6

Crystallite sizes measured by X-ray diffraction

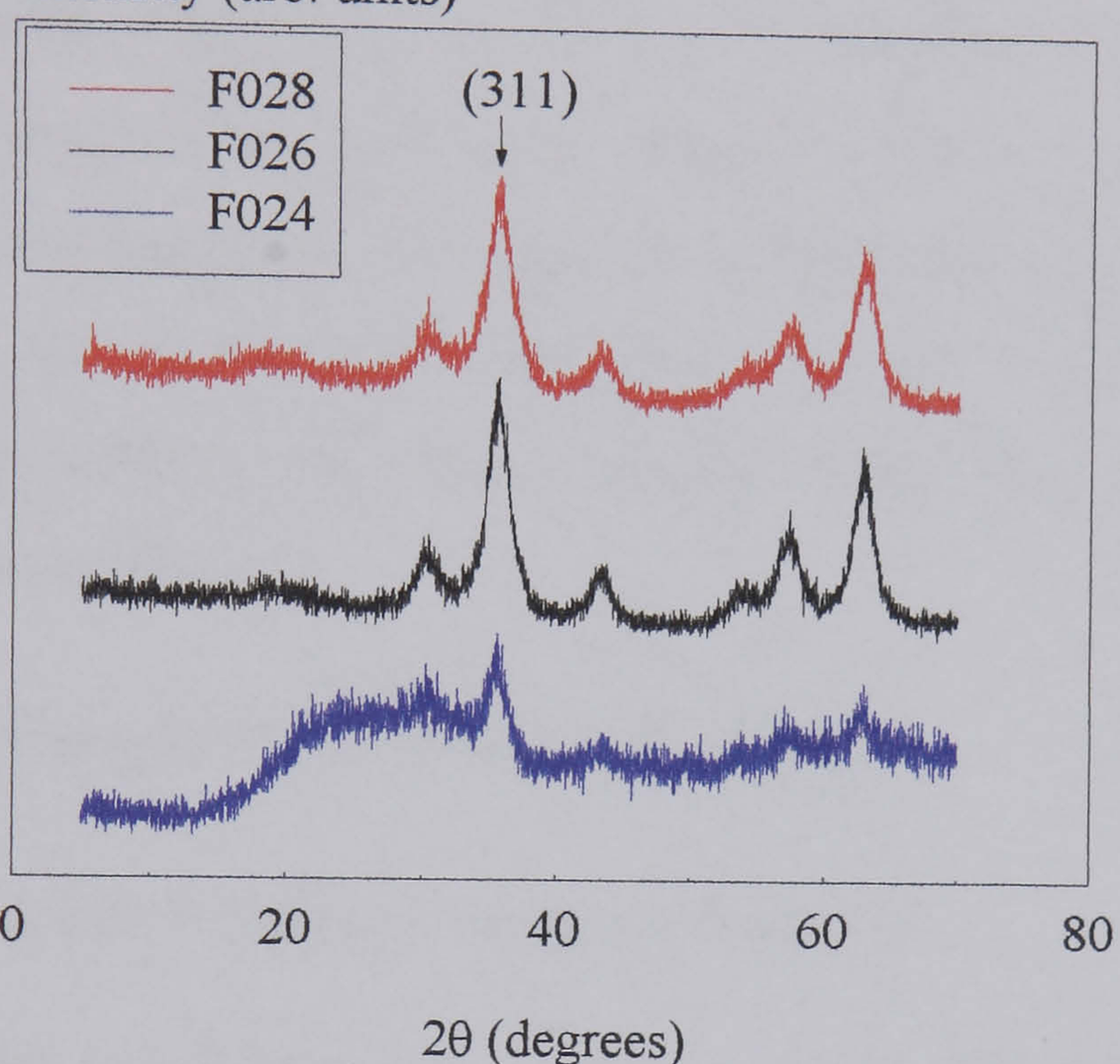

Figure 5-8

X-ray diffraction spectra for samples F024, F026, and F028

There appears to be less crystalline material than TEM and magnetic measurements seem to indicate. This may imply that the surface of these particles is not crystalline, due to the discontinuity that a surface constitutes. Atoms are expected to lie on the surface with no nearest neighbours, giving no contribution to the X-ray diffraction.

A very interesting comparison between the sizes obtained by X-ray diffraction and TEM microscopy is given in the original work by Duvigneaud and Derie [1980] who states that: 'In order to compare the "microscopic" (TEM) and "X-ray" mean particle sizes, one has to keep in mind that the X-rays *see* the particles as multiple unit cells so that the mean crystallite size of a perfect homogeneous sphere is less than its true diameter. It is well known [Guinier (1964)] that $M = 0.67D$, where M is the mean value calculated by X-rays and D is the diameter of the particle observed by TEM. The agreement between the X-ray and microscopic sizes (M / D close to 0.75) confirms that the particles of a sample can be considered as isotropic single crystallites'. This is the case, for example of sample F024,

where $M / D = 57 / 77 = 0.74$. Thus for this sample it can be said that it is constituted by a single crystal of magnetite, and has a surface of around 10Å thick, which is approximately the lattice parameter, 8.39Å, for magnetite. The same conclusions can be drawn for sample F026, where $M / D = 46 / 64 = 0.72$. For sample F028, $M / D = 40 / 48 = 0.83$.

From these measurements the lattice parameter of the crystals can also be estimated. The value obtained is 8.35Å which lies between 8.33Å for bulk maghemite ($\gamma - Fe_2 0_3$) and 8.39Å for bulk magnetite (Fe_3O_4). This value seems reasonable for two reasons; firstly, some oxidation from magnetite to maghemite is expected with time, especially because the samples for the X-ray measurements had to be left to dry in an open atmosphere for more than two weeks. Also, due to the small sizes of the particles, some stresses might have been introduced, thus reducing the lattice spacing, effect that would be especially noticeable near the particle surfaces.

5.4. Temperature Decay of Remanence (TDR)

5.4.1. TDR and the distribution of energy barriers

The Temperature Decay of Remanence (TDR) measures the ratio of remanence to saturation at every temperature (see Fig. 5-9). At each temperature the system is saturated ($H_{sat} = 10kOe$), i.e., all the particle moments are aligned in the direction of the field. Once this field is removed, and depending on the time and temperature of the measurement, some magnetic moments will reverse back to their original easy axis positions (random, in our case) and others will not (blocked). The blocked particles are those which contribute to the remanence. Blocked particles have not been able to overcome their energy barriers to reversal ; thus TDR becomes a direct measurement of the energy barriers in the system [Tari et al. (1979)]. From the Arrhenius-Néel law (✣2.7.1.1),

$$M(t) = M(t=0) \cdot e^{-t/\tau}, \text{ where } \tau = f_0^{-1} e^{\frac{\Delta E}{k_B T}} \qquad \textbf{(Eq. 5.6)}$$

where ΔE is the energy barrier for reversal). Remembering the definition for the blocking temperature (✣2.4.1),

$$T_B = \frac{\Delta E}{k_B . \ln(\tau . f_0)} = (H = 0, \text{ for TDR}) = \frac{K.V}{k_B . \ln(\tau . f_0)} \qquad \textbf{(Eq. 5.7)}$$

it becomes clear that a measurement of the distribution of blocking temperatures, $f(T_B)$, gives a direct measure of the distribution energy barriers, $f(\Delta E)$, in a system [Tari et al. (1979)]. Thus, differentiating the TDR with respect to the temperature (Fig. 5-10),

$$d\left(\frac{M_R}{M_S}\right)\Big/dT \propto f(\Delta E) \propto f\left(T_B\right) \qquad \textbf{(Eq. 5.8)}$$

The TDR and its derivative are presented in Fig. 5-9 and Fig. 5-10, for all sizes, respectively. The fits and derivatives have been obtained using a FORTRAN program that includes NAG subroutines E02BAF, E02BBF, E02BCF and E02BEF. The program computes a weighted least-squares approximation to the experimental data points by a cubic spline. The cubic spline is calculated from its B-spline representation. The first three derivatives are finally evaluated from this B-spline representation.

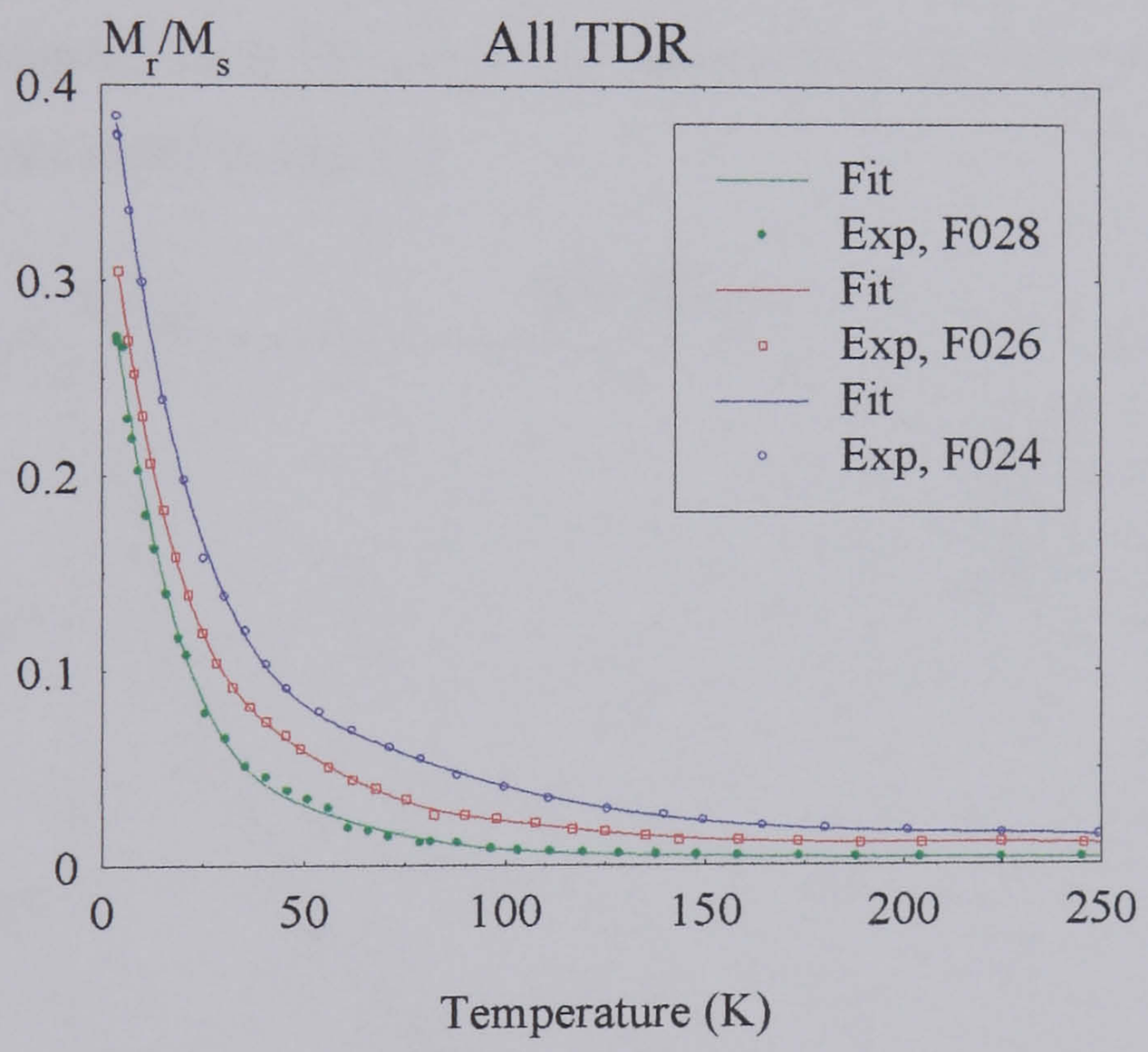

Figure 5-9

TDR for the 3 ferrofluid samples

If the applied field for saturation (here, $H_{sat} = 10kOe$) is not high enough, some of the existing energy barriers of the system (Fig. 5-10) will not be 'seen', because they have not been overcome by the saturating field in the first place (see following section 5.4.2). However, in the particles used for this thesis, 10 kOe is believed to be a high enough field to saturate the spins in the core of the particles ($H_K < 5kOe$, see ✣5.4.5 and ✣5.7.3), while the surfaces will remain canted [Hendriksen et al. (1994 *a*)] (see ✣5.11). Magnetisation curves taken with applied fields up to 8T (✣5.11) show that the slope of

these curves at high fields decreases for very low temperatures (T~4K), which indicates that saturating the surface spins is more difficult at low temperatures; it seems that the diminished thermal effects do not aid the applied field in aligning the surface spins, contrary to what would be expected for the core of the particle. These results are confirmed by Mössbauer data, in which the canting effect was found to decrease with increasing temperature for both small and large applied fields [Hendriksen et al. (1994 *b*), Parker et al. (1993), Morrish et al. (1976)].

For the same saturating field and the same measurement time, the remanence decreases as the temperature rises (see Fig. 5-9), due to the increasing contribution of thermal effects. Similarly, for the same temperature, the particles with smaller size (F026 and F028) will have a lower remanence to saturation ratio compared to the larger particle system (F024) as smaller particles are more susceptible to thermal effects, thus relaxing at lower temperatures, as expected from the simple Arrhenius-Néel law for relaxation (✣2.7.1.1). This can be observed clearly in Fig. 5-9.

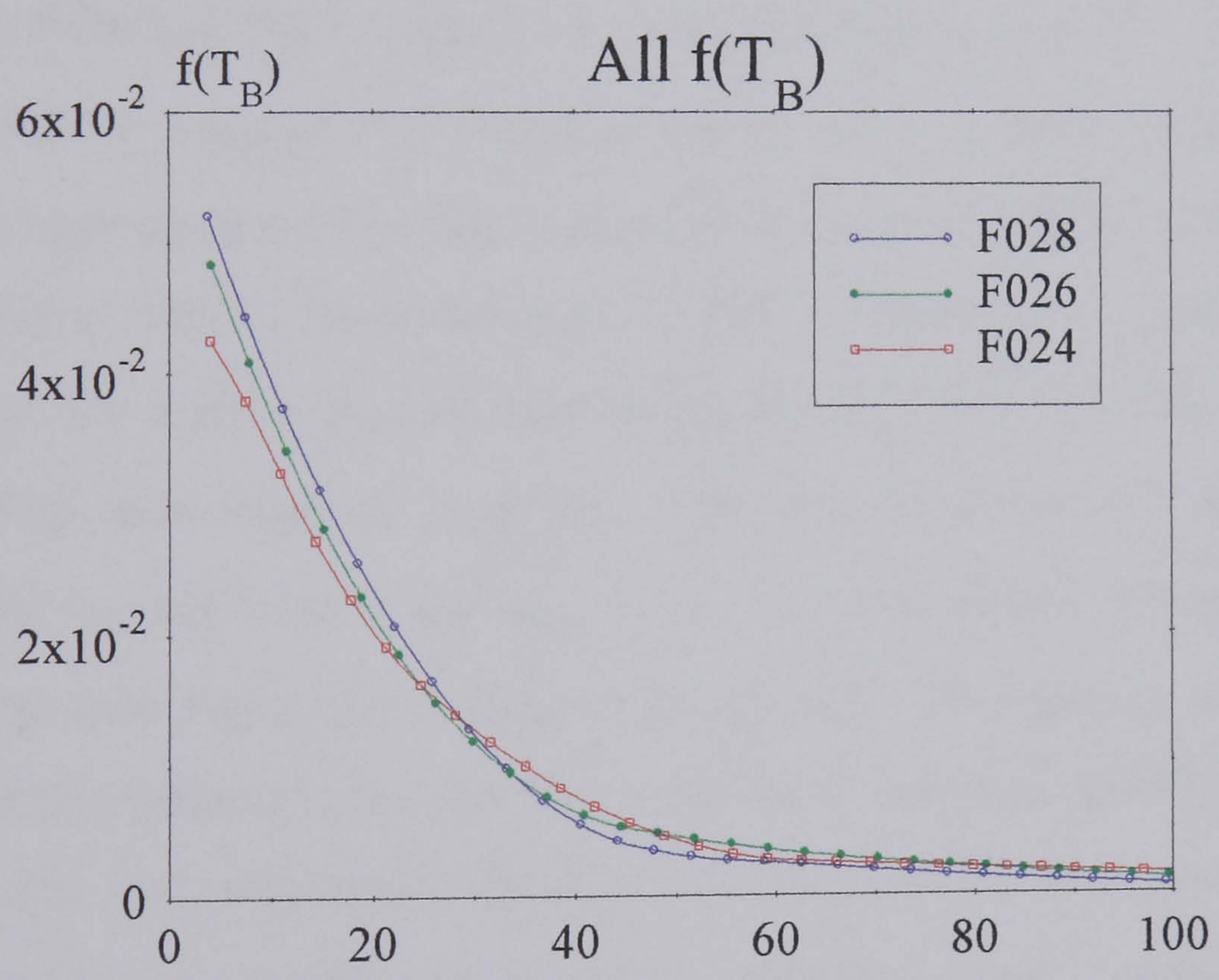

Figure 5-10

Distribution of energy barriers or blocking temperatures, $f(T_B)$ for the 3 samples.

From Fig. 5-10, the distribution of blocking temperatures has been obtained by differentiation of the TDR curve, as indicated in Eq. 5.8. This distribution has been fitted to a lognormal distribution of blocking temperatures and the median and standard deviation of the distributions, for the different particles sizes, are displayed in Table 5-8.

As expected, the systems with smaller particle size present the lower blocking temperatures.

SAMPLE	F024	F026	F028
T_{Bm}(K) ±1	17	16	14
σ ±0.01	1.02	1.08	0.91

Table 5-7

Median blocking temperatures, T_{Bm}, and standard deviation, σ, of the lognormal distribution of blocking temperatures (Fig. 5-10) for the 3 ferrofluid samples.

5.4.2. Non-ideal behaviour of TDR

It is important to emphasise the fact that the results presented in Fig. 5-9 indicate a remanence to saturation ratio of less than 0.5 (Stoner-Wohlfarth value for $T = 0K$) [Stoner and Wohlfarth (1948)]. At $T = 4K$, the values of M_r/M_s are 0.38, 0.30 and 0.27 for samples F024, F026 and F028, respectively; extrapolating to $T = 0K$, M_r/M_s becomes 0.43, 0.35 and 0.33, respectively. This decrease of M_r/M_s with respect to the 'ideal' value has also been observed by other authors [El-Hilo et al. (1990 *a*, 1992 *b*), Luo et al. (1991), Batlle et al. (1993), Hendriksen et al. (1994 *a*), Mørup et al. (1995)]. In the work by Mørup et al. the authors studied maghemite particles (Fe_2O_3) with $D_{vm} = 75$Å and $\sigma = 0.43$ Å. The value obtained to fit the TDR was $M_r/M_s = 0.37$ at $T = 0K$, for a saturation field (H_{sat}) of 1 Tesla, and $T_{Bm} = 17K$, $\sigma = 1.15$, values very similar to those of system F024 in this thesis (see Tables 5-8 and 5-9). The authors do not offer any explanation for this behaviour, but they acknowledge it. Luo et al. [1991] obtained a value of $M_r/M_s = 0.21$ (calculated from the hysteresis loop) at $T = 4.5K$ and for a saturating field $H_{sat} = 5kOe$, in a in a ferrofluid sample containing Fe_3O_4 particles ($D_{vm} = 50$Å, $\sigma = \pm 16$Å).

Obviously, the difference must lie on the fact that the S-W calculations were made for ellipsoidal (uniaxial anisotropy) single-domain particles of the same size, with no surface anisotropy and no interactions, and completely saturated before the remanence is recorded. Thus, there can be several reasons for the deviation from an ideal system,

1. Effects of dipolar interactions,

2. The presence of a microstructure, possibly small aggregates, in the system,

3. Not having a large enough saturating field,

4. The presence of a strong surface anisotropy.

Recent theoretical results by El-Hilo et al. [1998] and Kechrakos et al. [1998] predict a lowering in the remanence to saturation ratio due to the presence of *dipolar interactions*, overall demagnetising in nature. Hadjipanayis and co-workers [1981 *a*, *b*] pointed out that when there are magnetising interactions in the system, $M_r > 0.5M_s$, but if there are demagnetising interactions, $M_r < 0.5M_s$. The reduced M_r is thus evidence for interactions which lead to demagnetising effects.

Chantrell and Coverdale [1996] showed theoretically, for a suspension of magnetic particles, how the presence of a *microstructure* reduces the magnetisation of the system. Calculations were performed on a distributed system of 60 Å median diameter and $\sigma = 0.15$, with 1% packing fraction (see Appendix IV). It is shown that the reduced magnetisation in zero field, M_r/M_s, of the system with a realistic random initial configuration, i.e. with the presence of some microaggregates (see Fig. App-3, *a*) is 53% the value expected for an ideal random system ($M_r/M_s = 0.5$), i.e. 0.265.

An important fact that may have a strong bearing in the diminished value of M_r/M_s is the lack of a large enough saturating field. Measurements of initial magnetisation curves up to $8T$ show that for $T = 8K$, $M_s(1T) = pM_s(8T)$, where $p = 88\%$, 80% and 77% for F024, F026 and F028, respectively. For magnetite particles in a ferrofluid, with higher energy barriers ($T_{Bm} = 32$ and $T_{Bm} = 20$) than those studied in this thesis, El-Hilo et al. [1992 *b*] attributes the 'missing' contribution in the TDR at low temperatures to the lack of a sufficiently large field to saturate the particles with larger energy barriers (see ✣5.4.3).

Another possible reason for the low values of TDR at low temperature is the presence of a *surface anisotropy*. The influence of such an anisotropy may cause a lowering of M_r. As suggested by Aharoni [1987, 1997], the reversal mechanisms of particles with a non-negligible surface anisotropy, may go from coherent to non-coherent (curling or buckling mode) rotation, which lowers the energy barrier; in other words, the reversal from the saturation direction requires less energy in the presence of surface anisotropy, which would reduce M_r from its expected value, at each temperature. Also, the presence of a

strong surface anisotropy at low temperatures, as suggested by several authors [Hendriksen et al. (1994 a, *b*), Parker et al. (1993)], will make it difficult for the applied field to overcome the energy barriers presented by the system.

As presented here, all dipolar interactions, magnetic microstructure, the insufficiency of the saturating field and surface anisotropy, seem to lead to a reduction in the remanence to saturation ratio. It is difficult to analyse quantitatively how much each mechanism contributes (if anything) to this reduction. A theoretical model including all these effects could help in its quantitative evaluation. In this thesis, the Montecarlo model by El-Hilo et al. [1998] has been utilised (✣5.4.7) in an attempt to draw some light in the physical processes occurring in these systems

5.4.3. Theoretical predictions [Tari et al., 1979]

Following from Eq. 5.8, the TDR can be 'recovered' from the distribution of blocking temperatures [Tari et al. (1979), El-Hilo et al. (1992 *b*)] as,

$$\frac{M_r(T)}{M_s(T)} = 0.5 \int_{T/T_{Bm}}^{\infty} f(T_R) dT_R \text{, where } T_R = T / T_{Bm} \qquad \textbf{(Eq. 5.9)}$$

is the reduced blocking temperature and $f(T_R)$ the distribution of reduced blocking temperatures. This technique has also been used by other authors [e.g. Mørup et al. (1995)] to obtain T_{Bm} and σ in maghemite particles. In Fig. 5-11 a, b, c, M_r / M_s is calculated from the $f(T_B)$ (Fig. 5-10) as obtained from the differentiation of the TDR measurements (Fig. 5-9), using Eq. 5.9. In Fig. 5-11 a', b' and c', the values of $f(T_B)$ used were obtained from the experimental TDR corrected so that $M_r / M_s(T = 0\,K) = 0.5$. The parameters obtained are displayed in Table 5-9, below.

For $T > 70K$ both the theoretical and experimental TDR are very close (both in a, b, c and a', b', c'). For $T < 70K$, the values of the experimental M_r / M_s (a, b, c) lie below those calculated from Eq. 5.9. For $T > 70K$ the temperature is rather high and all the energy barriers present in the system are easily overcome with the saturating field available ($10kOe$), thus all the particles in the system contribute to the remanence. Also, at these higher temperatures the thermal effects possibly dominate any other effects, such as the effect of dipolar interactions or surface anisotropy, described in ✣5.4.2. As the temperature

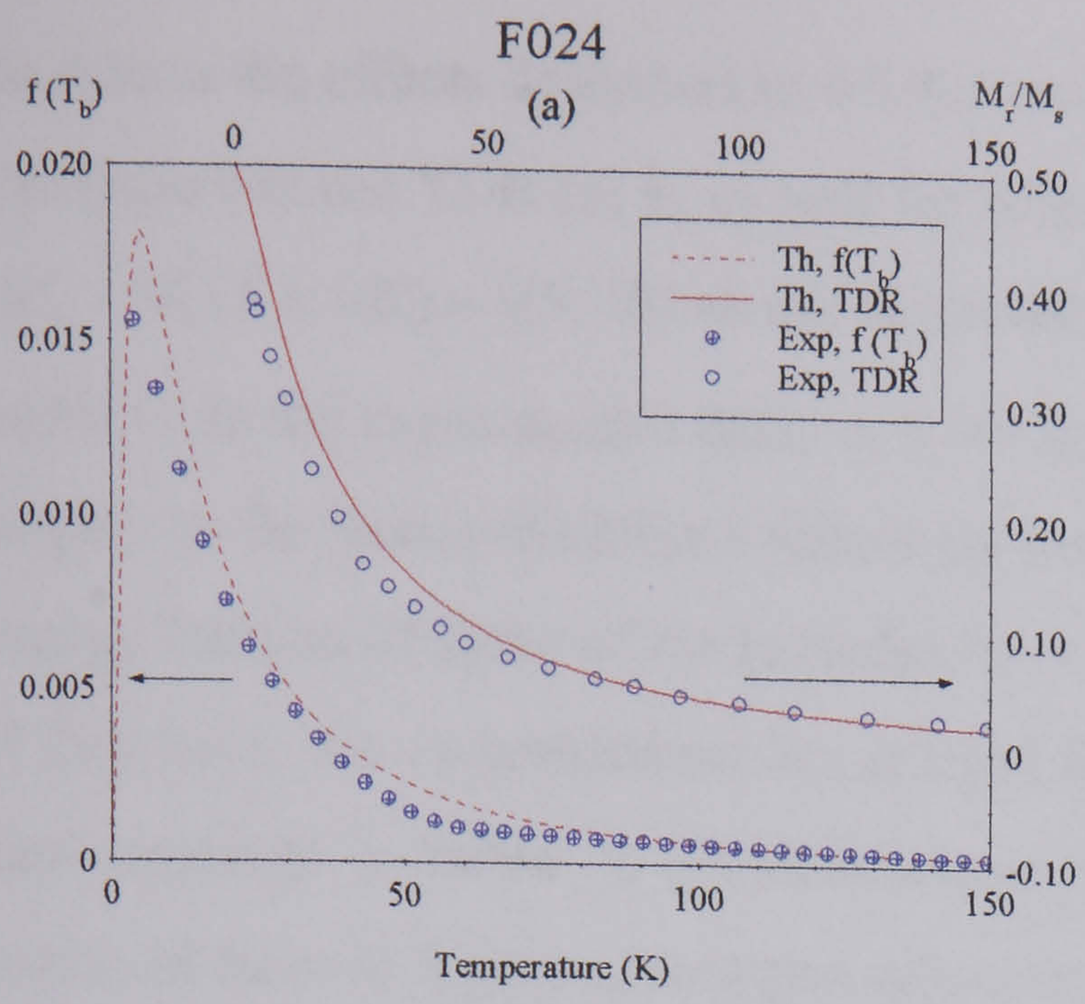

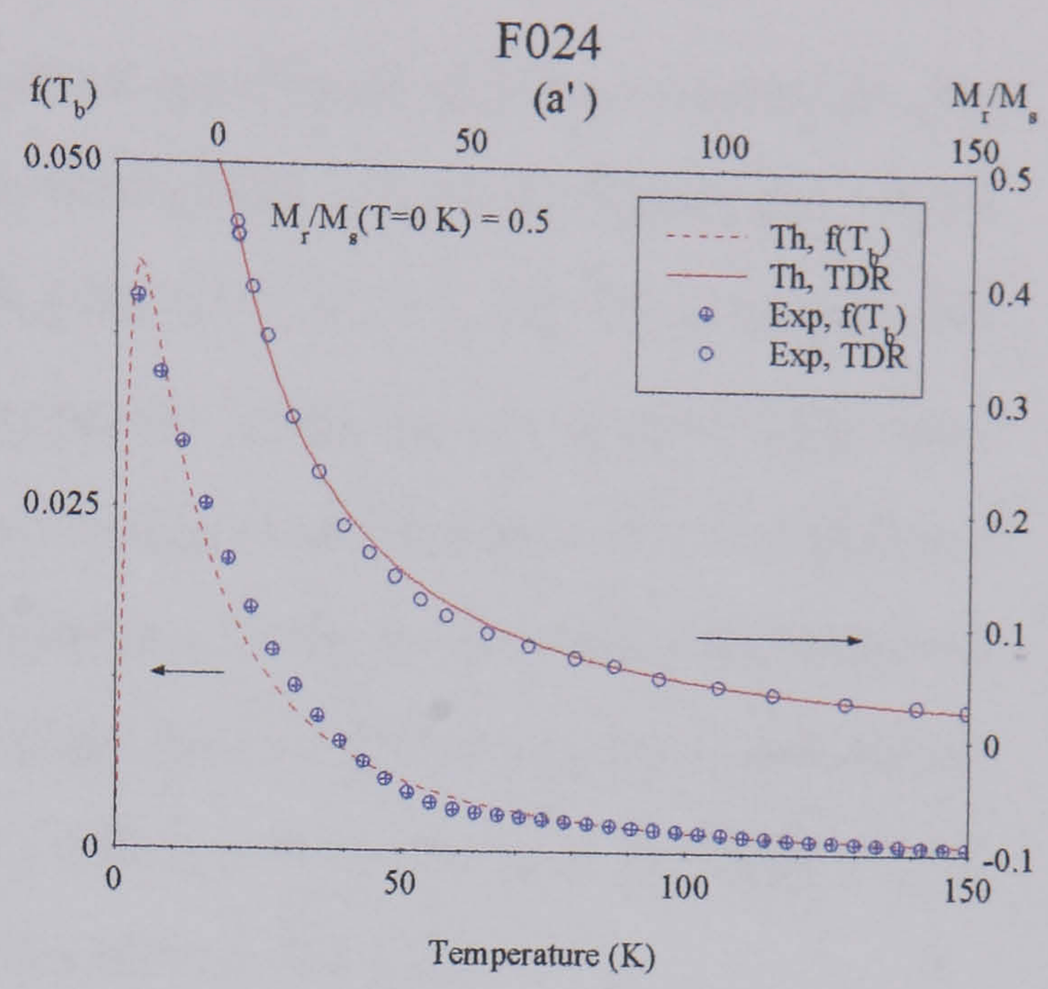

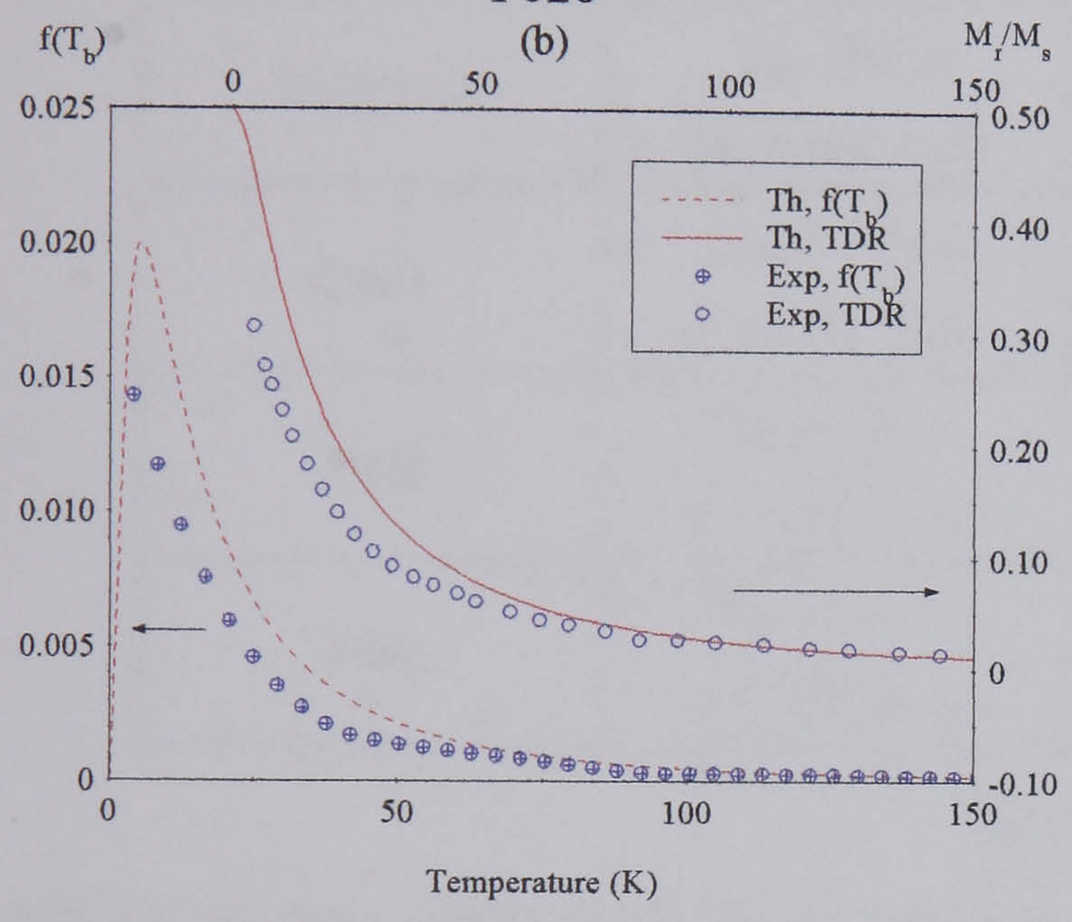

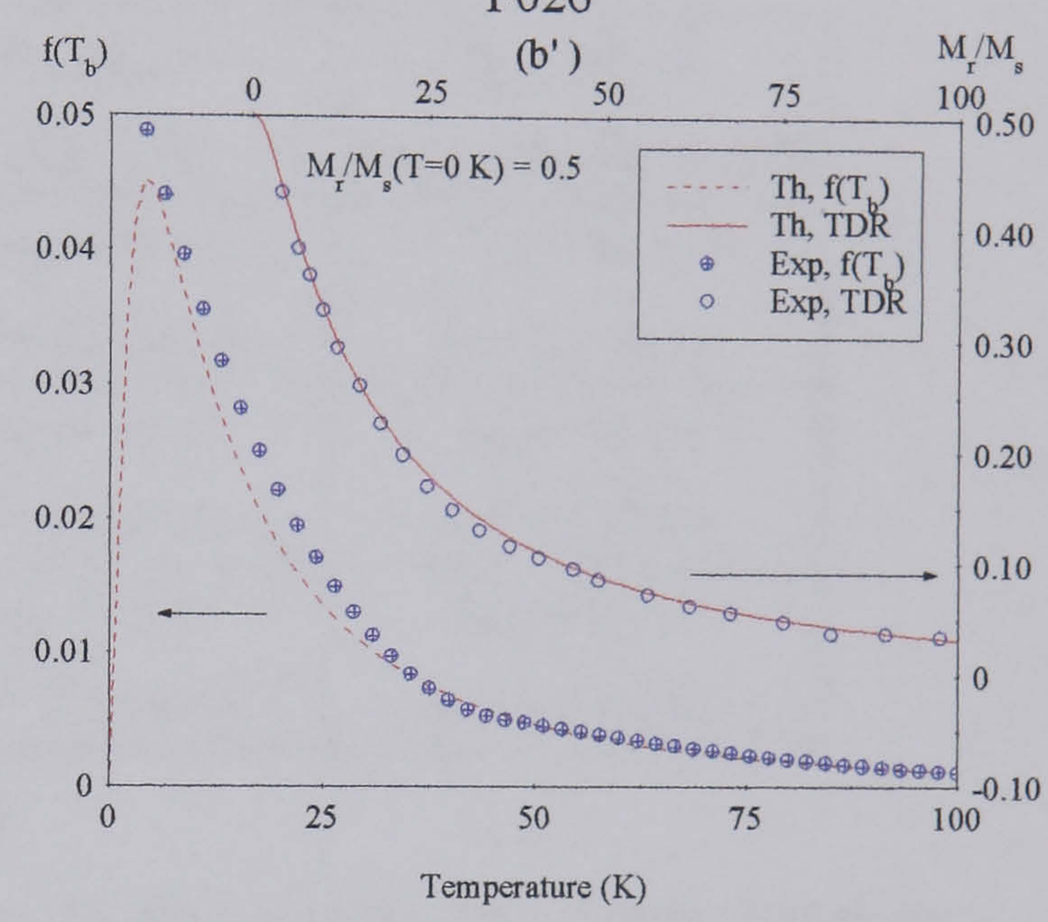

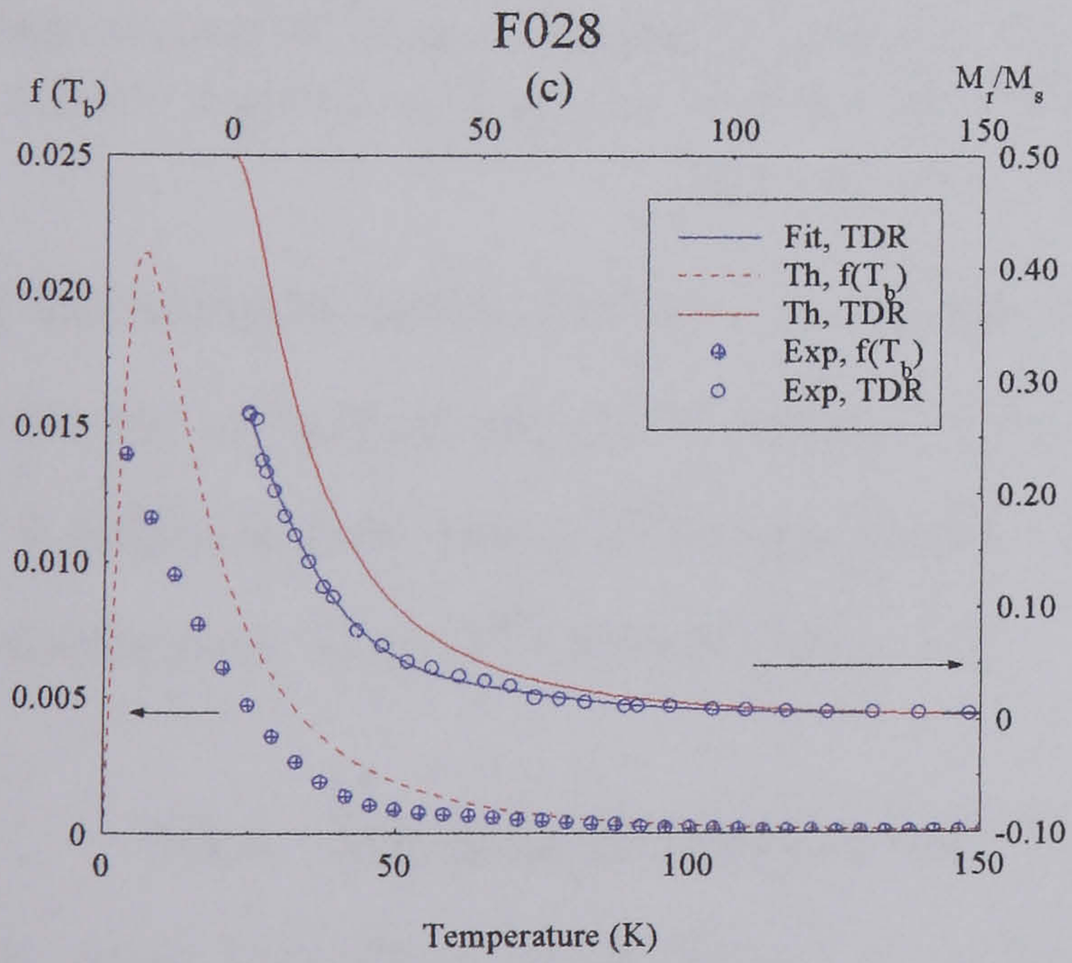

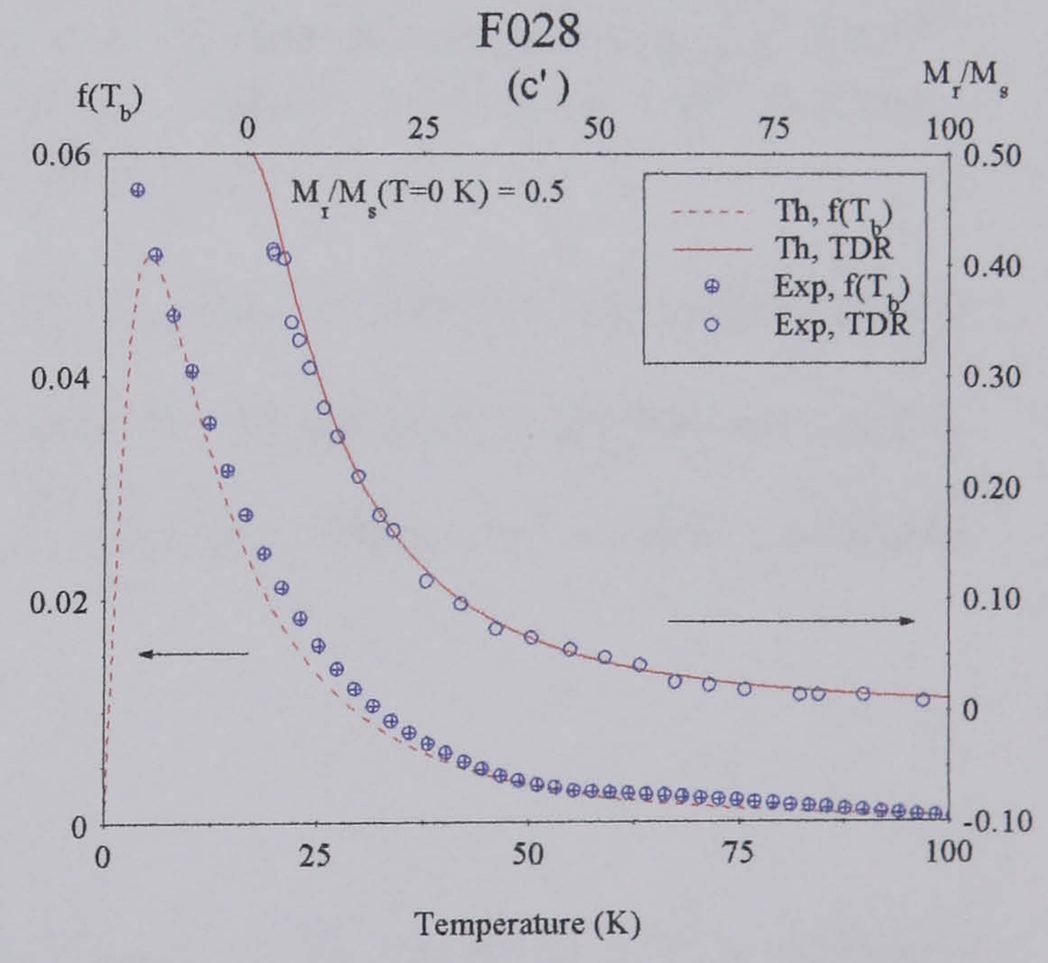

Figures 5-11

Theoretical(Th) curves (TDR and $f(T_b)$) for the 3 particle sizes, using Eq. 5.9 are obtained. In a, b and c the "Exp" curves are the experimental TDR curves, as measured. In a', b' and c', "Exp" represents the experimental TDR corrected so that $M_r / M_s(T = 0\ K) = 0.5$.

decreases the effects described in ✣5.4.2 become more significant and it is reasonable that the experimental TDR (a, b, c) will lie below the theoretical values predicted, for which $M_r / M_s(T = 0K) = 0.5$. When the corrected TDR is used (a', b', c'), Eq. 5.9 gives a much better fit to the experimental data, as it would be expected. Thus the decrease of TDR with respect to the Stoner-Wohlfarth values for low temperatures may be due to the fact that the energy barriers of some of the particles have not been overcome by the saturating field, or if they have, the magnetisation has relaxed faster than 100 sec (TDR measurement time), thus resulting 'invisible' to the measurements. This effect is more obvious for F028 (c), as expected from its higher anisotropy, calculated in the section ✣5.4.5.

SAMPLE	**T_{Bm} (K), σ (as measured)**	**T_{Bm} (K), σ (Eq. 5.9))**	**T_{Bm} (K), σ (exp. Corrected to 0.5)**
F024	T_{Bm} = 17 ±1 σ = 1.02 ±0.01	T_{Bm} = 18 ±2 σ = 1.2 ±0.02	T_{Bm} = 18 ±1 σ = 1.3 ±0.01
F026	T_{Bm} = 16 ±1 σ = 1.08 ±0.01	T_{Bm} = 16 ±2 σ = 1.1 ±0.02	T_{Bm} = 16 ±1 σ = 1.2 ±0.01
F028	T_{Bm} = 14 ±1 σ = 0.91 ±0.01	T_{Bm} = 15 ±3 σ = 0.9 ±0.02	T_{Bm} = 13 ±1 σ = 1.0 ± 0.01

Table 5-8

Median blocking temperatures and standard deviations for the 3 particle sizes, obtained from the experimental TDR as measured (2nd column, Fig.5-10), from the data as measured via Eq. 5.9 (3rd column, Fig.5-11 a, b, c) and from the data corrected to $M_r / M_s(T = 0\ K) = 0.5$ (3rd column, Fig.5-11 a', b', c') also via Eq. 5.9.

It interesting to notice (Table 5-9) that the values of T_{Bm} and σ do not vary significantly from the experimental fit (2nd column, Table 5-9) and the theoretical calculations via Eq. 5.9 obtained from fitting the experimental TDR (3rd column, Table 5-9) or the corrected experimental TDR (4th column, Table 5-9).

5.4.4. Influence of interactions on TDR

To study the effect of interactions, TDR curves need to be measured for different concentrations. According to El-Hilo et al. [1990, 1992 *b*] the TDR measurements are not susceptible to interactions. The same results are obtained by Mørup et al. [1995] for coated particles in a ferrofluid, while a different behaviour is observed in uncoated particles.

Mørup et al. [1995] studied maghemite particles with a magnetic particle size of 75 Å and standard deviation $\sigma = 0.43$. Measurements were performed on coated and uncoated particles, exerting pressure on the dry powders to study the effect of the interparticle interactions. For the coated particles (Fig. 5-12 *a*), the effect of increasing interparticle distance seems to have no effect on the value of the TDR. However, the uncoated systems show an increase of the remanence as the particles lie closer to each other (Fig. 5-12 *b*). They attribute this behaviour to the effect of strong magnetic interactions that result in the formation of an ordered state with a spin-glass-like structure, a 'super-spin-glass' [Mørup et al. (1983 *b*)].

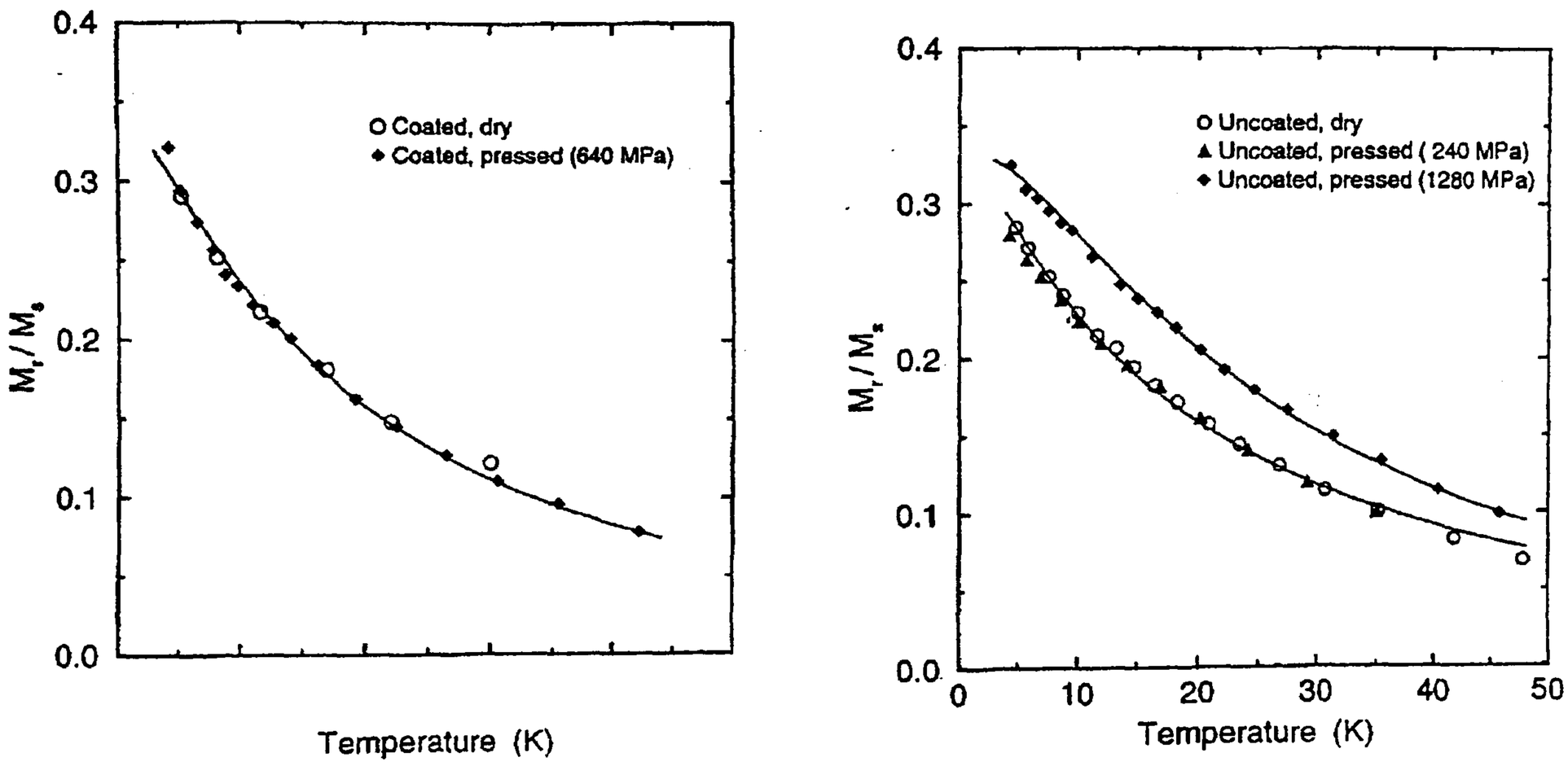

Figure 5-12

Variation of the remanence to saturation ratio with temperature (TDR) for (a) coated and (b) uncoated maghemite particles. The solid lines represent the best fit of the data with a standard decay of remanence model (data extracted from Mørup et al., 1995)

It is interesting to note the results of M_r / M_s obtained for the magnetisation curves at low temperatures (see ✣5.7), which indicate a reduction of the remanence to saturation ratio with increasing concentration. These latter results agree with the theoretical predictions by El-Hilo et al. [1998].

5.4.5. Determination of the effective anisotropy constant, K_{eff}

Following the definition of the blocking temperature given in ✣2.4.1, an effective anisotropy constant of the systems can be calculated using,

$$K_{eff} = \frac{\ln(\tau \cdot f_0) k_B T_{Bm}}{V_m} \qquad \textbf{(Eq. 5.10)}$$

In Table 5-10 below, values for the effective anisotropy constants are calculated, using the median magnetic volume (Table 5-2) and a measurement time $\tau = 100\,\text{sec}$. The value of the attempt frequency, f_0, has been determined in ✣5.10 for the 3 samples, via the method of Dickson et al. [1993 *a*]. The values of the blocking temperatures are given in column 4 of Table 5-9.

	F024	**F026**	**F028**
K_{eff} (10^5erg/cc)	3.3 ±0.2	4.0 ±0.4	4.6 ±0.5
H_{Keff} (Oe)	1650 ±130	2370 ±220	2730 ±280
ΔE_{eff} (10^{-14} erg)	6.6 ±0.1	5.0 ±0.1	5.0 ±0.1

Table 5-9

Effective anisotropy constant, anisotropy field and energy barrier, as extracted from the TDR data.

The anisotropy constant of the smallest particle size is the largest of the three, decreasing as the particles size increases. The origin of this higher anisotropy for smaller particle systems could possible lie in the larger surface/volume ratio of the smaller particle systems (see ✣5.11), as it has also been proposed by Chen and co-workers [1995] and Respaud et al. [1998] to explain the increase in the anisotropy constant as particle size decreases, for coated spherical Co particles with D_m in the range 18 to 40Å. The higher surface anisotropy of the smaller particles is also supported by the deviation from the Langevin behaviour of the room temperature magnetisation curves, especially important for these smaller sizes, as observed in ✣5.2.1.2.

There is no reason to think why the smaller particle systems would have a higher interaction-induced anisotropy, as suggested by some authors [Dormann et al. (1997) p. 322]. Precisely, the contrary is expected from Montecarlo calculations [Menear et al. (1984)] at high temperatures.

5.4.6. Bimodal behaviour

Assuming that the energy barriers are lognormally distributed (based on the lognormal distribution of particle sizes), it has been observed that these samples present a bimodality in the distribution of energy barriers (see Fig. 5-13) [Blanco-Mantecón and O'Grady (1999)]. In Table 5-11, the parameters for the lognormal distributions are displayed, noting the percentage of each distribution for the case of bimodal behaviour.

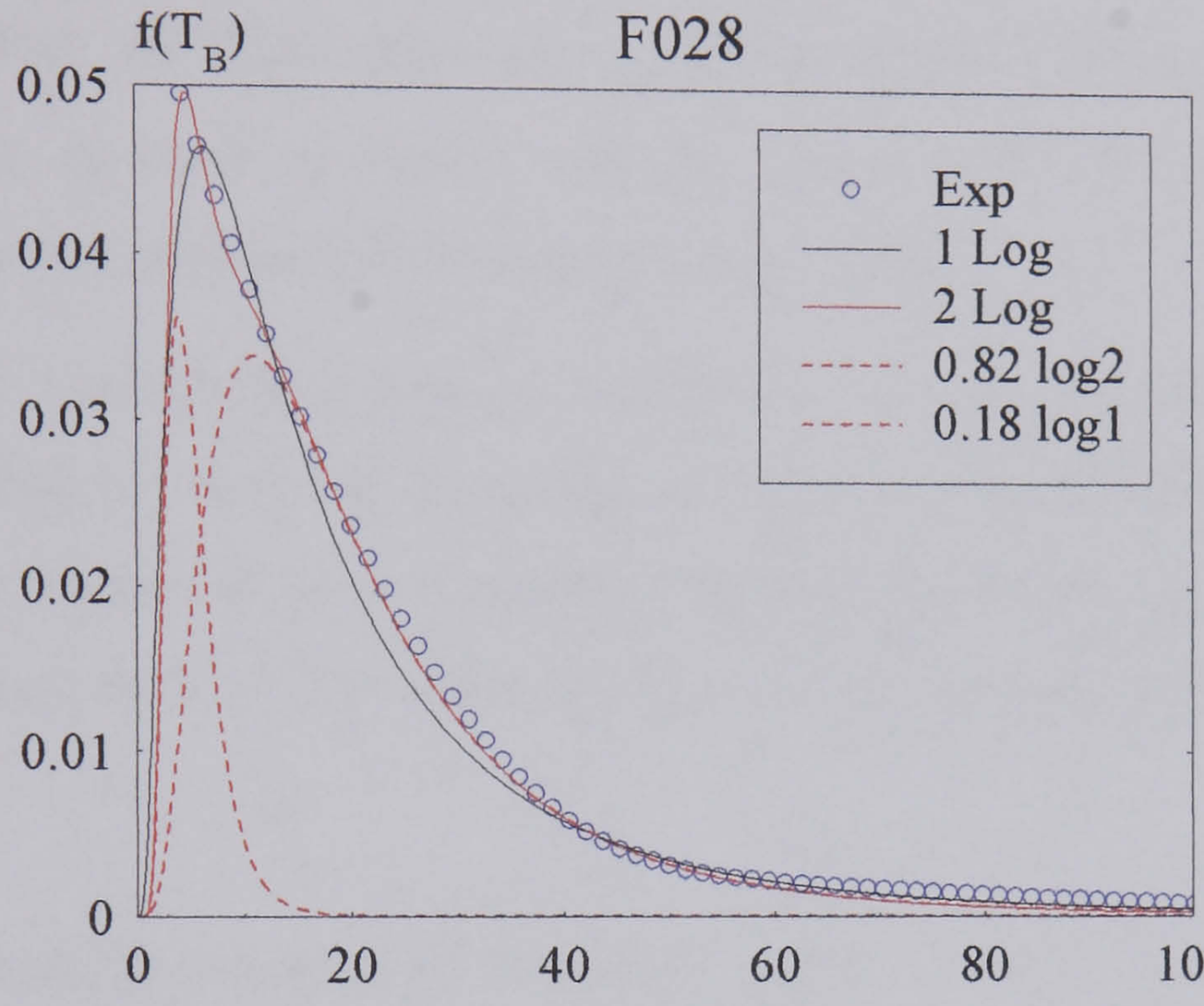

Figure 5-13

Bimodal behaviour of the distribution of energy barriers for sample F028 (59 Å)

SAMPLE	T_{Bm}(K), σ (1 Log)	T_{Bm1}, σ_1 , T_{Bm2}, σ_2 (2 Log)	Percentage (%)
F024	T_{Bm}= 17 ±1 σ = 1.02 ±0.01	T_{Bm1}= 4.7 ±0.1 σ_1 = 0.40 ±0.03 T_{Bm2}= 18.9 ±0.2 σ_2 = 0.91 ±0.01	7% 93%
F026	T_{Bm}= 16 ±1 σ = 1.08 ±0.01	T_{Bm1}= 3.9 ±0.1 σ_1 = 0.33 ±0.03 T_{Bm2}= 16.93 ±0.14 σ_2 = 0.99 ±0.01	3% 97%
F028	T_{Bm}= 14 ±1 σ = 0.91 ±0.01	T_{Bm1}= 4.8 ±0.1 σ_1 = 0.45 ±0.02 T_{Bm2}= 17.8 ±0.2 σ_2 = 0.70 ±0.01	18% 82%

Table 5-10

Median blocking temperatures and standard deviations assuming a single and a bimodal distribution (lognormal) of energy barriers.

The obvious explanation for this bimodality would be the presence of a bimodal distribution in the sizes of the particles, as it has been observed in ✣5.3. Considering the bimodal distribution of physical particle sizes (Table 5-6), the corresponding blocking temperatures have been calculated for each of the median diameters of this bimodal distribution, obtaining blocking temperatures in close agreement with those obtained in the analysis of the $f(T_B)$. For example, in sample F028, $D_{vm1} = 28$ Å (36%) and $D_{vm2} = 47$ Å (74%); for these values the calculated blocking temperatures are 3.2 and 15.5, respectively, in close agreement with the values 4.8K (18%) and 17.8K (82%) obtained from the fitting of the distribution of energy barriers.

For the fitting to a single or a bimodal distribution, a Levenberg-Marquardt algorithm [Press et al. (1988)] has been used, which is a common method for non-linear fitting. It finds the solution iteratively, varying smoothly between the inverse of the Hessian method and steepest-descent method. The value chi-square is used to control the goodness of the fit.

5.4.7. Model predictions [El-Hilo et al., 1998]

The model by El-Hilo et al. [1998] (see Appendix III) has been used in this section to try and reproduce the TDR curves obtained experimentally. Different variables such as anisotropy constant, K, concentration, ε, and the range of the dipolar interaction, R, affect the behaviour of the remanence to saturation ratio, and have been adjusted to fit the experimental results. Fig. 5-14 *a*, *b* and *c* show different results for sample F028, and the best fits for F024 and F028 are presented in Fig. 5-14 (d). Firstly, the qualitative results obtained from the model are going to be revised. Afterwards, a comparison of the theoretical and experimental results is presented.

The effect of concentration is reflected in Fig. 5-14 *a*: the lower the concentration, the lower the values of M_r/M_s, given all the other parameters remain constant. This reduction in the remanence to saturation ratio is stronger for the systems with lower anisotropy, i.e., K=4-6.10^4 erg/cc (see Fig. 5-14 *a*). Also, for the lower anisotropy values, higher concentrations (10%) give a flatter TDR, while lower concentrations (1%, 3%) give steeper curves, closer to the experimental curves. Similar behaviour with anisotropy constant is observed in Fig. 5-14 *b*. Thus, smaller anisotropy constants (~10^4 erg/cc) give steeper curves, closer to the experimental results, for the same interaction range and

concentration. It can also be observed in Fig. 5-14 *b*, that the lower the anisotropy constant the lower the values of M_r/M_s, as would be expected. In Fig. 5-14 *c* it is interesting to note that for ranges up to R=1, the curves are fairly similar, although flatter the larger the range; for R>1 a noticeable difference is observed in the curves, which become much flatter for the higher values of R, also presenting lower values of the remanence to saturation ratio.

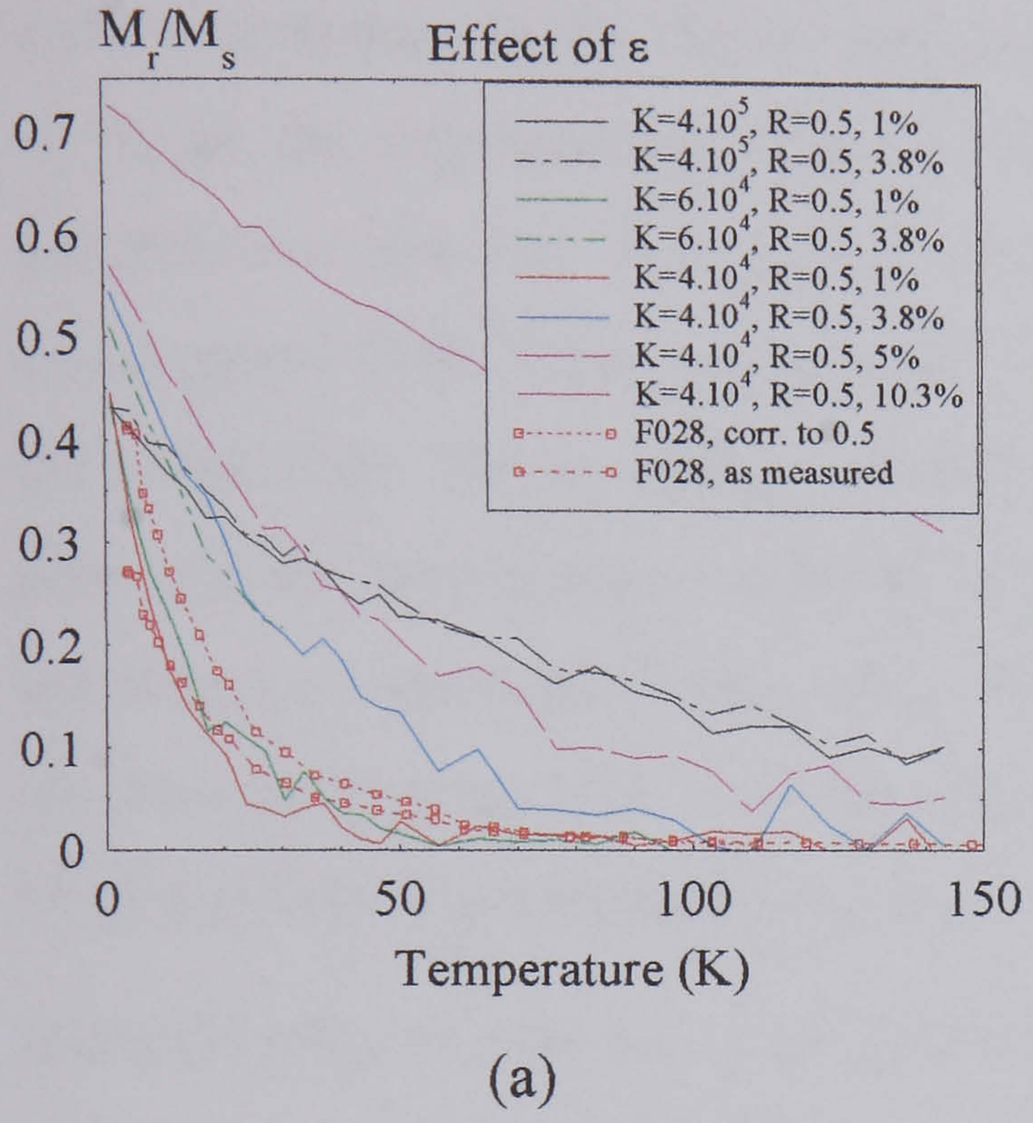

(a)

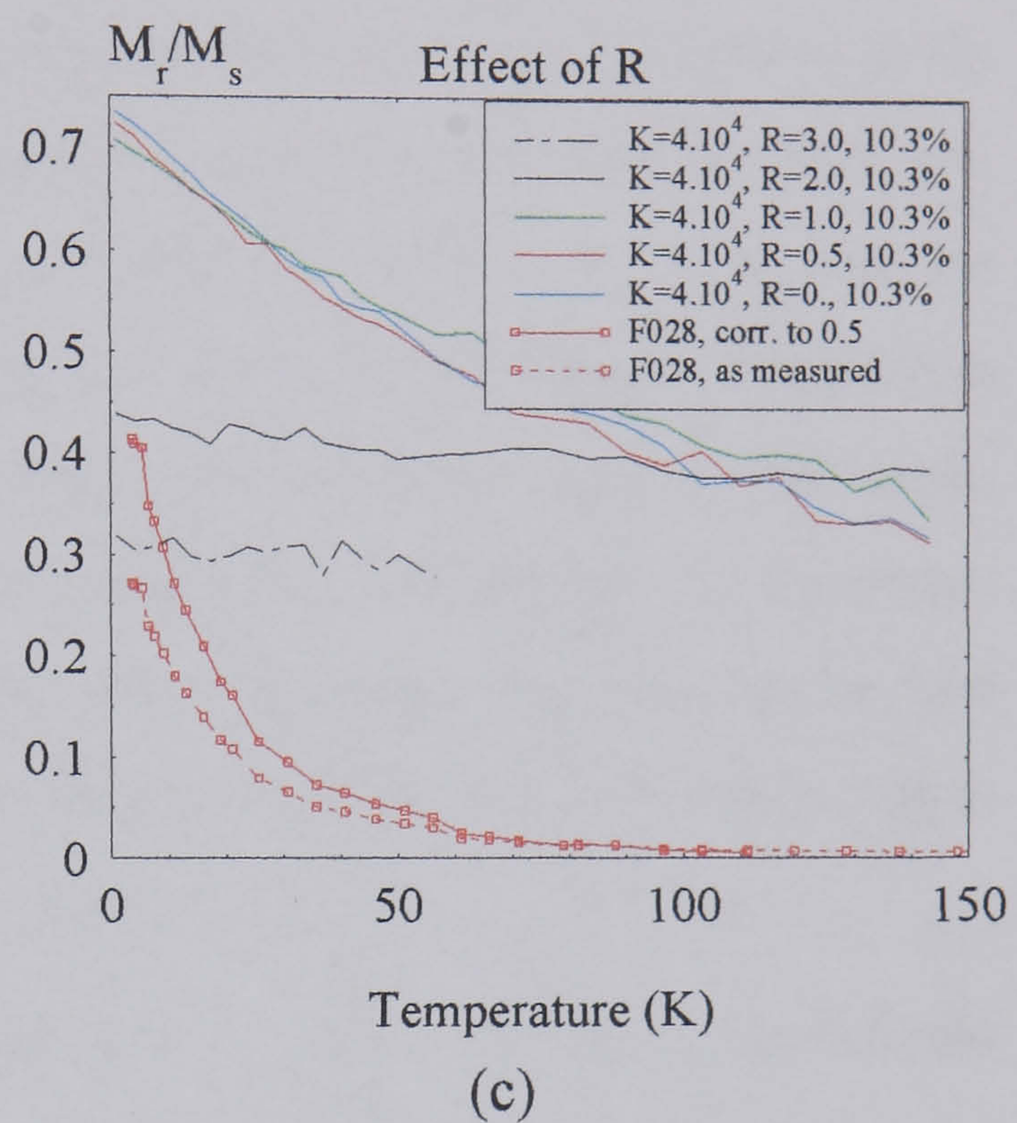

(c)

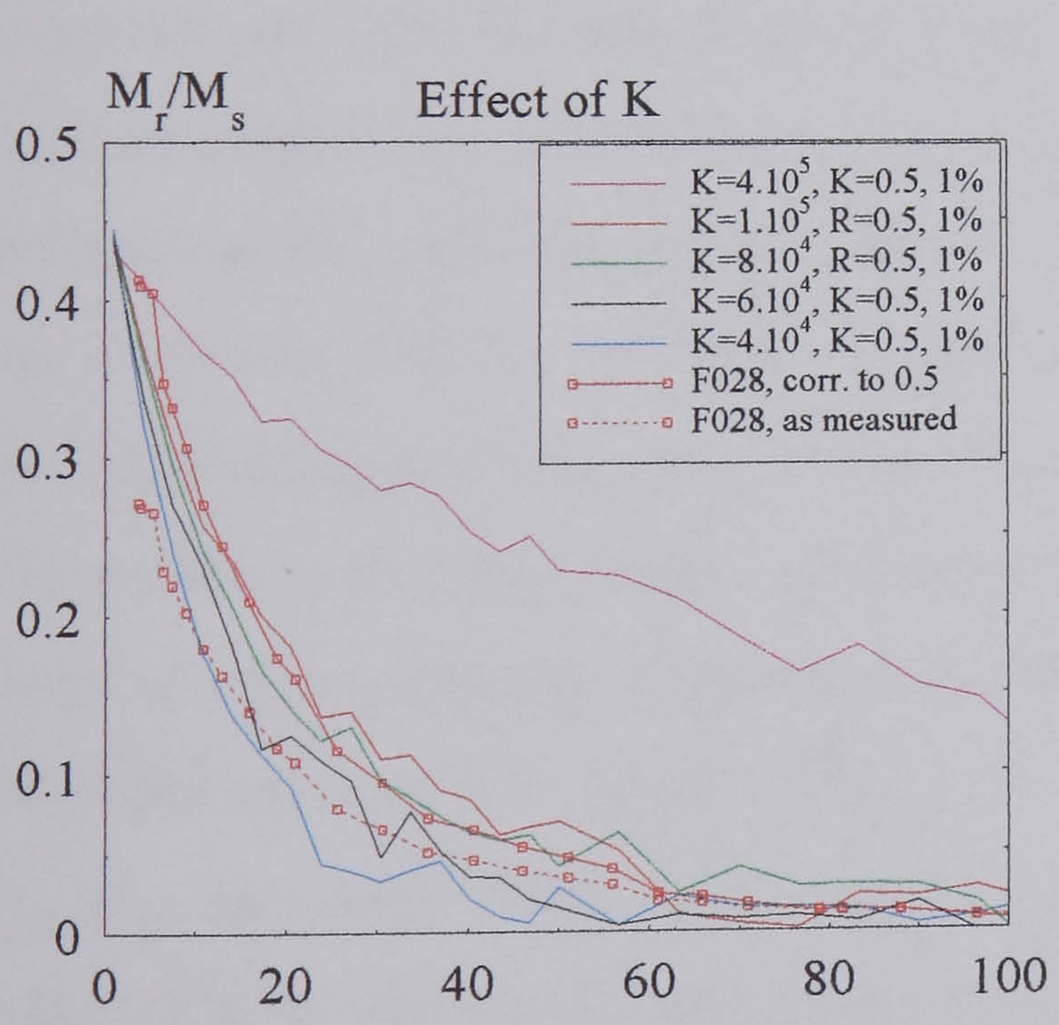

(b)

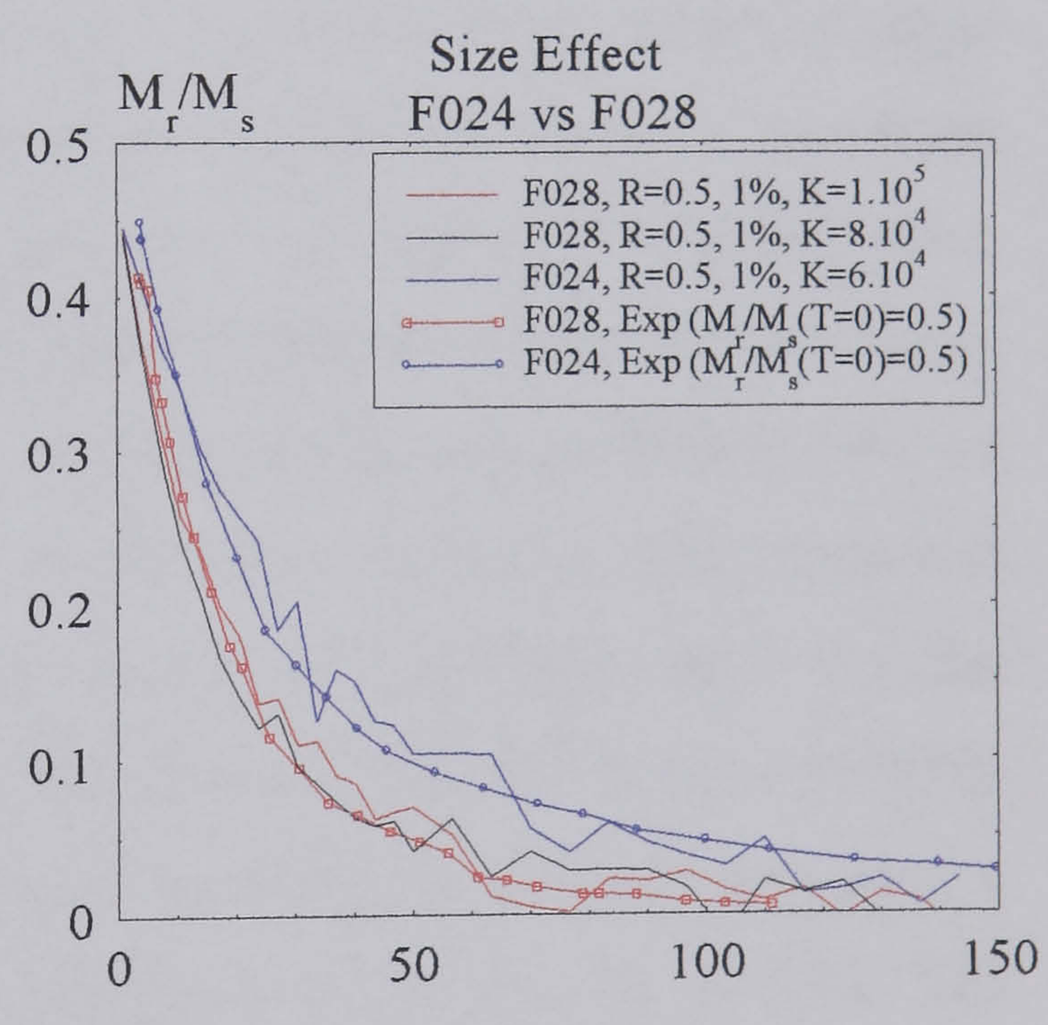

(d)

Figures 5-14

TDR curves as obtained using the model by El-Hilo et al. [1998], for different values of the concentration ε (a), *the anisotropy constant K (erg/cc)* (b), *and range of the interaction, R.* (c) *for sample F028 (59Å); in* (d), *the best fits to the experimental data, obtained for F024 and F028, are presented.*

As mentioned above and according to the model of El-Hilo et al., it seems that the concentration of the particles that best reproduces the experimental data is ~1%, which is much smaller than the actual concentration of the samples, ~10%. It is not clear why this is so. With regard to R, the range of the interaction that seems to provide the better results is R=0.5. According to the model, this means that only particles within half a diameter of a particle contribute to the dipolar interactions. Although the results for R=2.0 seem to lie closer to the experimental values of the remanence to saturation ratio for very low temperatures (see Fig. 5-14 *c*), the curve is much flatter for this value of R than the experimental TDR. Thus, according to the model, only really close particles contribute to the interactions. The anisotropy constants that seem to reproduce the experimental results more closely are almost an order of magnitude smaller (Fig.5-14 *d*) than the calculated anisotropy constants (see Table 5-10). For example, the mean anisotropy constant that best fits the experimental TDR curve for F028 lies between $K=8\cdot10^4$ and $K=1\cdot10^5$ erg/cc (Fig.5-14 *d*) while the experimental value was $4.5\cdot10^5$ erg/cc (see ✣5.4.5).

It is interesting to note that some of the values of M_r/M_s at 0K are larger than 0.5, the expected value [Stoner and Wolfarth (1948)] for a purely non-interacting system of single domain particles at zero Kelvin. This is attributed to the fact that when the anisotropy constant of the system is relatively low (4.10^4 erg/cc) so is the anisotropy field, H_K, which has a value of 115 Oe. As studied by Zhu and Bertram [1988] the dipolar interaction can be tensioned against the anisotropy field to see the effects that both contributions have on the system. If this anisotropy field is particularly small, then the dipolar interactions can overcome the anisotropy effects and increase the remanence to saturation ratio from the expected value of 0.5. An estimate of the coupling constant [Zhu and Bertram (1988)], H_{dip}/H_k, for sample F028 (59 Å), with an interparticle separation of 100 Å (ε~5%), gives a value of 0.24, which according to the authors would lead to a value M_r/M_s of 0.76. This seems to be the case for the systems with low anisotropies (~10^4 erg/cc) and higher concentrations (3.8%, 5%, 10.3%) while for the systems with the lowest concentration (1%) the dipolar interactions are too weak to overcome the effects of the anisotropy field. As the interparticle separation increases, i.e., the systems have lower concentration, the effect of the dipolar interactions becomes weaker and the anisotropic effects dominate the magnetic behaviour of the system.

It has also been predicted by other authors [Walsmley et al. (2000)] that dipolar interactions can be magnetising in weakly dipolar interacting systems, in the absence of anisotropic effects. Magnetising interactions have been predicted [Hadjipanayis et al. (1981 *a*, *b*)] to increase the value of 0.5, as seems to be the case of the calculations in this section for low anisotropies and concentrations from 3.8% to 10%. In the case of the systems in this thesis, the anisotropy fields oscillate between 1000 and 3000 Oe for the different particle size systems, which dominate the magnetisation processes and thus a value for M_r/M_s of 0.5 or less is expected for these systems as found.

It appears to be the case that this theoretical model produces TDR curves which have higher energy barriers than those present in real systems; this is manifest in the larger values of M_r/M_s for the theoretical curves, with respect to the experimental curves, when using the anisotropy constants and concentrations calculated experimentally (Table 5-10). This is possibly one of the reasons why to reproduce the experimental curves, the theoretical anisotropy constants are much smaller than the experimental values. This could also be due to the lack, in the model, of a good account of thermal activation, which for real systems, and in these small size ranges, (D~50-80Å) seems to have a strong effect in the magnetic relaxation of the particles, as it shows the rather steep slope in the relaxation data. The possible effect of the initial microstructure of the sample may hold the explanation for the value of the range, R, being so small (best fits with R=0.5). In this sense, if the particles form small aggregates of a few particles, it is only the particles within these aggregates, very close to each other, that contribute to remanence in the TDR curves. It is not clear, however, why the values of the concentration that best reproduce the experimental values are so small, ~1%, compared to the experimental values, ~10%.

5.4.8. Summary

There are several important results obtained in this section 5.4. Firstly, the distribution of blocking temperatures (and/or energy barriers) of the systems, as well as the standard deviations of these distributions, have been obtained. Secondly, a deviation of the TDR value from the expected value predicted by Stoner and Wohlfarth [1948] has been observed. An effective anisotropy constant has been calculated from the TDR data, the smallest particle systems presenting the highest anisotropy, probably due to the surface contribution as already predicted from the magnetisation curves at room temperature.

Also, a bimodal distribution of energy barriers has been detected in agreement with the bimodality obtained from the physical particle analysis. The model of El-Hilo et al. [1998] has been used to obtain some preliminary results, and at the moment it can only reproduce some of the experimental results qualitatively.

'Know ye, O man, that all that exists, is
only an aspect of greater things yet to come.
Matter is a fluid and flows like a stream,
constantly changing from one thing to another.
The key to worlds within thee,
is found only within,
for man is the gateway of mystery,
and the key is that One is within One'.
(Adapted from *The Emerald Tablets of Thoth*)

5.B. Interactions and particle size effects

5.5. Geometry of small aggregates in zero and non-zero applied fields

Previous to the presentation of the main results on the interactions in the different magnetic systems, it is necessary to revise (partially treated in ✣2.5.1.2.a) in some detail what sort of geometries small agglomerates of a few magnetic particles can present. We refer here to Appendix IV where results showing the expected stable configurations of these small aggregates of particles, as a function of temperature and applied field, are presented. This is relevant for the interpretation of the results at low and high temperatures, as different configurations of the particles can give different (magnetising/demagnetising) interactions as was discussed in ✣2.5.1.2.a.

5.6. dc initial susceptibility (ZFC curves)

The measurement of the initial susceptibility with temperature is frequently called Zero Field Cooled (ZFC) measurement. Here the sample is frozen in a zero applied field, previous to the measurement of the susceptibility of the sample as a function of temperature. The susceptibility is measured in the presence of small applied field.

For a single particle which has been frozen in a zero applied field, its magnetic moment lies along its easy axis of magnetisation, which is oriented at random; then, there will exist an energy barrier if the particle's magnetic moment is to follow the field. As the temperature is raised, the probability for the moment to overcome its energy barrier will increase, and eventually it will align. When this happens the ZFC curve will have an abrupt peak. If the temperature is increased further, the magnetisation will gradually decrease due to randomising thermal effects.

In real systems the presence of a distribution of particle sizes determines a distribution of energy barriers, and consequently a distribution of blocking temperatures, T_B (defined in ✣2.4.1 and ✣5.4.1). Hence the susceptibility curves will not follow a step function but they will have a smooth increase followed by a smooth decrease. As the temperature rises and it approaches the blocking temperature of each particle, the 'unblocking' of the magnetic moments increases the magnetisation (susceptibility)(*), and eventually will manifest as a peak, T_m, in the ZFC. But soon after the particles have overcome their energy barriers, the temperature becomes high enough to make the moments quasi-paramagnetic; in this situation, the susceptibility will decrease again.

Initial susceptibility measurements have been used to study magnetic interactions since Weiss [1907] postulated the existence of a 'molecular field', or mean interaction field, which would account for the deviation of the susceptibility from the paramagnetic case. Many attempts have been done in the past [Söffge and Schmidbauer (1981), Fiorani et al. (1986 *a*, *b* and *c*), El-Hilo et al. (1988), Chantrell et al. (1991), Dormann et al. (1997)] to study the effects of particle size, interactions and applied field on the initial susceptibility or ZFC curves of different fine particle systems. For this purpose, ferrofluids F024 and F028, with different concentrations of magnetic material, have been used.

5.6.1. Effects of concentration and particle size on the ZFC curves

According to Weiss [1907], $\chi_i = C(T-\theta)^{-1}$ (Eq. 2.34), where C is a constant and θ is the Curie-Weiss temperature, which gives the strength of interactions in the systems. For the study of this Curie-Weiss temperature, χ_i^{-1} is plotted against temperature, and the intersection of this curve with the temperature axis obtained (see Fig. 5-17). This value is the so-called total ordering temperature, T_{0t}. Thus the susceptibility can be rewritten in terms of T_{0t} [El-Hilo et al. (1992 *b*)], $\chi_i \propto c\left(T+T_{0t}\right)^{-1}$, where $T_{0t} = -\theta$, and $T_{0t} = T_{0B} - T_{0i}$ (see ✣2.5.2.3). Once T_{0t} is corrected from the effects of blocking, T_{0B}, (see ✣2.5.2.3), considering the distribution of particle volumes (✣5.2) for the corrections [Chantrell (1998), private communication], the interaction temperature, T_{0i}, is obtained.

Due to the narrow distribution of particle sizes ($\sigma < 0.5$), the correction factors due to blocking effects are very small and the total ordering temperatures, T_{0t}, are almost genuine interaction temperatures, T_{0i}, due solely to interaction effects or better, due to the deviation of the systems from the pure paramagnetic behaviour. In fact, as already noted in ✣2.4.1, at 100K (T_{0i} has been calculated at 100<T<180 K (see Fig. 5-17)) the contribution to the total susceptibility due to blocked particles is only 1% of the total susceptibility, which is negligible. At higher temperatures, this contribution will be zero.

Fig. 5-15 and 5-16 show the ZFC curves obtained for different concentrations of samples F024 and F028, respectively. The temperature of the maximum, T_m, and the interaction temperature T_{0i}, corrected for the blocking contribution, T_{0B}, are shown in Table 5-12, A and B, for the different particle sizes and dilutions.

(*)In the case that no energy barrier is present, the effect of temperature will also facilitate the alignment of the spins in the field direction, leading to an increase of the susceptibility, as in the case of the presence of an energy barrier.

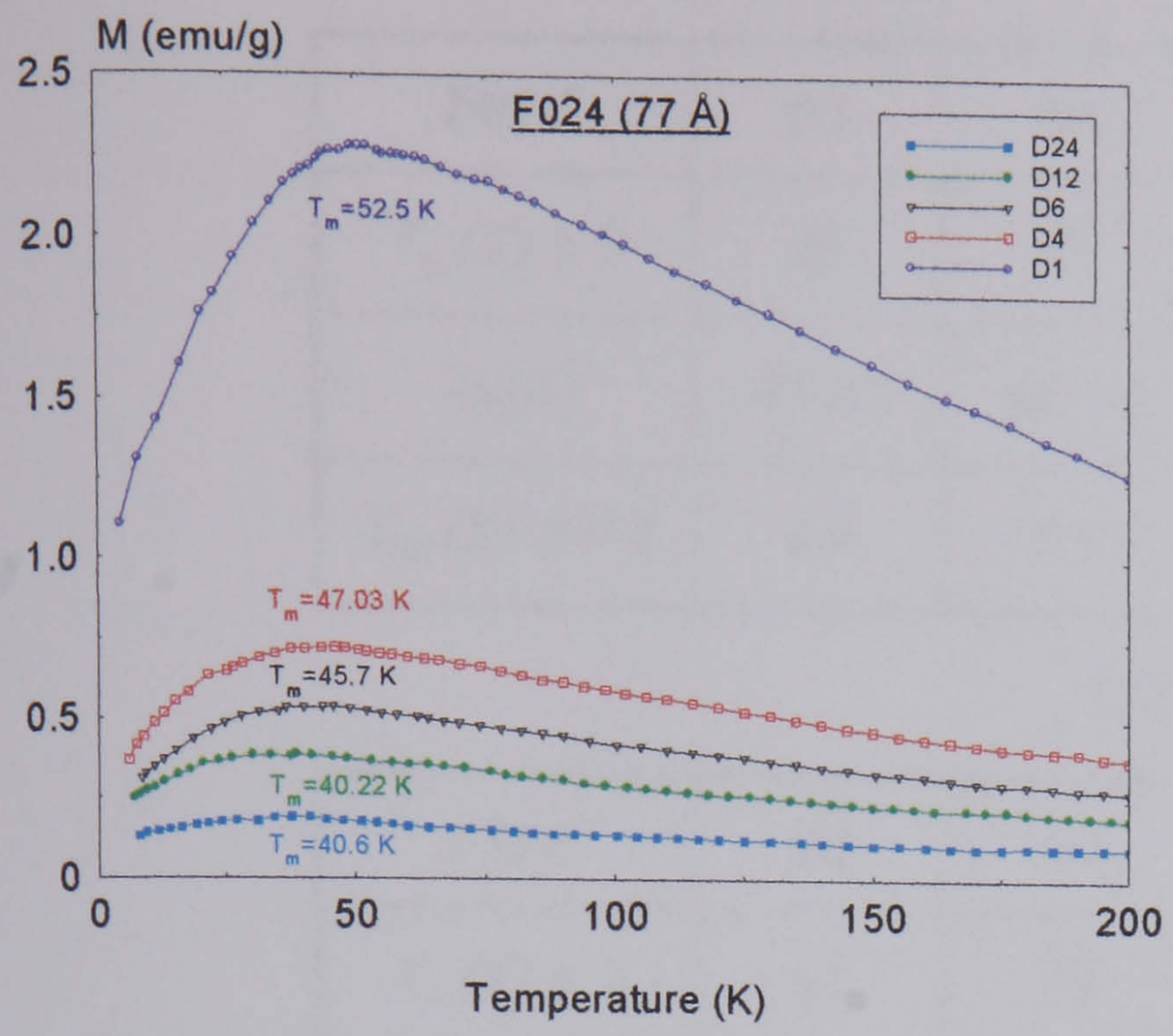

Figure 5-15

ZFC curves for sample F024, in $H_{app} = 25\ Oe$

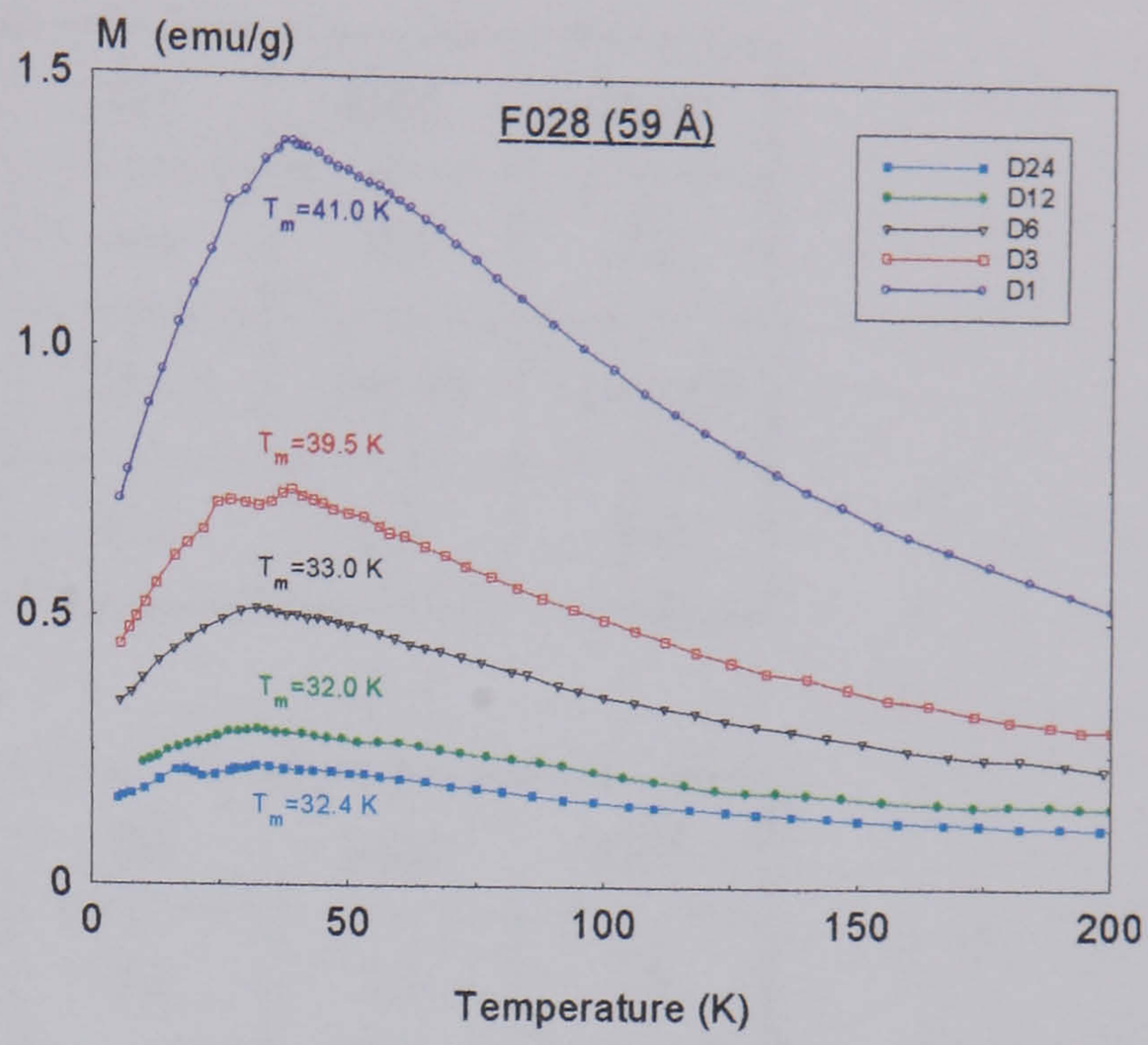

Figure 5-16

ZFC curves for sample F028, in $H_{app} = 25\ Oe$

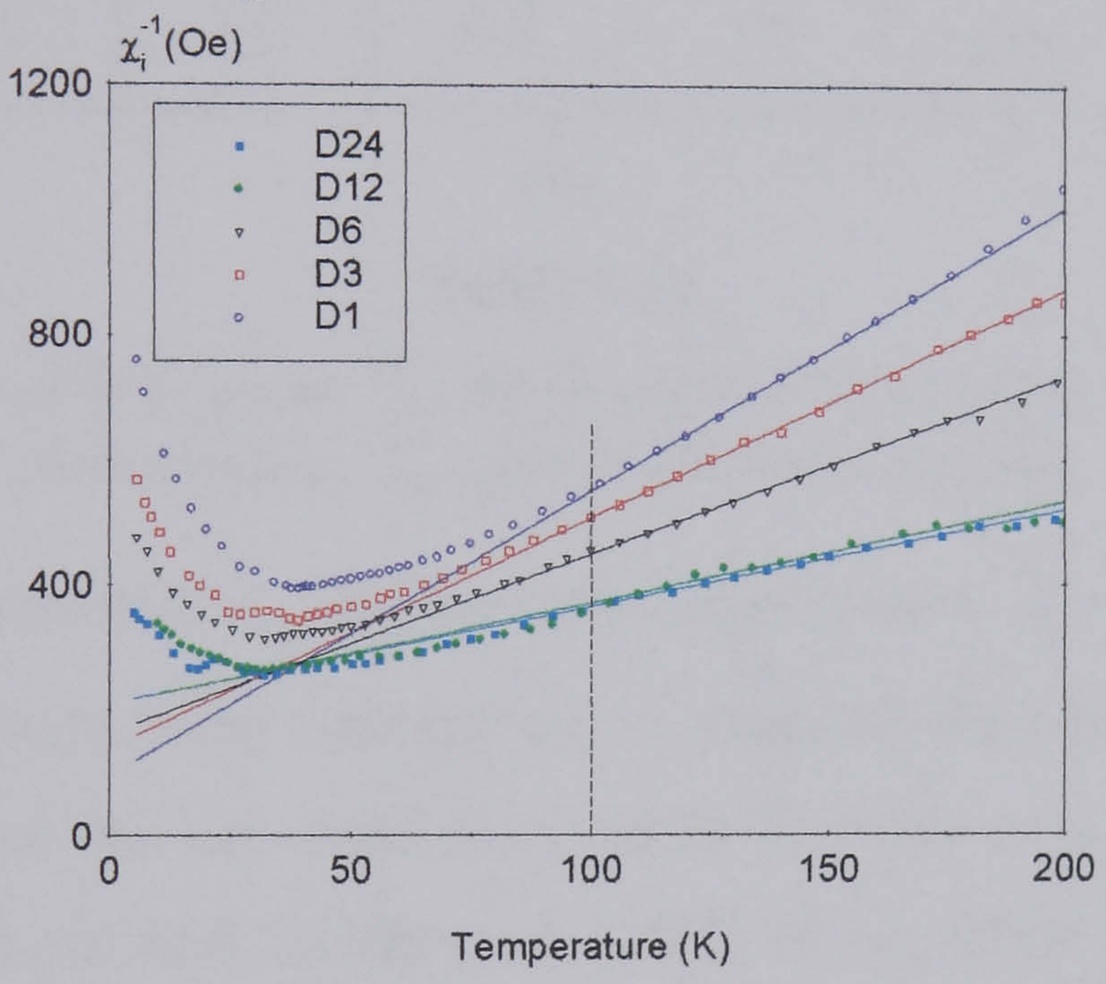

Figure 5-17

Linear fit of $\overline{\chi}_i^{-1}$ *vs T in the temperature range* 100<T<180 K *for sample F028.*

From Fig. 5-15 and 5-16 and Tables 5-12, A and B, it can be observed that for concentrations D1, D3 and D6, T_m decreases with decreasing concentration as has been observed in many systems [El-Hilo et al. (1992 *b*); Tronc et al. (1995); Dormann et al. (1996, 1998 *c*)]. For systems D12 and D24, T_m seems to remain constant, indicating no further effect with dilution. It is also evident that T_m depends on particle size, being lower for the smaller particle sizes, as would be expected from the lower energy barriers present in these systems.

F024	**D1**	**D4**	**D6**	**D12**	**D24**
$T_m\,(K) \pm 2$	53	47	46	40	41
$T_{0i}\,(K)$	-81 ±3	-66 ±3	-71 ±4	-98 ±4	-103 ±5
$T_{0B}\,(K) \pm 0.1$	8.4	6.9	6.7	5.9	5.9

(A)

F028	**D1**	**D3**	**D6**	**D12**	**D24**
$T_m\,(K) \pm 2$	41	39	33	32	32
$T_{0i}\,(K)$	-17 ±5	-34 ±7	-54 ±5	-126 ±8	-132 ±4
$T_{0B}\,(K) \pm 0.2$	3.6	3.5	2.9	2.8	2.8

(B)

Table 5-11

Values for the maximum of ZFC curves, T_m, the interaction temperature, T_{0i}, and the contribution from blocking, T_{0B}, for (A) F024 and (B) F028.

Another interesting quantity is T_{0i}, the interaction temperature. T_{0i} is negative in all cases indicating overall demagnetising interactions, as expected for purely dipolar interacting systems. This behaviour has also been observed by Godinho et al. [1995] in maghemite particles dispersed in a polymer, Söffge et al. [1981] in magnetite ferrofluids, and El-Hilo [1990] in ferrofluid systems similar to the ones measured in this thesis. Also, negative interactions temperatures have been predicted by Chantrell et al. [1999 *a*].

With respect to *particle size*, the values of $|T_{0i}|$ are larger for F024 ($D_{vm} = 77$ Å) than for F028 ($D_{vm} = 59$ Å), which could be interpreted as stronger interactions or more stable magnetic configurations, possibly initiated by small aggregates [Buzmakov et al. (1995)], in these larger particle systems. In this sense, the higher stability of the magnetic configurations of F024 would be manifest as a less magnetising effect giving rise to a more negative T_{0i}.

The variation of T_{0i} with *concentration* is another important source of information; for the smaller particle size sample, F028, $|T_{0i}|$ decreases with increasing concentration. This

means that the interactions are more magnetising as the concentration grows. Similar effects have been observed in previous works [e.g. Godinho et al. (1995)]. El-Hilo et al. [1992 *d*] performed similar studies on frozen ferrofluids of magnetite particles with a mean diameter, $D_{vm} = 50$ Å. Although El-Hilo et al. obtained positive ordering temperatures, in the temperature range where the particles are superparamagnetic, they also observed the same trend, i.e., more magnetising effects as the concentration increased. For sample F024, the trend is not clear, although it seems opposite to that observed in F028, i.e., the interactions are more demagnetising with concentration. This latter behaviour was observed in previous measurements for different dilutions of F024. However these early data had to be repeated, because only values up to 160 K had been recorded. There exists a possibility that sample D6 has agglomerated with time. An extensive study on the effect of concentration on the value of T_{0i} is to be carried out in the future.

This difference in the value of T_{0i} with particle size and its evolution with concentration, seems to indicate that although all interactions are globally demagnetising, the sample with the largest particle size (F024) has stronger dipolar interactions (higher $|T_{0i}|$) which may dominate other local effects, compared to the samples with the smaller particle sizes. The larger the dipoles (for F024), the stronger the dipolar interactions, thus being more difficult for the system to move out of this energetically stable configuration, which manifests in more demagnetising effects as the concentration increases. The local effects in F028 seem to lead to more magnetising interactions as the concentration grows. This may be due to the weaker interactions (smaller dipoles) present in these systems, which makes the magnetising effect of the surrounding media to be noticeable, decreasing the demagnetising effect of the dipolar interaction, as suggested by Kechrakos and Trohidou [1998]. Also, it may be the case that smaller particles take on totally different microstructures than larger particles, thus leading to different local microscopic interactions. In this sense T_{0i} could give information of local differences in the samples. It is difficult, however, to extract any valuable information unless more simulations and/or new measurement techniques are developed to predict the configurations for systems with different sizes and their influence, if any, on the value of T_{0i}.

Rather higher values of T_{0i} for dilutions D12 and D24 (see Table 5-12), in both F024 and F028, with respect to the other dilutions, seem to indicate the presence of agglomerates, or

bigger agglomerates, in these samples. Larger agglomerates would have larger effective moments and stronger dipolar interactions. This effect is particularly noticeable in F028 (see Table 5-12). Also, possible agglomeration was suggested in ✣5.2.3, due to the increase of initial susceptibility of samples D12 and D24 with respect to the values of the previous dilutions, as obtained from the room temperature magnetisation curves. The constancy of T_m for the very diluted samples D12 and D24 could also be an indication of agglomeration in these systems.

As already stated T_m decreases as concentration decreases for all particle sizes, as expected, but in apparent contradiction with the trend observed in the value of T_{0i} where more magnetising effects with higher concentration are observed for F028. For this sample, interactions seem to be more magnetising, as demonstrated by lower values of $|T_{0i}|$ as concentration is increased, which is not expected. The reason for this behaviour probably lies in the fact that the dependence of the peak in the χ vs T curve on concentration is determined when the system presents a mixture of superparamagnetic and blocked particles, and both systems (F024 and F028) seem to have the same behaviour in this temperature range. However, T_{0i} is measured in a temperature range where all the particles are superparamagnetic, and at these temperatures local effects seem to dominate, which may strongly depend on the particle size of the systems.

The fact that $|T_{0i}|$ increases with increasing dilution, for F028, could suggest the presence of agglomerates as samples are diluted; agglomerates would produce effectively bigger particles with increased magnetic moments and enhanced demagnetising effects. This seems possible in the case of the samples with greater dilution (D12, D24), where the values of T_{0i} become much higher than the values for the rest of the dilutions, as shown in previous paragraphs. However, for concentrations D1, D3 and D6 of F028 the decrease of $|T_{0i}|$ as concentration seems a genuine effect. The same evolution of $|T_{0i}|$ with concentration ($|T_{0i}|$ decreases as the concentration is increased) has also been observed by Godinho and co-workers [1995] in systems of $\gamma - Fe_2O_3$ nanoparticles dispersed in a polymer.

At room temperature, dipolar interactions in a ferrofluid system can lead to very specific microstructures [Menear et al. (1983, 1984), Martin et al. (1987, 1992), Buzmakov (1995),

Chantrell et al. (1996), Trohidou and Blackman (1995), Jund et al. (1995)], due to cluster or micro-aggregate formation (see ✣2.5.1.2.a and Appendix IV). Whatever these microstructures may be, they are 'frozen' as the ferrofluid is cooled down (in $H = 0$) to perform the susceptibility measurements. The presence of these microstructures would support the argument of *local* effects affecting the evolution of T_{0i}. Luo et al. [1991] calculated the Arrot plot(*) for a ferrofluid sample of magnetite, obtaining a change of curvature near the maximum of the ZFC curves, T_m, thus indicating that there may be local random uniaxial anisotropy that will destroy the long-range order [Aharony and Pytte (1980)]. This seems reasonable for the very diluted ($\varepsilon < 10\%$) systems that ferrofluids constitute.

An intuitive explanation in terms of 'magnetic stability' can also be given to explain the evolution of T_m with concentration, as suggested by Chantrell et al. [1999 *a*]. Local effects make the more concentrated systems more 'stable' in their initial configurations, the effect manifesting itself as a higher energy barrier to be overcome; in other words, in these systems higher temperatures are needed for them to become superparamagnetic, because of the 'local coupling'. The contrary will occur for the more diluted systems: not so much cohesion or coupling requires lower temperature for the particles to overcome their energy barriers and become superparamagnetic. This can be called the 'local trapping net' effect or 'local coupling', and can be seen as an stability effect.

5.6.2. Normalised susceptibility

The curves in Fig. 5-18 show two interesting effects, due to different concentrations and particle sizes; firstly, the effects of dilution are an enhancement in the value of the normalised susceptibility, $\overline{\chi}_i$, and a reduction of T_m, for decreasing concentrations. Less concentrated samples have a smaller interaction contribution, i.e., are less stable in their interacting positions, thus making it easier for the individual particles to rotate towards the field, showing a smaller value of T_m and higher values of $\overline{\chi}_i$. This is the case for all particle sizes. The same results were obtained by El-Hilo et al. [1992 *c*] and predicted by

(*) In an Arrot plot, M^2 is plotted versus H/M. They were used by Aharoni and Pytte [1980] to develop a theory for random uniaxial anisotropy systems. In 1982 [1982 *a*], von Molnar, Barbara and co-workers used the Arrot plots to distinguish between alloys with random anisotropy and normal spin-glasses. Also, the systems with random anisotropy, presented no spontaneous magnetisation at any temperature.

the same authors [El-Hilo et al. (1998)] with a Montecarlo model developed to explain the behaviour of small magnetic particle systems.

It is interesting to note that the evolution of $\overline{\chi}_i$ with concentration at these low temperatures is opposite to that observed at room temperature. While at room temperatures $\overline{\chi}_i$ is a good indicator of the agglomeration in the system (see ✣5.2.3) [O'Grady et al. (1986), Holmes (1990)], at lower temperatures it is the interaction effects and the unblocking of the particles which seem to dominate the evolution of $\overline{\chi}_i$, the aggregation state having possibly remained the same upon freezing the samples.

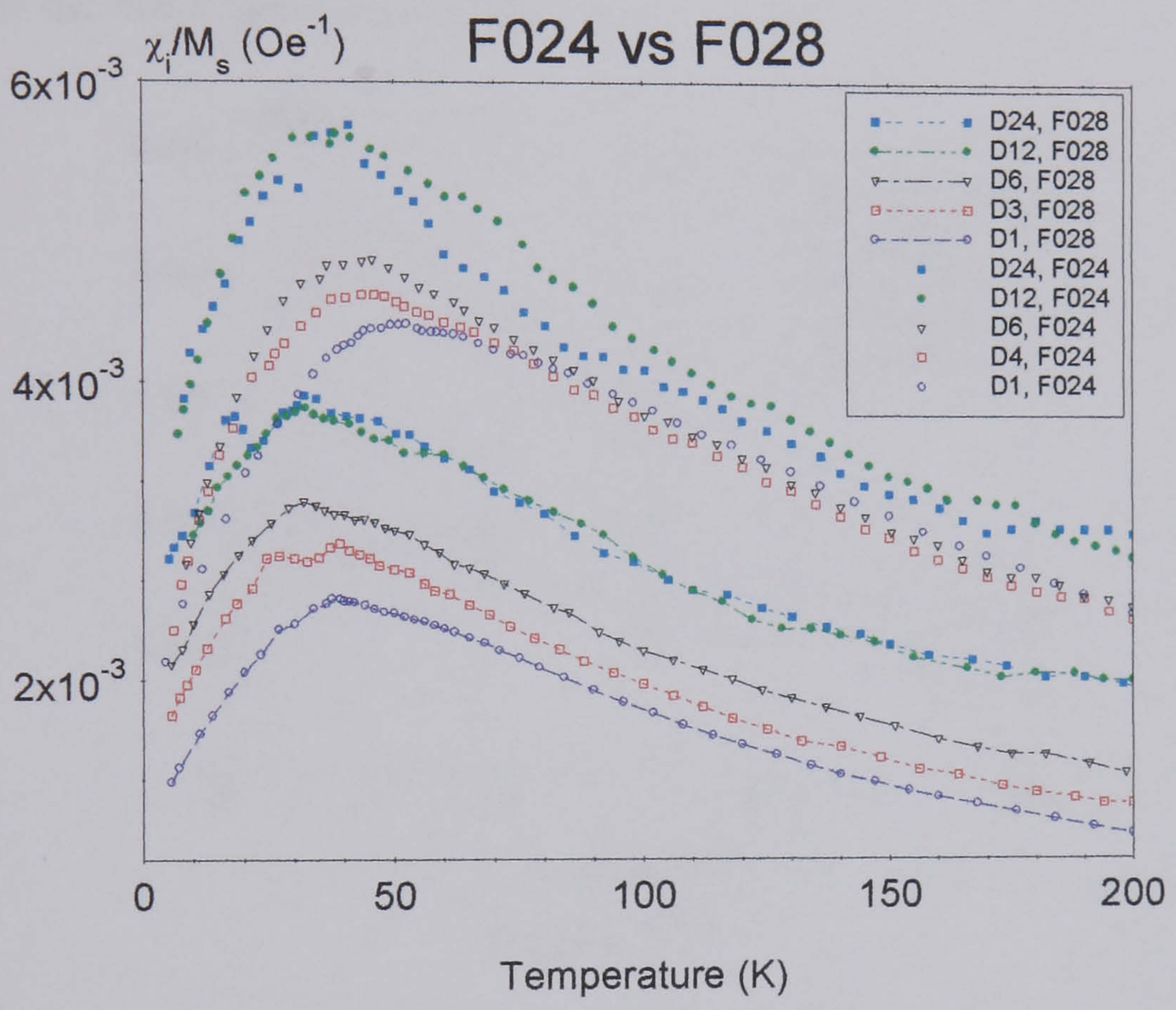

Figure 5-18

Normalised (to M_s) ZFC curves for F024 (D_{vm} = 77 Å) and F028 (D_{vm} = 59 Å).

Secondly, the samples with the bigger particle sizes seem to have a higher susceptibility, in agreement with the results obtained from the room temperature magnetisation curves (✣5.2.3), in the superparamagnetic state, in which the enhancement of the magnetisation was more obvious in the bigger particle sizes, as predicted and observed by Bradbury et al. [1985, 1986]. This is because the initial susceptibility is dominated by the largest particle in a system [O'Grady et al. (1986), Holmes et al. (1990)]. Similar behaviour has also been observed in many other systems, e.g., in Fe-Cr-B nanoparticles embedded in an alumina matrix by Dormann and co-workers [1998 *a*].

5.6.3. Effects of an applied field

In this thesis the effect of an applied field has been investigated in sample F024, for $H \approx 25\ Oe$ and $H \approx 45\ Oe$. For this purpose, the reduced susceptibilities for both fields have been compared (see Fig. 5-19). The effect that the applied field has on the energy barrier is clearly seen in Fig. 2-7 (b), for a uniaxial particle where the field is applied in the direction of the easy axis. Basically, the higher the field the lower is the energy barrier that the particle needs to overcome to align into the field direction. In this sense, it is reasonable to observe a lower T_m for larger values of the applied field (see Fig. 5-19 and Table 5-13), for the same sample dilutions.

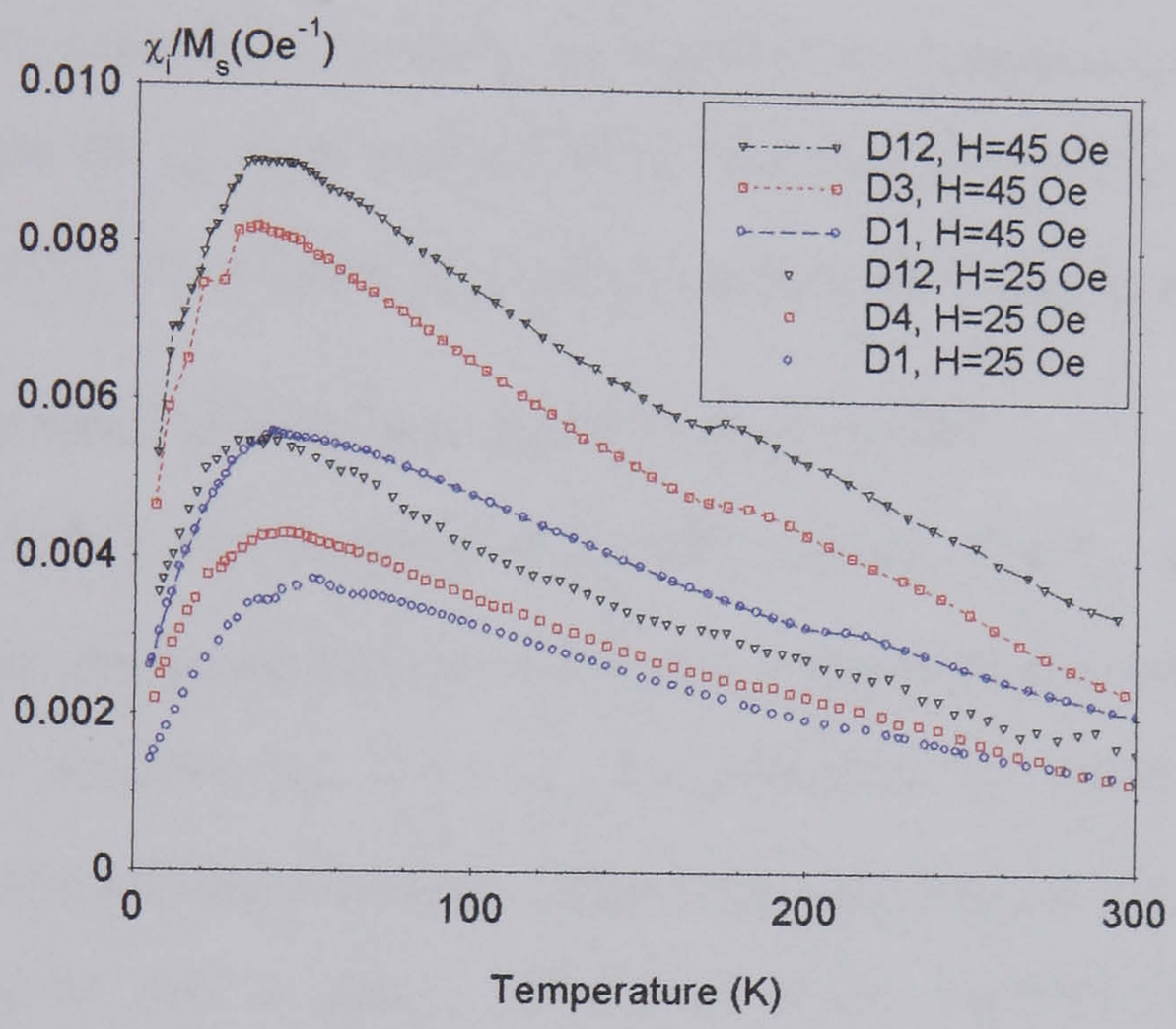

Figure 5-19

Effect of different applied fields on the ZFC curves, for different dilutions of sample F024

	H=25 Oe			***H=45 Oe***		
F024	**D1**	**D4**	**D12**	**D1**	**D3**	**D12**
$T_m\,(K) \pm 2K$	53	47	40	41	35	34
$T_{0i}\,(K)$	-81 ±3	-66 ±3	-98 ±4	-89 ±3	-82 ±2	-138 ±2

Table 5-12

Parameters obtained from the ZFC curves of sample F024, for 2 magnetic fields, 25 and 45 Oe.

Another observation is the increase in the normalised susceptibility (Fig. 5-19) with applied field. This behaviour would not be expected if the low field approximation, $\overline{\chi}_i \approx \mu / 3kT$ ($\mu = VM_s$ is the magnetic moment for a single particle), is considered.

However, this approximation arises from considering the first term in the Taylor expansion of the Langevin function. It is possibly the case that this is not a valid approximation for 45 Oe, and that higher terms of the expansion may be necessary to explain the behaviour of $\overline{\chi}_i$. This being the case, $\overline{\chi}_i \approx \mu / 3kT - (1/45) \times (\mu H / kT)^2 + (1/945) \times (\mu H / kT)^4$, which would account for the increase in susceptibility with applied field.

Additionally, the interaction temperature, T_{0i}, shown in Table 5-13, seems to increase in absolute value for the 45 Oe field compared with the corresponding values obtained for $H \approx 25\ Oe$. This implies that the interactions are more magnetising for the lower field ($H = 25\ Oe$) or the magnetising part of the dipolar interaction is more effective for these field. At the present moment, however, no appropriate explanation has been found to describe the evolution of T_{0i} with applied field, but similar behaviour has been observed by Godinho et al. [1995] for maghemite particles dispersed in a polymer.

5.6.4. Theoretical predictions [El-Hilo et al., 1998]

It must be born in mind that at the peak of the ZFC curves, $T \approx T_m$, a mixture of blocked-blocked and blocked-superparamagnetic interactions exist; on the other hand the ordering temperature, T_{0i}, is studied for $T >> T_m$, temperatures in which superparamagnetic-superparamagnetic interactions dominate. Thus only a theoretical model, that accounts for all these effects, will be able to give a prediction of the experimental results as well as provide an interpretation for them.

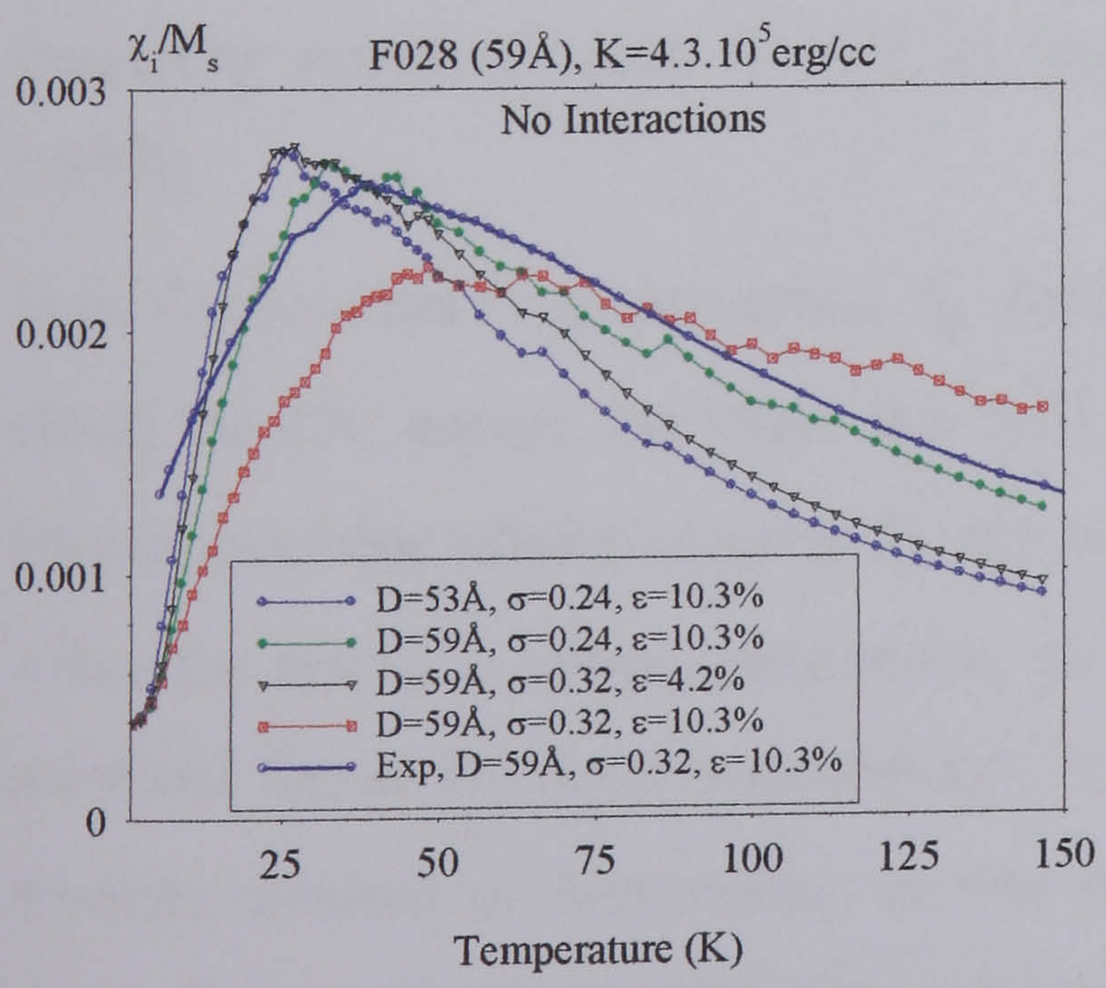

(a)

Curves for F028 for different concentrations and anisotropy constants

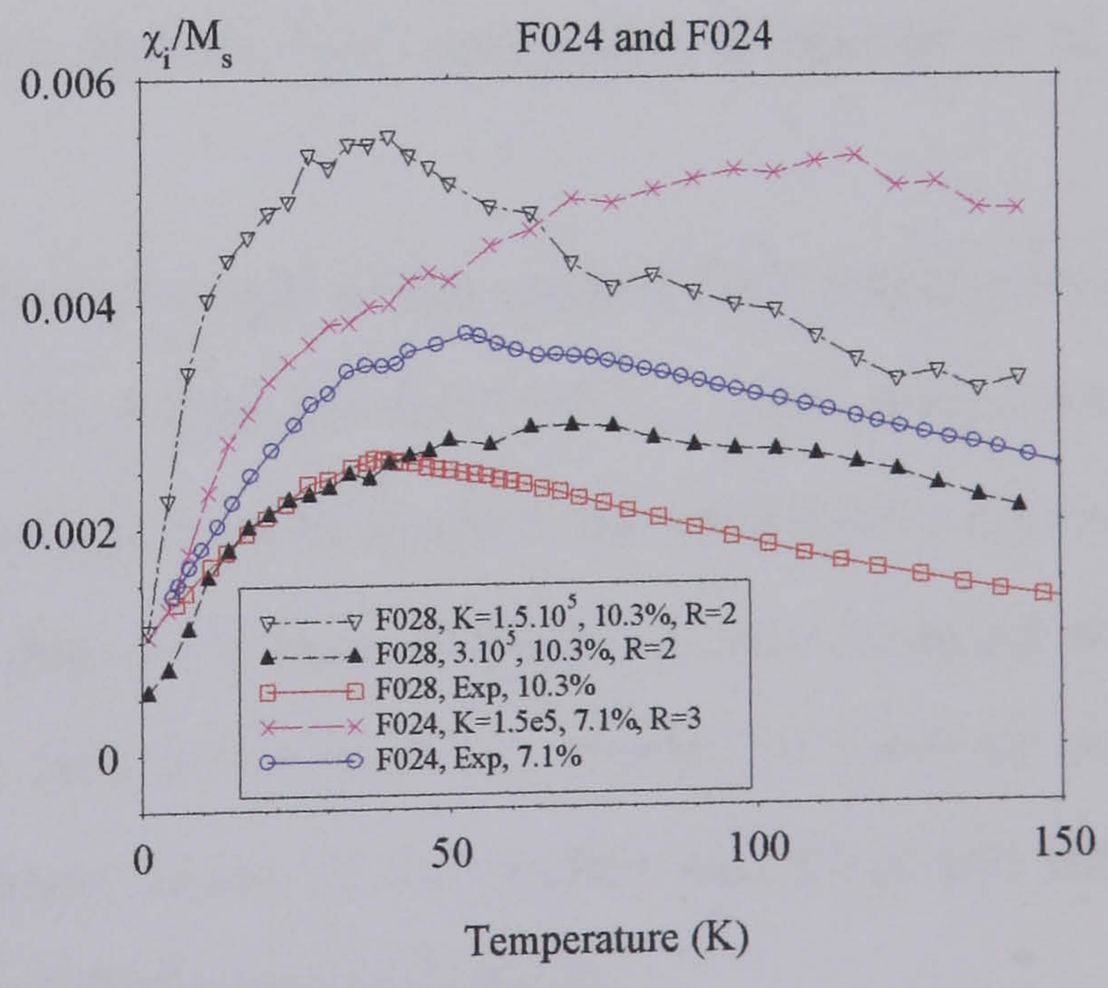

(b)

Predicted ZFC curves for F024 (77Å) and F028 (59Å) via the Montecarlo model

Figure 5-20

With this in mind, a Montecarlo model by El-Hilo and co-workers [1998] has been utilised (more details in Appendix III). Fig. 5-20 (a) shows susceptibility curves using a direct calculation of the particle's susceptibility due to non-interacting superparamagnetic particles, which are assumed to have Langevin behaviour. In Fig. 5-20 (b), the results from the Montecarlo model are presented. In both cases, the parameters used in the calculation have been obtained from the basic magnetic analysis performed in ✣5.2.

In Fig. 5-20 (a) and (b) it can be seen how the main characteristics are reproduced, i.e., the more concentrated samples have a higher T_m (see Fig. 5-20 (a)), and the absolute value of $\overline{\chi}_i$ is higher for the larger particles, F024 (see Fig. 5-20 (a)), as observed in experiment. However the exact numerical values are not reproduced. In fact the model predicts the 'trends' observed in experiments, but much more information about the microscopic configuration of the systems and the influence of anisotropy is required for an exact analysis. This will be object of future work.

5.6.5. Discussion

It has been shown that T_{0i} and T_m enable us to understand the behaviour of a system qualitatively. Although some conclusions about how interactions behave in weakly interacting systems are drawn from the study of the ZFC or susceptibility curves, an exact determination of the type and intensity of interactions cannot be obtained from these studies. For example, a zero ordering temperature cannot be used as evidence of a non-interacting system [El-Hilo (1990)], as some authors have considered [Linderoth et al. (1993)].

In particular it has been shown that T_{0i} depends strongly on the applied field employed to obtain the ZFC curves: the larger this field, the higher the value of T_{0i}. Also, it must be born in mind that when evaluating T_{0i} the analysis must be made in the temperature region where the system is superparamagnetic, so that the effects of blocking are minimised or corrected for, at the lower temperatures. In fact the value of T_{0i} cannot be taken as an absolute measure of interactions. In this sense, many of the studies published and the conclusions reached in the literature require carefully reconsideration.

The interaction temperature, T_{0i}, and the maximum of the ZFC curves, T_m, depend strongly on the magnetic state of the system, whether this is induced by an external applied

field, internal field (due to interactions) and/or the physical microstructure of the particles in the system. So, although both temperatures give some idea of the interactions, when compared for differently diluted samples, particle sizes and applied fields, it should only be considered as a trend, the absolute value being influenced by so many microscopic parameters that are difficult to identify and even more difficult to control.

The only feasible solution seems to be the use of computer model that takes all considerations into account: applied field, microstructure, interparticle distance, surface effects, local interaction effects, etc. Using the Montecarlo model by El-Hilo et al. [1998] it has been shown that the qualitative behaviour of the systems can be reproduced. However, no quantitative agreement has been reached. The main problem lies in the fact that microscopic behaviour is intended to be understood via macroscopic-type measurements. In this sense, the recent development of micro-squid susceptometers [Wernsdorfer et al. (1995 *a*, *b*)] which measure the magnetisation of isolated particles, is expected to play an essential role in the understanding of the interactions and other effects such as magnetisation reversal mechanisms, surface properties, etc. of small particle systems [Dormann et al. (1997)].

5.6.6. Effects of texture induced by a small field on the ZFC curves

During the measurement of the ZFC curves it was observed that all the characteristic parameters vary if the samples are frozen in a field not exactly equal to zero. To show this effect, sample F028 was used. Studies were performed on sample D1 (10%).

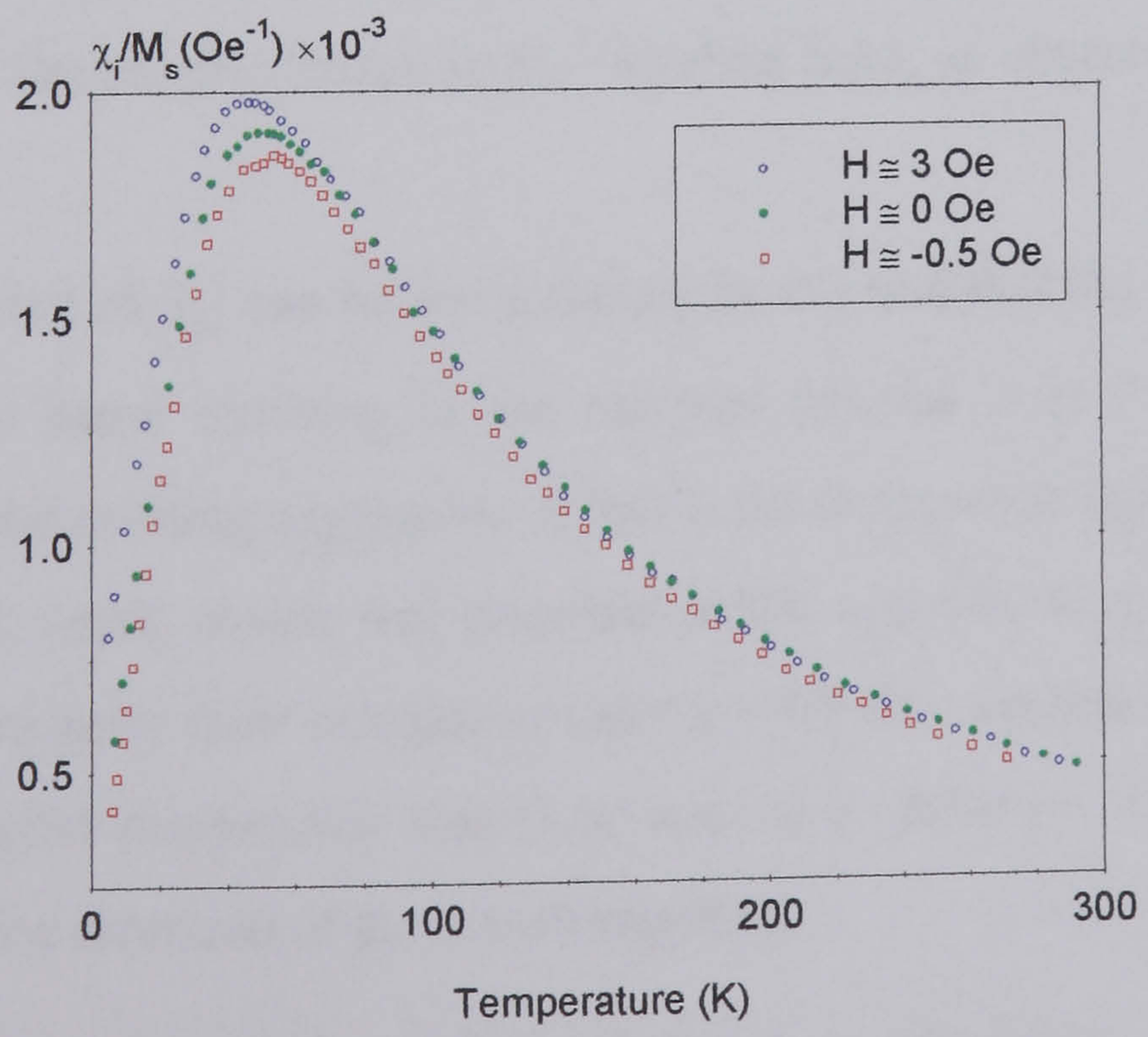

Figure 5-21

ZFC curves, measured in a H=15 Oe, for sample F028 (D1), frozen in different small fields.

In a ZFC measurement the samples are frozen in a zero applied field, and then the susceptibility is measured, $\chi = M/H$, by recording the magnetisation in a small applied magnetic field. To be able to see any texture effects induced by very small applied fields, the samples have been frozen in 3 different very low fields of *-0.5, 0* and *3 ± 0.1 Oe*, and the initial susceptibility measured.

H_{app} (Oe) ±0.1	T_m ±2	T_{0B} (K) ±0.2	T_{0i} (K)
-0.5	54	0.9	-6 ±3
0	53	1.0	-4 ±4
3	48	0.9	3 ±2

Table 5-13

Textured effects induced in sample F024, studied for different dilutions.

❖ Value of T_m for different textures

If the sample is frozen in a positive field (3 Oe) the easy axis of some of the particles would already lie in a direction θ close to 0^0 (θ being the angle between the easy axis and the H_{app}), because the field is applied from room temperature, where the particles are able to physically rotate. When the susceptibility is measured in a positive field (15 Oe, in this case) in that same direction, the overall energy barrier for reversal of the system will have diminished, as some of the particle magnetic moments have already rotated, presenting no energy barriers; thus T_m will be lower for the sample frozen in the 3 Oe field, and higher for the sample frozen in the negative field, as observed in Fig. 5-21 and Table 5-14.

This effect on the value of T_m can be strengthened by the fact that the applied field, small as it is, may induce some chaining in the samples (maybe 2 or 3 particle-chains) or reorientate some of the existing aggregates. If this is the case, when the sample is frozen in a $H \approx -0.5\,Oe$ field, small chains will orientate in the opposite direction of the applied field. They will try to keep their orientation (along $-0.5\,Oe$) against the measuring field ($+15\,Oe$), thus a higher temperature should be needed to drive the moments out of their easy directions into the direction of the measuring field.

Hence both effects, texture and possible chaining or alignment of existing micro-aggregates, would contribute (affecting the overall energy barriers) in the same direction,

and it may be the addition of both effects that explains the fact that such small fields produce measurable effects.

✣ Value of T_{0i} for different textures

The same arguments given to explain the evolution of T_m with the freezing field, are valid to explain the evolution of T_{0i}, in particular, the microstructure present in the system. When the freezing field is $-0.5\,Oe$, chain formation or reorientation would imply magnetising interactions in this direction, i.e., in the opposite direction to the measuring field ($+15\,Oe$); thus, overall, more demagnetising interactions are expected in this latter case than when a zero or a $+3\,Oe$ freezing field is applied (see values of T_{0i} in Table 5-12). Alternatively, it can be argued that even for individual particles, some of the particles' easy axis will lie close to the direction of the $-0.5\,Oe$ freezing field, due to particle rotation and it will be more difficult for these moments to rotate out of their now stable configurations, into the $+15\,Oe$ field. This stability manifests itself in the value of T_{0i}: more negative (demagnetising interactions) for the $-0.5\,Oe$ freezing field.

✣ Other effects due to texture

The effect of different freezing fields is also manifested in the absolute values of the normalised susceptibility, $\overline{\chi}_i$ (Fig. 5-21). As expected, $\overline{\chi}_i$ is higher for the *3 Oe* freezing field, as it is in this field when the value of the magnetisation in the direction of the field is higher. Also, magnetisation curves were taken at $T = 77\,K$ of the sample frozen in a *-0.5 Oe* applied field to see if any texture was being induced. The value of M_r / M_s in the direction where the field had been applied was higher (0.027 ±0.002) than the value obtained in the perpendicular direction (0.012 ±0.002) indicating the presence of some texture in the sample.

✣ SUMMARY

Up to date no other studies have been carried out which show any texture with such small fields. Curie-Weiss behaviour was studied by Ayoub et al. [1989] in magnetite ferrofluids, for different positive ($0 < H < 210\,Oe$) freezing fields, and the opposite behaviour (i.e. more demagnetising interactions the higher the field) to the systems in this thesis was observed. Also, induced texture, by freezing the sample in rather high fields ($H \approx 2.5\,T$)

has been studied via Mössbauer spectroscopy by Hendriksen and co-workers [1994 *a*]. Although the fields used in that work were too high to draw any similarities between the data, they arrive at an interesting result which is worth commenting: the degree of alignment of the easy axis in the direction of the field is higher when the anisotropy of the system is also higher.

At present the results in this thesis are the only evidence of very small magnetic fields inducing a real texture or at least some special microstructure in the samples. More measurements with different fields and particle sizes are needed to draw definite conclusions. This section is dedicated to draw attention to the important effect that the freezing field may have on the ZFC curves measured.

5.6.7. Spin-glass behaviour

A spin-glass is a magnetic material in which the spins are frozen in random orientations. Originally, the term spin-glass was applied to dilute metallic alloys such as Cu(Mn), Ag(Mn) and Au(Fe) [Canella et al. (1971), Zibold (1979), Tholence (1980)]. In these systems, random interactions arise due to the dominant Ruderman-Kittel-Kasuya-Yosida (RKKY) interaction, where the magnetic moments are coupled via the induced polarisation in the conduction electrons of the host. In the case of the particles in this thesis, it is obvious that if the systems have been frozen in a zero applied field, their magnetic moments will lie at random, along the directions of the easy axis of the particles. Thus a system of magnetic nanoparticles could be considered a spin-glass where the interactions are now dipolar and the moments are those on particles rather than on atoms.

Spin-glass systems present a sharp peak in the temperature variation of the low field susceptibility (ac and dc), a similar characteristic to the peak presented in susceptibility curves of magnetic nanoparticles. For this reason, many studies have been dedicated to the study of spin-glass properties of nanoparticle systems. Although some properties of spin-glasses such as the dependence of T_m with concentration have been analysed in our systems, such an approach was undertaken by El-Hilo et al. [1990, 1992 *a*, *b*], who concluded that the spin-glass behaviour observed in fine particle systems could be explained in terms of the blocking model of Néel [1949 *a*] modified to take into account the effect of dipolar interactions. Similar conclusions were obtained earlier by Wohlfarth [1980] and Wenger and Mydosh [1984].

More recently Jonsson dedicated his Ph.D. thesis [1998 *a*] and many of his papers to the investigation of the spin glass behaviour in 'typical' spin-glass systems [Mattsson et al. (1995), Anderson et al. (1996)] and in magnetic nanoparticles [Jonsson et al. (1995, 1998 *a*, *b*)]. One of their results is that the more concentrated (17%) systems, Fe_20_3 ferrofluids with $D_m = 70$ Å, show typical spin-glass dynamics at low temperatures, e.g., the time dependent relaxation depends on the time spent at constant temperature before applying the magnetic field - the system 'ages' [Jonsson et al. (1995)]; while diluted (0.03%, 0.3%) systems show isolated particle dynamics, with no ageing. The spin-glass-like behaviour is attributed to the influence of the dipolar interactions. Unfortunately, no results are presented of samples with concentrations in between these low and high extremes.

Mørup [1994] revised magnetic data taken of different ferrofluid systems obtained by different authors [Luo et al. (1991), Prené et al. (1993), Hendriksen et al. (1993)] concluding that when the interactions are weak in a magnetic nanocomposite, both Mössbauer spectra and ZFC magnetisation measurement can be explained by superparamagnetic blocking while for the case of strong interactions they can only be explained by ordering of the magnetic moments. Unfortunately again, the author did not give any quantitative estimation of the concentration required in a system for it to be 'weak' or 'strongly' interacting. In the same work, Mørup presents a phase diagram which illustrates the behaviour (or phase) of magnetic nanoparticles as a function of temperature and interaction strength.

From the work in this thesis it appears that for weakly interacting systems ($\varepsilon < 10\%$) there is no such a thing as a transition to an ordered state below a certain temperature, as suggested for a spin glass. All the properties observed in the systems can be explained in terms of the superparamagnetic model.

5.7. Effects of interactions and particle size on the shape, remanence and coercivity of the low temperature magnetisation curves

Magnetisation curves at low temperatures give information of the influence of interactions when thermal effects are diminished. A study of the magnetisation curves up to 10 kOe on the ZFC ferrofluids for different temperatures is presented in this section. This study gives a good insight into how coercivity and remanence to saturation ratio are influenced by concentration and particle size.

5.7.1. Effects of interactions

5.7.1.1. Basic results

Data of coercivity and remanence to saturation ratio are presented in Table 5-15 for samples D1 and D3 diluted from F028, for 12, 20 and 30 K, respectively. From Table 5-15 it seems clear that the coercivity is higher if the system is more concentrated. On the contrary, M_r / M_s seems to be within error lower for the samples with higher concentration.

	T = 12 K		*T = 20 K*		*T = 30 K*	
Sample	D1	D3	D1	D3	D1	D3
M_s(emu/g)	27.2 ±0.5	12.1 ±0.2	27.4 ± 0.6	11.9 ± 0.3	26.2 ± 0.7	12.0 ± 0.3
M_r / M_s	0.162 ±1.10^{-3}	0.165 ±2.10^{-3}	0.109 ± 2.10^{-3}	0.104 ±2.10^{-3}	0.069 ±3.10^{-3}	0.067 ±4.10^{-3}
H_c(Oe)	188 ±4	177 ±2	90 ±3	75 ±3	44 ±2	40 ±1

Table 5-14

Coercivity and remanence to saturation ratio obtained from the magnetisation curves, at 12, 20 and 30 K, for different dilutions (D1 and D3) of sample F028 (59 Å).

As discussed in ✣2.5.1.2.a, when dipolar interactions are dominant in a system, a decrease of coercivity with dipolar interactions is predicted [Néel (1947 *b*), Wohlfarth (1955)]. This may well be the case for a strongly interacting system. However, for the ferrofluids in this work, which are weakly interacting ($\varepsilon < 10\%$) the opposite behaviour is observed.

It is difficulty to calculate the coercivity of a system of small particles when dipolar interactions are present, as pointed out by some authors [e.g. Wohlfarth (1955)]. Dipolar interactions depend on the shape or arrangement of the particle moments, determined by the actual physical geometry of the particles and/or the magnetic microstructure in the system. When a saturating field ($H_s = 10kOe$) is applied, all the moments are assumed to align in that direction. Then, slowly, this field is progressively increased in the opposite direction, until it comes a point (coercivity) that the total magnetisation of the system is zero. For the more concentrated sample, it is harder for the particles to rotate out of their local stable magnetic configurations. They have more interactions, which keep the system more 'fixed' thus needing a higher field to reach zero magnetisation. This effect is manifested in the higher coercivity of the more concentrated samples.

A similar explanation can be provided for the evolution of M_r / M_s with concentration. In the presence of a zero applied field (M_r / M_s), the particles magnetic moments go back to their more stable configurations of lower magnetisation, being this effect stronger for the more concentrated samples. A reduction of the remanence to saturation ratio as concentration increases, has also been predicted recently by Chantrell et al. [1999 *a*] and Kechrakos and co-workers [1998] for weakly dipolar interacting systems. In the words of Chantrell et al. [1999 *a*], 'the decrease in remanence with increasing concentration can be associated with an increased tendency of the system to form flux closure structures in zero applied field'.

The absolute values of the M_r / M_s obtained via TDR and the hysteresis loops differ due to the differences in the measurements. In the TDR the sample is saturated, the field reduced to zero and the remanence to saturation ratio measured. In the magnetisation curves the field is progressively diminished to zero. Thus the value of M_r / M_s is expected (and observed) to be smaller for the hysteresis curves than from the TDR, because in the former the particles have more time to relax out of the saturation direction.

✣ *Discussion:*

According to the results presented above, it is clear that interactions affect the magnetic response of the system. It also seems obvious that the applied field has a strong bearing on the type, strength, and behaviour of the interactions, as observed in the ZFC curves. In the presence of an applied field the interactions make the magnetic system more stable, i.e., higher H_c, while for a zero applied field, interactions reduce the remanence to saturation ratio. This apparently contradictory behaviour has been justified in the previous paragraphs.

It must also be born in mind that all these results are for a temperature range where there is mixture of blocked and superparamagnetic particles. To be able to study interactions between purely superparamagnetic particles arranged at random, the only macroscopic magnetic measurements available are the ZFC curves (✣5.6) and the magnetisation curves at room temperature (✣5.2.1). In any case, to thoroughly quantify the effect of interactions and temperature on H_c and M_r / M_s more measurements need to be taken, which will be the object of future work.

5.7.1.2. Behaviour at high fields

Another interesting feature that is observed from the magnetisation curves occurs at intermediate and high fields. It so happens that the diluted sample (D3) appears to saturate more easily (Fig. 5-22, inset) than sample D1. For the higher concentration sample (D1), the magnetic microstructure is possibly more stable and it is more difficult for the spins to rotate into the direction of the applied field. On the contrary the particles in the diluted sample (D3) follow the applied field easier, which can be seen in the high field region of the hysteresis loop.

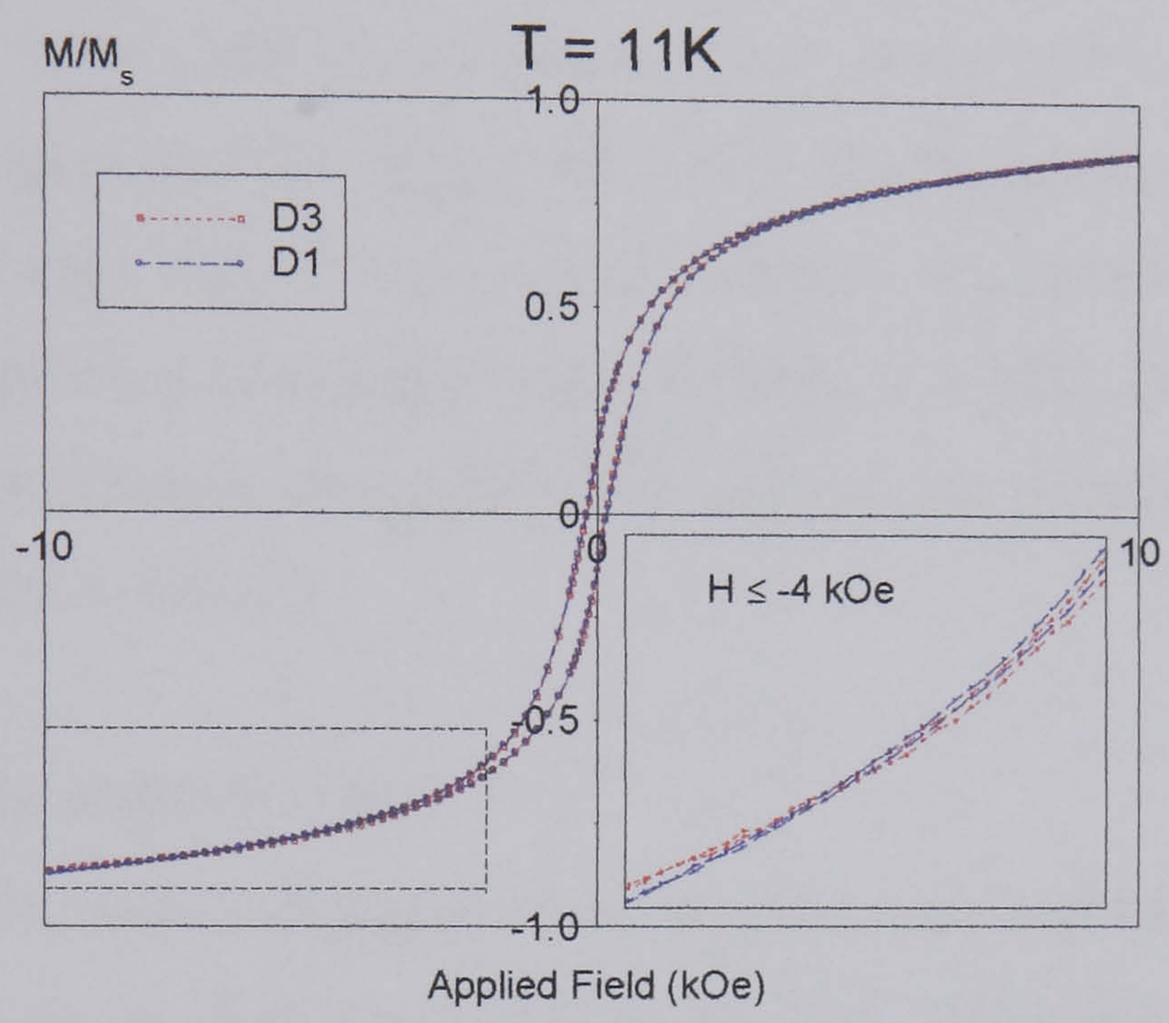

Figure 5-22

Magnetisation curves for dilutions D1 and D3 of sample F028. Detail shows the effect of sample dilution for high fields at 11 K.

However there is another possible or perhaps parallel or complementary explanation for this behaviour: the fact that the particle's surface may affect the interactions [Dormann et al. (1996)]. The results in Fig. 5-22 suggest that the interactions between particles may be enhanced or mediated by the surface of the particles. Thus the closer the particles the closer their surfaces are and the stronger this 'surface-channelled-coupling' effect [Dormann et al. (1996)] is, thus resulting in samples more difficult to saturate when the concentration is higher. This is supported by some experimental evidence by Dormann and co-workers [1996], in which they observed that the saturation magnetisation at zero Kelvin is reduced by 30% in the low concentration samples, while it only reduces by 10% in the high concentration samples. According to the authors, 'the reduction can be due to magnetic disorder occurring at the particle surface, which seems to be lower in the presence of interactions. In this case we can assume that the surface energy varies with the

interactions, owing to the modifications of the magnetic state at the particle surface. Besides, superexchange interactions could also occur via the water molecules that may have remained trapped between the particle surface and the polymer'.

The fact that this effect is stronger at high fields seems to support the 'surface-channelling' argument, because it is at high fields when the effects of the particle surface becomes more obvious (see ✣5.11). At $20K$, the effect observed in Fig. 5-22 is not so obvious, and at $30K$ it cannot be observed. This evolution with temperature may also support the surface argument. Chen et al. [1995] suggest that in a small particle there is a very well defined shell-core structure, with a surface of paramagnetic spins, and a magnetic core which exhibits superparamagnetism; the surface spins are a smaller portion and are less coupled than the spins in the core, thus being much more sensitive to thermal effects and remain paramagnetic at much lower temperatures (presumably, $T \geq 30K$, as observed by Kodama et al. [1996]). On the contrary the spins in the core become superparamagnetic at rather higher temperatures ($T > 100\ K$).

5.7.2. Effects of particle size

It is also interesting to note the evolution of the coercivity and remanence to saturation ratio with particle size, at different temperatures (see Table 5-16). The values of the coercivities are, for the same temperatures, higher for the larger particles; however, when the temperature reaches $T = 4K$ this trend is inverted. The same occurs for the predicted values of $H_c(0K)$ (✣5.7.3).

	Temp (K)	*4 K*	*10 K*	*15 K*	*20 K*
F024 (77 Å)	$M_r / M_s \pm 6.10^{-3}$	0.370	0.362	0.230	0.180
	H_c(Oe) ± 4 Oe	380	262	139	91
F026 (66 Å)	$M_r / M_s \pm 5.10^{-3}$	0.296	0.225	0.182	0.118
	H_c(Oe) ± 4 Oe	406	245	172 (14K)	109(19.5K)
F028 (59 Å)	$M_r / M_s \pm 4.10^{-3}$	0.261	0.186	0.136	0.098
	H_c(Oe) ± 4 Oe	450	230	140	78

Table 5-15

Coercivity and remanence to saturation ratio for the three particle sizes (D1) and different temperatures

It seems to be the case that while at temperature $T > 4K$, the particle size (core) regulates the behaviour of the coercivity, when the temperature becomes low enough ($T \leq 4K$) the surface has an important contribution to the reversal mechanism of the particles and dominates the coercivity of the system, acting as a hindrance for spin rotation, in the surface as well as in the core. This effect will be stronger for the particles with a higher surface area/volume ratio, i.e., the smaller particles (F028). Systematic studies of the coercivity at very low temperatures ($0K$- $4K$) would be very interesting and clarifying. Unfortunately these measurements are not possible in our laboratories.

The evolution of M_r / M_s with temperature and particle size can be seen in Table 5-16. As expected the remanence to saturation ratio diminishes with temperature for all particle sizes. Also, this ratio is higher for the largest particles diminishing with decreasing particle size, for all temperatures. This behaviour seems to indicate that M_r / M_s is regulated by the spin at the core of the particle and is not susceptible to surface effects, as it seem to be the case for the coercivity. In this latter case, the surface seems to affect the reversal processes, thus influencing the value of the coercivity.

5.7.3. Determination of the anisotropy constant

For a group of non-interacting ferromagnetic particles, with uniaxial anisotropy, it has been predicted that the evolution of the coercivity with temperature can be expressed as,

$$H_c(T) = H_c(0) \cdot \left[1 - \left(\frac{V_p}{V}\right)^{\alpha}\right], \qquad V \geq V_p$$
$$H_c(T) = 0 \qquad V \leq V_p \qquad \textbf{(Eq. 5.11)}$$

where $H_c(0)$ is the coercivity of the system at absolute zero, V_p is the critical volume for superparamagnetic behaviour at each temperature, and α takes the value of 0.5 in the case of *aligned* particles [Bean and Livingston (1959)] and 0.77 for a *random* assembly of small particles [Pfeiffer (1990 *a*)]. The uniaxial character can be assumed from two reasons; firstly, due to shape and/or interaction (dipolar) effects; secondly, magnetite experiences the so-called Verwey transition which induces a change from a cubic to a monoclinic crystalline structure, at the Verwey temperature, T_v. This temperature decreases with decreasing particle size, going from 119 K for bulk magnetite to about 100K for 100 Å particles [Mørup et al. (1983 *a*)].

Expressing the value of V_p as a function of temperature, and using the value of α for a random assembly of magnetic moments, Eq. 5.11 can be written as (see ✣2.5.3.2),

$$H_c(T) = H_c(0) \cdot \left[1 - \left(\frac{\ln(\tau \cdot f_0) k_B}{K_{eff} V_m} \right)^{0.77} T^{0.77} \right], \qquad \textbf{(Eq. 5.12)}$$

where K_{eff} and V_m are the effective anisotropy constant, and median volume of the particles, respectively. The values used for f_0 have been calculated in ✣5.10.

Eq. 5-12 is only applicable for $V \geq V_p$, since no coercivity would be present otherwise. Linearity of $H_c(T)$ with $T^{0.77}$ takes place at low temperatures, as shown Batlle et al. [1993] who observed linearity for $T \leq 28K$ in nanoparticles of barium hexaferrite ($BaFe_{10.4}Co_{0.8}Ti_{0.8}O_{19}$). Although in our systems complete linearity has not been observed, Eq. 5-12 is going to be used to draw a comparison between the values obtained with this technique and those calculated in ✣5.4.5.

In Fig. 5-23 the coercivity is plotted against $T^{0.77}$ for the three particle sizes, F024, F026 and F028. The value of the coercivity at zero Kelvin as well as the effective anisotropy constant, K_{eff}, and the effective energy barrier, $\Delta E_{eff} (= K_{eff} \cdot V_m)$, are obtained. The results are displayed in Table 5-17.

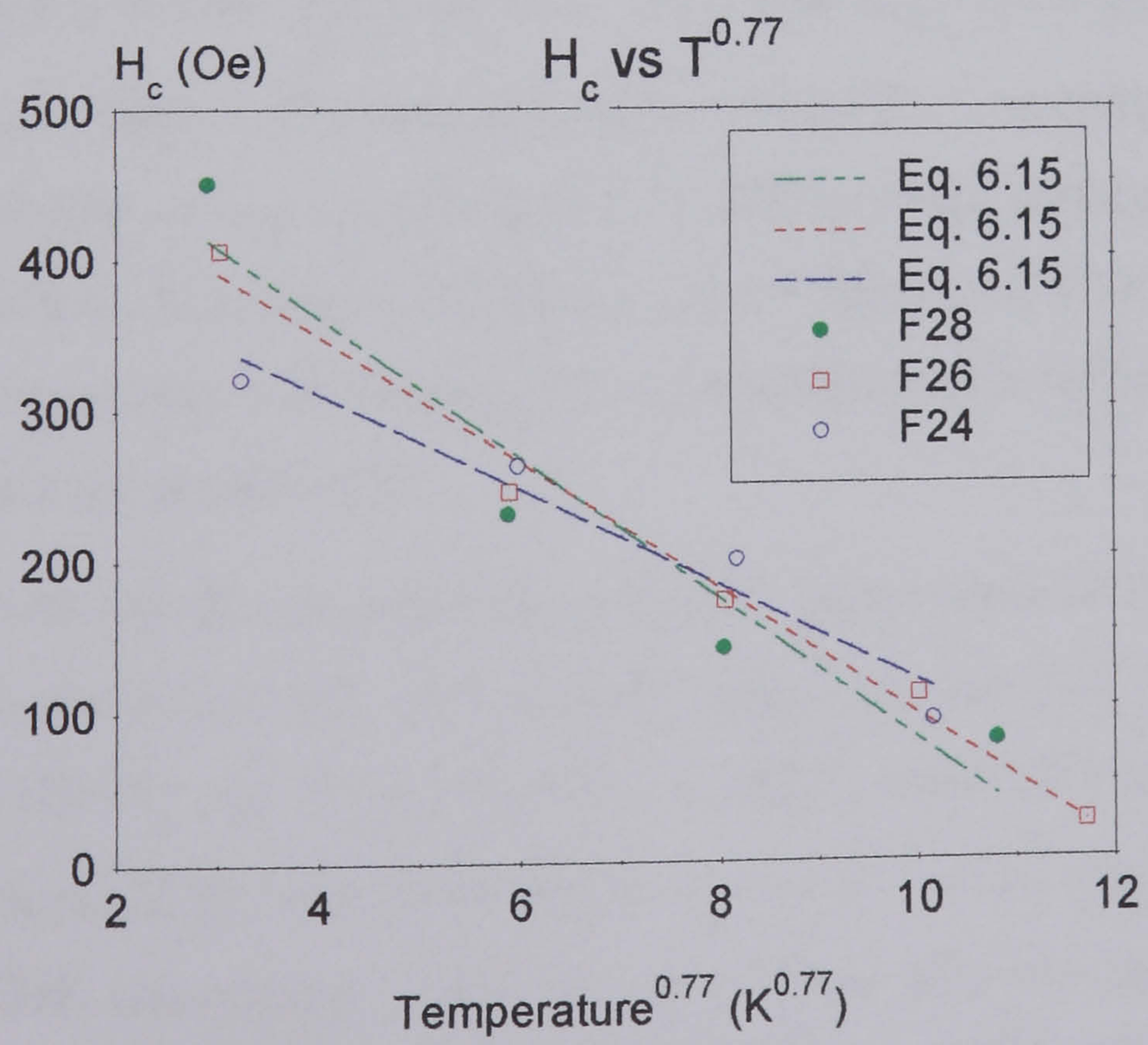

Figure 5-23

Coercivity vs temperature (Eq. 5-12) as calculated by Pfeiffer [1990 a], for all particle sizes

The anisotropy constant (column 2, Table 5-17) increases as particle size decreases, in agreement with the results obtained from the TDR measurements (✣5.4.5, and column 3 of Table 5-17). The anisotropy constants are, for all particle sizes, higher than the value for bulk magnetite, $1.1 \cdot 10^5$ (erg / cc) [Morrish (1965) p. 507]. An enhancement of K_{eff} with decreasing particle size was also observed by Chen et al. [1995] in Co particles with sizes $18 < D_m < 44$ Å, where a core-shell structure was inferred as the reason for this behaviour (see ✣5.11.1). A similar increase in the anisotropy constant was observed by Batlle and co-workers [1993] in doped nanocrystalline barium ferrite particles.

<u>k=0.77</u>	K_{eff} (10^5erg/cc)	K_{eff} TDR (10^5erg/cc)	ΔE_{eff} (10^{-14} erg)	ΔE_{eff} TDR (10^{-14} erg)	$H_c(0K)$ (Oe)	H_{Keff} (Oe)	$H_{Keff\ TDR}$ (Oe)
F024	3.4 ±0.5	3.3 ±0.2	8.1 ±1.2	6.6 ±0.1	439 ±38	2022 ±293	1647 ±129
F026	4.8 ±0.5	4.0 ±0.4	7.3 ±0.8	5.0 ±0.1	517 ±23	2861 ±317	2370 ±217
F028	6.4 ±1.1	4.6 ±0.5	6.9 ±1.1	5.0 ±0.1	549 ±68	3825 ±631	2728 ±279

Table 5-16

Effective anisotropy constant, K_{eff}, and energy barrier, ΔE_{eff}, coercivity at zero K, and effective anisotropy field, $H_{Keff} = 2K_{eff} / M_S$, as calculated from Eq.5-12, for all particle sizes. The results are compared with those obtained from the TDR analysis

An interesting result is that the values of K_{eff}, ΔE_{eff} and H_{Keff} are higher using Eq. 5.12 than via the TDR (see Table 5-17). This is possibly because the 'coercivity method' studies values of the coercivity at low temperatures ($T \leq 20K$), where surface effects seem to become more significant [Kodama et al. (1996)]. On the other hand TDR gives a value for the anisotropy constant over a wider range of temperatures where surface may not be so significant or at least not predominant.

Stoner and Wohlfarth [1948] calculated the coercivity for a system of randomly oriented non-interacting magnetic moments with uniaxial anisotropy that had coherent reversal, obtaining: $H_c = 0.479 \cdot H_k$ (A). If the values for H_k (TDR) obtained in column 8 of Table 5.17 are substituted in (A) the coercivities obtained are 1207, 1115 and 1307 for samples F024, F026 and F028, respectively, which are much higher than the experimental values (439, 517 and 549, respectively) for the coercivity at 0 Kelvin (Table 5-17, col.6). Similar results are obtained if the column 7 is used. This seems to indicate that the reversal

mechanism, at least at these low temperatures, is not coherent rotation of particles but a mechanism that takes the system through a less energetic path, such as curling or buckling as suggested by Aharoni [1988], possibly due to the presence of the surface which introduces irregularities and defects that may act as nucleation sites, lowering the coercivity.

5.7.4. Theoretical predictions [El-Hilo et al., 1998]

The main predictions of El-Hilo et al. model are given in the paper by the authors [1998]. The effect of particle size is shown in Fig. 5-24 (a). As expected, smaller particles give lower coercivities and remanence to saturation ratios. Fig. 5-24 (b) shows the magnetisation curves obtained at 4K using the mean anisotropy constants calculated in ✣5.4.5, showing, in all cases, higher values of coercivities and remanence to saturation ratio, compared to the experimental values. These results, together with the data obtained at higher temperatures (see Fig. 5-24 (c)), indicate, as suggested in ✣5.4.7 for the theoretical TDR, that for T>4K the anisotropy constants required to reproduced the experimental results are smaller than the calculated in ✣5.4.5, except at 4K (see Fig. 5-24 (a)), when higher values of K_{eff} are required for the theoretical model to reproduce the experimental results. It is interesting to note, that although the numerical values of the coercivities at 4K are not the same as the experimental values, at this temperature the model seems to predict a higher coercivity for F028 (59Å) compared to F024 (77Å), as observed in the experiments. The value of H_c for F026 (66Å), i.e., H_c=439 Oe, is lower than the values for both F024 or F028, giving evidence of the complicated interplay among particle size, width of the distribution, anisotropy, concentration and thermal effects.

Also, it is clear from the shape of the loops in Fig. 5-24 (c) that the thermal effects for T=12 K are much stronger in the experimental results. The same has been observed for T>12K, when comparing theoretical and experimental results. At 4K (Fig. 5-24 (b)), however, both the theoretical and experimental magnetisation curves are very similar. Thus, at this very low temperature, where thermal effects are very small, the theoretical model predicts curves very close to the experimental data.

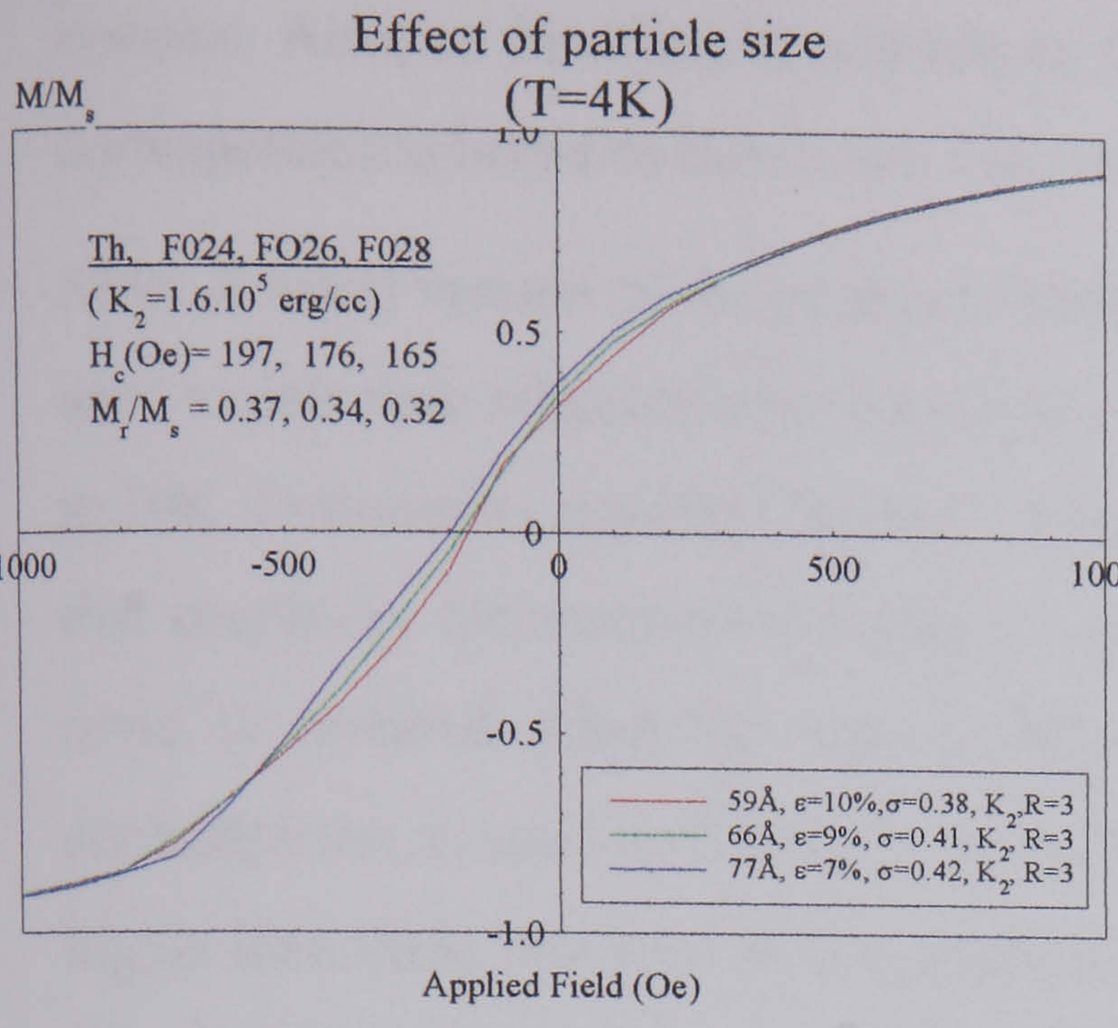

(a)

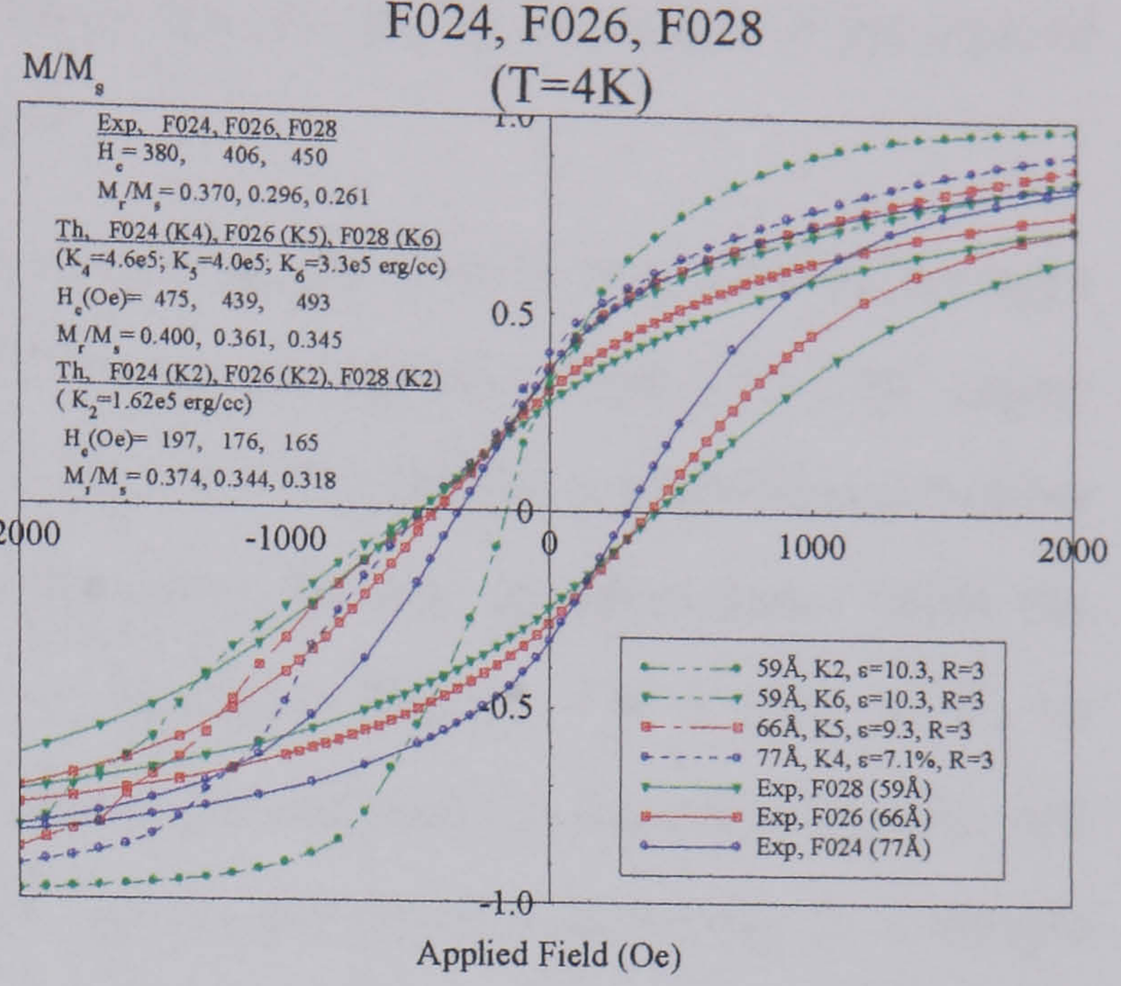

(b)

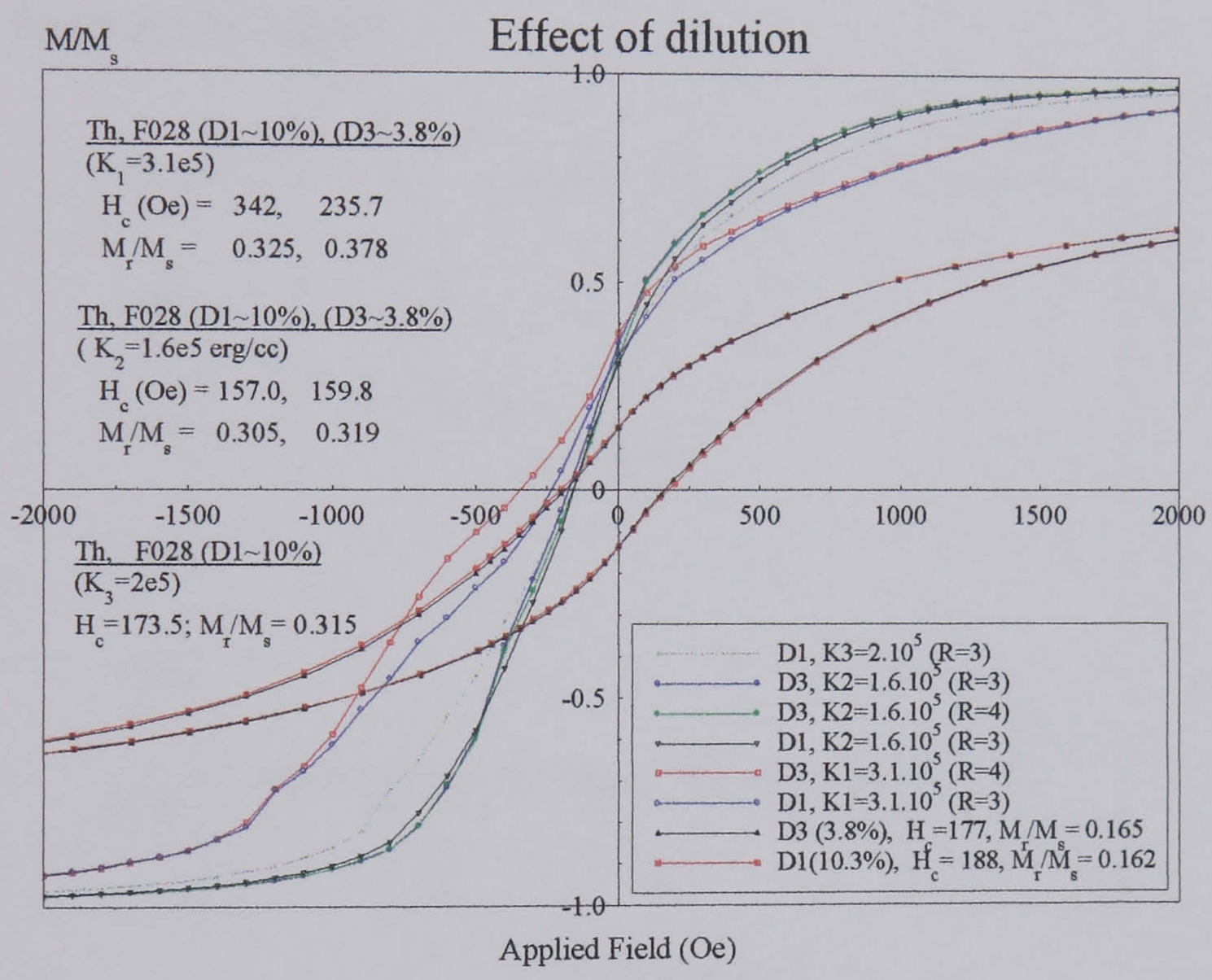

(c)

Figure 5-24

(a) *Effect of particle size according to the model of El-Hilo et al. [1998];* (b) *Comparison experiment-theory at 4K, for the 3 particle sizes;* (c) *Experimental and theoretical results for sample F028 (59 Å) at 12K, for different concentration and anisotropy constant.*

In general, and as already stated in ✣5.4.7, this model seems to predict higher energy barriers than the real barriers existing in the systems, which is manifested in the higher H_c and M_r/M_s calculated from the theoretical magnetisation curves with respect to the experimental values, when using anisotropies and concentrations calculated experimentally. It is a possibility that these higher energy barriers calculated by the model may be due either to an overestimated anisotropy constant or volume of the particles in the

systems. Also, an insufficient account of thermal effects can be the cause of the lack of correspondence between theory and experiment.

Note: A latest version of the program initially developed by El-Hilo et al. [1998] has been used to calculate magnetisation curves, for 60 Å diameter particles, with $K=5.1.10^5$ erg/cc at 10K. Preliminary results [Claudio Verdes, February 2000, private communication] show that coercivity increases for increasing concentrations, for low concentrations, while the trend is inverted when the concentration in increased further. For a plot of H_c vs concentration, ε, see Fig. 5-24 (d). Although the values obtained for the coercivity are still higher than those observed in the experimental results, the trend of coercivity with sample dilution observed in the experiments (Table 5-15) seems to be reproduced in this new version of the Montecarlo model.

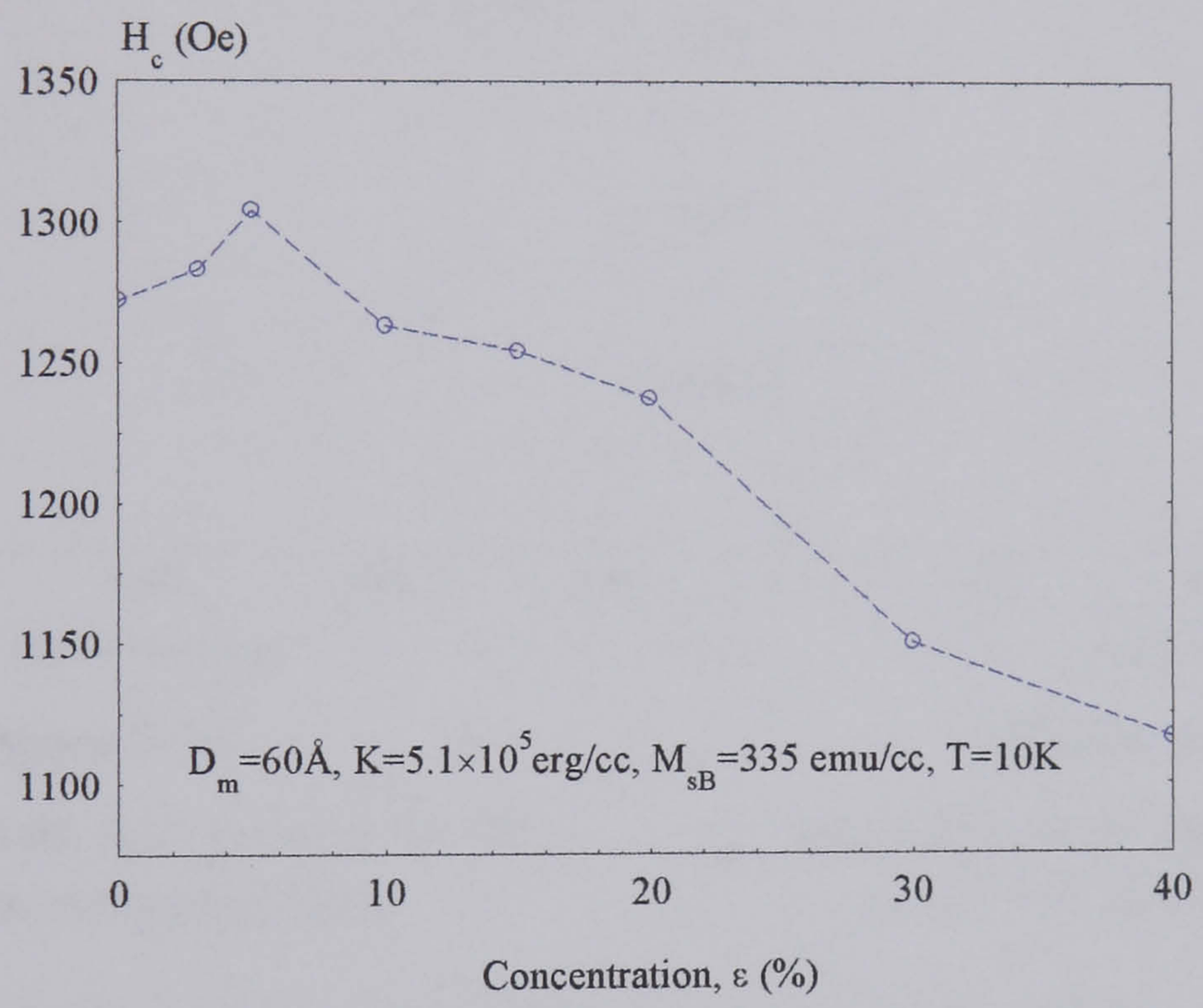

Fig. 5-23 (d)

Coercivity vs concentration of magnetic material, for a 60 Å sample, with $K=5.1.10^5$ erg/cc at 10K, as obtained from the latest version of El-Hilo et al. [1998] model [Claudio Verdes, private communication].

5.8. IRM, DCD and ΔM curves at different temperatures

In this section the remanence curves have been utilised to extract information about interactions and particle size effects. The well-known ΔM plot [Kelly et al. (1989)] (see also ✣2.5.3.1) has been studied and its applicability for fine particle systems evaluated. It seems to be the case that the irreversible susceptibility curves, χ_{irr}, which are the derivatives of the remanence curves with respect to the field, give very valuable and easy

to interpret information about the influence of interactions and particle size in these systems.

5.8.1. Effects of particle size

It has been observed that the χ_{irr} curves are very informative. In fact, the effect of particle size on the remanence curves is best studied by means of these curves. The irreversible susceptibility has been calculated for all particles sizes at 4K. The results are shown in Fig. 5-25 and 5-26. The values of the remanence coercivity, H_r, for which χ_{irr} is maximum, are shown in Table 5-18.

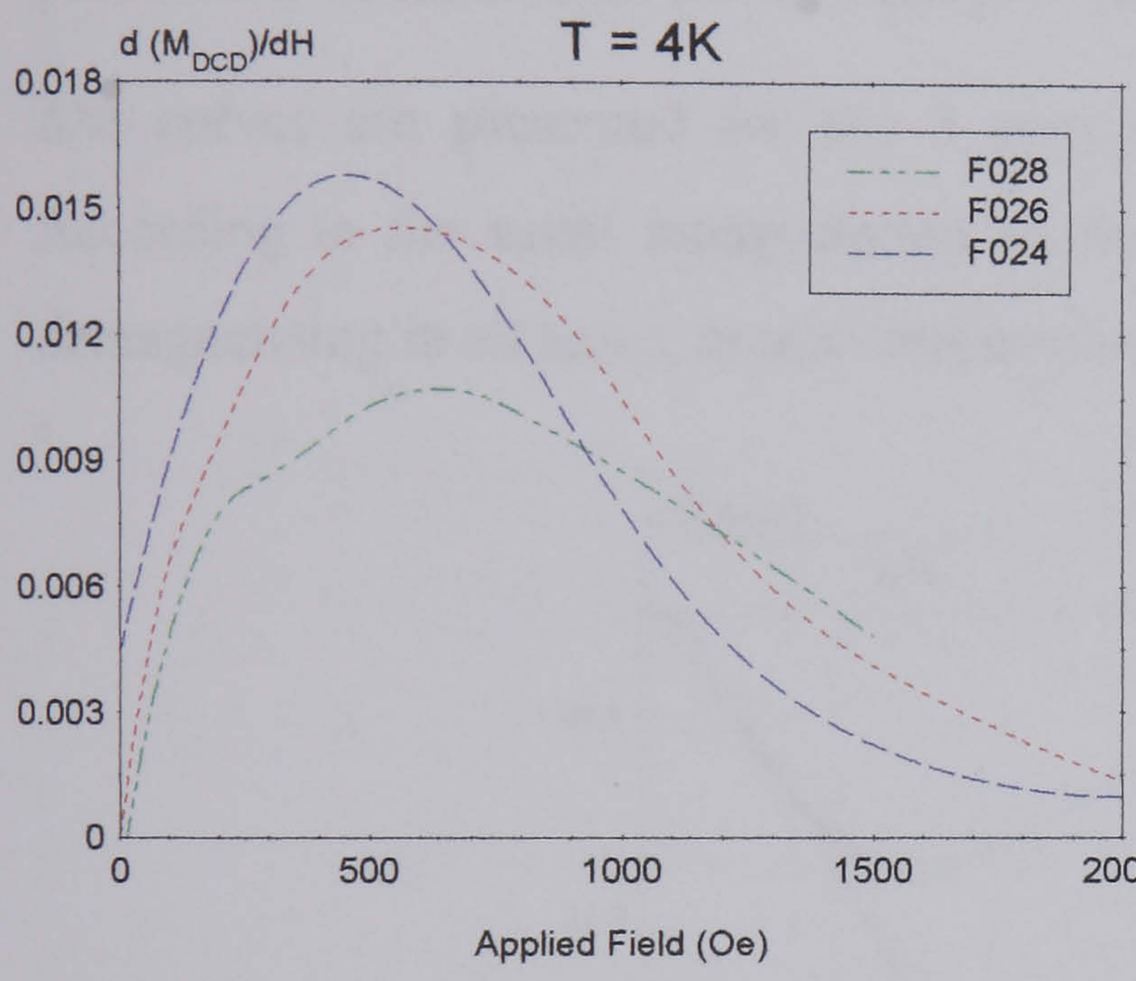

Figure 5-25

χ_{irr} obtained from the differential of the DCD curves with the applied field.

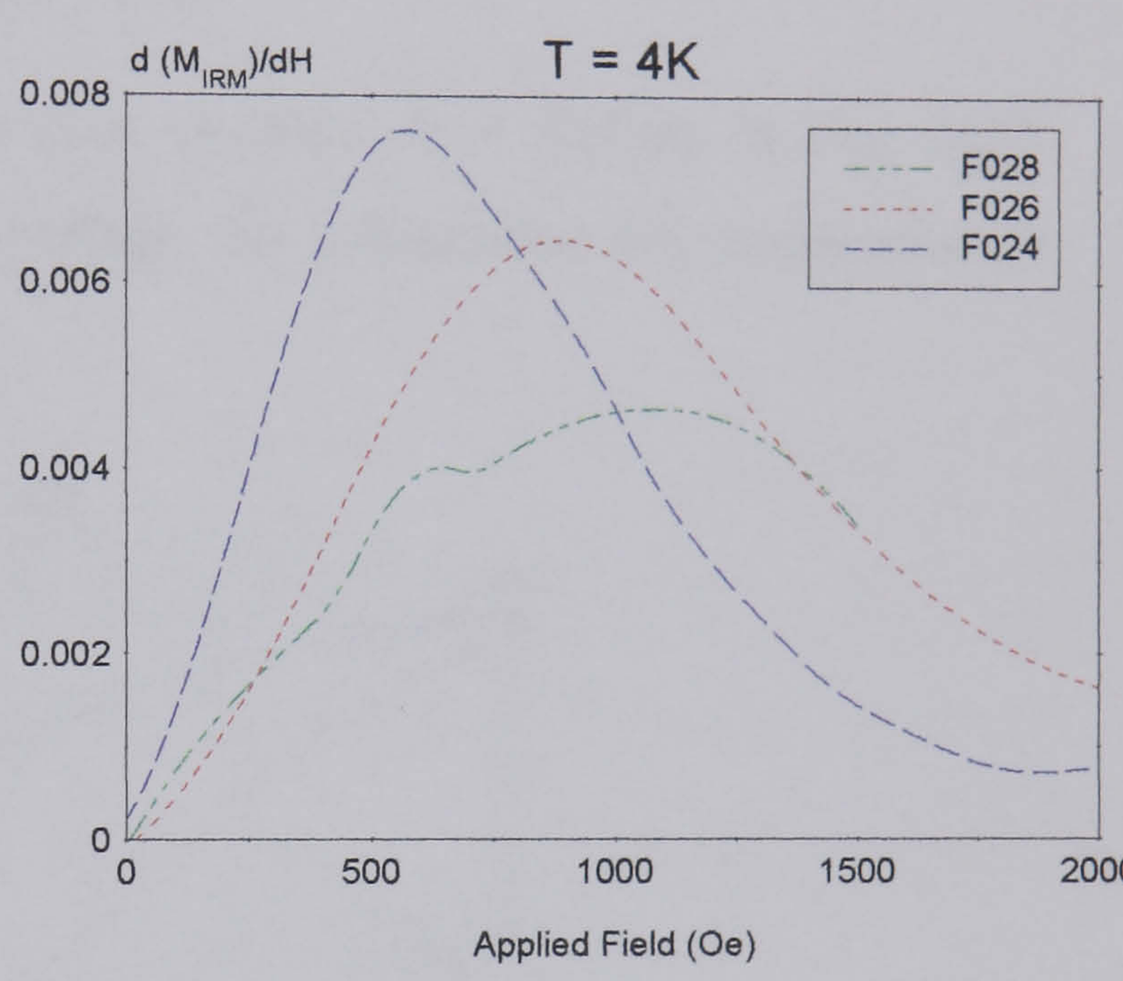

Figure 5-26

χ_{irr} obtained from the differential of the IRM curves with the applied field

From Figs. 5-25, 5-26, it can be seen that H_r increases as particle size diminishes, as observed in the evolution of coercivity with particle size at 4K (Table 5-16) and 0K (Table 5-17). Thus these results are consistent with those obtained from the hysteresis loops at the same temperature. The reason for this increase in H_r with decreasing particle size, contrary to what is expected and unlike the observed results at other temperatures, must lie in the manifestation of a strong anisotropy that seems to become more obvious for lower temperatures [Kodama et al. (1996)], presumably due to the spins in the surface of the particles as suggested in other sections.

T = 4K	F024	F026	F028
$H_{r(DCD)}(Oe)$	458 ± 4	565 ± 4	633 ± 3
$H_{r(IRM)}(Oe)$	469 ± 4	886 ± 4	1085 ± 3

Table 5-17

Remanence coercivity, H_r, for the IRM and DCD curves for all particle sizes, at 4K.

Another interesting result is the fact that the χ_{irr} curves become wider with decreasing particle sizes. This fact may be a further evidence of the bimodal behaviour, observed particularly in the smaller particle samples (see ✣5.3.1).

ΔM curves are presented for the 3 particle size samples, at 4 Kelvin in Fig. 5-27. According to the usual interpretation of these plots, the interactions are predominantly demagnetising in all cases, at that temperature.

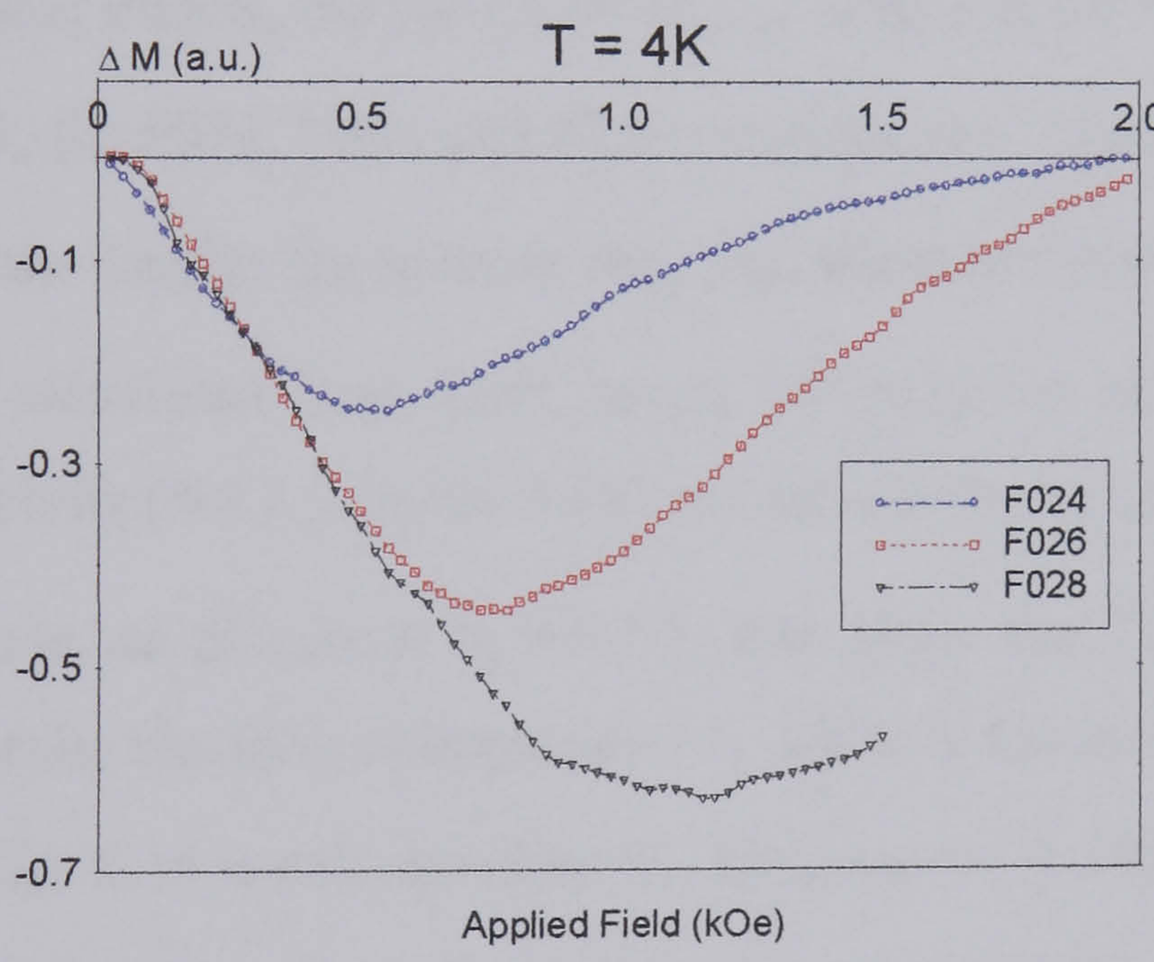

Figure 5-27

ΔM for the 3 particle sized samples, measured at T=4 K.

5.8.1.1. Distribution of anisotropy fields

Neglecting the contribution from superparamagnetic particles, the distribution of anisotropy fields, $g(H_K)$, can be determined from the switching field distribution (SFD) as obtained from the differential of the IRM curve [Pfeiffer (1990 *a*)], as the remanence curves represent the irreversible changes in magnetisation. According to Pfeiffer, for a system with particles oriented at random,

$$g(H_K) = \frac{1}{2} \cdot SFD\left(\frac{H_K}{2}\right) = \frac{1}{2} \cdot \left.\frac{dM_{IRM}}{dH}\right|_{H=H_K/2} \qquad \textbf{(Eq. 5.13)}$$

An order of magnitude of the effective anisotropy field, H_{Keff}, is twice the remanent coercivity obtained from the IRM curve, i.e., $H_{Keff} = 2 \cdot H_{r(IRM)}$. According to this, the effective anisotropy fields corresponding to the 3 particle sizes are 958, 1772 and 2170 Oe, for F024, F026 and F028. These values are for 4 K, where the thermal effects are small. In the same paper, Pfeiffer gave an expression that corrected the anisotropy field for thermal effects present, so that the intrinsic anisotropy field, $H_{Ki,\,eff}$, is given solving the following equation,

$$H_{Keff} = H_{Ki,\,eff} - H_{Ki,\,eff}{}^{0.3}\left(\frac{2 \cdot \ln(\tau \cdot f_0) k_B T}{V_m M_{sB}}\right)^{0.7} \qquad \textbf{(Eq. 5.14)}$$

Correcting from thermal effects, the values of $H_{Ki,\,eff}$ obtained for the 3 particle sizes are 1537, 2486 and 3463, for F024, F026 and F028, respectively. Although, in general, K_{eff} and H_{Keff} are higher the smaller the particle size, regardless of the measurement technique used, the anisotropy calculated from TDR curves (✣5.4) gives lower values than those obtained via the coercivity (✣5.7.3, Table 5-17) and remanent coercivity data.

It seems to be the case, as discussed in ✣5.7.3, that while the TDR gives an effective anisotropy constant at the blocking temperature ($T_B \approx 15K$), the intrinsic anisotropy field, $H_{Ki,\,eff}$ obtained via Eq. 5.14 is calculated at 4K, temperature at which the surface effects are presumed (✣5.7.2) to be much stronger [Kodama et al. (1996)]. Consequently, it seems logical that this latter measurement technique gives higher values of anisotropy constants, as at low temperatures the measurements are dominated by these effects. According to this reasoning it could be possible to extract a surface anisotropy constant from the anisotropy constants obtained from TDR and $H_c(T)$ (or $H_{ki,eff}$). This will be the object of ✣5.11.1.

5.8.2. Effects of interactions

The effect of interactions on the remanence curves and ΔM plots has been studied at T=11.5 K for samples D1 and D4 of F024 (see Figs. 5-28 and 5-29).

It can be observed that both the DCD and IRM curves for sample D4 lie 'on top' of the corresponding curves for D1 (Fig. 5-28). This is consistent with the remanence to saturation ratio values obtained in ✣5.7.1. The results are also consistent with the ΔM plots obtained in Fig. 5-29, where the more concentrated sample (D1) seems to have more demagnetising interactions than the more diluted D4, for all the applied fields.

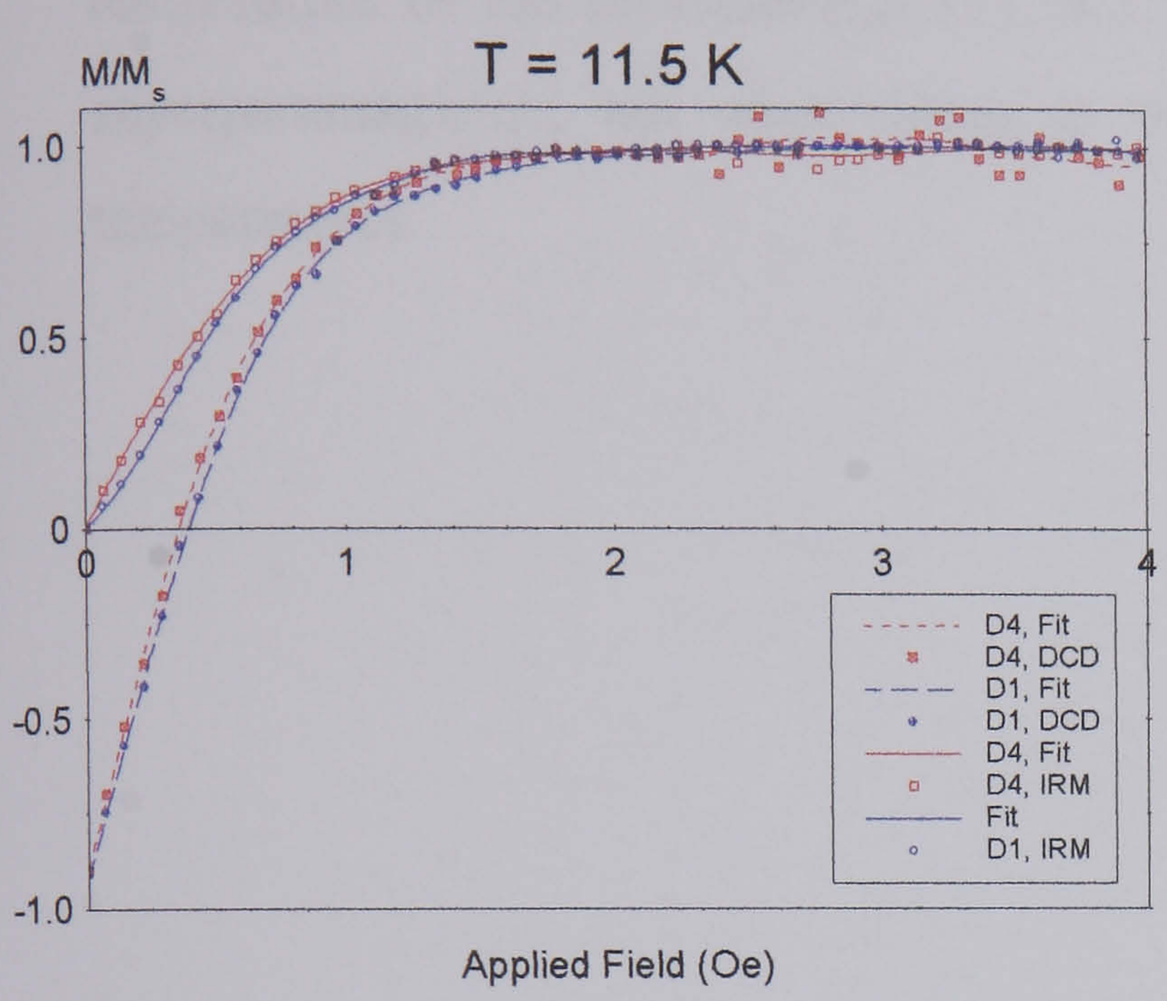

Figure 5-28

IRM and DCD curves for D1 and D4 of F024 at 11.5 K.

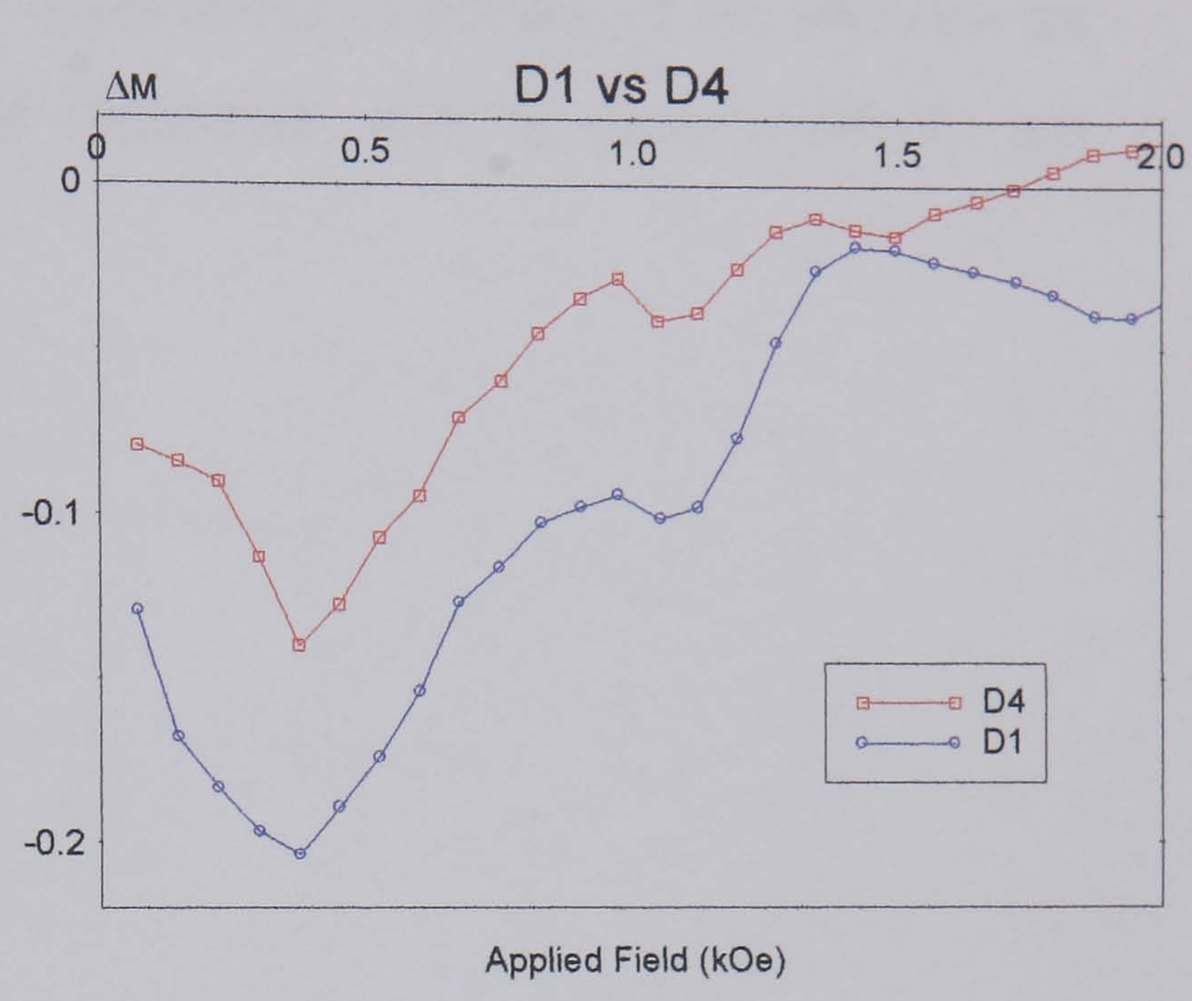

Figure 5-29

ΔM curves for D1 and D4 of F024 at 11.5 K

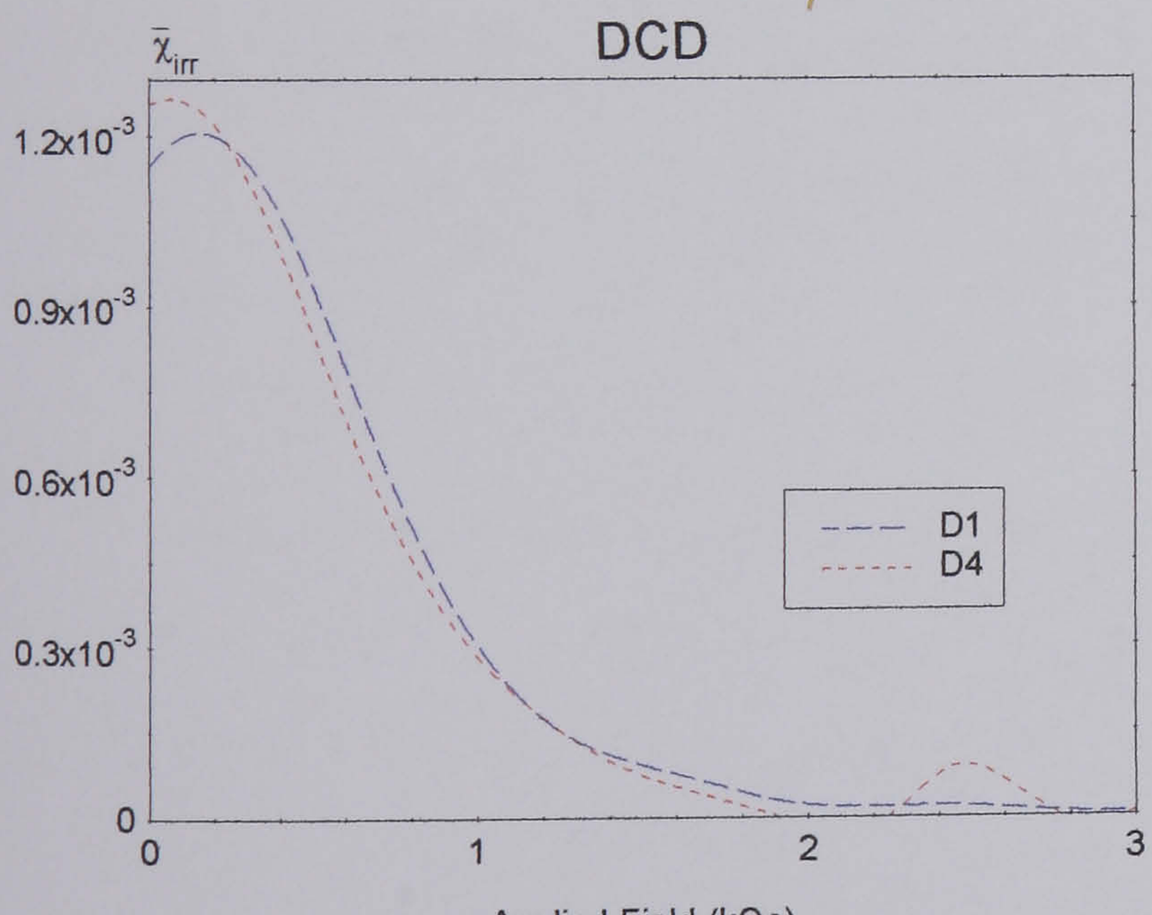

Figure 5-30

χ_{irr} *obtained from the DCD curves of samples D1 and D4 of F024, at T=11.5 K.*

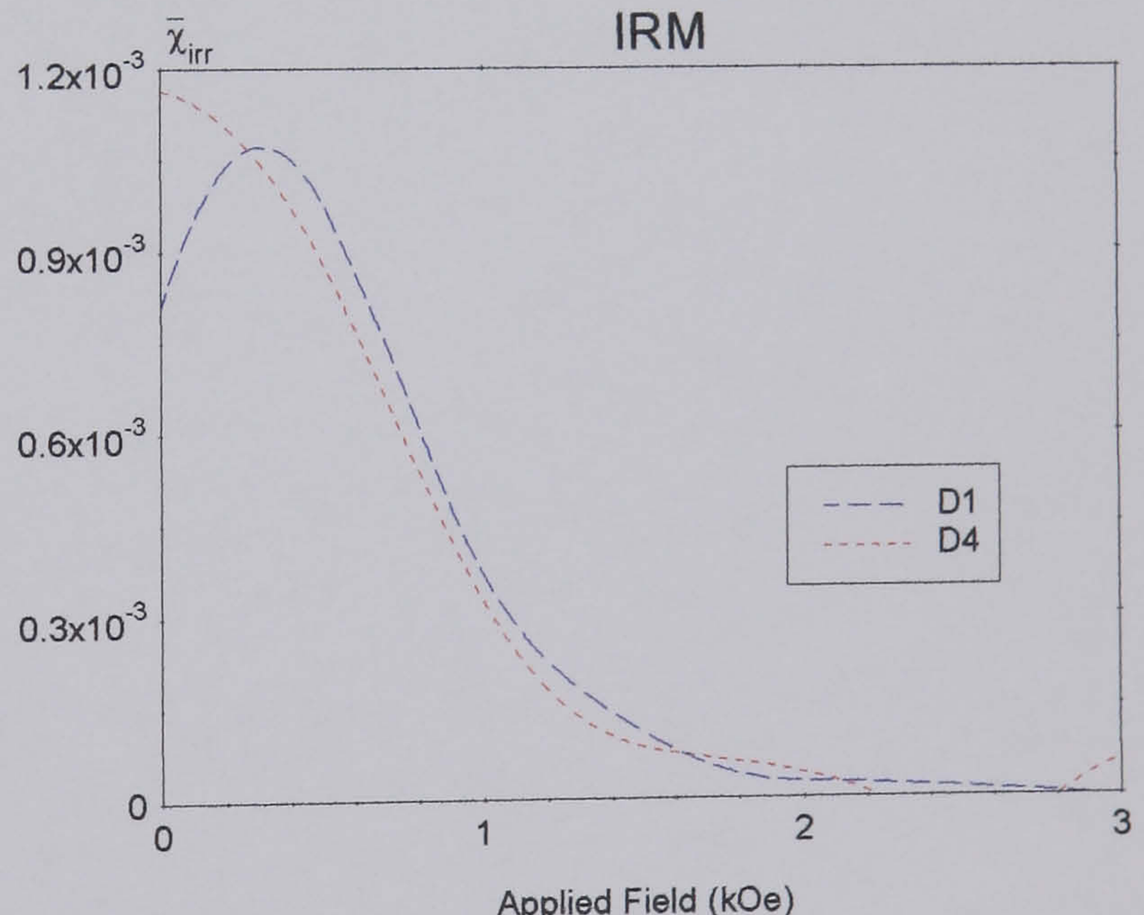

Figure 5-31

χ_{irr} *obtained from the DCD curves of samples D1 and D4 of F024, , at T=11.5 K.*

As it was shown in the previous section, the derivatives of the remanence curves, χ_{irr}, give valuable information. From the Fig. 5-30 and 5-31 it is clear that the remanence coercivity, H_r, from both the IRM and the DCD curves is higher for D1 than for D4, mirroring the

behaviour of coercivity with dilution as observed in the hysteresis loops (✣5.7.1), for the same temperature. This is another manifestation of higher anisotropy or more stable microstructures of the more concentrated sample.

It is significant that both χ_{irr} curves are 'cut' at the lower fields; this indicates that at the temperature of the measurement (11.5K) a considerable proportion of the particles are superparamagnetic, not contributing to the remanence, even at these relatively low temperatures.

" It is utterly beyond our power
to measure changes of things by time.
Quite the contrary, time is an abstraction
at which we arrive by means of the changes of things ".
(*Ernst Mach*, Austrian physicist, 1872)

5.C. *Time dependence, attempt frequency and surface effects*

5.9. Viscosity measurements

For the time dependence measurements, all the samples have been frozen in a zero magnetic field. In each case, a saturating field of $-10kOe$ has initially been applied. Then different positive fields are applied in the opposite direction and the magnetisation measured during 900 seconds. The magnetisation relaxes linearly with the logarithm of the measurement time.

5.9.1. Relaxation of magnetisation

In this section the relaxation of the magnetisation is going to be studied assuming a logarithmic law (see ✣2.7). In Fig. 5-32 below, it is clear that the magnetisation relaxes linearly with the logarithm of the measurement time, over the time-scale of the measurement (15min). This is the case for all the samples studied.

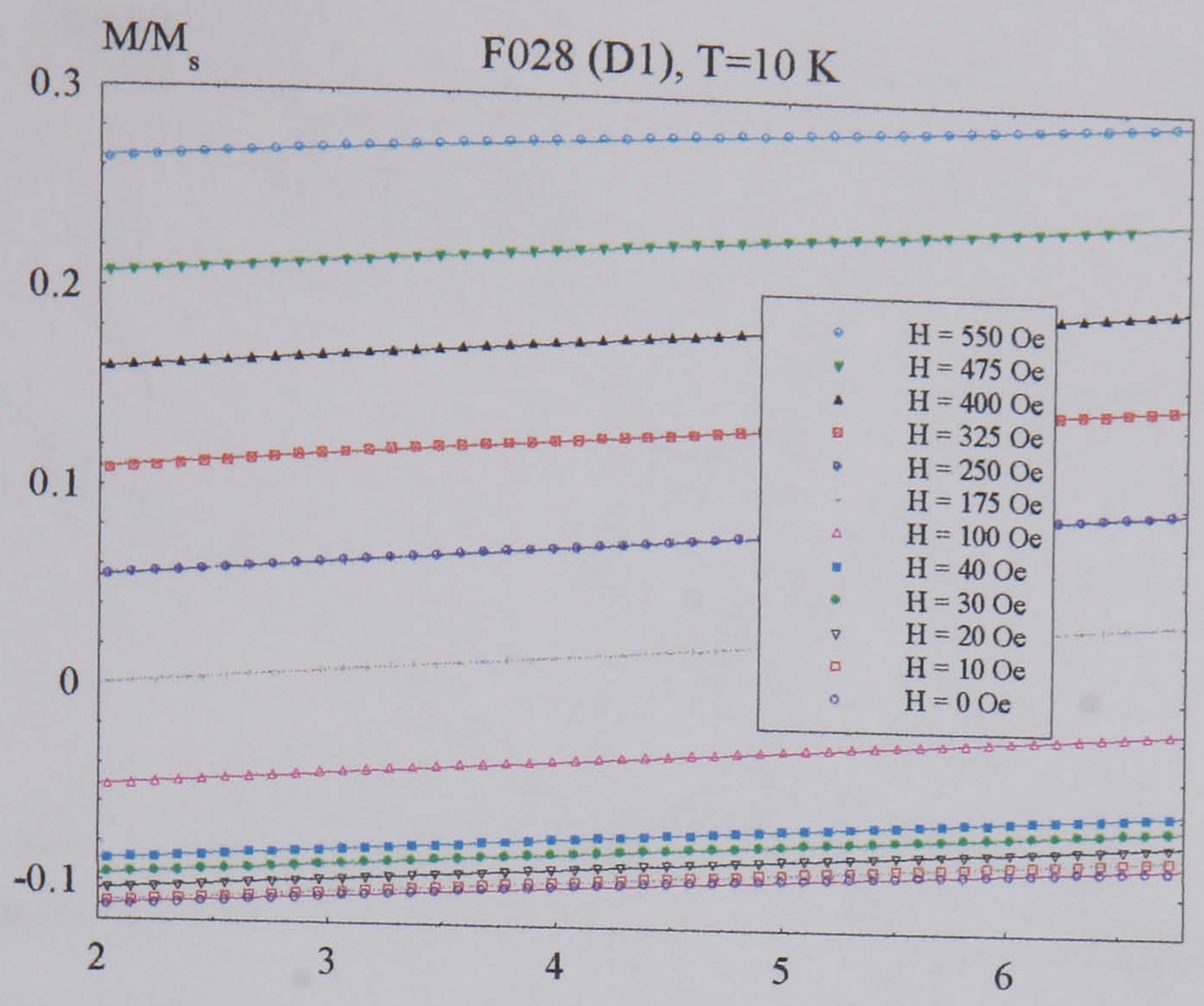

Figure 5-32

Normalised magnetisation plotted versus the logarithm of time. Linear behaviour is clearly observed.

In this section the relaxation of the systems is studied via S, the coefficient of magnetic viscosity, which is the slope of the relaxation curves (see ✣2.7.3) vs the logarithm of time, i.e.,

$$S = \frac{d\left(M(T)/M_s(T)\right)}{d\ln(t)} \qquad \textbf{(Eq. 5.15)}$$

At each temperature, the magnetisation is normalised to the saturation value so it is possible to compare relaxation measurements for different particle sizes and dilutions.

Data over longer times (t > 900 sec) have not been recorded, but linear behaviour has been observed in similar systems by other authors [O'Grady et al. (1981), El-Hilo (1990)] for times up to 1200 sec. In fact, unless a really long observational time window is available, a linear behaviour with ln(t) is expected for these fine particles systems. In this sense, a simpler way of mapping the distribution of energy barriers is to study the relaxation at different temperatures, as shown in Fig. 5-33, 5-34 and 5-35.

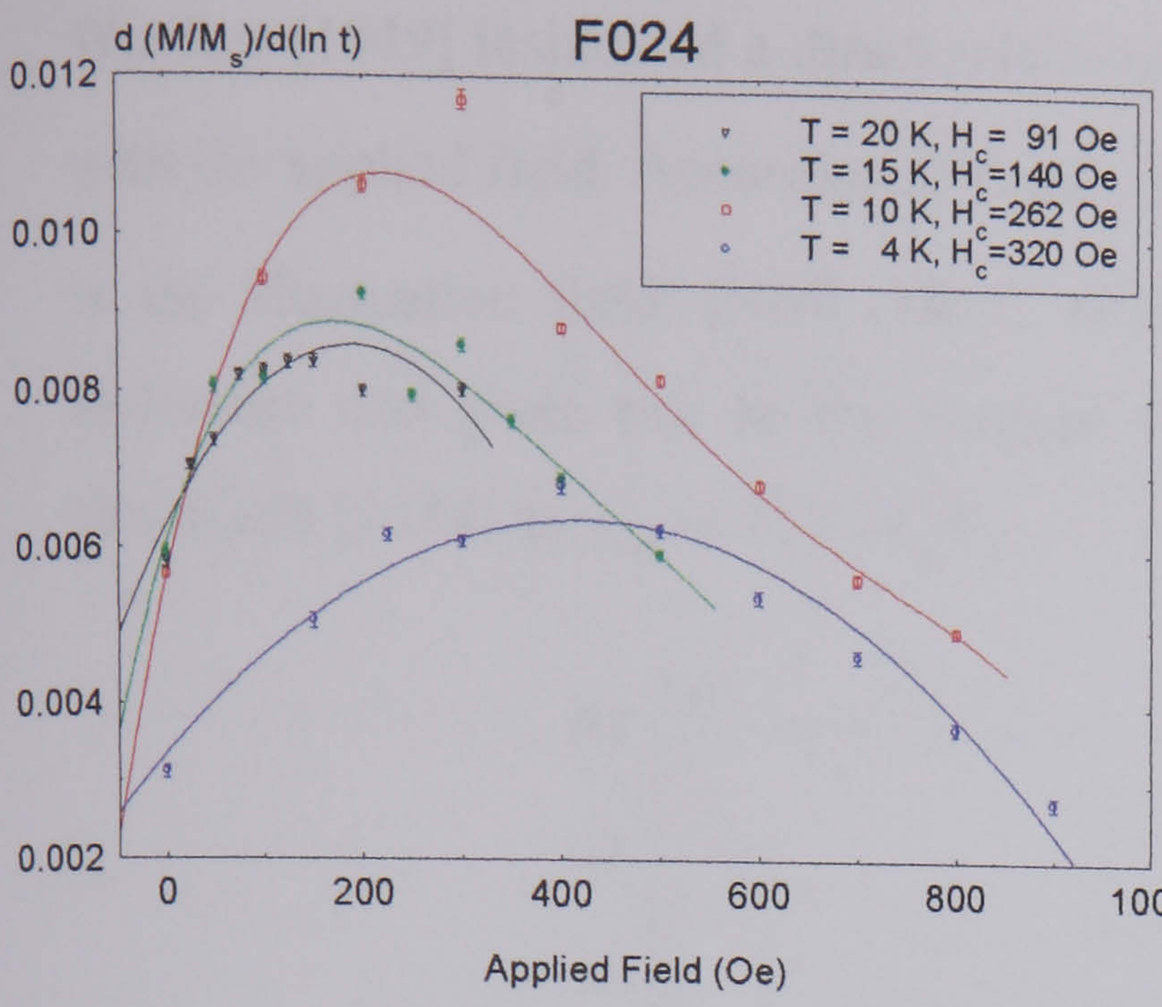

Figure 5-33

Coefficient of magnetic viscosity vs applied field for sample F024

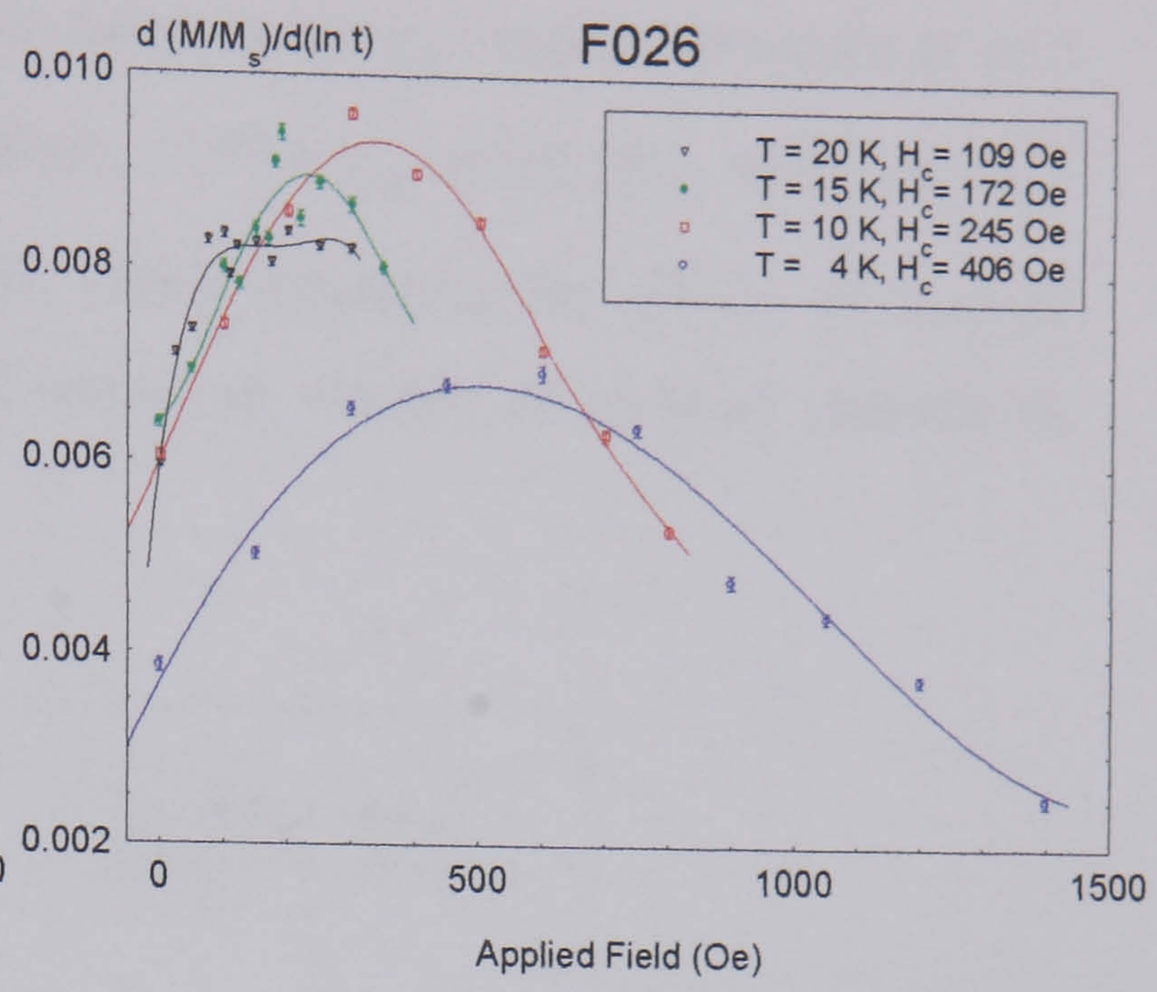

Figure 5-34

Coefficient of magnetic viscosity vs applied field for sample F026

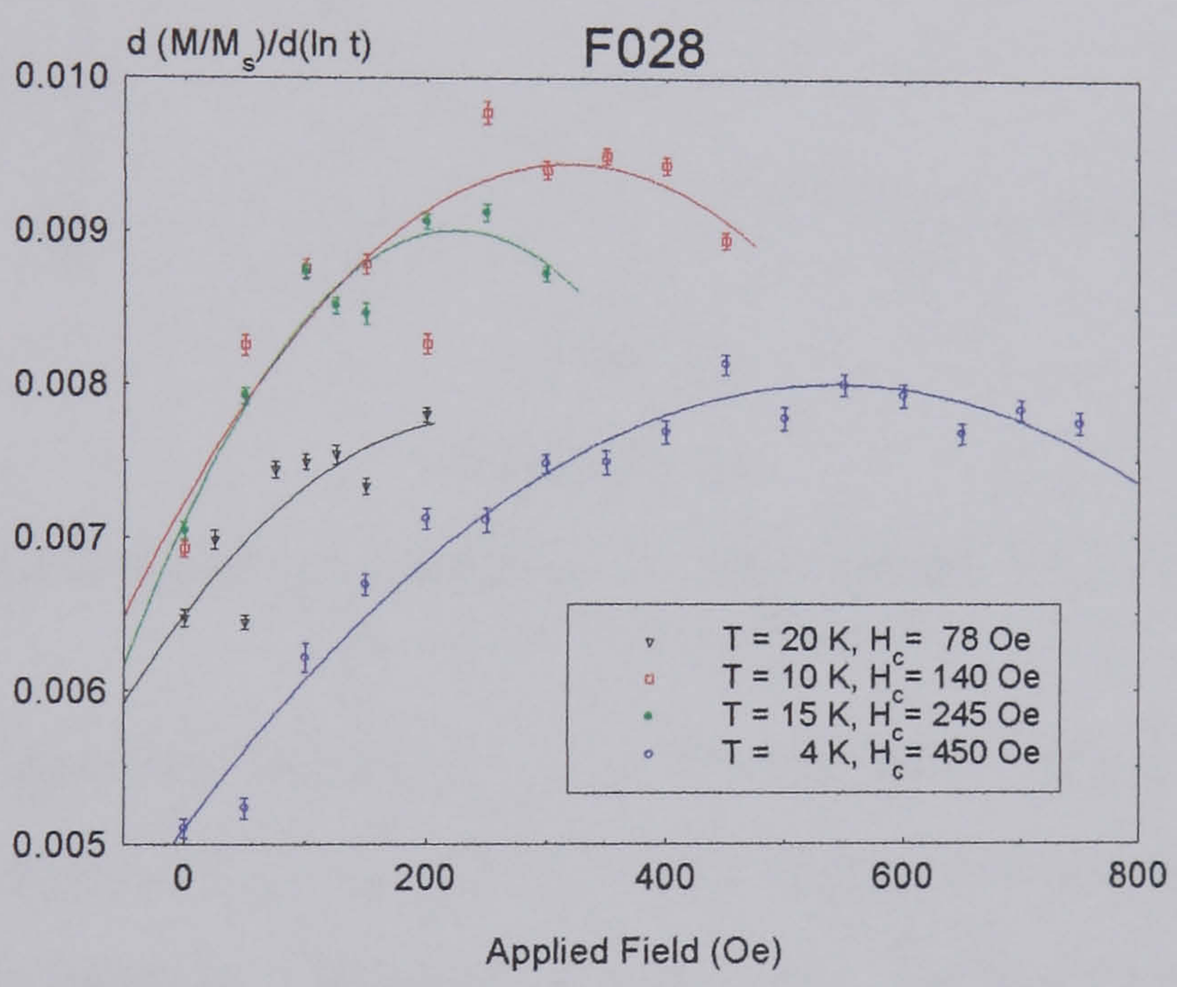

Figure 5-35

Coefficient of magnetic viscosity vs applied field for sample F028

There are two main conclusions to be drawn from the data. Firstly, the dependence of the coefficient of viscosity, S, with applied field; secondly, the evolution of S with temperature. It has been traditionally accepted [O'Grady et al. (1981)] that the maximum value of S will happen around the coercivity value. This is not the case for these samples, where the maximum is found near the remanence coercivity, H_r, as obtained from the maximum of the χ_{irr} of the DCD curve (see ✣5.8), as it would be expected. This is the case for all particle sizes. This has also been observed by other authors [e.g. Uren et al. (1988), Garcia del Muro et al. (1997)]. Although treating a different problem, Street and

Woolley [1949] insinuated a direct relationship between the χ_{irr} and the dependence of S with the applied field. According to these authors, $S(H) = \chi_{irr}(H)H_f(H)$, where $H_f(H)$ is the 'fluctuation field' [Néel (1950, 1951)], which represents the effects of thermal activation and gives rise to the concept of activation volume of reversal, defined by Wohlfarth [1984] as $v_{act} = kT / M_s H_f$.

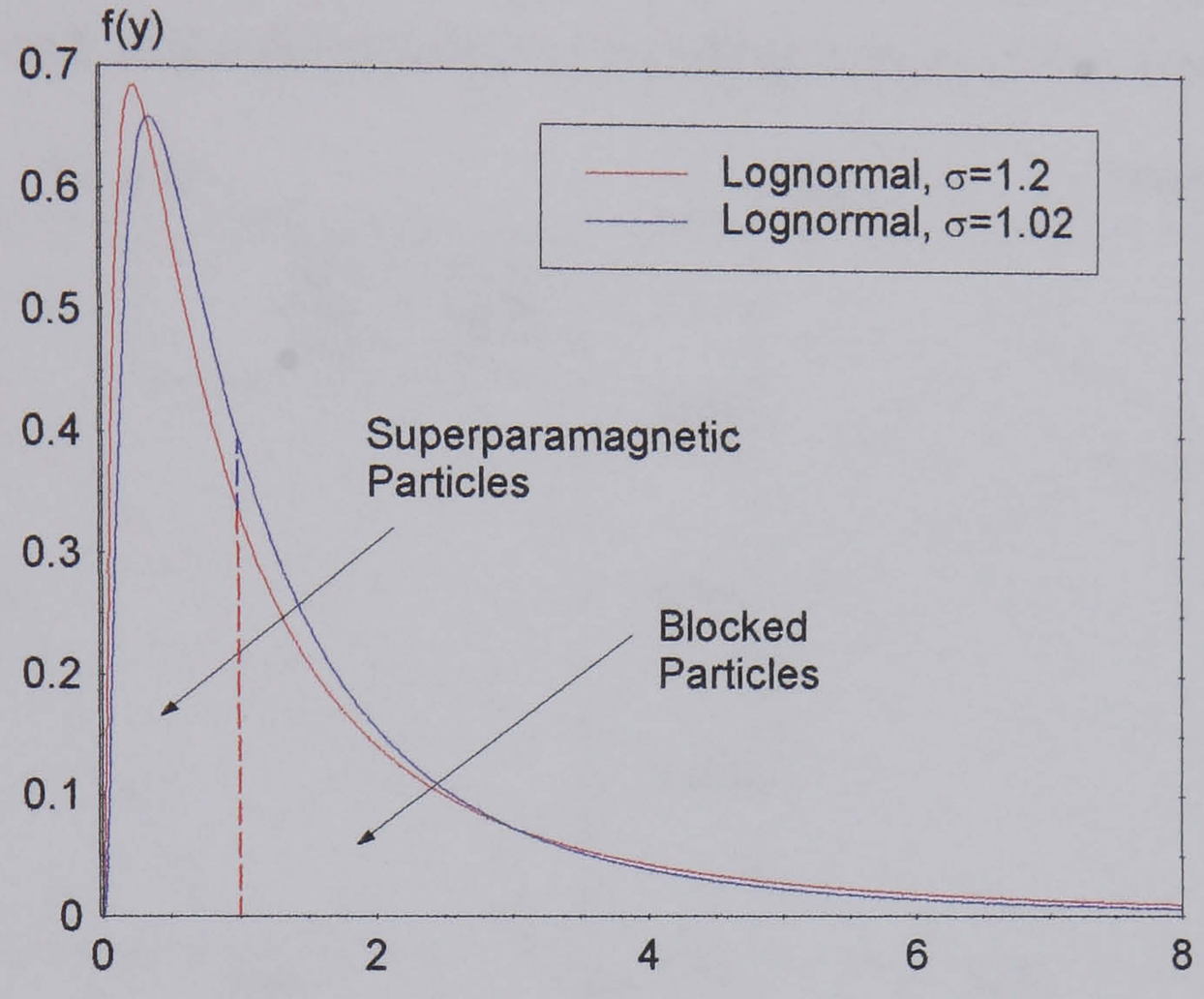

Figure 5-36

Distribution of (reduced) blocking temperature as obtained from ✣5.4.1 (σ=1.02) and ✣5.4.3 (σ=1.2) for sample F024.

With respect to the apparent slowing down of the relaxation as temperature is raised (T ⩾10K), it can be understood if a clear picture of the blocking temperatures or diameters of the systems is kept in mind (see diagram of Fig. 5-36). At higher temperatures the small particles, that would contribute with a fast relaxation. i.e., higher S, relax almost instantaneously, i.e., they are superparamagnetic, as observed in the χ_{irr} curves at 10K in the previous section (✣5.8.2). At this and higher temperatures, the particles that contribute to the relaxation are the largest ones (see Fig. 5-36), with higher blocking temperatures, at the tail of the distribution. These larger particles will relax slower than the smaller ones (see curves for 15 and 20K, in Fig. 5-33, 5-34 and 5-35). Alternatively the relaxation behaviour can be explained using the expression, $S = 2M'_s kTf(\Delta E)$ [Gaunt (1986)] where $f(\Delta E)$ is the value of the distribution of energy barriers of the active regions of the sample (regions which are changing their magnetisation in the field and at the time of the measurement), and M'_s is the spontaneous magnetisation. Thus S is proportional to the

value of the energy barrier that is being overcome and it will increase if the value of this value increases, and decrease if $f(\Delta E)$ decreases (see Fig. 5-36 and ✣2.7.3).

5.9.1.1. Influence of particle size

The effect of particle size on the relaxation data is shown for temperatures 4 and 10 K (see Fig. 5-37 and 5-38), where the thermal effects are small. At these temperatures, it is the particles at the low end of the distribution of blocking temperatures which are relaxing.

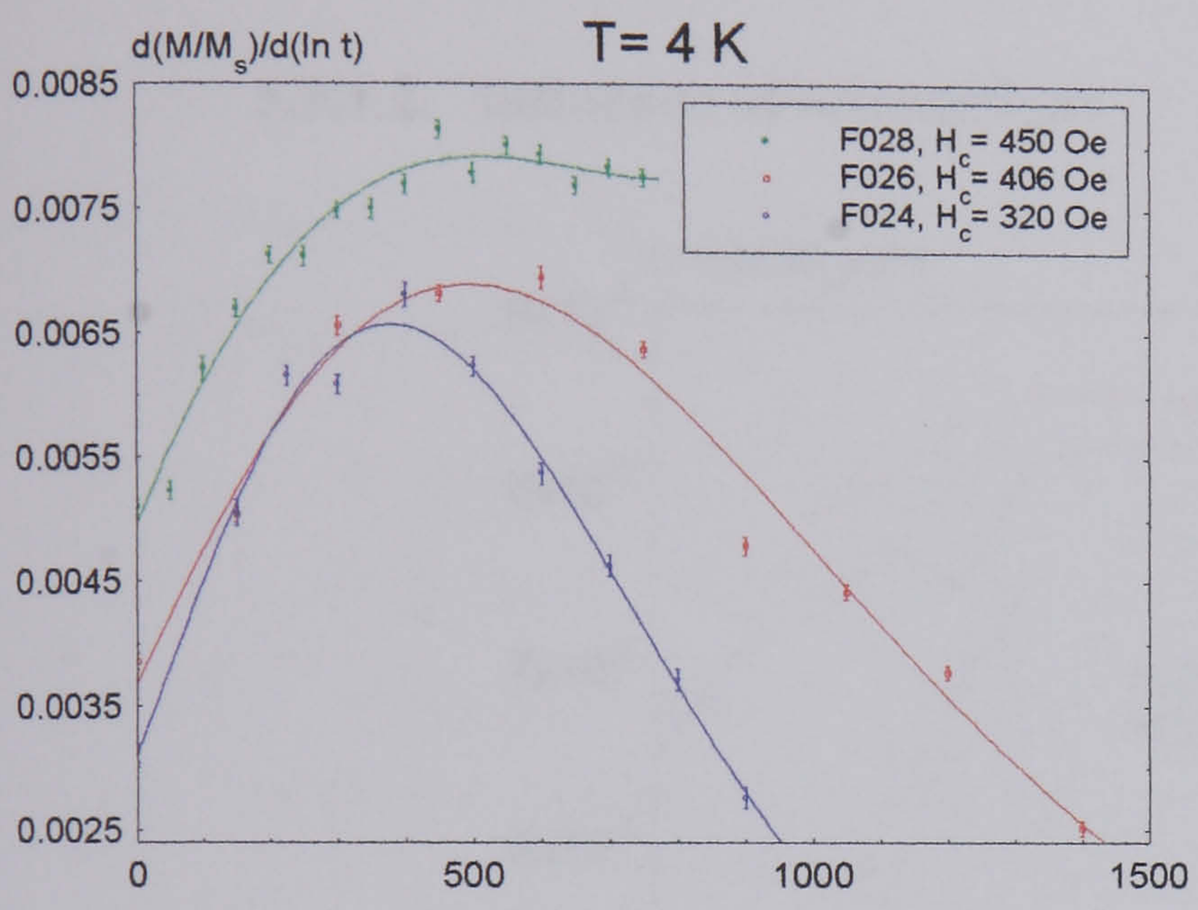

Figure 5-37

Coefficient of magnetic viscosity vs applied field for sample F024.

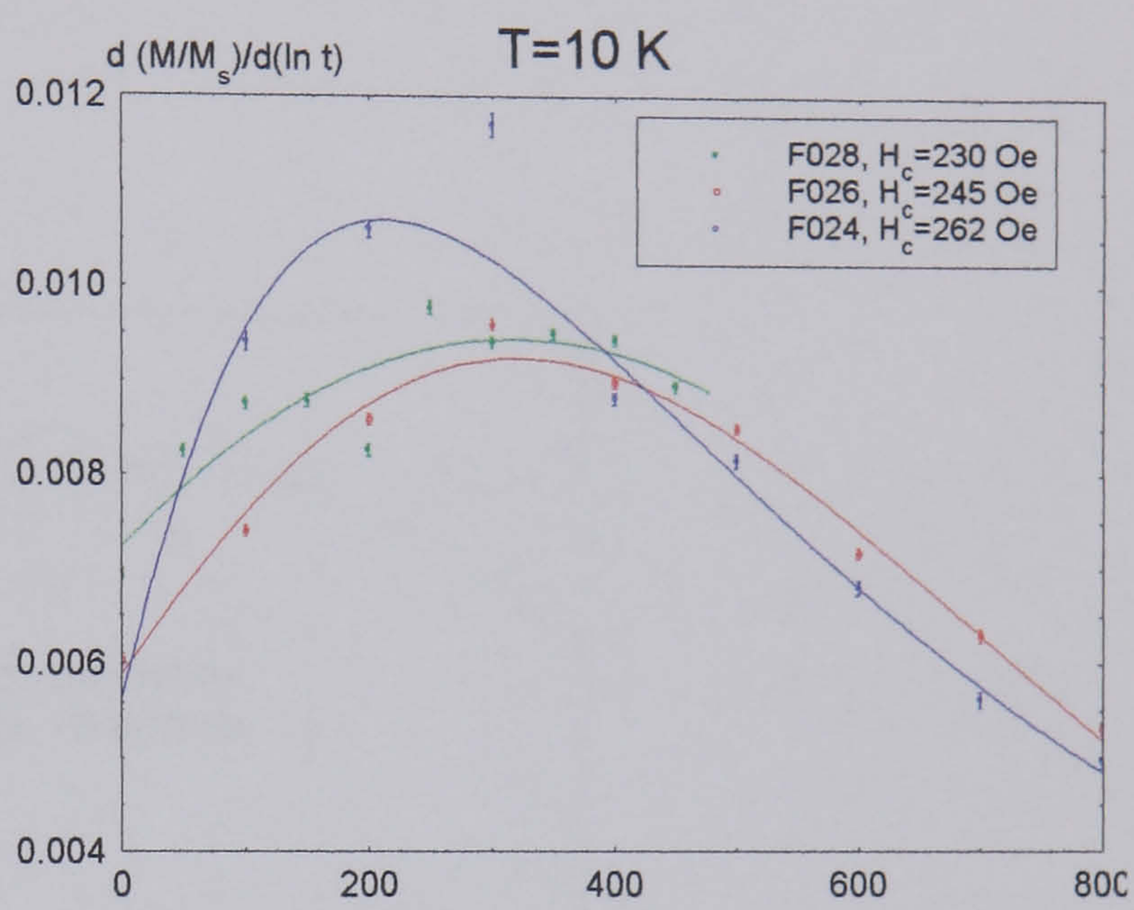

Figure 5-38

Coefficient of magnetic viscosity vs applied field for sample F024

The effect of the particle size is clearly seen in the figures. The fastest (higher S) sample to relax is F028, as expected from its smaller energy barrier (Table 5-17). The effect is not so obvious for F024 and F026 whose values of S seem to be fairly close. However, S of F026 lies clearly 'on top' of the values of F024 for higher fields. This can also be an effect due to the larger H_r of F026 (✣5.8.1) compared to that of F024, so that the particles in F026 relax faster at higher fields because these are closer to their remanent coercivity, H_r.

An interesting result, that can be observed especially at the lowest temperatures ($T \leq 10K$), is the fact that S vs H becomes broader and the peak appears at higher fields, for the smaller particle sizes, following the same trend observed in the derivatives of the IRM and DCD curves. This is possibly due to anisotropic effects, dominant at these low temperatures, as observed from the behaviour of both H_r (✣5.8.1) and H_c (✣5.7.2) with particle size at low temperatures.

At higher temperatures, 10, 15 and 20 K, the curves of all samples intermix, and it is not clear which one lies over or underneath. At these temperatures all the energy barrier distributions and sizes are quite complex. For example, at higher temperatures, in F028 may be only the larger volume particles are relaxing and these are similar to the ones in F026 and F024 (Fig. 5-36, distribution of blocking temperatures). It is not clear why having practically no error in the M vs ln(t) plots (Fig. 5-32), the S vs H curves present so much scatter.

5.9.1.2. Influence of interactions

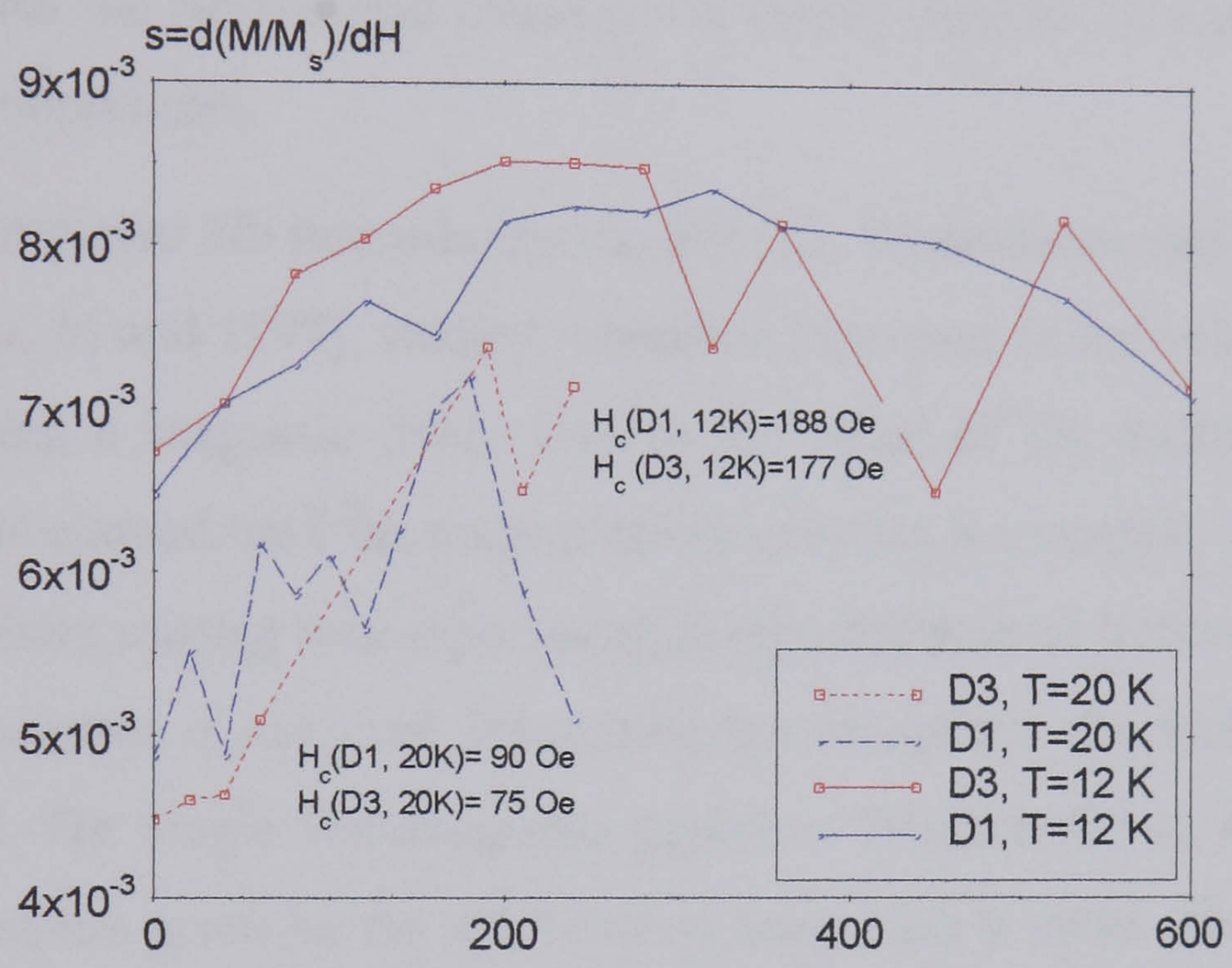

Figure 5-39

Coefficient of magnetic viscosity, S, obtained from the slope of the normalised magnetisation against ln(t), plotted vs the applied field for dilutions D1 and D3 of F028.

For the study of the influence of interactions in the time dependence, dilutions D1 and D3 of sample F028 have been used. From Fig. 5-39, it can be seen that at 12K the diluted samples seem to relax faster than the concentrated ones, for applied fields between zero and the maximum of the curves. For fields above the maximum, the noise in the curve for sample D3 is too high to draw any reliable conclusions. For $T = 20K$, although D3 seems to relax slower, again the data are too noisy. The noise in these curves seems surprising due to the very clear linearity and absence of noise in the M vs lnt curves (Fig. 5-32).

5.9.2. Discussion

Néel-Brown relaxation (✣2.7.1) has been assumed as the relaxation mechanism for a single particle. Due to the presence of a distribution of particle sizes, in practice, a linear dependence of the magnetisation with logarithm of time has been observed.

To test the validity of the exponential behaviour as well as other laws of relaxation, it is useful to use the $T.\ln(t/\tau_0)$ scaling (see ✣5.10.3), in which the relaxation data at different temperatures are plotted in a master curve, essentially mirroring relaxation processes over a large time window (see Fig. 5-41). Using the $T.\ln(t/\tau_0)$ Labarta et al. [1993] showed that the Néel-Brown relaxation is indeed realistic for a distributed systems of hexaferrite nanoparticles.

Making used of a planar Nb micro-bridge-dc SQUID, Wernsdorfer and co-workers [1995 (*a*, *b*, *c*), 1996 (*a*, *b*) and 1997], studied relaxation processes in individual single domain particles. Applying a magnetic field close to the value of the switching field of the particles, the time elapsed until the magnetisation switches is recorded. This measurement, called by the authors *waiting time experiment*, is repeated several hundred times, so that a waiting time histogram is obtained. Integrating this histogram, the switching probability can be obtained. For single ferromagnetic particles, Wernsdorfer et al. found that the exponential relaxation given by the Néel-Brown expression is valid. This doesn't seem to be the case, however, for antiferro and ferrimagnetic particles [Wernsdorfer et al. (1995 *a*, *b*, 1996 *a*), Lederman et al. (1993)], where the probability of not-switching is flatter than exponential at low temperatures (typically T<1K) and steeper at higher temperatures (1K<T<6K). Similar behaviour has been predicted by Chantrell et al. [1997] (see ✣2.7.3). For very low temperatures (2K<T<4K) the system seems to relax faster than the expected from an exponential decay, i.e. the relaxation curve is steeper than exponential.

5.10. Determination of f_0

Although the attempt frequency, f_0, depends on different parameters (see ✣2.7.1.2 and Klik et al. (1990), Jones et al. (1989)] such as temperature, gyromagnetic ratio or anisotropy constant, in the majority of experimental studies it is considered as a constant, an assumption that has become known as the Néel-Brown model. The exact analytical expression of f_0 remains an unresolved problem.

Experimentalists have developed different methods to calculate f_0 in magnetic materials. In the following sections three methods have been used and discussed.

5.10.1. f_0 using magnetic and Mössbauer studies

Assuming Néel relaxation (see ✣2.7.1.1) of the magnetisation, Dickson and co-workers [1993 *a*, *b*] developed a technique by which f_0 can be calculated knowing the blocking temperatures of a system via two different magnetic measurements, namely Mössbauer spectroscopy and TDR (see ✣5.4) measurements. In the present section, this technique is used in order to calculate the attempt frequency of the magnetite particles in the ferrofluid. According to Dickson et al.,

$$f_0 = \left[(t_1)^{\beta} / (t_2)^{\alpha} \right]^{1/(\alpha-\beta)} \qquad \textbf{(Eq. 5.16)}$$

where β is the ratio of the median blocking temperatures, $\beta = T_{B1m} / T_{B2m}$, and α is the ratio of the median anisotropy energy barriers of the system, $\alpha = \Delta E_1 / \Delta E_2$, for both measurement techniques with corresponding measuring times t_1 and t_2, respectively. For Mössbauer spectroscopy, $t_1 = 5 \times 10^{-9} s$, while the typical measuring time for the TDR is $t_2 = 100 s$. The value of α is taken as 1 if there is a linear relation between the magnetic moment of each particle and the number of atoms in such particle [Dickson et al. (1993 *a*)].

The Mössbauer relaxation spectra (see Fig. 5-40) were taken at Liverpool University by G. H. Milford and D. P. E. Dickson.

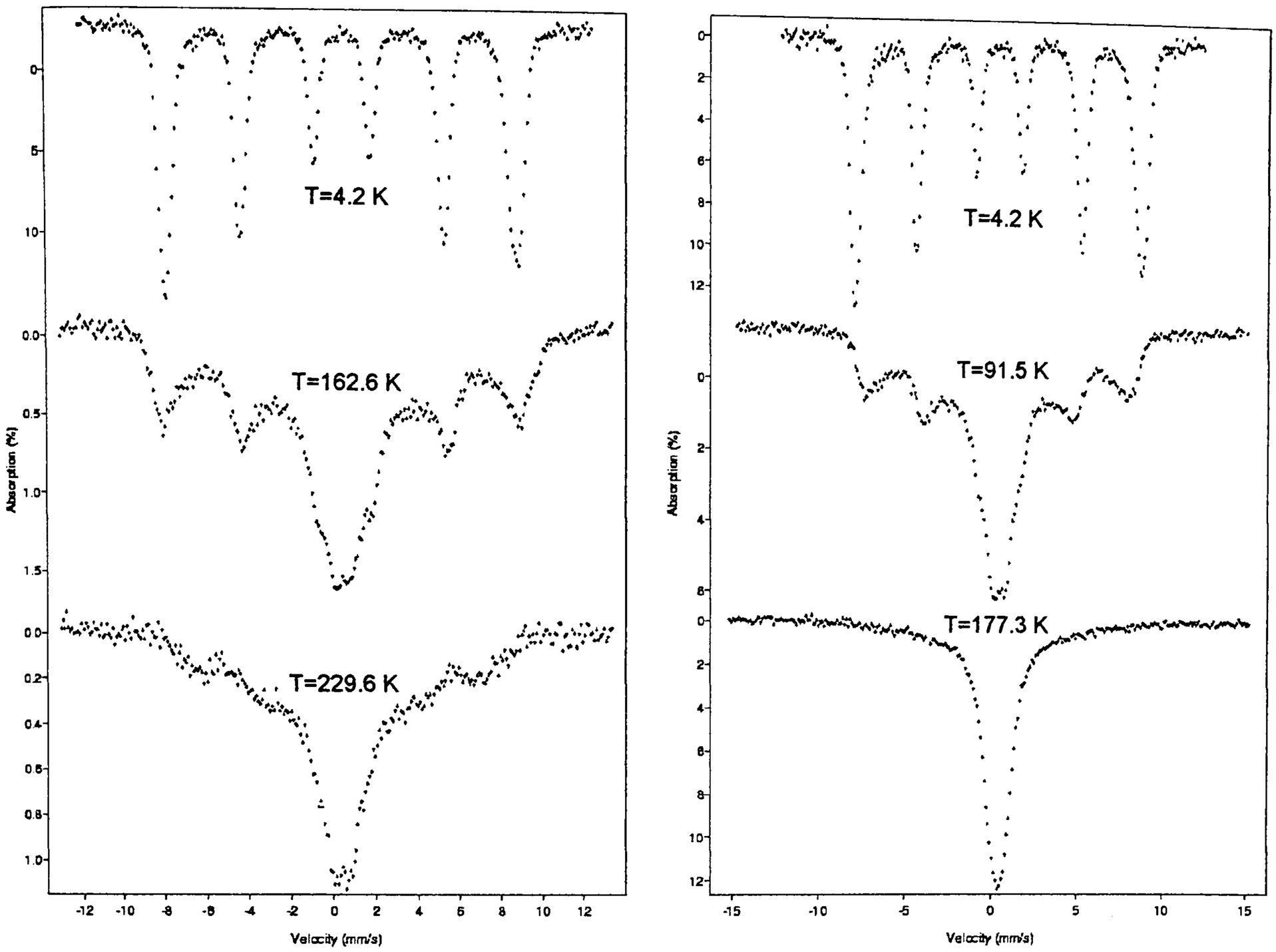

Figure 5-40

Mössbauer spectra for samples F024 (a) and F028 (b), for temperatures such that all the moments are blocked (lower temperature), 50% are relaxed and all of them are superparamagnetic.

T (K)	**F024**	**F026**	**F028**
T_{Bm} (TDR)	18	16	13
T_{Bm} (Mössb.)	170.2 ±0.5	130.1 ±0.5	97.4 ±0.5
$f_0 \times 10^9$ (Hz)	3.31 ± 0.74	5.56 ±1.27	7.72 ±1.7

Table 5-18

Values of f_0 (Hz) calculated with the method of Dickson et al. [1993].

Mössbauer data were taken at different temperatures, and the area under the superparamagnetic and blocked (six-line spectra) spectra measured, to obtain the temperature for which half of the sample is superparamagnetic, i.e., the median blocking temperature, T_{Bm} (see Fig. 5-40). Values of the median blocking temperatures, both from TDR (✣5.4) and Mössbauer spectroscopy, are shown in Table 5-19, as well as the values of f_0 obtained for the different particle sizes.

It seems clear that the value of f_0 increases with decreasing particle size. According to Brown's expression [1959] for the attempt frequency,

$$f_0 = \gamma_0 H_k \left(KV/\pi k_B T\right)^{1/2} \qquad \textbf{(Eq. 5.17)}$$

where $H_k = 2K / M_s$ and γ_0 is the gyromagnetic ratio, it is clear that $f_0 \alpha (KD)^{3/2}$. Thus the ratio $f_0(\text{F028})/ f_0(\text{F024})$, as given by Eq. 5.17, would be 1.1, while this ratio is 2.3 from the values obtained in Table 5.19. Although both values are not equal, possibly due to the non-constancy of M_s in these small particles, it is clear that the higher values of f_0 for the smaller particles seem reasonable, due to the higher anisotropy observed (see ✣5.4.5) in these systems.

For a brief overview of the values obtained for other magnetic systems, using this and other techniques see ✣5.10.4.

5.10.2. f_0 via Brown's (1959, 1963) formula

Brown [1959] derived an expression for f_0 at zero applied field (Eq. 5.17), in which it depends on the volume, anisotropy and temperature of the particle. In Table 5-20, the values of f_0 for 4K and room temperature have been calculated using Eq. 5.17.

$f_0 \times 10^{10}$ (Hz)	**F024**	**F026**	**F028**
T_{Bm} (TDR)	18	16	13
f_0 (T = 4K)	8.9 ±1.1	11.2 ±1.8	12.8 ±2.1
f_0 (T = 297K)	1.0 ±0.1	1.4 ±0.2	1.5 ±0.2

Table 5-19

Values of f_0 (Hz) for 4 and 297K, as calculated making use of Eq. 5.17 [Brown (1959)].

According to Brown's formula, the value of f_0 depends on the temperature considered. It can be observed in Table 5-20 that the values calculated using the method of Dickson et al. seem to be approximately intermediate values of the attempt frequencies calculated for 4 and 297 K via Brown's formula. Thus it seems that Brown's formula is possibly close, if not the actual formula, of the analytical expression of f_0. However, the dependence of f_0 on other parameters, such as K and M_s is difficult to evaluate, as these parameters also

change with temperature. The effect of interactions on the value of f_0 also needs to be studied if the attempt frequency in real systems is to be understood. Experiments like the ones performed by Wernsdorfer et al. [1995, 1996, 1997] on single particles, where f_0 can be calculated at different temperatures and applied fields, seem to provide interesting data for Eq. 5.17 to be tested.

5.10.3. f_0 using T.ln (τ/τ_0) scaling

This technique, briefly introduced in ✣2.7.4, was initially developed to study magnetic relaxation in spin-glasses [Prejean and Souletie (1980)]. Using this scaling the relaxation data obtained at different temperatures lie in a master curve, M/M_s vs $T.\ln(t/\tau_0)$, which is equivalent to study the data over a very long time window (see Fig. 5-41), not available in experimental set-ups. This technique was adopted by Labarta et al. [1993] to study the relaxation mechanisms in small magnetic particle systems. The attempt frequency, f_0, is obtained as a fitting parameter of the scaling, i.e., there is a value of $\tau_0 (= f_0^{-1})$, for which the relaxation data taken at different temperatures fall in the same master curve.

In the present section, sample F028 has been studied using the $T.\ln(t/\tau_0)$ scaling. The system was cooled down in a zero field (ZFC) and the relaxation of the magnetisation at zero field, after previous saturation ($H_{sat} = -1\,T$), has been recorded for different temperatures during 900 sec. Then, all the curves recorded for the different temperatures have been fitted to a master curve. From the scaling, a value for the inverse of the attempt frequency, $\tau_0 = (f_0^{-1})$, is obtained as a fitting parameter. The results from the scaling are shown in Fig. 5-41. For the fitting, 40sec were added to the measuring time, which means that the relaxation started 40 sec before the time started to be counted, which is possibly due to the time it takes for the field to achieve saturation and return to zero again. $\tau_0 = 3.0 \cdot 10^{-10}\,\text{sec}$ has been obtained as the fitting parameter. Thus the attempt frequency is given by $f_0 = 3.3 \cdot 10^{-9}\,Hz$ which is close to the values obtained by the method of Dickson et al. in ✣5.10.1.

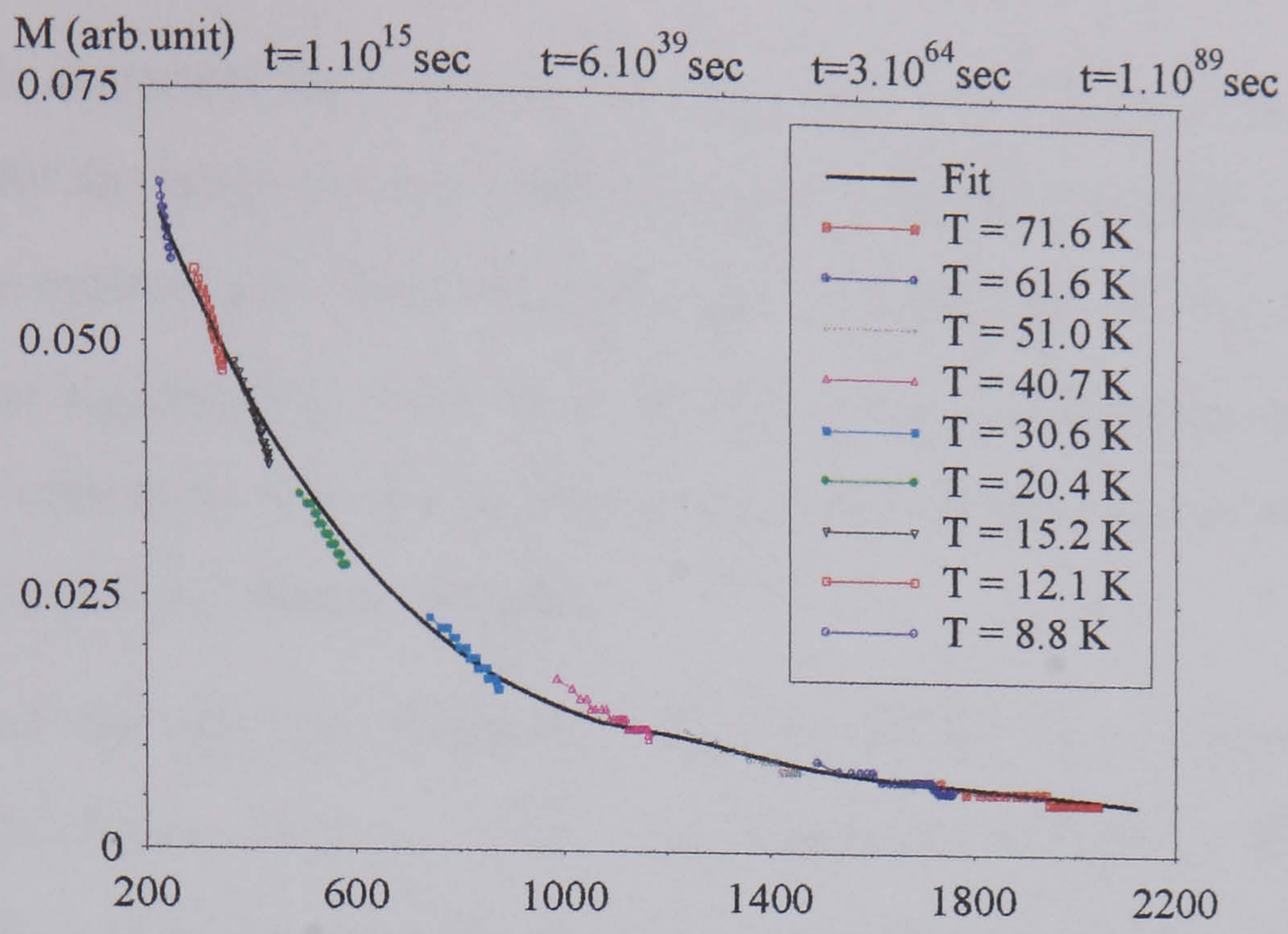

Figure 5-41

$T.\ln(t/\tau_0)$ scaling for sample F028, where relaxation data for temperatures 8K<T<80K have been plotted in the same master curves

It necessary to note that although the value of f_0 obtained using the $T.\ln(t/\tau_0)$ scaling is close to the value calculated using other methods the scaling does not seem as good as that obtained by other authors [Labarta et al. (1993), Batlle et al. (1997 *b*)]. Perhaps, this is not the most appropriate technique for the study of the small magnetite particles in this thesis.

5.10.4. Values of f_0 using different techniques for different materials

Using the same technique of ✣5.10.1, Moskowitz et al. [1997 *a*] obtained a value of $f_0 \approx 10^9\,Hz$ for maghemite cores in magnetoferritin, which agrees with the value $f_0 = 1.1 \cdot 10^9\,Hz$ obtained by McNab et al. [1968] for 100Å magnetite particles, which they calculated by fitting Mössbauer data at 4.2 K. Kneller [1964] reported a value of $f_0 = 2.8 \cdot 10^9\,Hz$ for α-Fe particles. These values of f_0 are almost three orders of magnitude lower than the value determined by Dickson et al. [1993 *a*], where $f_0 = 5.4 - 9.5 \cdot 10^{11}\,Hz$ for the iron oxyhydroxide particles in the protein ferritin. According to Moskowitz et al. [1997] the difference may be related to the different types of magnetic spin ordering and anisotropy of the core of the materials in the two varieties of ferritin: ferrimagnetic (maghemite) in magnetoferritin and antiferromagnetic (ferrihydrite cores) with uncompensated spins in native ferritin. In the same work [Moskowitz et al. (1997)] it is also suggested that higher values of f_0 ($\sim 10^{11}$ Hz) are more appropriate for

antiferromagnetic materials like hematite [Hansen et al. (1997)], goethite or ferrihydrite particles, while for ferrimagnetic materials like maghemite and magnetite, lower values of f_0 ($\sim 10^9$ Hz) are encountered. Different values for f_0 depending on the type of magnetic ordering was also suggested by Jones et al. [1989]. Jones and co-workers also predict a reduction in the relaxation rate due to interactions, as it would have an effect similar to that produced by a direct magnetic coupling.

Lower values of the attempt frequency, $f_0 = 2.5 \cdot 10^8 Hz$, have been obtained for ferromagnetic Co clusters with $D_m = 300$ [Wernsdorfer et al. (1997)]. However, in this case, the method used to obtained the attempt frequency was different to the method of Dickson et al. and it is not known if both results can be fully compared. Using the same technique as Dickson et al., Linderoth and co-workers [1993] studied ultrafine ($D_m(TEM) = 31$ Å) amorphous Fe-C particles, obtaining a value $f_0 = 1 \cdot 10^{12} s$ for these systems.

The influence of interactions, particle size, temperature and applied field on the value of the attempt frequency is of vital importance. Although the majority of the methods calculate a mean value of f_0 for the whole assembly of particles [Dickson et al. (1993), Labarta et al. (1993)], there have been some recent attempts [Wernsdorfer et al. (1995, 1996, 1997)] to study the relaxation processes in individual particles. A comparison among the results obtained via the different methods available as well as the validity of each method are fundamental to understand the behaviour of f_0, and check the validity of the analytical expressions derived for this constant [Néel (1949 *a*), Brown (1959, 1963), Jones et al. (1989)].

5.11. Surface properties

Although it is well known that the surface of small particles has a strong bearing on their properties, it is difficult to characterise these effects or derive an expression for the surface anisotropy.

Some authors [Aharoni (1987)] have included surface anisotropy in their calculations of reversal mechanisms, predicting buckling instead of the expected coherent rotation for spherical particles (see ✣ 2.3.1). The presence of a non-coherent reversal mode seems clear in ✣5.7.3 where the experimental coercivity at 0 K in a system of random distributed

easy axis is much smaller than that predicted by coherent rotation. Thus, it may be the case that the surface anisotropy, high at low temperatures (✣5.7.3), does influence the rotation mechanisms in these small particle systems. Also, some authors [e.g. Wernsdorfer et al. (1995 *b*, 1997), Schabes and Bertram (1988)] have attributed the non-coherent reversal of individual single-domain particles to different effects arising from the presence of a surface in the particles.

From the measurements of the crystalline and the magnetic particle size, a rough estimate of the thickness of the non-crystalline or not perfectly crystalline surface layer can be made, as shown in Table 5-21 below. As it was commented in ✣5.3.2, the surface thickness is within the error, one unit cell, considering the lattice constant for magnetite is 8.39 Å, which is reasonable.

SAMPLE	Mag. size (Å)	X-ray size (Å)	Estimated thickness (Å)
F024	77 ±2	57 ±2	10 ±4
F026	66 ±2	46 ±1	10 ±3
F028	59 ±2	40 ±1	9.5 ±3

Table 5-20

Estimate of the surface thickness for the different particle sizes

It was shown in ✣5.7.2, that below 20K the coercivity of the smaller particles is higher than that of the bigger particles. This was attributed to the surface effects, that seem to become more obvious for T<20K, also suggested by other authors [Kodama et al. (1996)]. Morrish et al. [1976] observed increased canting as the temperature was lowered. Initial magnetisation curves taken at high fields ($H \leq 8T$), in the superconducting VSM at Liverpool University (see ✣3.2), show, as observed in ✣5.2.2, that the smaller particles are more difficult to saturate (see Fig. 5-42). Although this effect can be attributed to higher influence of thermal activation on the smaller particles, it is possibly an intrinsic property of small particles due their strong surface anisotropy.

The slope, s', of the magnetisation curves for $H > 5T$ has been recorded for several temperatures. It has been observed that this slope increases, and then decreases for the lower temperatures (T=4K). The initial trend in s' seems logical because as the thermal effects diminish it is easier for the particles to align in the magnetic field. However, the evolution of s' for very low temperatures does not seem logical, unless, as suggested by

Kodama and Berkowitz [1996], the surface spins undertake a transition into a glassy type state, in which the lower the temperature the more difficult it is for those spins to align in the field direction, which become locked in their structures as the temperature is lowered. This argument seems to be supported by the results obtained in ✣5.7.1.2, i.e., the fact that the particle surface anisotropy becomes more significant for $T < 30K$, which is also manifested in the higher coercivities of the smaller particle sizes with respect to the larger particles, for these low temperatures.

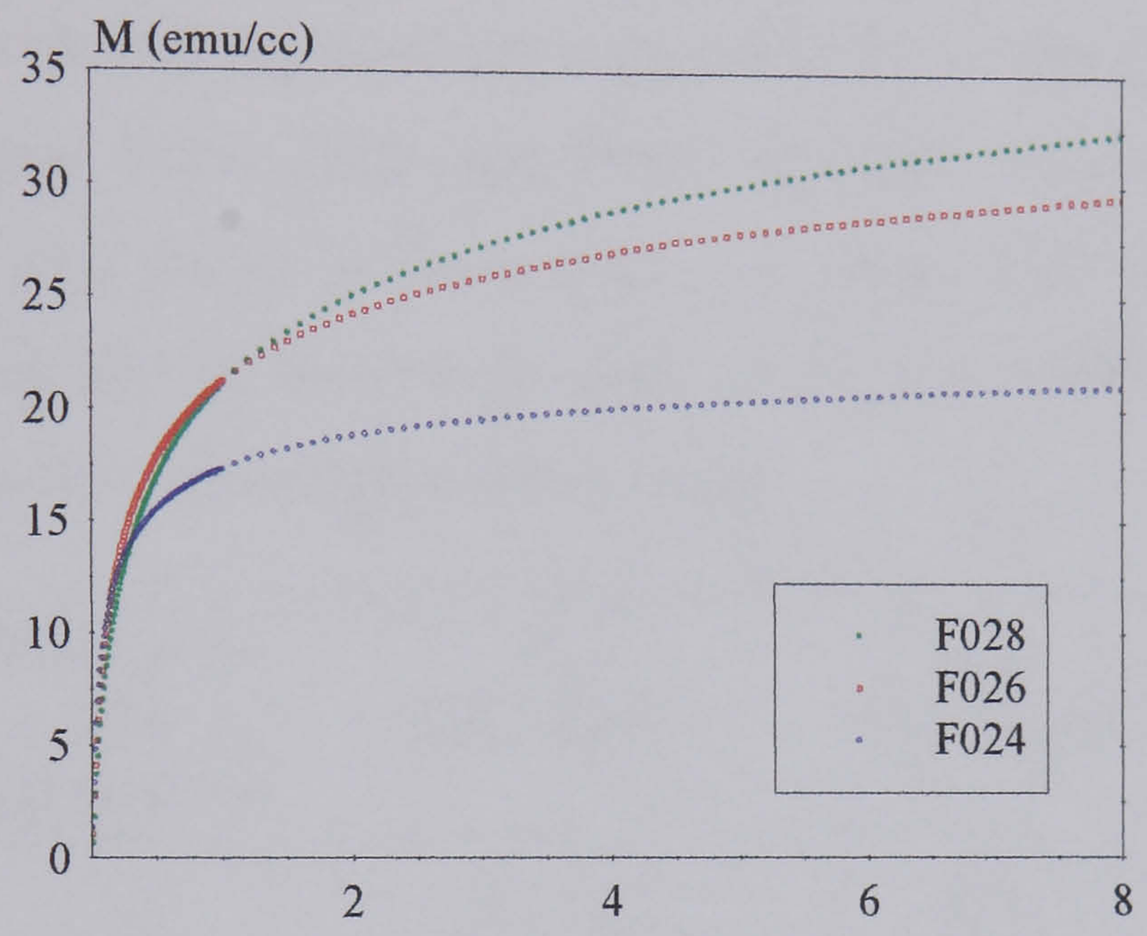

Figure 5-42

High field magnetisation curves of the 3 particles size ferrofluid samples, at room temperature.

In any case, more detailed measurements need to be recorded to draw any definite conclusions about the real presence of this effect in the particles in this thesis.

5.11.1. An estimate of the surface anisotropy constant, K_S

Assuming the simplest case where the effective anisotropy constant, K_{eff}, is the sum of the volume (or crystalline), shape and surface uniaxial anisotropies in the particles,

$$K_{eff} = K_V + K_{shape} + K_{surf}, \qquad \textbf{(Eq. 5.18)}$$

$$K_{shape} = \frac{1}{2}(N_a - N_c)M_s^2 \qquad \textbf{(Eq. 5.19)}$$

where N_c and $N_a = N_b$ are the demagnetising factor of a prolate spheroid, along the major and minor axis [Cullity (1972) p. 56], an approximate surface anisotropy constant

can be calculated. Considering that the volume anisotropy is the crystalline anisotropy of the bulk, $1.1.10^5$ erg/cc for magnetite, and considering the shape anisotropy as defined in Eq. 5.19, an estimate of the effective surface anisotropy can be derived (see Table 5-22). Although the surface anisotropy is generated mainly by the spins near the surface, it has indeed a volume effect, i.e. is not merely a surface effect. As such, the surface anisotropy constant would be given by direct subtraction of the effective and the crystalline and shape anisotropy constants, as shown in Table 5-22, and measured in erg/cc. For this purpose, the values for the effective anisotropy constants obtained in ✣5.7.3 have been used. The mean axial ratio for systems F024, F026 and F028 has been measured from the TEM photographs and are also shown in Table 5-22. The values used for the demagnetising factors are those calculated by Bozorth [p. 846 (1951)] for cylinders with permeability $\mu \approx 5$, which is the case for the samples in this thesis.

SAMPLE	Mean axial ratio (long/short)	K_{eff} (10^5.erg/cc)	K_{shape} (10^5.erg/cc)	K_{surf} (10^5.erg/cc)
F024 (77Å)	1.2	3.3 ±0.2	1.9	0.3 ±0.2
F026 (66Å)	1.3	4.0 ±0.4	2.0	0.9 ±0.4
F028 (59Å)	1.2	4.6 ±0.5	1.9	1.6 ±0.5

Table 5-21

Estimated value of the surface anisotropy for F024, F026 and F028.

From Table 5-22 it can be observed that the surface anisotropy is higher as the particle size decreases, as expected from the increase in surface to volume ratio as the particle size diminishes. Thus, while for both F026 and F028 the surface anisotropy is significant, this does not seem to be the case for F024. These observations seem to support the results obtained in the previous sections at room (✣5.2.1.2) and low temperatures (✣5.7.1.2, 5.7.2, 5.8.1).

5.11.2. Discussion

Hendriksen et al. [1994 *b*], studying γ-Fe_20_3 particles in a frozen ferrofluid, observed that the degree of spin alignment is independent of the orientations of the different easy axis directions of the samples. The authors field cooled the sample and measured the Mössbauer spectra in different applied fields, parallel and perpendicular to the sample, observing that above 7.5kOe, the degree of alignment is always the same. This observation

is consistent with the concept of spin-canting suggested by Coey [1971, 1972] (see ✣5.4.1) and in agreement with many experimental observations [Coey (1971), Morrish et al. (1976), Parker et al. (1993), Prené et al. (1994), Linderoth et al. (1994), Respaud et al. (1998), Dorman et al. (1998 *a*, *b*)]. The origin of the canting of the magnetic moments has been attributed to the reduced coordination and broken exchange bonds between surface spins [Kodama et al. (1996)]. This spin canting effect has been more frequently observed in ferrimagnetic oxide particles, rather than in metallic particles although some non-collinearity effects have been reported in this latter systems [Dormann et al. (1997) p. 406]

In recent experiments, Wernsdorfer and co-worker [1997] explained why the relaxation of antiferro/ferrimagnetic particles is flatter than exponential at low temperatures (~0.2K) and steeper at higher temperatures (T~4.5K) in the following terms: 'We believe that the magnetisation reversal of these particles is influenced by spin frustration of non-compensated spins at the interface between the ferromagnetic core and the antiferromagnetic surface layers or at the surface of a ferrimagnetic particle. This frustration could differ slightly from one hysteresis loop to another, thus producing slightly different energy barriers. This effect is less important at higher temperatures when the thermal energy is much larger than the energy barrier variations, whereas at low temperatures this effect may flatten the probability of not switching and increase the width of the switching field distribution'. The same workers [Wernsdorfer et al. (1995 *b*)] explained the increasing width, σ, in the distribution of switching fields, for decreasing temperatures as 'induced by topological fluctuations of the magnetisation state, due to sample imperfections, which become energetically distinct at very low temperatures. This separation of states can sometimes be very pronounced and a splitting of the switching field in two or more switching field distributions is observed'.

According to Kodama et al. [1996] the canted spins on the particle surface of Ni ferrites ($NiFe_2O_4$) nanoparticles undergo a glass-type transition below 50K, at which point they present multiple stable configurations. This is manifested in the open hysteresis loops observed even for fields up to 16 T, time-dependent magnetisation in a 7 T applied field and shifted hysteresis loops after field cooling the samples. These observations are attributed to the transitions between surface spins rather than magnetisation reversals of whole particles. Similar results have been reported by Garcia del Muro et al. [1999] in barium hexaferrite nanoparticles.

" If you could ask a gift for your children,
you should ask for curiosity "
(Inductions, *The Geenom Manuscripts*).

6. Results II. *Co-Cu Nanoclusters*

Introduction

The materials under study in this chapter are clusters of magnetic atoms (*Co*) in a non-magnetic matrix (*Cu*). Because the clusters are in the nanometer range they are called *nanoclusters*. Using mainly magnetic measurements, the effects of the different particle sizes and concentrations have been studied.

6.1. The samples

The nanoclusters were made in a magnetron cluster source at Daresbury Laboratory (for more details about the manufacture process see ✣3.8). The approximate number of atoms per cluster, as well as the concentration of the different samples, are given in table 6-1.

Samples	*S1-5*	*S1-10*	*S1-50*	*S8-5*	*S8-10*	*S8-50*
No. Atoms	1000	1000	1000	8000	8000	8000
ε (%)	5	10	50	5	10	50

Table 6-1

Number of atoms per cluster and concentration of magnetic material (Co) in the nanoclusters, as facilitated by the manufacturers.

6.2. Magnetic Particle Size

6.2.1. Magnetisation curves at room temperature. Superparamagnetism in nanoclusters

6.2.1.1. Magnetic size parameters

Assuming a lognormal distribution of particle volumes, and a sum of Langevin functions the magnetisation curves at room temperature ($T = 297K$) are used to calculate the median magnetic diameter, D_{vm}, and standard deviation, σ_v, of the distribution. Only the samples which are superparamagnetic at room temperature can be described by a sum of Langevin functions. For the particles to be truly superparamagnetic not only must they have no coercivity or remanence but also present H/T superposition (see ✣6.2.1.2). This is the case for samples S1-5, S1-10, S8-5. Although sample S8-10 is not truly superparamagnetic, there being some coercivity in the system, ($H_c(S8-10) \approx 37\,\mathrm{Oe}$), a sum of Langevin functions has been assumed to fit the magnetisation curves of this sample, as the system follows very closely Langevin behaviour. In this way, it is possible to get an idea of the magnetic particle size, and compare it with that of S8-5, which has the same number of atoms per cluster but lower concentration (5%).

Due to the low signal of some of the samples, some noise is appreciable in the magnetisation curves. For this reason, and the absence of detailed susceptibility data at low fields, the 'best fit' method (✣5.2.1.2) was considered more appropriate for the determination of the magnetic size in the systems. For the sake of comparison, the method of Chantrell et al. [1978] has also been used in order to test the validity of the method for the determination of the particle size distribution, even with the very few data points available at low fields.

As described in ✣5.2.1.2, the 'best fit' method fits the magnetisation curves to a sum of Langevin functions, from which the median magnetic diameter and the standard deviation of $\ln D$ are obtained. In the absence of any data for small particles, the *Co* clusters are assumed to have the same saturation magnetisation of bulk *Co*, i.e., $M_{sB} = 1400\ (emu/cc)$. The parameters obtained for the different samples, as well as the best fit magnetisation curves for all the nanocluster samples, are given in Table 6-2 and Fig. 6-1 (*a*, *b*, *c* and *d*),

respectively. The theoretical curves obtained by the method of Chantrell et al. and the corresponding parameters obtained are shown in Fig. 6-2 and Table 6-3, respectively.

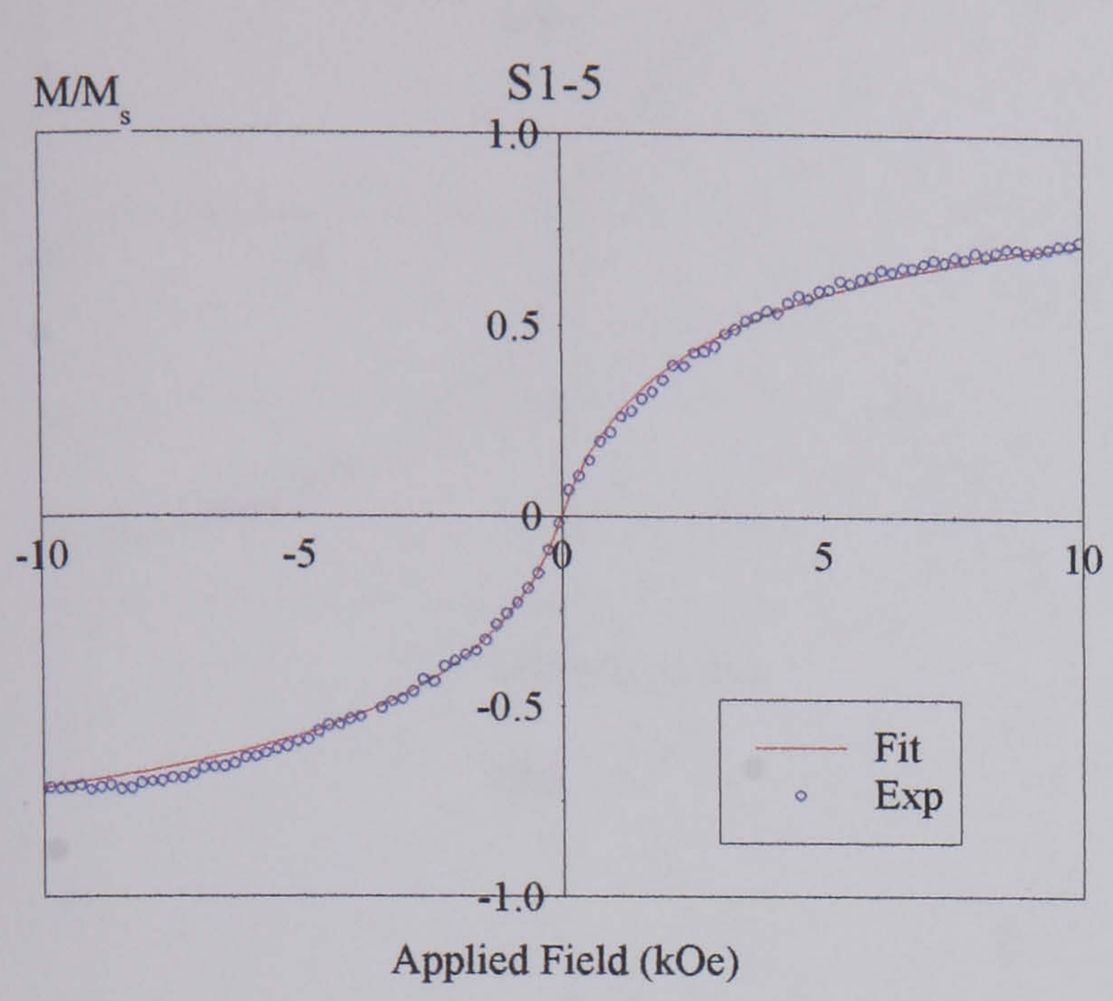

(a)

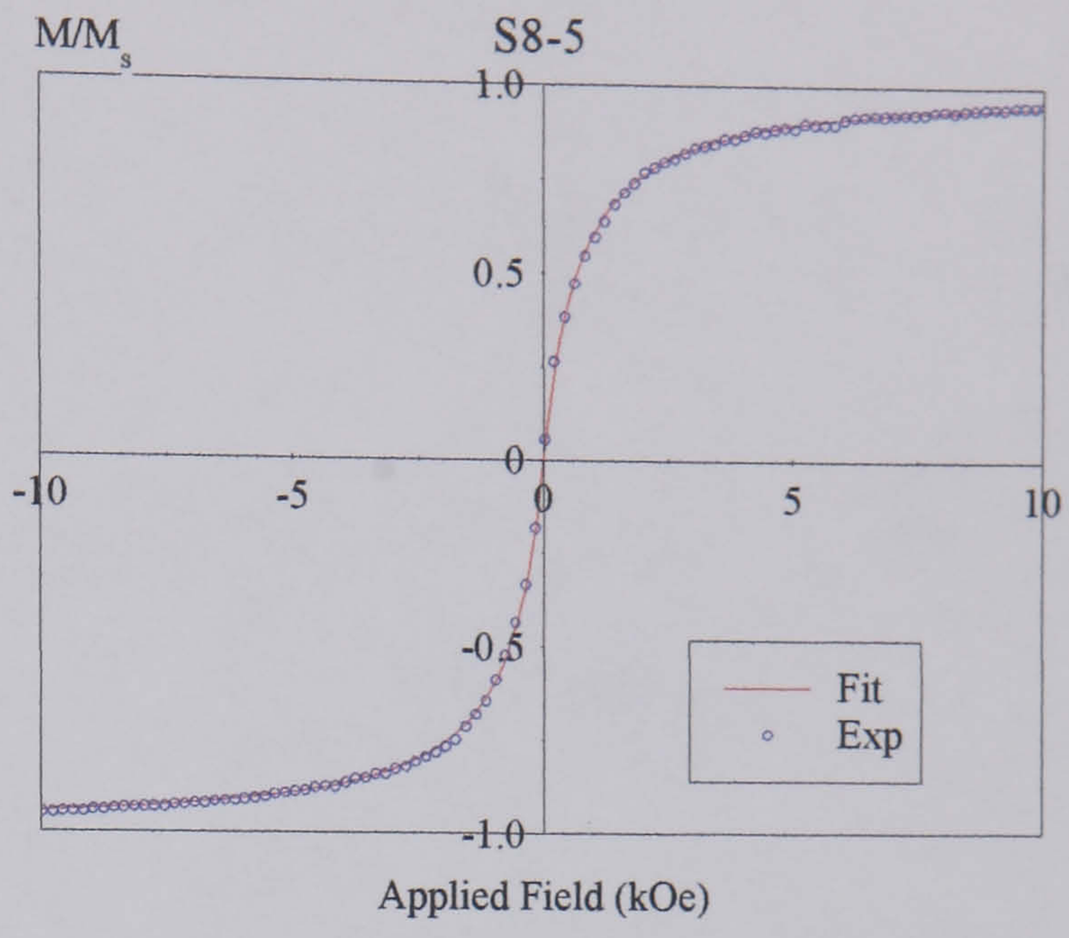

(c)

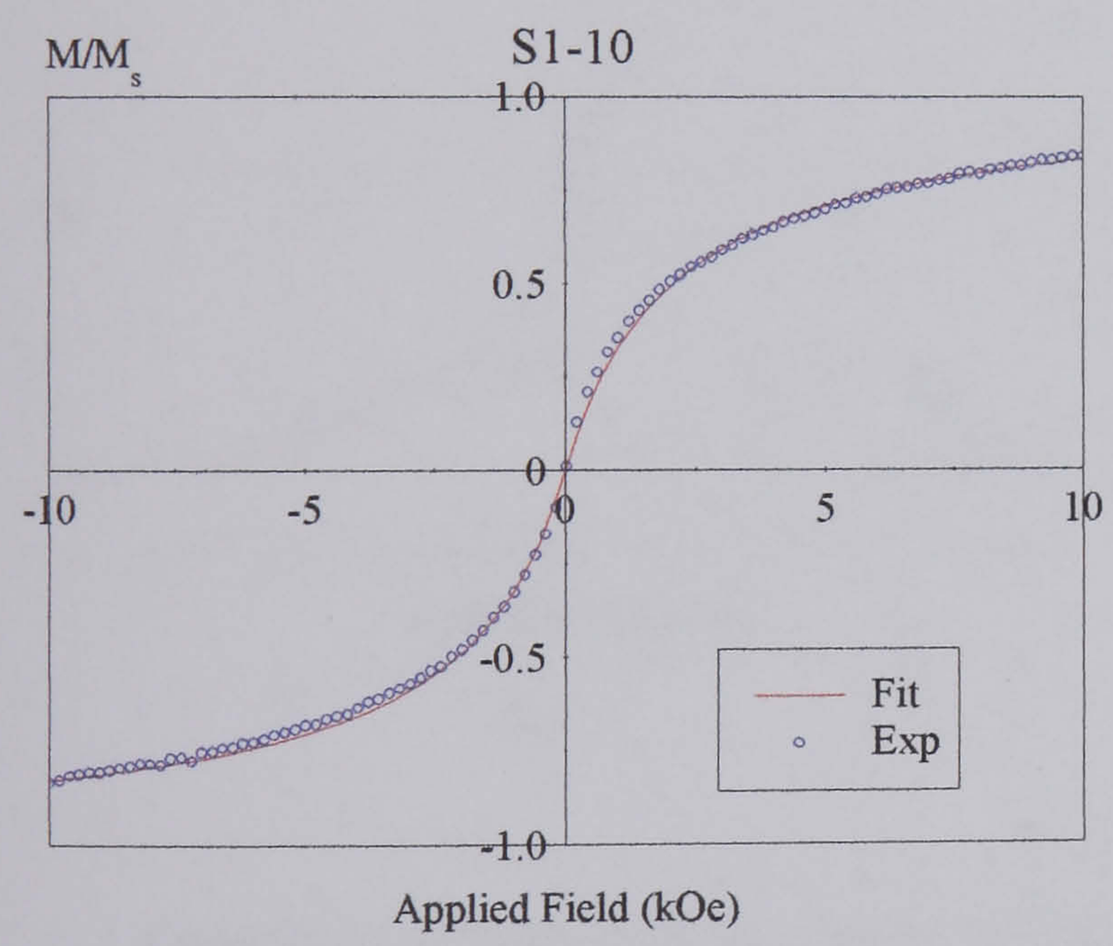

(b)

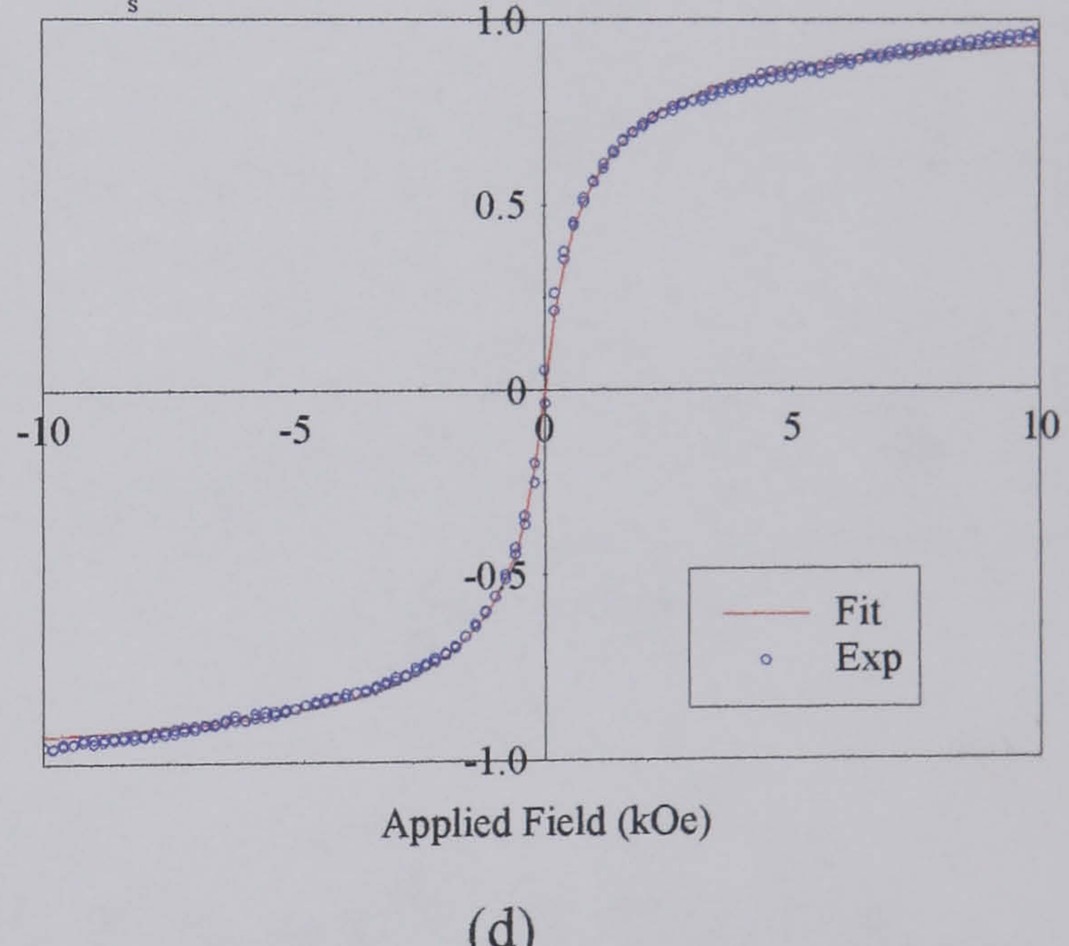

(d)

Figure 6-1

Experimental magnetisation curves (Exp) for S1-5 (a), S1-10 (b), S8-5 (c), S8-10 (d) fitted *to a sum of Langevin functions (Fit).*

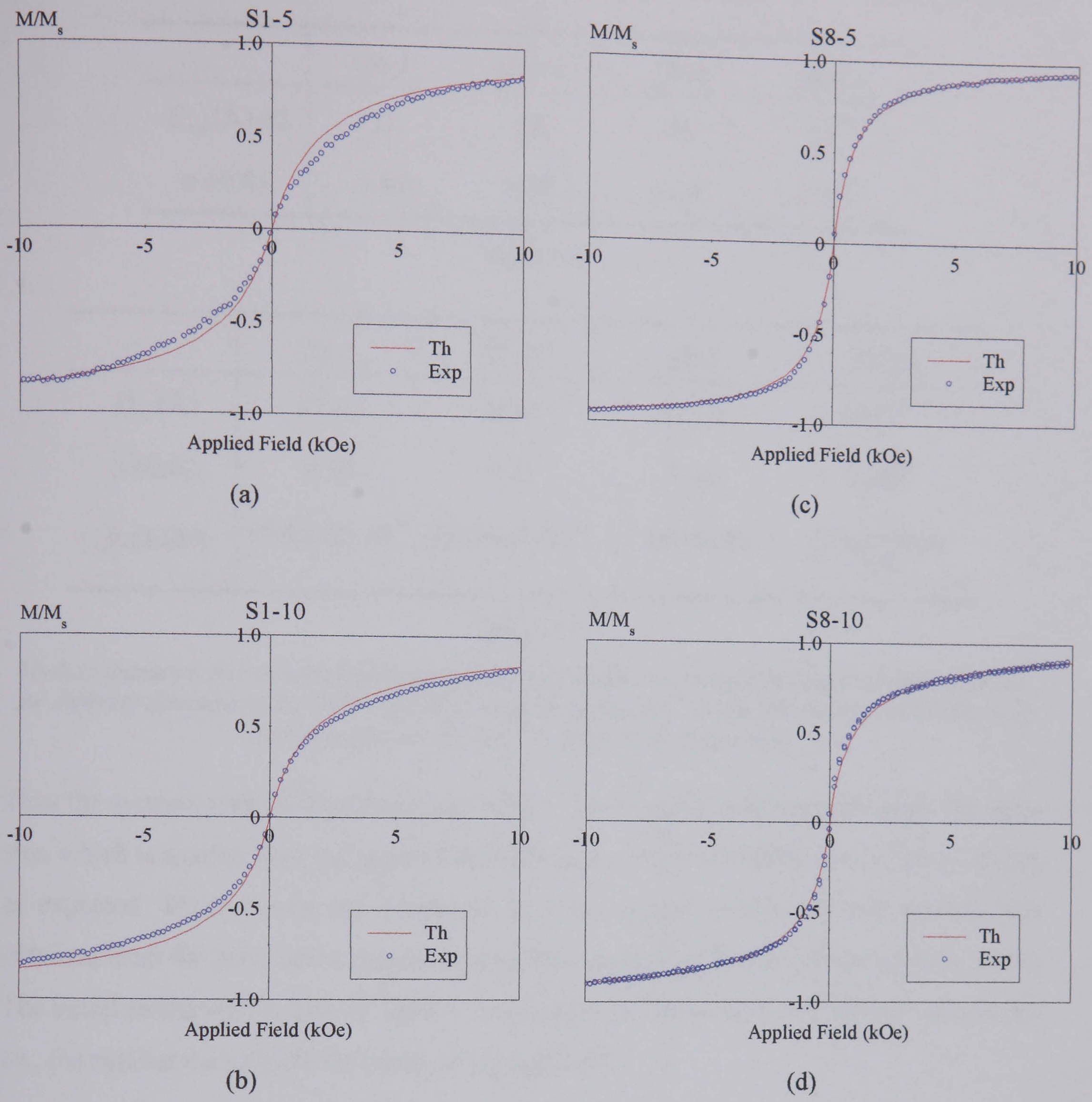

Figure 6-2

Experimental magnetisation curves (Exp) for S1-5 (a), S1-10 (b), S8-5 (c), S8-10 (d) and theoretical (Th) Langevin (sum) curves generated using the parameters obtained via the method of Chantrell et al.

As it is observed from Fig. 6-1 and Fig. 6-2 the best fit method follows the experimental data more accurately. The method of Chantrell et al. does not achieve very good fits due, as already commented, to the lack of detailed data in the low field part of the magnetisation curves. The parameters obtained using both methods are shown in Tables 6-2 and 6-3 below.

	S1-5	*S1-10*	*S8-5*	*S8-10*
D_{vm}(Å) ±2	31	36	53	51(*)
σ ±0.01	0.44	0.32	0.28	0.36(*)

Table 6-2

	S1-5	*S1-10*	*S8-5*	*S8-10*
D_{vm}(Å)	37 ±3	38 ±3	51 ±2	46±2(*)
σ ±0.02	0.30	0.35	0.28	0.38(*)
$\overline{\chi}_i$(1/Oe)	$(4.6\pm0.2).10^{-4}$	$(5.6\pm0.3).10^{-4}$	$(1.1\pm0.6).10^{-4}$	$(1.1\pm0.6).10^{-4(*)}$

Table 6-3

Median diameter and standard deviation of the lognormal distribution of magnetic particle sizes, for different dilutions of the 1000 and 8000 atom nanoclusters, via the best fit method (Table 6-2) and using the method of Chantrell et al. (Table 6-3).

Thus the systems with 1000 atom clusters (*S1-5*, *S1-10*) have both approximately the same size, which is smaller than the samples with the larger clusters of 8000 atoms (*S8-5*, *S8-10*), as expected. These results are consistent with the values for the physical particle size obtained from the mass spectrometer data and the number of atoms per cluster (see ✣6.3). The initial susceptibility data in Table 6-3 also supports the evolution of particle diameters, i.e., the smaller the particle the lower its susceptibility.

6.2.1.2. Langevin behaviour

In general, it can be affirmed that the cluster samples with the lower concentrations (5% and 10%) have approximately Langevin behaviour. This is to be expected because these cluster samples are well below the superparamagnetic limit which for small fcc Co particles, and assuming $K = 5 \cdot 10^5 erg / cc$ [Rodbell (1962)] is 150 Å. Later calculations of the anisotropy constant in fine Co fcc particles gave a value of $\approx 2 \cdot 10^6 erg / cc$ [O'Grady et al. (1980)], which the authors attributed to shape effects. This latter value may be in fact

(*) It is convenient to remember at this point that the values obtained for the median particle size and the standard deviation of S8-10 are smaller than those obtained for S8-5. These results can be somewhat fictitious due to the fact that this sample is not truly superparamagnetic, as it shows the presence of some coercivity (37 Oe). Thus complete Langevin behaviour cannot be expected, and the size distribution characterisation obtained from this assumption may not be totally accurate.

the anisotropy constant of small Co particles, as from the TDR results obtained in this thesis (see ✣6.4) the value of the anisotropy constant does oscillate between 1 and $3 \cdot 10^6 erg/cc$ (see Table 6-5). These anisotropies would lead to values for the superparamagnetic diameter of 90Å and 130Å for the 1000 and 8000 atom clusters, respectively. According to the values obtained for the superparamagnetic limit the sizes of the clusters studied in this chapter lie below this limit. However, there is a distribution of particle sizes, and in the case of the 8000 atoms clusters it is possible that there exist some blocked particles (see Fig. 6-3) which would account for the observed coercivity in the S8-10 sample.

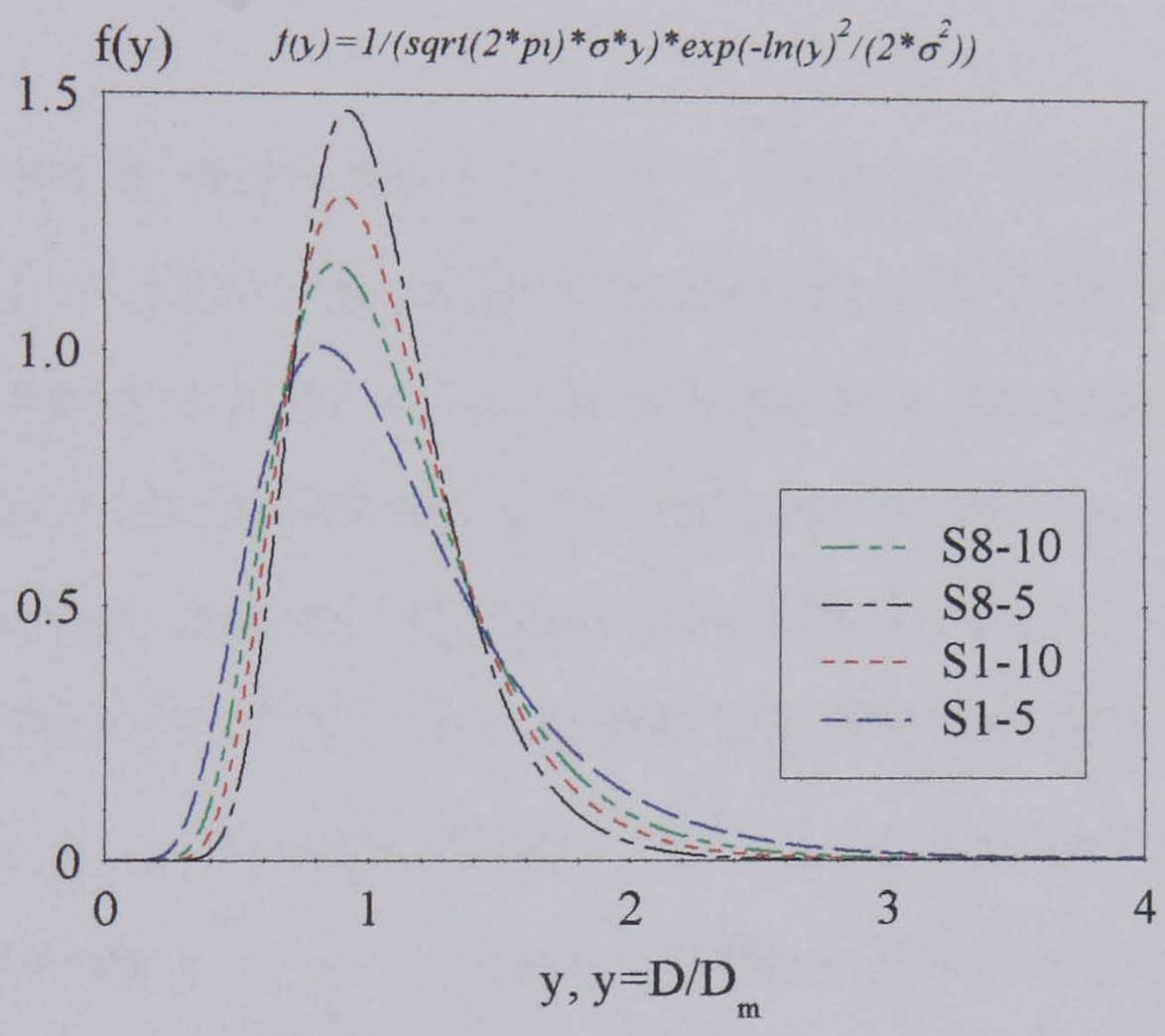

Figure 6-3

Lognormal distribution, f(y), of the reduced (magnetic) diameters, $y=D/D_m$, for the cluster samples.

Samples S1-5 and S1-10 (Fig. 6-1, *a* and *b*) seem to deviate slightly from the Langevin behaviour as it was observed in Fig. 5-2 for the ferrofluid samples. The reason for this deviation is most certainly due to the contribution of a strong anisotropy, either due to surface or strain effects and/or perhaps due to the crystalline anisotropy in the Co particles. Crystalline anisotropy, however, would not be expected to be higher in the smaller particles systems. In fact, if anything, it would be expected to be smaller due to the unpaired spins on the surface. In these very small systems a non-crystalline icosahedral structure has been found theoretically [Leary (1997)], as previously observed in other metallic and non-metallic nanocluster systems [Mackay (1962), Farley et al. (1989), Schriver et al. (1989)]. The study of Shapiro et al. show that the icosahedral structure minimises the surface energy, although the inner energy of the cluster is higher than in the case of the *fcc* Co,

which increases as the particle size is reduced and more atoms are on the surface. The larger clusters have the expected *fcc* structure. Experimental evidence suggests that the critical size is in the range of 1500-3000 atoms, which is supported by recent theoretical calculations [Leary and Shapiro (1999)] which found the crossover between the *fcc* and the icosahedral structures at 2869 atoms. Leary and Shapiro found a new fcc minimum-energy structure for a 2869-atom cluster. By modifying the exterior cuboctahedral *fcc* crystal geometry, an optimised 26-polyhedral configuration was obtained that minimised the surface/volume ratio of the crystal. With the information supplied, however, it is not possible to pinpoint the exact reason for the slight deviation of S1-5 and S1-10 from Langevin behaviour.

Except for the presence of some coercivity ($H_c = 37Oe$) in S8-10, possibly due to some blocked particles in this system, the magnetisation curves of both S8-5 and S8-10 follow the Langevin curve closely, and the surface anisotropy does not seem to make an important contribution. This seems reasonable as the *Co* lattice parameter ($a = 3.55$ Å , assuming *fcc* Co) is much smaller than that for magnetite ($a = 8.39$ Å) and thus the size for the *Co* clusters to present comparable surface anisotropic effects is smaller than that of magnetite.

Using the liquid drop model [Jortner (1992), ✣4.2.2], the fraction F of surface to volume atoms can be calculated by $F = 4 / n^{1/3}$, where n is the number of atoms in the cluster. Thus $F = 0.47$ and 0.28, for a 30 and 50 Å cluster, respectively, and $F = 0.57,\ 0.51$ and 0.44 , for the F028 (59Å), F026 (66Å) and F024 (77Å) ferrofluids, respectively. This means that although the samples with 8000 atoms have a size ($D_{vm} \approx 50$ Å) comparable to that of the ferrofluid F028 ($D_{vm} \approx 59$ Å), no deviation from the Langevin behaviour is observed in these clusters. Only for the smaller particle sizes ($D_{vm} \approx 30$ Å) do the anisotropic effects become more obvious, as the surface to volume ratio becomes significant, and comparable to that of the smaller ferrofluid systems.

The observation of H/T superposition in samples S1-5, S1-10 and S8-5 also supports the existence of superparamagnetism in these samples. Fig. 6-4 shows H/T curves obtained for sample S1-10 at 300 K and 270K. At 250 K, the magnetisation curve does not superimpose in the M vs H/T graphs, indicating that some blocking may be happening already at this rather high temperature. In fact, for this temperature the superparamagnetic limit for the

small nanoclusters is $D_p \approx 80\text{Å}$ and it is very probable that some of the particles in sample S1-10 are in this size range.

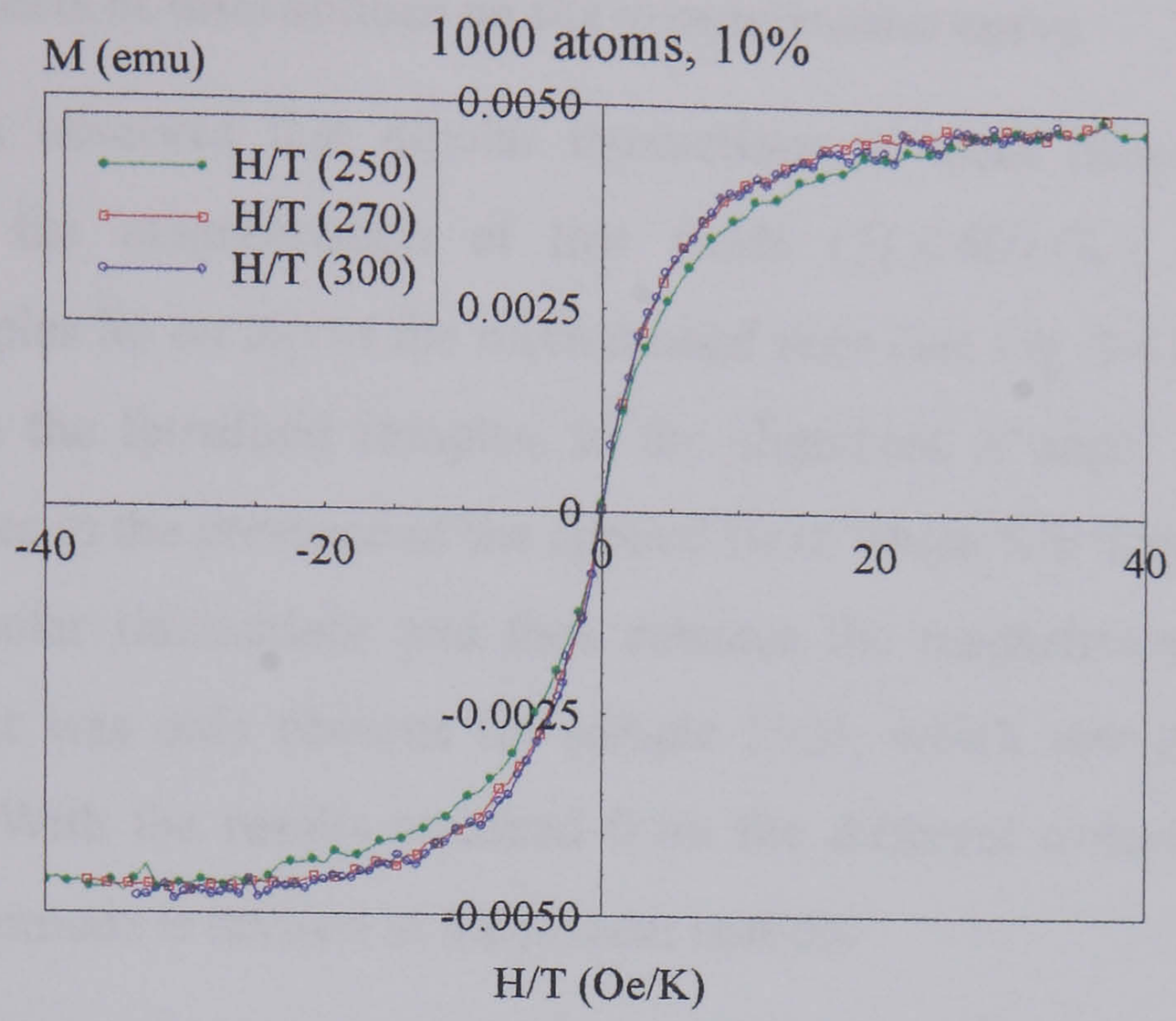

Figure 6-4

H/T superposition in sample S1-10

6.2.2. Effects of particle size on the magnetisation curve

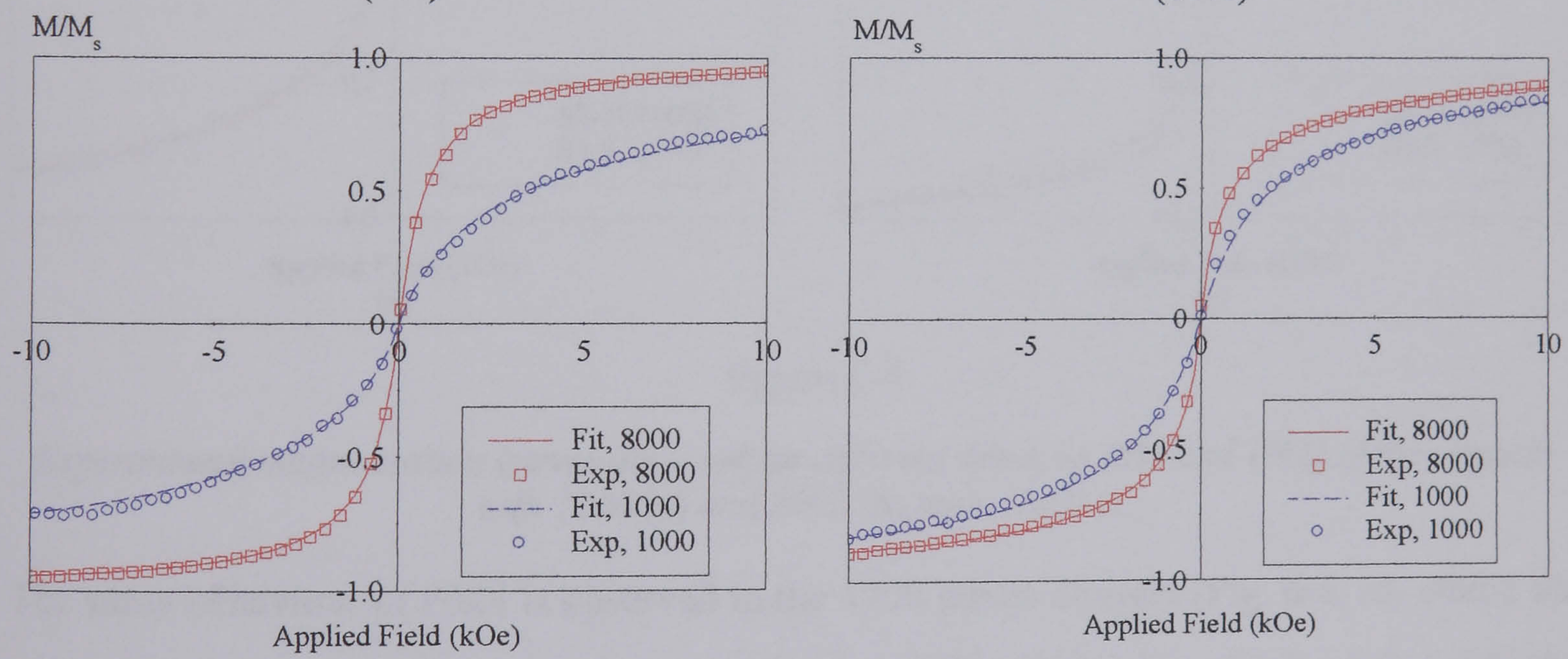

Figure 6-5

Influence of the particle size on the shape of the magnetisation curves, for different concentrations: (a) 5% and (b) 10%

The effect of particle size on the magnetisation curves is clearly seen in Fig. 6-5. As explained in ✣5.2.2, as particle size decreases, the saturation is more difficult to approach.

This is expected as the randomising effects of temperature will be more effective the smaller the particles, at a constant temperature.

6.2.3. Effects of interactions on the magnetisation curve

In ✣5.2.3 it was observed that dipolar interactions at room temperature produce an enhancement of the magnetisation at low fields ($H \leq 500\ Oe$), so that the more concentrated samples lie on top of the more diluted ones (see Fig. 5-4). This enhancement was attributed, in the ferrofluid samples, to the alignment of small chains (dimers and trimers) of particles in the presence of the applied field, which will display the magnetising aspect of the dipolar interactions and thus enhance the magnetisation. In the previous chapter this effect was only obvious for sample F024, which was the sample with the largest particles. With the results obtained from the different concentration nanocluster samples this phenomena is revised in the present section.

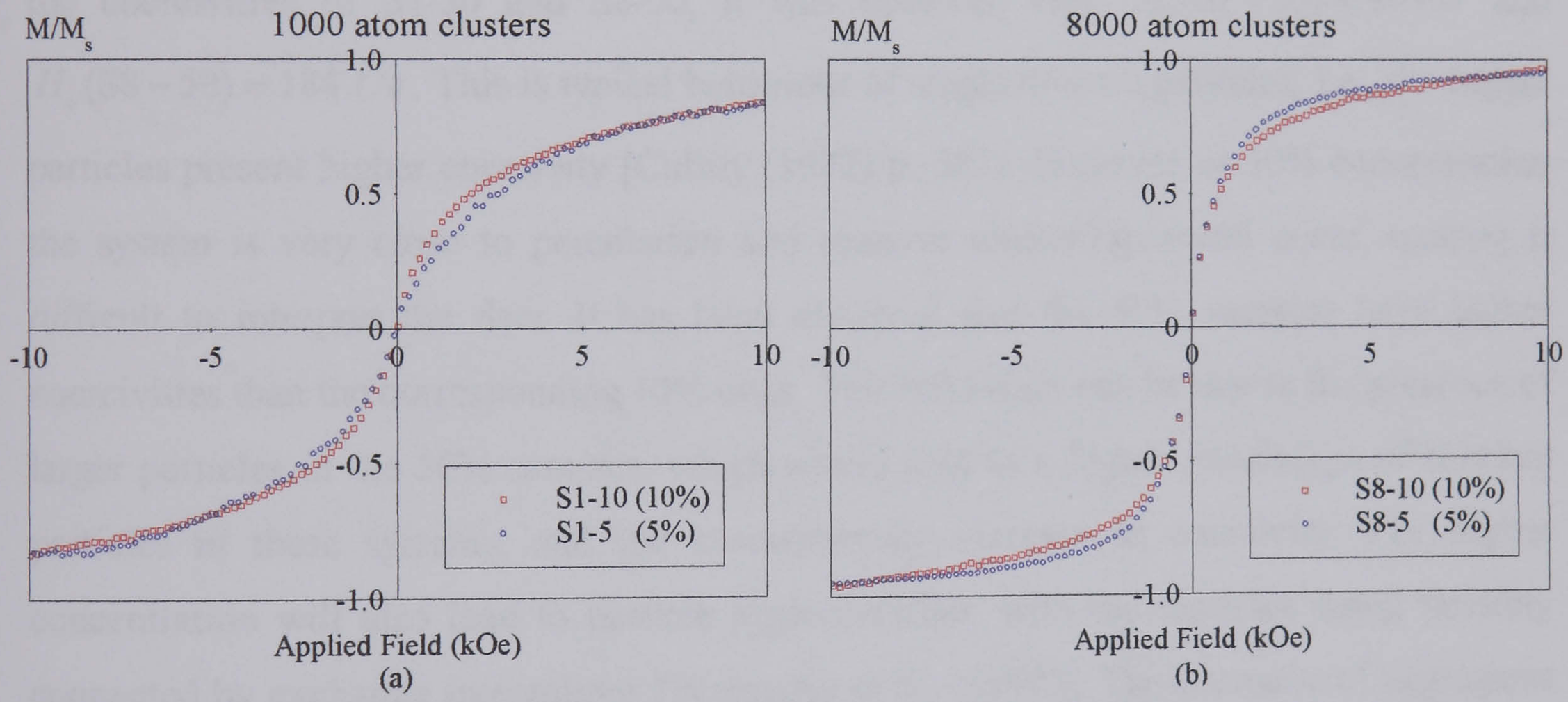

Figure 6-6

Experimental magnetisation curves obtained for different dilutions (5% and 10%) of the samples with 1000 (a) *and 8000* (b) *atom clusters.*

The same behaviour of F024 is observed in the 1000 atoms clusters (Fig. 6-6, *a*), where the magnetisation curves of the more concentrated samples (10%) lie on top of those of the diluted (5%) samples. This is observed up to larger fields ($H \leq 5\ kOe$) than for the case of ferrofluids. At the moment it is not clear why such an enhancement would take place in these systems. One possible explanation is the fact that sample S1-10 has a larger size, as obtained by the magnetic size characterisation (see Table 6-2), contributing with higher magnetisation, especially at the lower fields, as observed in Fig. 6-6 *a*. Another possibility

is the existence of a genuine interaction effect in these samples. The opposite behaviour to that of samples S1-5 and S1-10 is observed for the 8000 atom clusters, S8-5 and S8-10 (Fig. 6-6, *b*). This is the expected behaviour of dipolar interacting systems [El-Hilo et al. (1998)]. However, according to Table 6-2, sample S8-10 seems to have smaller particle size or more coupled particles, possibly behaving effectively as a smaller particle system, which would account for the lower magnetisation values of S8-10 with respect to S8-5.

At the present moment no conclusive explanation has been found for either type of behaviour observed in Fig. 6-6. Localised microscopic magnetic measurements as well as precise information of the film structure will be the key to understand interaction processes in these small particle systems, as well as the influence of size and concentration on such processes.

It is also interesting to analyse the magnetisation curves of the 50% samples. Comparing the coercivities of S1-50 and S8-50, it was observed that: $H_c(\mathrm{S1}-50) = 89\ Oe$ and $H_c(\mathrm{S8}-50) = 184\ Oe$. This is typical behaviour of single domain particles, i.e., the bigger particles present higher coercivity [Cullity (1972) p. 387]. However, at 50% concentration the system is very close to percolation and massive clustering would occur, making it difficult to interpret the data. It has been observed that the 50% samples have higher coercivities than the corresponding 10% ones. This behaviour can be due to the presence of larger particles in the 50% samples, which would lead to a higher percentage of blocked particles in these systems, and the corresponding increase in coercivity. The higher concentration will also lead to particle agglomeration, with the particles being possibly connected by exchange interactions [Walmsley et al. (1999)]. The presence of aggregates would lead to higher effective magnetic moments, and thus higher coercivities, as far as the particles still remain in the single-domain regime. However, in a system with a 50% concentration of magnetic material the interactions can be complicated and their impact on the magnetic characteristics of these systems difficult to evaluate.

6.3. Physical particle size

The particle sizes were measured using a time of flight mass spectrometer, during the manufacture of the samples. After being produced in a magnetron cluster source (see ✣3.8), the clusters of Co are co-deposited with an atomic beam of copper, in a high

vacuum deposition chamber. In this process, the pulsed beam of clusters travels a distance d in a time t, with a velocity v; using the equation for the kinetic energy,

$$E = \frac{1}{2} mass \times velocity^2 \text{, where} \qquad \text{(Eq. 6.1)}$$

$$velocity = distance / time\ of\ flight \qquad \text{(Eq. 6.2)}$$

the mass of the particles can be calculated. A counter records the number of clusters arriving at different times. As the distance between the cluster source and the counter is constant, different times of arrival will mean different masses, and the mass spectrum can be worked out by changing the pulse time or the distance source-detector. This will give a distribution of the masses, or number of atoms in the cluster, for every sample.

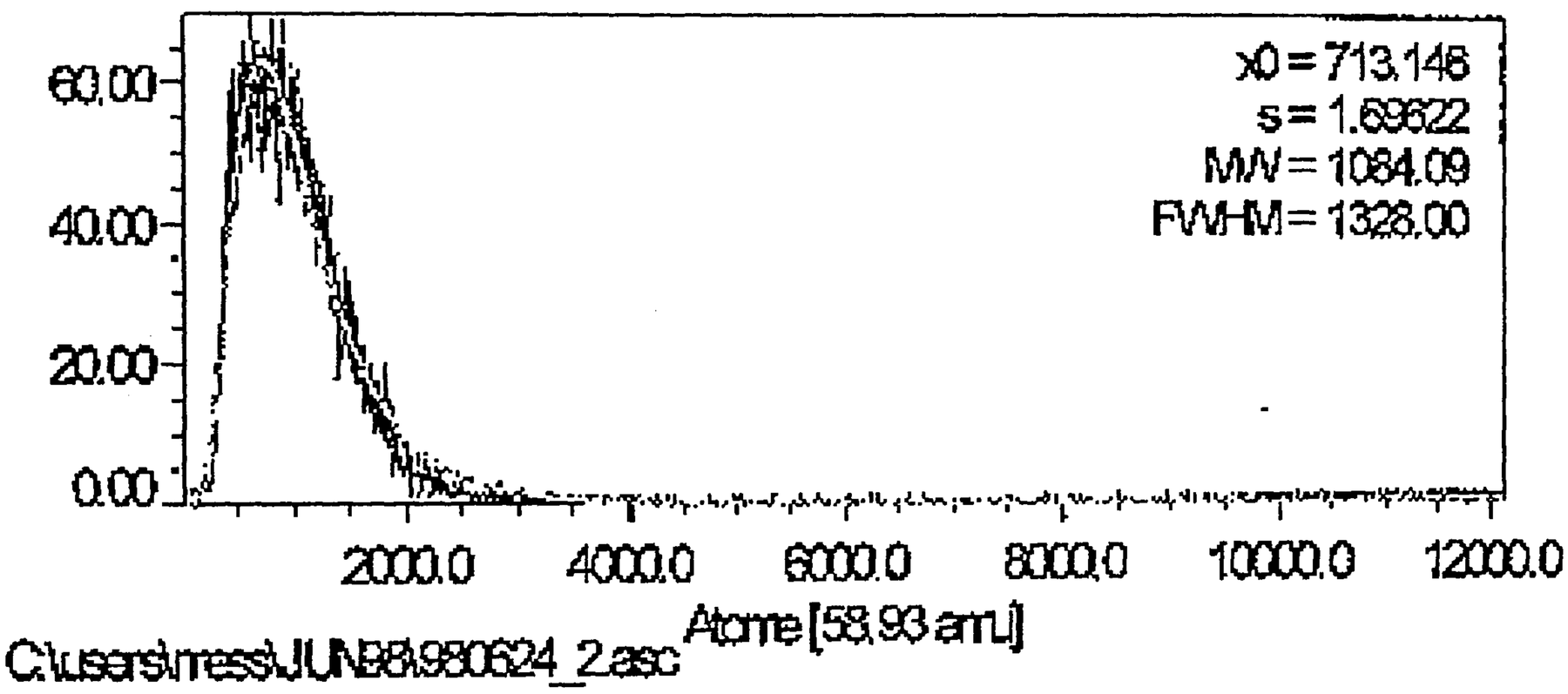

Figure 6-7

Distribution of number of atoms per Co cluster in the S1-5 nanocluster film, fitted to the distribution described in Eq.6.3 (courtesy of Derek Estham, at Daresbury Laboratory).

The cluster size distributions were fitted (see Fig. 6-7) by the manufacturers to a distribution of the form,

$$f(n)dn = n \cdot \exp\left(\frac{-(\ln(n/n_0)^2}{2 \cdot (\ln(\sigma))^2}\right) dn \qquad \text{(Eq. 6.3)}$$

where n and n_0 are the number of atoms and the mean number of atoms per cluster, respectively, and σ is the standard deviation of the distribution. In Fig. 6-7, $n_0 = x_0$ and $\sigma = s$. According to this, the values given by the manufacturers are,

	S1-5	*S1-10*	*S1-50*	*S8-5*	*S8-10*	*S8-50*
x_0	713	708	750	6794	6382	5726
s	1.70	1.69	1.80	1.38	1.48	1.68

Table 6-4

Mean number of atoms per cluster and standard deviation, for the different nanocluster systems, as defined in Eq. 6.3.

If a spherical shape is assumed for every cluster, and considering that the *Co* clusters have an *fcc* structure (lattice constant $a = 3.55$ Å) a distribution of the cluster diameters, $f(D)$, can be obtained based on the distributions of the number of atoms per cluster obtained in the time-of-flight spectrometer. Following the same procedure described in ✣5.3.1, the median diameters and the standard deviations of the lognormal distribution of particle diameters can be calculated, as shown in Table 6-5.

	S1-5	*S1-10*	*S1-50*	*S8-5*	*S8-10*	*S8-50*
D_{vm} *(Å)*	42	42	46	91	94	96
σ_v	0.18	0.17	0.20	0.17	0.15	0.14

Table 6-5

Median cluster diameter and standard deviation for the different nanocluster systems, as defined in Eq. 5.2.

As it can be observed from the results in Table 6-5, the physical size of the nanoclusters is larger than the magnetic size (Table 6-2) as observed by other authors [Chantrell et al. (1978)]. This would be expected if there exists a surface in the clusters with no magnetic behaviour, which could be the case for these samples [Chen et al. (1995)].

For the clusters that contain 8000 atoms the data obtained for the physical diameters (table 6-5) seem too large to be realistic. If a spherical shape is assumed, and an *fcc* lattice is considered, the diameter of a 1000 atom cluster would be 38 Å, while it would take the value of 76 Å for an 8000 atom cluster. Thus, while the values obtained in Table 6-5 for the 1000 atom clusters seem reasonable, the same cannot be said of the 8000 atom clusters. It is not clear why such a difference is obtained. It may be due to the fact that while for the 1000 atoms clusters the assumption of a spherical shape is probably reasonable this is not

the case for the larger clusters; or perhaps the lattice constant in small clusters is different from that assumed for bulk *fcc* Co.

6.4. Temperature Decay of Remanence (TDR)

6.4.1. Experimental data

From the data presented in this section some interesting conclusions can be drawn. Firstly, it can be seen from Fig. 6-8 that the smaller nanocluster sample (S1-10) presents a lower value of the remanence to saturation ratio, as expected and also observed in ✣5.4 in the ferrofluid samples. This, as already commented in the relevant section, may be partly due to the fact that smaller particles are affected more strongly by thermal effects, the remanence being lower for the same temperature; also, the lack of a high enough saturating field and/or the presence of a strong anisotropy (surface and/or strain) due to the reduced size of these particles could be the cause of the low values of M_r / M_s, as discussed in ✣5.4. From Fig. 6-8, it can be observed that this does not seem to be the case for the 8000 atom clusters whose $M_r / M_s(T = 4.5K)$, for both concentrations, presents almost the same value very close to 0.5.

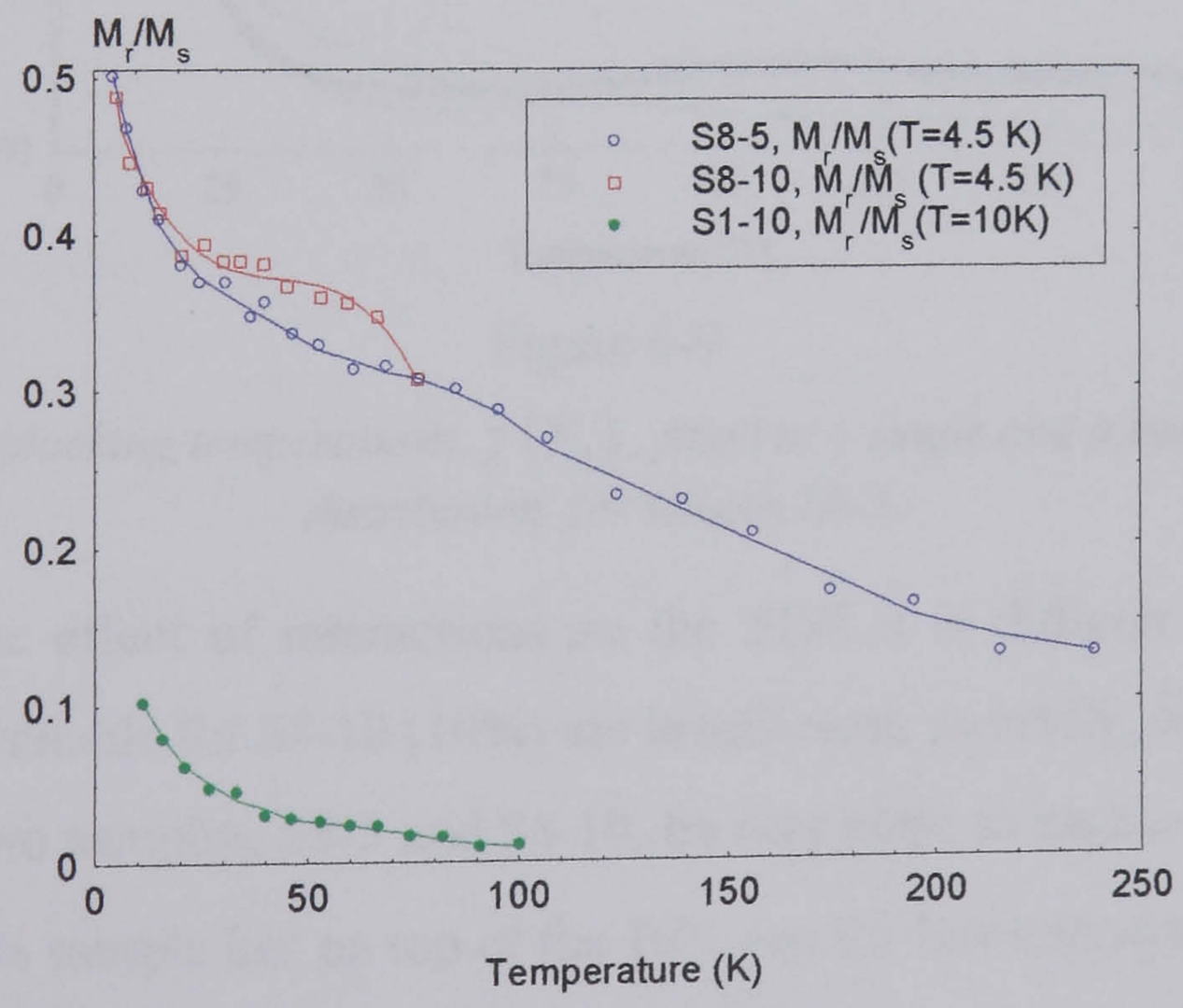

Figure 6-8

Temperature Decay of Remanence (TDR) for samples S8-5, S8-10 and S1-10.

The TDR have been differentiated to obtain the distribution of blocking temperatures or energy barriers (✣5.4.1), and fitted to a lognormal distribution function of reduced temperatures. The median blocking temperatures and standard deviations are obtained, as

well as the corresponding anisotropy constants (✣5.4.5), which are shown in Table 6-6. Sample S8-10 has not been used due to the lack of data.

An interesting observation is that for both samples, S1-10 and S8-5, some bimodality (see Fig. 6-9 and Table 6-6) is present, as it was the case for the ferrofluid samples. An initial steep slope of $f(T_B)$ followed by a smoother slope leads to two different energy barriers. This bimodality may be due to the presence of very small particles and larger ones, and/or to the presence of two sources of anisotropy. However, more measurements need to be taken to be able to draw any real conclusions. With the only data taken in this section any conclusion seems speculative.

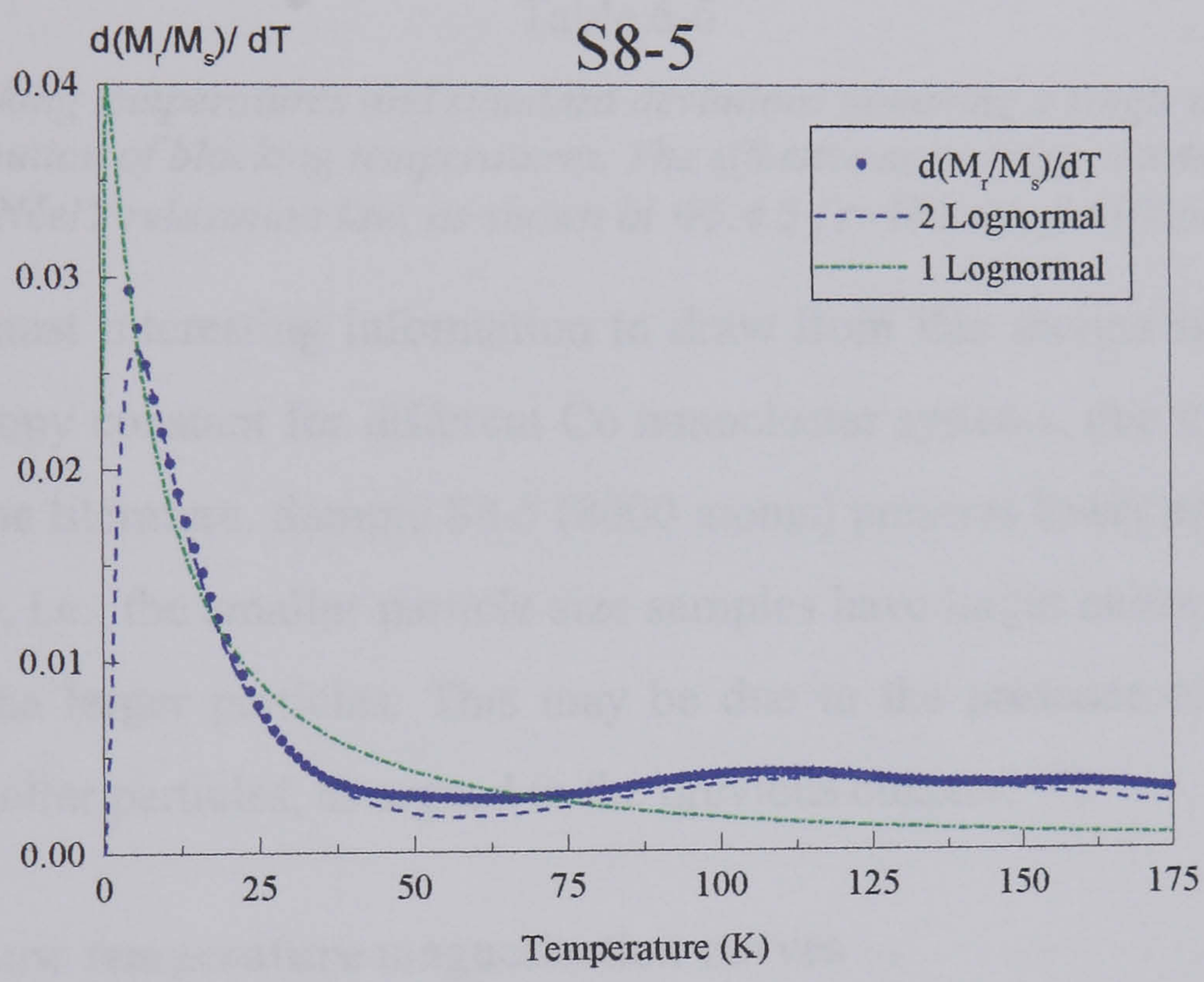

Figure 6-9

Distribution of blocking temperatures, $f(T_B)$, fitted to a single and a bimodal lognormal distribution, for sample S8-5.

With respect to the effect of interactions on the TDR it is difficult to evaluate. Firstly because the data available for S8-10 (10%) are insufficient; secondly, because the values of M_r / M_s for the two samples, S8-5 and S8-10, lie very close to each other. Thus, although it seems that the 5% sample lies on top of the 10% one for low temperatures, this is not the case anymore for $T > 10K$. This could be a real effect or equally a result of the noise in the measurements. To discern the behaviour of the systems, experimental devices with more resolution would be required.

SAMPLE	T_{Bm} (K), σ (1 Log)	K_{eff} (10^6 erg/cc)	T_{Bm1}, σ_1, T_{Bm2}, σ_2 (2 Log)	Percentage (%)	K_{eff1}, K_{eff2} (10^6 erg/cc)
S1-10	T_{Bm} = 17.0 σ = 0.6	2.4 ($f_0=10^9$ Hz) 3.1 ($f_0=10^{12}$ Hz)	T_{Bm1}= 13.7 σ_1 = 0.3 T_{Bm2}= 27.1 σ_2 = 0.6	38% 62%	1.9 ($f_0=10^9$ Hz) 2.5 ($f_0=10^{12}$ Hz) 3.8 ($f_0=10^9$ Hz) 4.9 ($f_0=10^{12}$ Hz)
S8-5	T_{Bm} = 27.4 σ = 1.8	1.2 ($f_0=10^9$ Hz) 1.6 ($f_0=10^{12}$ Hz)	T_{Bm1}= 13.4 σ_1 = 0.9 T_{Bm2}= 140.9 σ_2 = 0.4	53% 47%	0.6 ($f_0=10^9$ Hz) 0.8 ($f_0=10^{12}$ Hz) 7.7 ($f_0=10^9$ Hz) 8.1 ($f_0=10^{12}$ Hz)

Table 6-6

Median blocking temperatures and standard deviations assuming a single and a bimodal lognormal distribution of blocking temperatures. The effective anisotropy constants are calculated assuming Néel's relaxation law, as shown in ✣5.4.5 (τ=100 sec, $f_0=10^9$ and 10^{12} Hz).

At present the most interesting information to draw from this section is the value of the effective anisotropy constant for different Co nanocluster systems, due to the lack of such information in the literature. Sample S8-5 (8000 atoms) presents lower anisotropy than S1-10 (1000 atoms), i.e., the smaller particle size samples have larger anisotropy compared to the values for the larger particles. This may be due to the presence of stronger surface effects in the smaller particles, as argued in the previous chapter.

6.5. Low temperature magnetisation curves

The main results of this section are presented in Table 6-7, below. It can be seen how, for the low temperatures studied ($T = 10K$) the coercivity of samples S1-5 and S1-10, with the 1000 atom clusters, decreases as dilution increases, as observed in ✣5.7 (Table 5-16) in the ferrofluid systems. Also, for these two samples the evolution of the remanence to saturation ratio seems to follow the same behaviour with concentration as in the ferrofluids, i.e. higher remanence to saturation ratio the more diluted the sample is, which also agrees with predictions by El-Hilo et al. [1998]. This is so for the lower concentration samples, S1-5 and S1-10, which lie within the weakly interacting regime, i.e., $\varepsilon \leq 10\%$ [Martin et al. (1986), El-Hilo et al. (1992 *b*)]. S1-50 is probably a totally different sample, possibly with a higher particle size and complicated interactions, which make it difficult to interpret the coercivity and remanence to saturation ratio. It is possibly the case that S1-50 presents a larger particle size, as shown by the higher coercivity of this sample.

In the case of the 8000 atom clusters ($T = 4.5K$), however, the coercivity follows exactly the opposite behaviour, i.e., it diminishes with particle concentration, in this case for all particle concentrations. This is expected from systems with strong dipolar interactions [El-Hilo et al. (1998), Wohlfarth (1955)]. For S8-50 it is difficult to ascertain if the decrease in coercivity and remanence to saturation ratio is due to increasing dipolar interactions and/or to the presence of significant exchange interactions, which would not be surprising with such a concentration (50%).

Sample	*S8-5*	*S8-10*	*S8-50*
$H_c(T = 4.5K)$ *(Oe)*	690 ±5	653 ±5	554 ±4
$M_r / M_s(T = 4.5K)$	0.21 ±0.02	0.18 ±0.02	0.15 ±0.01
Sample	*S1-5*	*S1-10*	*S1-50*
$H_c(T = 10K)$ *(Oe)*	80 ±7	117 ±6	299 ±4
$M_r / M_s(T = 10K)$	0.25 ±0.03	0.18 ±0.02	0.278 ±0.02

Table 6-7

Coercivity and remanence to saturation ratio at low temperatures for different concentrations of the 8000 and 1000 atom nanoclusters

Although the 8000 atoms clusters (S8-5, S8-10, S8-50) are smaller ($D_m = 50$ Å) than the F028 ferrofluid particles ($D_m = 59$ Å) they have coercivities (compare Tables 6-7 and 5-16) which are higher than those of magnetite particles in F028. This is probably due to rather higher anisotropy of the Co clusters (see ✣6.4), as compared to the anisotropy of the magnetite particles.

Unfortunately, the effect of particle size on the loop characteristics cannot be studied properly, because the magnetisation curves have been taken at different temperatures (4 and 10 K, for samples S8 and S1, respectively). Still it can be observed that the 8000 atoms (S8) clusters have a much higher coercivity than the 1000 (S1) clusters, given the difference in temperature, as expected for single domain particles, where at a constant temperature, the larger the size, the higher the coercivity.

" As the sky touches land,
the sea touches the shore,
so heaven touches the earth and time touches eternity "
(*Celtic Reflections*)

7. Conclusions and future work

Conclusions

In this work a basic understanding of the mechanisms that drive the magnetic behaviour of small magnetic particle systems with weak interactions has been developed. Such processes include time dependence of the magnetisation, temperature decay of remanence (TDR), magnetisation curves at different temperatures, initial susceptibility (ZFC), remanence curves, etc. In all cases, the influence of particle concentration, size, measurement time and temperature has been studied, using the whole range of magnetic and non-magnetic experimental techniques.

Superparamagnetic behaviour has been observed in both ferrofluid and nanocluster systems at room temperatures. From the magnetisation curves at room temperature, the median and standard deviation of the lognormal distribution of particle sizes have been calculated. The median diameters of the three ferrofluid samples are 77, 66, and 59 Å, respectively. The size distributions have been found to be very narrow, with standard deviations of ln(D) of 0.42, 0.41 and 0.38, respectively. In the magnetisation curves interactions has been found to enhance the magnetisation of the system only for the larger

particle systems (77 Å) and for low magnetic fields ($H < 500$ Oe). The median diameter of the Co/Cu clusters are 31, 36, 53 and 51 Å, with standard deviations of 0.44, 0.32, 0.28, 0.36, for the S1-5 (1000 atoms, 5%), S1-10 (1000 atoms, 10%), S8-5 (8000 atoms, 5%) and S8-10 (8000 atoms, 10%), respectively. In the nanoclusters some effects of concentration on the room temperature magnetisation curves have also been observed, although at the moment it is not clear if such effects are only due to dipolar interactions or there are other variables involved in this behaviour, such as different particle sizes (for the different concentration clusters) or the presence of some exchange in the clusters.

In the ferrofluid samples, the particle size distributions do not seem appreciably changed by dilution, as it had been suggested by some authors [Menear et al. (1984)]. The presence of some aggregation in the more diluted samples, D12 and D24, has been detected both in the 77 and 59 Å ferrofluid samples, via the initial susceptibility values, which are strongly influenced by the bigger particles [O'Grady et al. (1986)].

A best fit routine has been written to test the validity of the method of Chantrell et al. [1978], which has also been used as an alternative method for the determination of magnetic particle size distributions. The method of Chantrell et al. has been found to be very reliable in giving the particle size distribution of the samples. However, in both cases the best fit method seems to provide theoretical magnetisation curves that lie closer to the experimental data.

Some deviation from the purely Langevin behaviour has been observed at room temperatures at intermediate and high applied fields, specially in the lower particle size samples. This has been attributed to the presence of surface anisotropy, which makes it hard for the field to completely saturate the sample. Following theoretical studies by Hanson et al. [1993] and Chantrell [1977] the energy term that describes the magnetic system has been modified to include an anisotropic contribution, $K\cos^2\theta$, in an attempt to account for the deviation from the Langevin behaviour. The subroutine is still under testing, and its optimisation as well as the use of different anisotropy terms, will be the object of future work.

In the ferrofluid systems, the particles physical and crystalline sizes have been calculated via TEM and X-ray diffraction, respectively. For the nanocluster samples a time of flight spectrometry has been used to measure the number of atoms per cluster. The TEM micrographs were studied with a Zeiss analyser and the median diameters and standard

deviations obtained [O'Grady et al. (1983)], which are very close to those acquired from the magnetic characterisation, namely, 77, 64 and 46 Å, with 0.26, 0.30 and 0.39 standard deviations, respectively. The crystalline sizes are 57, 46 and 40 Å. From the relation between the sizes found by TEM and X-ray diffraction, it can be said [Duvigneaud and Derie (1980)] that the crystalline part is a single crystal. The presence of bimodality has been detected in the particle size distribution, that has been attributed to the preparation process of the samples. An estimate of the surface thickness has been given, by direct subtraction of the magnetic and the crystalline diameters, and a value of approximately 10 Å has been obtained. This is roughly the lattice constant for magnetite particles, 8.39 Å.

The temperature decay of remanence has been used to calculate the distribution of blocking temperatures or energy barriers in the system [Tari et al. (1979)]. The median blocking temperatures, T_{Bm}, and standard deviations of these distributions have been obtained. The T_{Bm} are 13, 16 and 18 for the 59, 66 and 77 Å particle systems, respectively. From the median blocking temperatures, effective values of the anisotropy constants, K_{eff}, have been obtained for the different systems, which are 3.3, 4.0 and 4.6×10^5 erg/cc, for decreasing particle sizes. The values obtained indicate the presence of a higher anisotropy in the smaller particle systems, which has been attributed to surface effects, as expected from the higher surface to volume ratio as particle size decreases. In the nanocluster samples, K_{eff} has been calculated via the TDR, and higher values of the anisotropy constant have been found for the smaller cluster systems. Bimodality has been observed in the distribution of energy barriers of the systems, both in the ferrofluids and the nanoclusters. While for the ferrofluids the bimodality seems to stem from the bimodality observed in the particle size distribution, it is not clear why there should be any bimodality in the nanocluster samples.

Another interesting result is the low value of M_r / M_s obtained from the TDR at low temperatures. The reason for this low value of the remanence to saturation ratio ($M_r / M_s < 0.5$) is not clear at the present moment. As discussed in ✣5.4 there are several reasons, such as the lack of a high enough saturating field, the presence of dipolar interactions, the existence of a certain microstructure in the system or surface effects, that could account for the deviation of M_r / M_s from the Stoner-Wohlfarth prediction for a random distribution of easy axis.

Low temperature magnetisation curves have been taken for all the samples. The coercivity at low temperatures has been measured for F028 (59 Å) and has been found to decrease with increasing dilution. This behaviour has been attributed to the presence of more stable microstructures in the more concentrated samples compared to those of the diluted materials. The same evolution with concentration has been found in the smaller nanoclusters (30Å). In the case of the larger nanocluster samples (50Å), even for the lower concentrations (5% and 10%) the evolution of coercivity with concentration follows the opposite trend, i.e., decreases with increasing concentration. In the case of the nanoclusters, the variation of coercivity with concentration is difficult to interpret, as there might be a combination of dipolar and exchange interactions, and possibly some other effects due to the specific microstructure of the systems.

In the ferrofluid systems, the remanence to saturation ratio, M_r / M_s, as obtained from the low temperature magnetisation curves seem to follow the expected behaviour for a purely dipolar interacting system, i.e. it decreases with higher concentrations. This has also been explained as a consequence of the more stable local microstructures for the higher concentration samples, to which the moments will return once the applied field is zero, when the remanence to saturation is recorded.

It has been observed at low temperatures that the coercive field of the smaller particle ferrofluid sample (59Å) is higher than the value recorded for the largest particle size sample (77Å). This is only observed for temperatures lower than $10K$. For temperatures above this value, the trend is as expected for single domain systems: larger particles have higher coercivities. This behaviour at the lower temperatures seems to indicate the manifestation of a strong anisotropy in the smaller particles when they are cooled down. This anisotropy has been attributed to surface effects and the lower the temperature, the harder it is to bring the surface moments out of their stable positions, as it has been reported by several authors [Morrish et al. (1976), Kodama et al. (1996)].

The initial susceptibility χ_i or ZFC curves have also been studied for the ferrofluid systems. Several features have been observed. The evolution of the maximum of these curves, T_m, with applied field and concentration has been described. T_m decreases with decreasing concentration as, in this case, the local interactions will be weaker than in the more concentrated samples, making it easier for the moments to rotate over the energy

barriers. T_m also decreases as the field is increased, as the applied field lowers the energy barrier for reversal.

From the ZFC curves, Curie-Weiss behaviour has also been studied. The value of the interaction temperature, T_{0i}, has been obtained by plotting χ_i^{-1} vs T, once the effects from blocking have been corrected. T_{0i} has been found to be negative for all particle sizes, indicating overall demagnetising interactions. This is supported by the negative ΔM plots obtained at 4K, for all samples. However, unexpected results for T_{0i} have been obtained depending on the particle size of the sample under study. For F028 (59Å) interactions have been found to be more magnetising as concentration is increased, while the contrary is observed for the larger particles (77Å). Although it is still not clear why this behaviour is observed, it may be due to the different microstructures present in the system, induced by the different sizes in the systems. In this situation it may be the case that for the smaller particle sizes (F028), the antiferromagnetic part of the dipolar interaction is decreased, causing the interactions to be more magnetising for more concentrated samples [Kechrakos et al. (1998)]. The larger particle systems present the expected more demagnetising interactions as concentration increases.

The normalised susceptibility, $\overline{\chi}_i$, has been compared for the different systems. It has been found that the values of $\overline{\chi}_i$ increase for larger particle sizes, as expected if Langevin behaviour is assumed, i.e. $\overline{\chi}_i = \mu / kT$, where $\mu = VM_S$, which seems to be the case for the low fields ($H = 25\,\mathrm{Oe}$) used in these measurements. Higher applied fields ($H = 45\,\mathrm{Oe}$) have been used to study their influence in $\overline{\chi}_i$, which is enhanced for the larger fields. This can only be explained if more terms of the Taylor expansion of the Langevin function are considered, i.e. if $\overline{\chi}_i = \mu / 3kT - (1/45) \times (\mu H / kT)^2 + (1/945) \times (\mu H / kT)^4$. In this situation, which may be the case for the $H = 45\,\mathrm{Oe}$ susceptibility curves, the value of $\overline{\chi}_i$ is expected to increase for higher fields.

Texture effects induced by small applied fields when freezing the samples, is reflected in different T_m, T_{0i}, and values of $\overline{\chi}_i$. The presence of texture effects when a 0.5 Oe field is used has been seen in the remanence to saturation ratio of magnetisation curves at 77K. Thus care must be taken when measuring the ZFC curves.

Remanence curves have been measured for the three ferrofluid samples, at 4K. It has been found that the remanence coercivity, H_r, both from the DCD and IRM curves, follows the

same trend with particle size and concentration, as that observed in the coercivity of the magnetisation curves at 4K, i.e., H_r is higher the smaller the particle size, and the larger the concentration. The size effect is attributed to the presence of stronger surface anisotropy in the smaller particles, while the effect of concentration is due to the more stable, and thus more difficult to reverse, configurations of the more concentrated sample (D1) compared to those in the more diluted sample (D4), for F024 (77Å).

Time dependence of magnetisation in the ferrofluid systems show linear behaviour with ln(t) for all particle sizes. The maximum decay or time dependence is observed near the remanent coercivity, H_r, as obtained from the DCD remanence curve. This is reasonable as the measuring technique for the time dependence mimics that used to record the DCD curve. The time dependence has been studied for two different concentrations of the ferrofluid samples. Unfortunately, the noise in the data is too high to draw any firm conclusions.

The value of the attempt frequency, f_0, has been calculated for the Fe_3O_4 particles, using the method of Dickson et al. [1993 *a*, *b*]. Although it is known [Brown (1959)] that the attempt frequency varies with temperature and particle volume, an effective value of f_0 has been obtained. It has been found that for the magnetite particles studied in this thesis, the attempt frequencies are 3.31, 5.6 and 7.7×10^9 Hz, for the 77, 66 and 59 Å systems, respectively. The higher values of f_0 for the smaller systems have been attributed to the higher anisotropy presented by these systems. Comparing values of f_0 for different magnetic systems, it seems to be the case that while ferrimagnetic particles have a value f_0 of the order of $\sim 10^9$, this is not the case for systems with antiferromagnetic order, like hematite, goethite or ferrihydrite particles [Hansen et al. (1997), Moskowitz et al. (1997)], which present higher attempt frequencies, $f_0 \sim 10^{11}$ Hz. T.ln(τ/τ_0) scaling has been used as an alternative method to calculate the attempt frequency, and although the value of f_0 obtained is close to that calculated using the method of Dickson et al. [1993 *a*, *b*], the scaling does not seem to fit our relaxation data closely.

From the work in this thesis, it appears that for weakly interacting systems ($\varepsilon < 10\%$) there is no such a thing as a transition to an ordered state below a certain temperature, as it has been suggested for a spin glass. All properties in the systems can be explained in terms

of the blocking model [Néel (1949 *a*)], as suggested by several authors [Wohlfarth (1980), Mydosh et al. (1984), El-Hilo et al. (1992 *a*, *b*)].

A Montecarlo model by El-Hilo et al. [1998] has been used to try and reproduce the experimental data. The model has been used to calculate TDR, susceptibility and magnetisation curves. Using the basic parameters obtained from the characterisation of the ferrofluid systems, it has been observed that the model predicts higher energy barriers than those presented in the real systems. Thus the results closest to the experimental data are obtained for anisotropy constants which are lower than the experimental values and for systems with very weak interactions, which does not seem to be realistic. Also, it is a possibility that the model does not account efficiently for thermal effects. It will be the object of future work to refine this model in order to be able to use it as an interpretation tool of the experimental data.

Future work

As outlined briefly in the conclusions there is some experimental work that follows naturally from the work in this thesis. The method of Hanson et al. (see✣5.2.1.2 and Appendix II) needs to be implemented in an attempt to obtain the right expression and value for the surface anisotropy constant that accounts for the deviation at high fields from pure Langevin behaviour, in the room temperature magnetisation curves. Measurements of the TDR at very high magnetic fields (H>>1T) and very low temperatures (T<4K) are vital to investigate the deviation of the remanence to saturation ratio from the value predicted by Stoner and Wohlfarth [1948], $M_r / M_s(T = 0K) = 0.5$.

A systematic study of susceptibility curves for the whole range of concentrations and applied fields is required to understand the distinct evolution of the interaction temperature, T_{0i}, for different particle sizes, and to finally assess its validity as a measure of the strength and type of interactions. The effects of induced texture on the susceptibility curves needs to be further investigated by studying these curves for the different freezing magnetic fields. Measurements of the low temperature magnetisation curves for different concentrations and particle sizes are necessary in order to study the evolution of both coercivity and remanence to saturation ratio with particle size and interactions. It is also of prime interest to study the magnetic behaviour of the systems in the strong interacting regime, for which samples with higher concentrations than those used in this thesis need to

be manufactured. Also, magnetisation curves at very high fields (H>>1T) and very low temperatures (T<4K) are required to further investigate the behaviour of the surface in the systems, and the influence, if any, of interactions in such effects (see ✣5.7.1.2). More data are required of the coercivity at low temperatures, for the different particle size samples, to prove the validity of equation 5.13 (H_c vs $T^{0.77}$) for the systems in this work.

The study of Mössbauer spectra at very low temperatures (T<4K) and high applied magnetic fields can give a clearer insight of how the spins in the surface behave, especially at these low temperatures, as well as give a precise estimate of the surface thickness and the magnetic order that the surface spins present.

The nanocluster systems need to be subjected to some kind of microstructural analysis, so the aggregation state and precise microstructure of these materials can be known. Also the production of the whole range of different concentrations of magnetic clusters is required in order to study in depth interaction effects in these systems. Due to the low amount of magnetic material, as the nanoclusters are in the form of thin films, an instrument with higher resolution than the VSM is required to study the remanence and delta-M curves and the time dependence of magnetisation. A comprehensive study of the coercivity and remanence to saturation ratio, for different particle sizes, concentrations and temperatures would be very interesting to assess the effects of such variables in this type of systems.

Finally the Montecarlo model developed by El-Hilo et al. [1998] needs to be tested further in order not only to explain the trends observed in the experimental data, but also to actually predict the experimental results as closely as possible. This will help to understand which are the processes that regulate the magnetic behaviour in these very small particle systems.

Appendix I. The method of Chantrell et al. [1978]

Assuming that the particles follow a Langevin behaviour and present a lognormal distribution of particle sizes, Chantrell et al. [1978] obtained two expressions for the median diameter and standard deviation of the logarithm of the diameters of this distribution of particle sizes. These expressions are the following,

$$D_{vm} = \left[\frac{18kT}{\pi M_{sB}} \left(\frac{\chi_{ini}}{3M_s} \cdot \frac{1}{H_0} \right)^{\frac{1}{2}} \right]^{\frac{1}{3}} \quad \text{and} \qquad \text{(Eq. App. 1)}$$

$$\sigma_v = \frac{1}{3} \left[\ln \left(\frac{3\chi_{ini}}{M_s \cdot \frac{1}{H_0}} \right) \right]^{\frac{1}{3}} \qquad \text{(Eq. App. 2)}$$

where χ_{ini} is the initial susceptibility (see Fig. App-1), T absolute temperature, k Boltzman constant, and M_s and M_{sB} the saturation magnetisation of the ferrofluid and the bulk, respectively, so that, $M_s = \varepsilon M_{sB}$. $1/H_0$ is defined as the value for which the curve M vs $1/H$, plotted for high fields ($H > 7kOe$) crosses the x-axis ($1/H$) (see Fig. App-1).

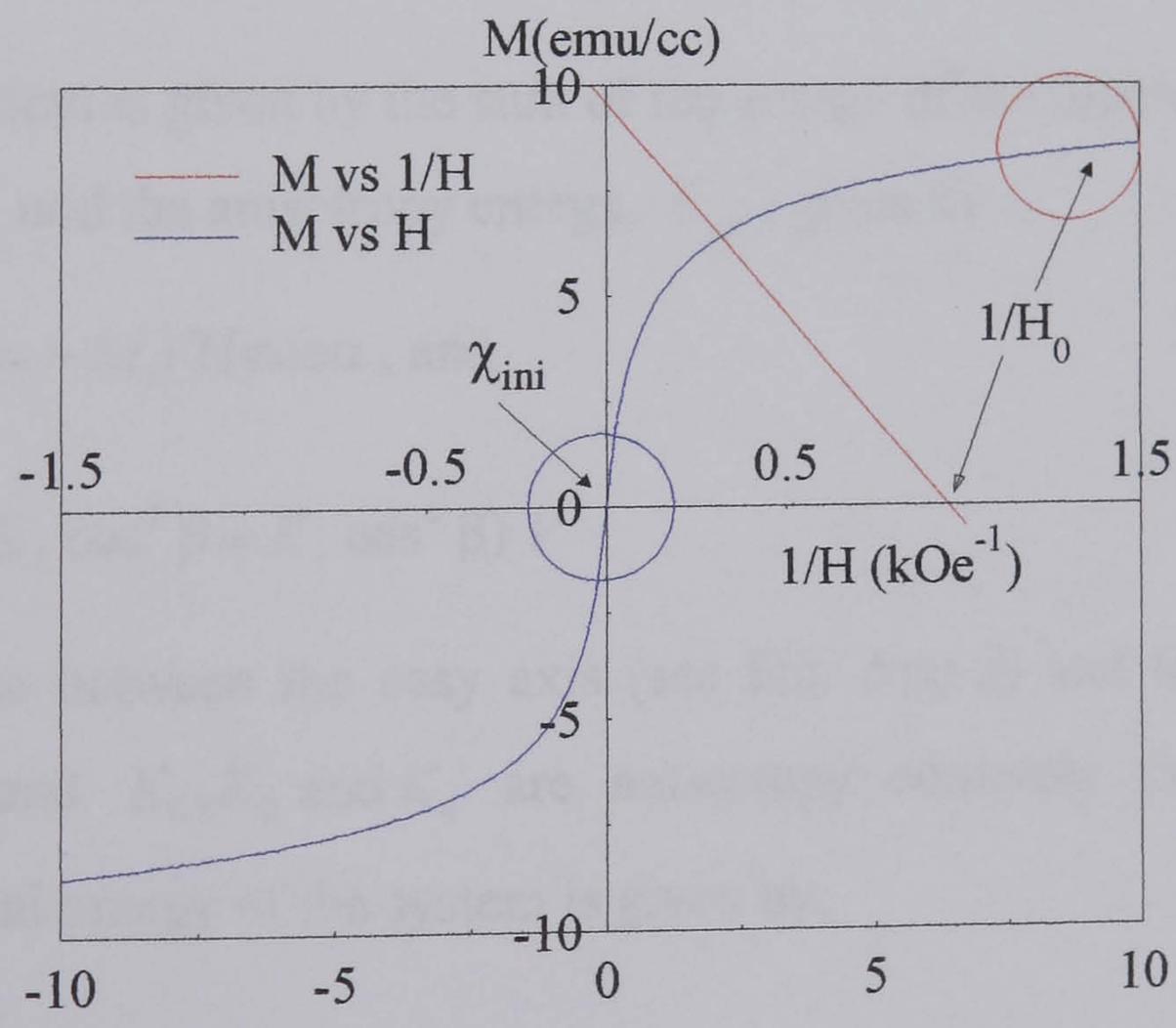

Figure App-1

Schematic of how to calculate the initial susceptibility, χ_{ini}, and the parameter $1/H_0$

The method of Chantrell et al. has been used in ✣5.2.1.1 and ✣6.2.1.1 to calculate the magnetic median diameter and standard deviation of the distribution of particle volumes in the ferrofluid and nanocluster systems, respectively.

Appendix II. Deviation from Langevin behaviour [Hanson et al. (1993)]

Hanson et al. [1993], measuring static magnetisation curves in fields up to 12 T, of magnetic particles in a frozen magnetic liquid, found that the data cannot be fully described by the Langevin behaviour, even when the size distribution is taken into account. Thus they were motivated to investigate if this deviation might be explained by the presence of some magnetic anisotropy. Hanson et al. [1993] used an energy term that included the energy of the magnetic moment in the presence of the field, as well as zero, second and fourth order anisotropy (uniaxial) terms. They found, with this approach, a better agreement between the experimental and theoretical field dependence of the magnetisation at low temperatures. In the present appendix we are going to briefly describe how the anisotropy energy modifies the field dependence of the magnetisation of an assembly of monodispersed non-interacting magnetic particles. Similar theoretical approach was developed by Chantrell in his Ph.D. thesis [1977], which was later applied by Williams et al. [1993 *b*] to explain the deviation of the magnetisation curves from the Langevin behaviour.

The energy of the system is given by the sum of the energy of the dipole in the presence of an applied field, E_H, and the anisotropy energy, E_{ani}, given by

$$E_H = -\mathrm{m}\cdot\mathrm{H} = -M_s V H\cos\alpha \text{, and} \qquad \text{(Eq. App. 3)}$$

$$E_{ani} = (K_0 - K_2\cos^2\beta - K_4\cos^4\beta)\,V \qquad \text{(Eq. App. 4)}$$

where θ is the angle between the easy axis (see Fig. App-2) and the direction of the magnetic moment, and K_0, K_2 and K_4 are anisotropy constants that depend on the material. Thus the total energy of the system is given by,

$$E = E_H + E_{ani} \qquad \text{(Eq. App. 5)}$$

In thermal equilibrium and for a fixed orientation of the easy axis (λ), the probability of finding the magnetisation in the direction of **u** (see Fig. App-2) is proportional to the Boltzmann factor,

$$f(\bar{u}) = e^{-E/kT} \qquad \text{(Eq. App. 6)}$$

where α is the angle between the magnetic moment and the applied field (see Fig. App-2). The expectation value of the z component of the magnetic moment will then be,

$$\langle m_z(\mathbf{e}) \rangle = M_s V \langle \cos\alpha \rangle = M_s V \frac{\int_{units\ phere} \cos\alpha f(\mathbf{u}) d\mathbf{u}}{\int f(\mathbf{u}) d\mathbf{u}} \qquad \text{(Eq. App. 7)}$$

units phere

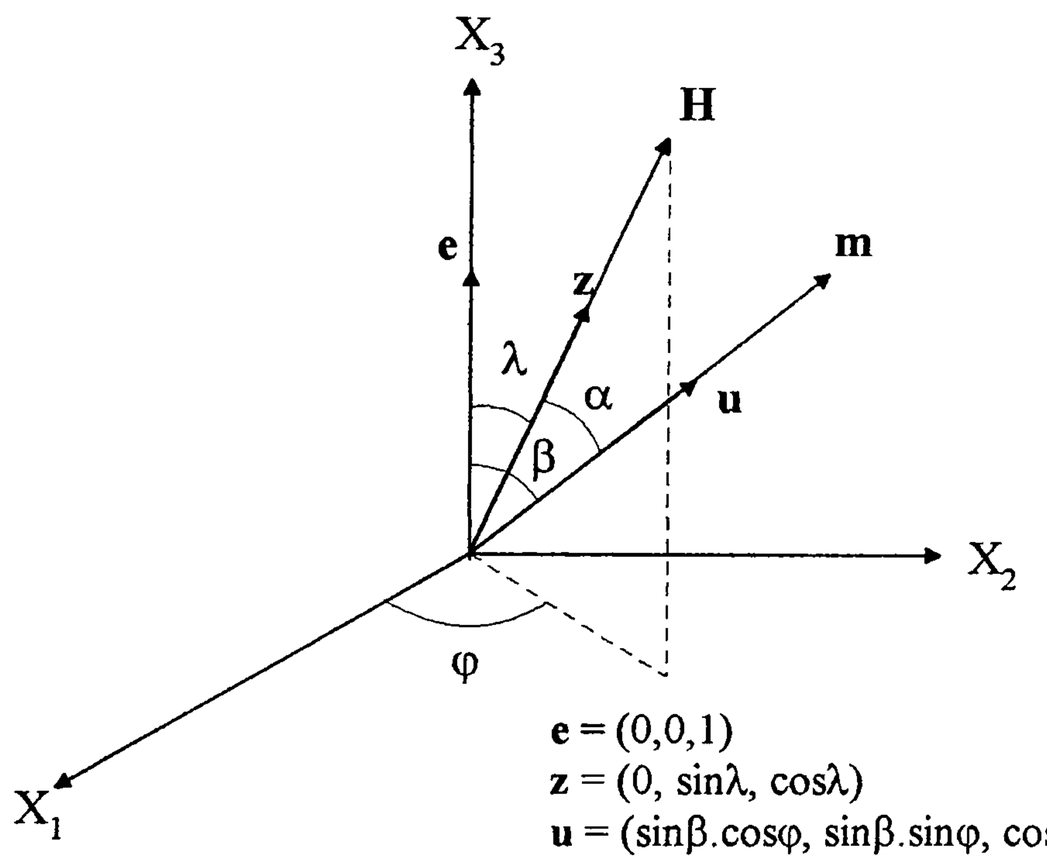

Figure App-2

Cartesian coordinate system, x_1, x_2, x_3, showing the unit vectors **e**, **u** *and* **z**, *in the directions of the easy axis, particle's magnetic moment,* **m**, *and magnetic field,* **H**, *respectively.*

Thus, substituting in Eq. App. 7,

$$\langle m_z(\mathrm{e}) \rangle = M_s V \int_0^{2\pi}\int_0^{\pi} \cos\alpha \exp(A\cos\alpha + B_1\cos^2\beta + B_2\cos^4\beta)\sin\beta d\beta d\varphi \times \left(\int_0^{2\pi}\int_0^{\pi} \exp(A\cos\alpha + B_1\cos^2\beta + B_2\cos^4\beta)\sin\beta d\beta d\varphi \right)^{-1} \qquad \text{(Eq. App. 8)}$$

where $A = M_s VB / kT$, $B_1 = VK_2 / kT$, $B_2 = VK_4 / kT$. The factor $\cos\alpha$ is given by $\cos\alpha = \mathbf{z}.\mathbf{u} = \sin\lambda\sin\beta\sin\varphi + \cos\lambda\cos\beta$ (see Fig. App-2). Using the transformation,

$$\bar{I}_0(x) = \exp(-|x|) I_0(x), \text{ and } \bar{I}_1(x) = \exp(-|x|) I_1(x) \qquad \text{(Eq. App. 9)}$$

where I_0 and I_1 are the modified Bessel functions of order 0 and 1, respectively, and integrating over φ in the numerator and the denominator of Eq. App. 8, the following expression is obtained,

$$m_z(\lambda) = T(\lambda)/N(\lambda)\text{, where} \qquad \text{(Eq. App. 10)}$$

$$T(\lambda) = \int_0^{\pi} [\cos\lambda\cos\beta \bar{I}_0(A\sin\lambda\sin\beta) + \sin\lambda\sin\beta \bar{I}_1(A\sin\lambda\sin\beta)] \times \qquad \text{(Eq. App. 11)}$$
$$\exp(A\cos(\lambda-\beta) + B_1\cos^2\beta + B_2\cos^4\beta)\sin\beta\, d\beta$$

$$N(\lambda) = \int_0^{\pi} \bar{I}_0(A\sin\lambda\sin\beta) \times \qquad \text{(Eq. App. 12)}$$
$$\exp(A\cos(\lambda-\beta) + B_1\cos^2\beta + B_2\cos^4\beta)\sin\beta\, d\beta$$

For a random distribution of easy axis directions, the z component of **m** is finally obtained from the statistical average,

$$m_z = \frac{1}{4\pi}\int_{\text{unit sphere}} m_z(e)de = \frac{1}{2}\int_0^{\pi} m_z(\lambda)\sin\lambda\, d\lambda \qquad \text{(Eq. App. 13)}$$

In this thesis the method of Hanson et al. has been extended, so that it accounts for a lognormal distribution of particle sizes.

Note: During the writing of this thesis, it was observed that in the original paper by Hanson et al. [1993] there was a misprint in Eqs. 8 and 9 (see original paper). The argument of the bar-modified Bessel functions (Eq. 6) is not ($A.\sin\lambda$) but ($A.\sin\lambda\sin\beta$) (see Eqs. App. 11 and 12). Also, there was a $\sin\beta$ missing in the integrand of both equations (8 and 9). The results, however, are calculated with the correct argument [Hanson (1999), private communication]. In this appendix, the right equations are reproduced (Eqs. App. 11, 12).

Appendix III. El-Hilo-Chantrell Montecarlo model [1998]

The study of interactions in a two particle system is a relatively simple problem and it can be solved. In real systems, however, there are many particles involved and their initial microstructures are not totally known (✣2.5.1.1.a). The exact analytical solution of the

many-body problem is virtually impossible to obtain. Hence, the use of the theoretical model seems indispensable to obtain the evolution of the system when interactions and particle size distributions are considered.

In a recent paper, 'A model of interaction effects in granular magnetic solids', El-Hilo et al. [1998] proposed a model for interacting single-domain particles considering thermal effects, based on the Montecarlo method to simulate the dynamic behaviour of a granular material. In the model the particles are assume polydispersed, with a lognormal distribution of particle sizes. The initial configuration of the system, calculated by the model, consists of a random distribution of easy axis. This model is capable of calculating the magnetisation of the system for different temperatures, sizes, concentrations, anisotropy constants and measurement times. The model includes the effect of thermal activation, assuming Néel-Brown relaxation law (see ✣2.7).

The model calculates the contribution of blocked and superparamagnetic particles to the magnetisation of the system. In this fashion, starting with an initial random configuration of magnetic moments (lognormally distributed), different versions of the program have been used to calculate TDR curves, ZFC curves and hysteresis loops. Interaction effects are taken into account via a total interaction field, which can include both dipolar and exchange contributions. The interaction strength is controlled by two parameters, that the user chooses, namely the concentration of magnetic material in the sample and the range of the interaction, which is given in units of particle diameter. The first qualitative results of the model were obtained in the same paper [El-Hilo (1998)]. Magnetostatic interactions are found to decrease both remanence and coercivity and the latter is predicted to decrease linearly with concentration. The model has also been design to calculate giant magnetoresistance (GMR).

Appendix IV. Review of the geometry of small aggregates in zero and non-zero applied fields

In this appendix, results by several authors, who calculate the stable configurations of small aggregates of particles as a function of temperature and applied field, are presented. As suggested in ✣2.5.1.1.a and ✣5.5, the knowledge of these microstructures is important for the interpretation of experimental data.

Hess and Parker [1966] were the first workers to detect the presence of aggregates in colloidal magnetic suspensions. Early studies by Menear et al. [1983, 1984] investigated

the degree of spatial ordering within a 2D system of small magnetic particles in the form of a colloidal suspension concluding that, in zero applied field, only dimers and trimers are present in the system. Using a 3D Montecarlo model, Martin [1987, 1992] confirmed Menear results, also showing the presence of some closed loop structures and larger aggregates as the temperature of the system was lowered.

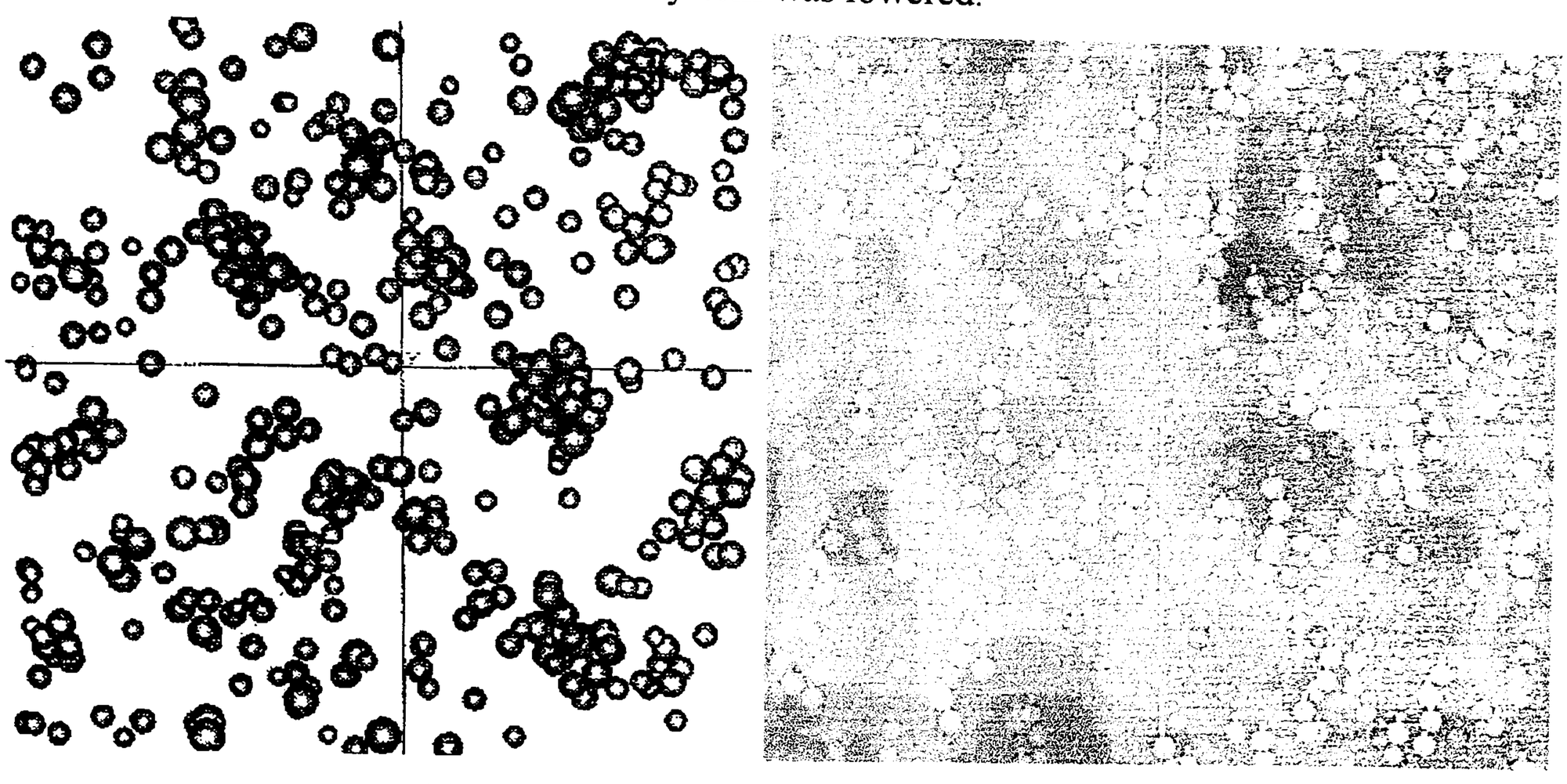

Figure App-3

Equilibrium configurations at room temperature for a magnetic dispersion containing particles with a D_{vm}=60 Å and σ=0.15. The microstructures have been calculated for (a) H=0 Oe and (b) H $\approx H_{sat}$, as obtained by Chantrell and Coverdale [1996]

More realistic is the microstructure of a ferrofluid as calculated by Chantrell and co-workers [1996] (see Fig. App-3). The authors used a 3D simulation for small (≈ 60Å) particles based on a Montecarlo model previously developed by Menear et al. [1984]. The energy of a given particle is due to the sum of all the dipolar fields within a cut-off radius and also a hard-sphere repulsion term preventing overlap of neighbouring particles. The predicted microstructures at $T = 297K$, for zero and a high applied field, are shown in Fig. App-3 (a) and (b), respectively. These microstructures are assumed to be preserved as the fluids solidifies (low temperature or polymerisation of the fluid matrix), giving a defined initial configuration which will be relevant for the further study of the magnetic behaviour in the systems.

In a series of papers Jund et al. [1995 *a* and *b*] and Tománek and co-workers [1997] studied systems of small magnetic particles ($D_{vm} = 100$Å) suspended in a fluid. They found [Jund (1995 *b*)] that the equilibrium configuration for agglomerates of $4 < N < 15$ (N = number of particles in the agglomerate) are planar and isotropic rings; for $N < 4$, the

system prefers to form linear chains and for $N > 15$, the fundamental state is structurally more complex than a single ring.

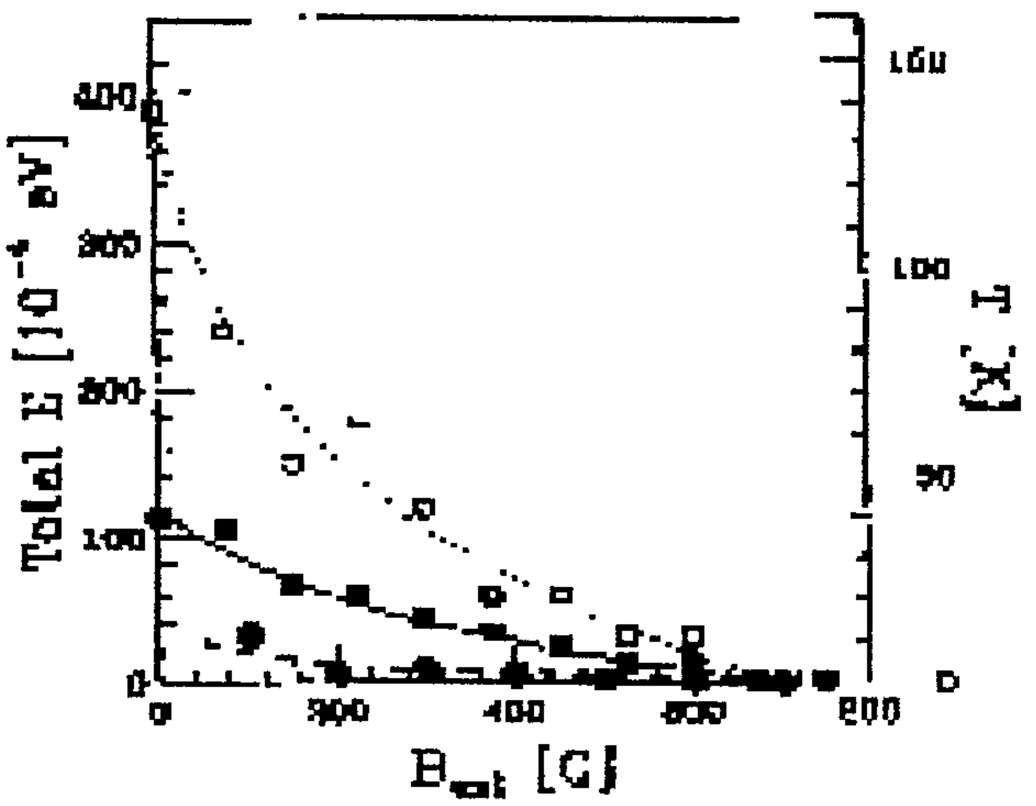

Figure App-4

Simulations for the activated transition from a N=10 ring to a chain, as a function of applied field. □ minimum total energy increase; ■ lowest potential energy barrier along a trajectory connecting a ring and a chain; ● activation barrier for the spiral opening mechanism of the ring.

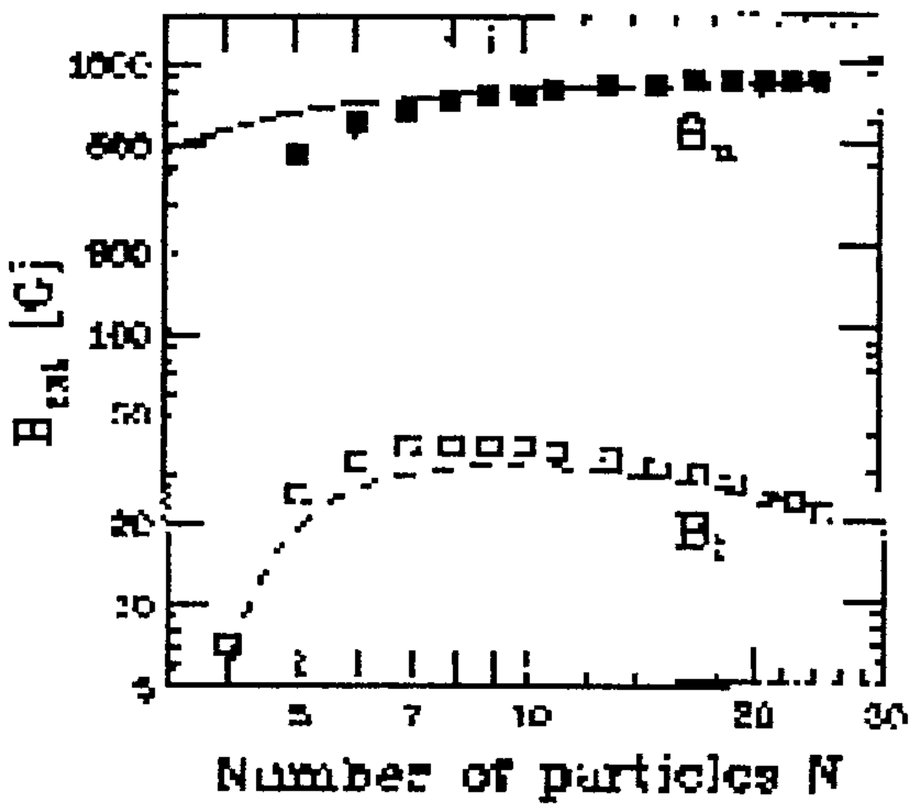

Figure App-5

Simulation results for the lower, H_l (□), and the upper, H_u (■), critical fields as a function of the aggregate size, N. The lines are the analytical results for H_l and H_u.

Jund et al. [1995 *a*] also presented studies of how the small aggregates change as a function of applied field, temperature and number of particles in the aggregate (see Fig. App-4 and App-5). For an applied field $H_{app} < H_1$, where H_l is the lower critical field, the stable configuration are rings. For $H_1 < H_{app} < H_u$ (H_u upper critical field), the dipoles in the rings start to rotate towards the direction of the field leading to a metastable state; however, for the ring to break up into chains(*), an extra activation energy is needed. Thus, only when $H_{app} > H_u$ will the rings brake up into chains, aligned in the field direction(**). With respect to the influence of the temperature in the process, the lower the temperature the highest the applied field required for the break up of the rings into stable chain configurations, as would be expected. The influence of the number of particles is best seen in Fig. App-5.

(*) For this to happen the particles in the magnetic suspension need to be able to rotate, i.e., need to be in the liquid state, which is not the case of ferrofluids are the low temperatures (T=0K) used for the work in this thesis.

(**) The property of inter-conversion (loop-chain and vice versa) of microstructures, due to the presence of an applied field and/or temperature has suggested several possible applications such as a high density memory [Tománek (1997)] (see Chapter 4 for more details).

To give an idea of the quantities involved, at sufficiently 'high' temperatures of typically a few tens of degree Kelvin, and activated transition to the more favourable chain structure can occur above a lower critical field of $H_1 \approx 50\ Oe$. These predictions are for relatively low temperatures (a few degrees Kelvin) and more extensive studies at room temperatures are necessary if realistic results are to be obtained.

Using a Montecarlo simulation Trohidou et al. [1995] studied cluster formation in systems with magnetic, non-magnetic and a mixture of both types of particles at zero temperature (see Fig. App-6). This study was performed to simulate cluster formation in the evaporation deposition technique. In this way, the particles were deposited on a substrate and allowed to move until they reached the equilibrium configuration. They found *fractal* structures in all cases. This means that the clusters are neither 2D nor 3D, because they cannot fill the whole space, but they have a fractal dimension. The non-magnetic particles diffuse by a random walk (slow), while the magnetic particles move due to the dipolar interactions (faster). In Fig. App-6 (*a* and *b*) clusters are presented for systems with magnetic and non-magnetic components, for two different concentrations.

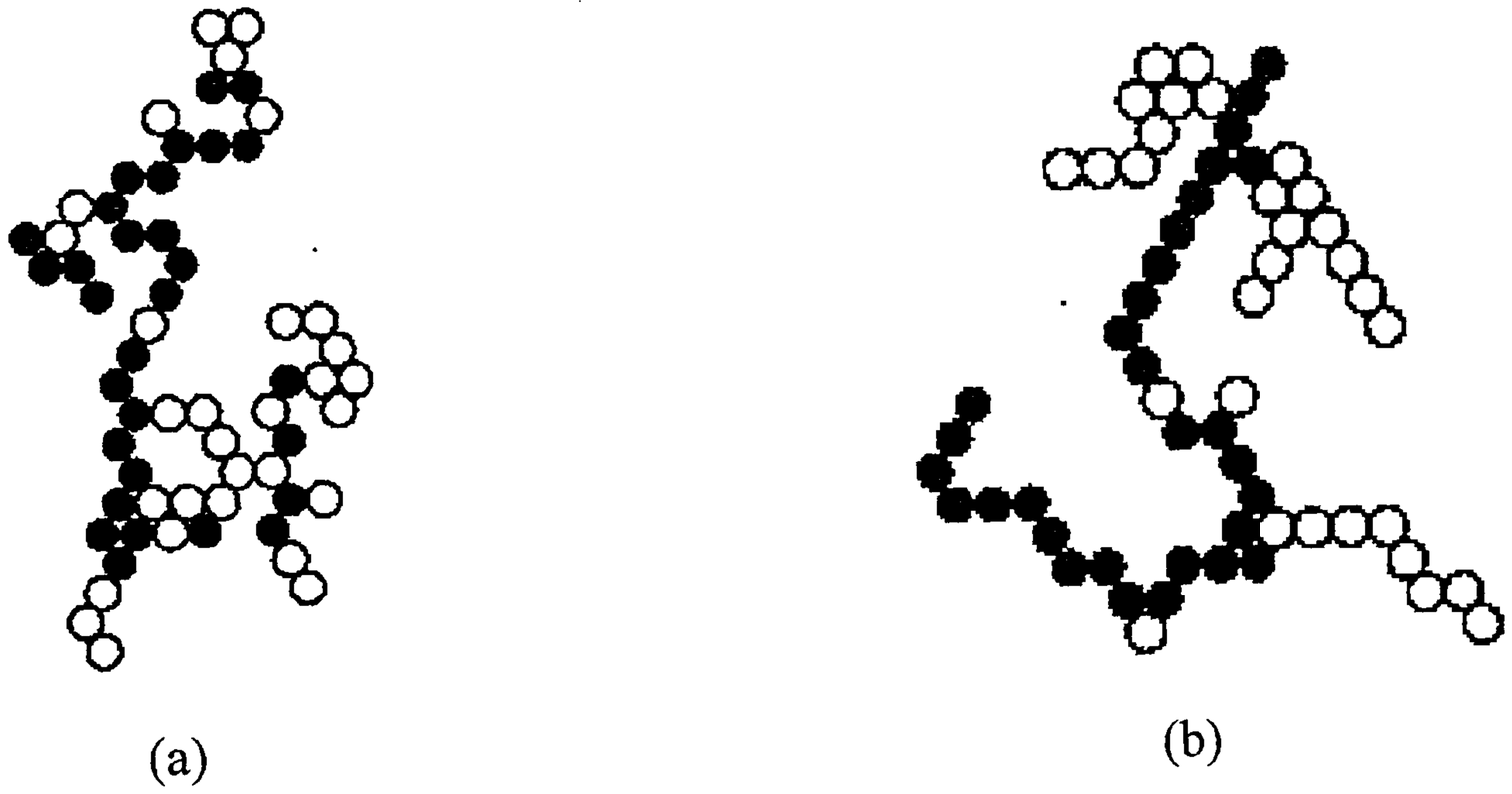

(a) (b)

Figure App-6

Clusters resulting from the zero temperature diffusion of 30 magnetic (filled circles) and 30 non-magnetic particles (open circles) for (a) a L=50 lattice (more concentration) and (b) a L=400 lattice (less concentration), as obtained by Trohidou et al. [1995]

Illuminating as the results by Trohidou et al. results might be, more calculations are required to know the exact cluster configuration of these systems at room temperature, and for different particle sizes with distributed properties. Especially interesting would be the simulation of the particles in a ferrofluid: a system filled with non-magnetic particles except for a few (~10%) that would be magnetic. For this calculation, the ratio of 30 (non-

magnetic particles)/30 (magnetic particles) utilised to obtain the cluster configurations shown in Fig. App-6, should change to, say, 30/3.

Although all these results give an idea of the microscopic structures that may be formed in colloidal systems, they only give a first approximation with regard to the actual microstructures present in these systems. In the ferrofluids used in these thesis, more precisely in sample F024 (see Fig. 5-6), different microstructures have been observed. In some areas of the fluid TEM has detected star-shaped agglomerates, similar to the fractal structures calculated by Trohidou et al. [1995]. In other photographs more 'bulky' aggregates can be seen, closer in structure to those obtained by Chantrell and Coverdale [1996]. In the photographs small chains of a few particles (two, three or four) can also be observed.

The presence of small aggregates has been measured in magnetite ferrofluids stabilised with oleic acid by Buzmakov and Pshenichnikov [1995]. These workers, making use of rheological and magnetic measurements were able to measure the mean number of particles in each aggregate. Measuring the complex component of the susceptibility, χ_2, the authors could detect the presence of single particles and small aggregates, presumably chains, with only 2 to 4 particles. These aggregates align via Brownian rotation, and thus can be detected from the peak in χ_2 at a certain frequency. Larger aggregates were also detected. From the measurement of the diffusion coefficient, sensitive to particle size, the mean diameter and the number of individual particles contained in these larger aggregates was measured. For a ferrofluid with particles of 100 Å, the number of particles contained in these aggregates would oscillate between 6.6-7.5 for a 4% concentration sample to 23 particles for a 10% concentration sample. These aggregates are thought to be spherical, to minimise the surface tension. According to Buzmakov and Pshenichnikov the aggregates are formed at the stage of preparation of the ferrocolloid, and are due to molecular forces, and not to dipolar forces, as suggests the fact that the aggregates are stable against temperature increases. In the opinion of the authors, the attraction between the colloidal particles within the aggregate is due to defects or dislocations in their protective layer. The surface of magnetite particles is not totally smooth and the adsorption of surfactant molecules cannot be equally dense throughout the surface. The occurrence of a defect in the protective layer results in a local decrease of the repelling forces and in predominant short-range molecular attractive forces. Mutual attraction of defects in different particles lead to the formation of aggregates. It is logical to think that smaller particles would

aggregate to a lesser degree due to the fact that molecular forces are weaker the smaller the particles [Hess and Parker (1966)] (see Eq. 4.2 in ✣4.1.4.1).

In general, although the theoretical studies presented in the previous paragraphs differ from each other, there seems to be a tendency in all the results, which agrees with the experimental observations: the absence of long-range order, and the predominant short-range (local) interaction effects, which lead to structures not totally 3 dimensional (fractal structures or 2D rings or chains), in the sense that they do not fill totally the whole space. This is probably a consequence of the nature of diluted systems with very small particles $D_m < 100\text{Å}$, which are weakly interacting, with only a small number of particles within the clusters or micro-aggregates (✣2.5.1.1.a).

Appendix V. Computer code (Fortran program)

As explained in ✣3.1.4, the low temperature measurements are subjected to screening effects. A FORTRAN program was originally developed by El-Hilo [1990 *a*] to correct susceptibility curves from this effect. For the work in this thesis, the original code has been modified and adapted to the different measurements performed.

A) Screening in the static cryostat (in the 455 PAR VSM)

This program corrects the magnetisation values from the screening effects in the 455 PAR VSM. There are two versions of the program. The one given below, 'screening_demag' corrects the screening and demagnetising effects in susceptibility measurements (χ_{ini} vs T). There is another version which corrects magnetisation data at a constant temperature.

! This code is based on the program written originally by M. El-Hilo to correct the measured magnetic moment for *screening* and then the susceptibility from the *demagnetising* (shape) effects.

!! It gives χ in EMU/(GR.OE) because in the small samples it is more reliable the measure of the mass than the measure of the volume, with the syringe.

```
! Ref. used: Pauthenet, J.Appl.Phys.53 ))1982((
      Program screening_demag
      integer,parameter::long=selected_real_kind(14,30), n=500
      character*20 file_input, file_output, ans1, ans2
      REAL (kind=long)  H, DMfact, Msat, VOL, pi, DM, mass, mass_gr, dens
      real(kind=long) F(500), FACT(500), GV(500), GM(500), Xt(500),RXt(500)
      real (kind=long) Ht(500), Mcorr(500),M_gr(500),Mmeas(500), T(500)
      integer ndata
      real(kind=long) input(500,2), output(500,2)
```

```
      write(6,*) 'This program corrects Magnetisation measurements'
      write(6,*) '(M in zfc, fc) from the screening in the cryostat'
      write(6,*) '
400   write(6,*) 'Please input the parameters for this sample'
      write(6,*) 'Input DMfact (in S.I. units), Msat (emu/gr)'
      read(5,*) DMfact, Msat
      write(6,*) 'Input Mass( mgr !!) and Density(emu/cc) of your sample '
      read(5,*) mass, dens
500   write(6,*) 'Please, enter the name of the INPUT file (M in emu)'
      read(5,*) file_input
      write(6,*) 'Input the field Happ(Oe) of this measurement'
      read(5,*) H
      write(6,*) 'Please, enter the name (10 letters) of the OUTPUT files'
      read(5,*) file_output
      write(6,*) 'You have the following files:'
      write(6,*) ' *.sus = Reduced X (1/Oe)'
      write(6,*) ' *.cor = Normal X (emu/gr.Oe)'
      write(6,*) ' *.gr  = Magnetisation (emu/gr)'
!     write(6,*) ' *.fac = Correction Factor (/100) with Temp'
!2    FORMAT (2F10.5, 2F12.8)
      OPEN (17, FILE=file_input, STATUS='old')
      OPEN (16, FILE=file_output//'.sus', STATUS='unknown')
      ! This file 16 gives the REDUCED Corrected X
      OPEN (18, FILE=file_output//'.cor', STATUS='unknown')
      ! This file 18 gives Corrected (Demag. Effects) X
      OPEN (19, FILE=file_output//'.fac',STATUS='unknown')
      !This file gives the CORRECTION-FACTORS divided by 100
      OPEN (20, FILE=file_output//'.gr', STATUS='unknown')
      !This gives the X in emu/cc
      OPEN (21, FILE=file_output//'.oe', STATUS='unknown')
      ! Which gives us Hreal applied on the sample
      OPEN (22, FILE=file_output//'.emu', STATUS='unknown')
      ! Which gives the M in emu, i.e. only the correction from screening
      ndata=1
3     continue
      read(17,*,end=4) input(ndata,1:)
      ndata=ndata+1
      goto 3
4     continue
      write (6,*) 'The number of rows is', ndata-1
```

```
      do 60 i=1,ndata-1
      T(i)=input(i,1)
      Mmeas(i)=input(i,2)        !Because input is M (emu)
      pi=3.1415927
      DM=4.0*pi*DMfact
!     write(6,*) 'The Demagnetising Factor *4 pi is = ', DM
      IF(T(i) > 20.0.AND.T(i) < 60.0) GOTO 10
      IF(T(i) >= 60.0.AND.T(i) <= 120.0) GOTO 15
      IF(T(i) > 120.0) GOTO 20
5     F(i)=.00047*(T(i)**3)-0.01324*(T(i)**2)+0.11601*T(i)+91.39153
      GOTO 50
10    F(i)=-0.00368*(T(i)**2)+0.4489*T(i)+84.66196
      GOTO 50
15    F(i)= -0.00013*(T(i)**2)+0.03677*T(i)+96.65267
      GOTO 50
20    F(i)= 0.00577*T(i)+98.59483
      CONTINUE
50    FACT(i)=F(i)/100.0       ! FACT= Correction Factor for Signal Screening
!     write(6,*) 'The correction factor is', FACT(i)
      mass_gr=mass/1000
!     dens=mass_gr/vol
      Mcorr(i)=Mmeas(i)/FACT(i)              ! Scorr= Corrected Sample Moment (emu)
      GV(i)=(Mcorr(i)/mass_gr)*dens  ! GV=   "      "  Magnetisation(emu/cc)
!     write(6,*) ' Magnetisation (emu/gr)', GV(i)
      GM(i)=Mcorr(i)/mass_gr          ! GM= Corrected  "       "      (emu/gr)
      Ht(i)=H-DMfact*GV(i)                   ! Ht = True Field acting on the sample (Oe)
      Xt(i)=GM(i)/Ht(i)                      ! True = True Susceptibility (emu/gr.Oe)
      RXt(i)=GM(i)/(Msat*Ht(i))              ! RXt= Reduced True Susceptibility (1/Oe)
!     write(6,*) 'Xreduced (1/Oe) = ', RXt(i)
      write (6,*) GM(i)
      write (6,*) input(i,1)
100   format(F10.3,1X,F10.8)
      write(16,100) input(i,1), RXt(i)
      write(18,100) input(i,1), Xt(i)
      write(20,*) input(i,1), GM(i)
      write(21,*) input(i,1), Ht(i)
      write(22,*) input(i,1), Mcorr(i)
      write(19,100) input(i,1), FACT(i)
60    continue
      write(6,*)'                                                    '
```

```
      write(6,*)'Do you want to use the same sample again '
      write(6,*)'but with another field, i.e., another file? (y/n)'
      read(5,'(a)') ans1
      if (ans1 == 'y') then
            goto 500
      else
            goto 600
      endif
600   write(6,*)'Do you want to work with a different sample? (y/n)'
      read(5,'(a)') ans2
      if (ans2 == 'y') then
            goto 400
      else
            goto 300
      endif
      close(UNIT=16)
      close(UNIT=18)
      close(UNIT=20)
      close(UNIT=21)
      close(UNIT=22)
300   end program screening_demag
```

B) *Screening in the dynamic cryostat (superconducting VSM)*

The program is the same as the one used for the screening in the 455 PAR VSM, but in this case, the correction factor is given by,

```
F(i)=. -6.74E-5*(T(i)**2)+0.0126*T(i)+57.1
```

References

- A. Aharoni, J. Appl. Phys. 30, 70S-78S (1959).
- A. Aharoni, Phys. Rev. 135, 2A (1964).
- A. Aharoni, Phys.Rev. 117, 2, 793-796 (1969).
- A. Aharoni, Phys. Rev. B. 7, 1103-7 (1973).
- A. Aharoni, Eisenstein, I., Phys. Rev. B. 11, 514-19 (1975).
- A. Aharoni, J. Appl. Phys. 57, 4702 (1985).
- A. Aharoni, J. Appl. Phys. 60, 1118-1123 (1986).
- A. Aharoni, J. Appl. Phys. 61, 3302-3304 (1987).
- A. Aharoni, J.App.Phys. 64, 6434-6438 (1988).
- A. Aharoni, J. Appl. Phys. 75, 5891-5893 (1993).
- A. Aharoni, 'Introduction to the theory of ferromagnetism' (Oxford University Press, New York, 1996).
- A. Aharoni, in Magnetic Hysteresis in Novel Magnetic Materials, edited by G. C. Hadjipanayis (Kluwer Academic Publishers, 1997), p. 1-20.
- A. Aharony, Pytte, E., Phys. Rev. Lett. 45, 1583 (1980).
- N. S. Akulov (1929), Z. Physik, 57, 249.
- J.-O. Anderson, Jonsson, T., Mattson, J., Phys. Rev. B 54, 14, 9912-9919 (1996).
- J. I. Arnaudas, del Moral, A., de la Fuente, C., de Groot, P.A.J., Phys. Rev. B 47, 11924 (1993).
- S. Arrhenius, Z. Phys. Chem. (Leipzig) 4, 226 (1889).
- D. D. Awschalom, Grinstein, G., McCord, M.A., Phys. Rev. Lett. 65, 6,783-786 (1990).
- D. D. Awschalom, Smyth, J.F., Grinstein, G., DiVincenzo, D.P., Loss, D., Phys. Rev. Lett. 68, 20, 3092-3095 (1992).
- N. Y. Ayoub, Abu-Aisheh, B., Dababneh, M., Laham, N., Popplewell, J., IEEE Trans on Magn. 25, 3860-3862 (1989).
- P. Bagchi, J .Colloid. Sci. 41, 380 (1972).

- S. Bandow, Kimura, K., Kon-No, K., Kitahara, A., Jap. J. Appl. Phys. 26, 713 (1987).
- B. Barbara, Gunther, L., 'Quantum tunneling of magnetization' (Kluwer Publishers, 1995 *a*).
- B. Barbara, Wernsdorfer, W., Sampaio, L.C., Park, J.G., Paulsen, Novak, M.A., Ferré , R., Mailly, D., Sessoli, R., Caneschi, A., Hasselbach, K., Benoit, A., Thomas, L., J. Magn. Magn. Mater. 140-144, 1825 (1995 *b*).
- P. Barnickel, Wokaun, A., Sager, W., Eicke, H.F., J. Colloid. Interface Sci. 148, 80 (1992).
- X. Batlle, García del Muro, M., Tejada, J., Peiffer, H., Görnert, P., Sinn, E., J. Appl. Phys. 74, 5, 3333-40 (1993).
- X. Batlle, Franco, V., Labarta, A., Watson, M.L., O'Grady, K., Appl. Phys. Lett. 70, 132-134 (1997 *a*).
- X. Batlle, García del Muro, Labarta, A., Phys. Rev. B 55, 9, 1-6 (1997 *b*).
- C. P. Bean, Jacobs, I.S., J. Appl. Phys. 27, 1448 (1956).
- C. P. Bean, Livingston, J.D., J. Appl. Phys. Supp. to Vol. 30, 4,1205-1295 (1959).
- J. J. Becker, Trans. AIME Pet. Eng. 209, 59 (1957).
- A. E. Berkowitz, Lahut, J.A., Jacobs. I.S., Phys. Rev. Lett. 34, 10, 594-97 (1975).
- A. E. Berkowitz, Lahut, J.A., VanBuren, C.E., IEEE Trans. on Magn. MAG-16, 2, 184-190 (1980).
- A. E. Berkowitz, White, R.M., Mater. Sci. Eng. B 3, 413 (1989).
- A. E. Berkowitz, J. Appl. Phys. 73, 5320 (1993).
- E. E. Bibik, Simonov, A.A., Lavrov, I.S., Colloid Journal 35, 4, 610 (1973).
- I. M. L. Billas, Becker, J.A., Châtelain, A., de Heer, W.A., Phys. Rev. Lett. 71, 4067 (1993).
- I. M. L. Billas, Châtelain, A., de Heer, W.A., Science 25, 1682 (1994).
- P. R. Bissell, J. Magn. Society of Japan 18, Suppl. S1, 261-264 (1994).
- Blakemore, Solid State Physics, Vol. 1, 2nd ed. (Cambridge University Press, 1985).

- M. Blanco-Mantecón, O'Grady, K., J. Magn. Magn. Mater. 203, 50-53 (1999).
- E. Blums, Chukhrov, A.Yu, J. Magn. Magn. Mater. 122, 110 (1993).
- F. Bødker, Mørup, S., Pederson, M.S., Svedlindh, Jonsson, G.T., Garcia-Palacios, J.L., Lazaro, F.J., J. Magn. Magn. Mater. 177-181, 925-927 (1998).
- R. M. Bozorth, 'Ferromagnetism', Vol. 1, (D. Van Nostrand Co., Princenton, N.J., 1951).
- A. Bradbury, Menear, S., Chantrell, R.W. and O'Grady, K., J. de Physique, Colloque C6 Supplément au No. 9, Tome 6 (1985).
- A. Bradbury, Menear, S., and Chantrell, R.W., J. Magn. Magn. Mater. 54-57, 745-746 (1986).
- L. Brillouin, J. de Physique 6, 74-81 (1927).
- W. F. J. Brown, Phys. Rev. 105, 1479-82 (1957).
- W. F. Brown, J.Appl.Phys. 30, 130-S (1959).
- W. F. Brown, Jr., Phys. Rev. 130, 5, 1677-1686 (1963 *a*).
- W. F. Brown, Jr., 'Micromagnetics' , 1st ed. (Intersience Publishers, a division of John Wiley & Sons, New York-London, 1963 *b*).
- R. Brown, Horsnell, T.S., Electr. Rev., 235 (1969).
- W. F. Brown, Jr., IEEE Trans. Mag. 15, 1196 (1979).
- J. P. Bucher, Douglas, D.C., Bloomfield, L.A., Phys. Rev. Lett. 6, 3052 (1991).
- V. M. Buzmakov, Colloid Journal 57, 1, 11-15 (1995).
- V., Canella ,Mydosh, J.A., Budnick, J.I., J. Appl. Phys. 42, 1689 (1971).
- M. Chagnon, J. Appl. Phys. 67, 5860 (1990).
- R. V. Chamberlin, J. Appl. Phys. 76, 6401-6 (1994).
- R. Chandrasekhar, Charles, S.W., O'Grady, K., J. Imaging Technol. 13, 55 (1987).
- R. W. Chantrell, Ph.D. Thesis, University of Wales, Bangor (1977).
- R. W. Chantrell, Popplewell, J. and Charles, S.W., IEEE Trans. Mag. Mag-14, 5, 975 (1978).

- R. W. Chantrell, Bradbury, A., Popplewell, J., Charles, S.W., J. Phys. D 13, L119 (1980).
- R. W. Chantrell, El-Hilo, M., O'Grady, K., IEEE Trans. Mag. 27, 4, 3570-3578 (1991).
- R. W. Chantrell, O'Grady, K., J. Phys. D: Appl. Phys. 25, 1-23 (1992).
- R. W. Chantrell, Coverdale, G.N., El-Hilo, M., O'Grady, K., J. Magn. Magn. Mater. 157/158, 250-255 (1996).
- R. W. Chantrell, Hannay, J., J. Mag. Soc. Jap. 21, Suppl. S2, 283-289 (1997).
- R. W. Chantrell, Hannay, J., Wongsam, M., Schreff, T., Richter, H.J., IEEE Trans. Mag. 34, 4, pt. 1, 1834-44 (1998).
- R. W. Chantrell, Walmsley, N.S., Gore, J., Maylin, M., J. Magn. Magn. Mater. 196-197, 118-119 (1999 *a*).
- R. W. Chantrell, Walmsley, N.S., Gore, J., Maylin, M., J. Appl. Phys. 85, 8, 4340-42 (1999 *b*).
- S. W. Charles, Chem. Eng. Comm. 67, 145 (1988).
- Chem. Rev. 86, entire issue (1986).
- D.-X. Chen, J. A. Brug, and R. B. Goldfarb, IEEE Trans. Mag. 27, 4, 3601-3619 (1991).
- J. P. Chen, Sorensen, C.M., Klabunde, K.J., Hadjipanayis, G.C., Phys. Rev. B 51, 17, 11527 (1995).
- O. Cheshnovsky, Taylor, K.J., Conceicao, J., Smalley, R.E., J. Chem. Phys. 64, 1785 (1990).
- C. L. Chien, Ziao, J.Q., Jiang, J.S., J. Appl. Phys. 73, 5309 (1993).
- S. s. Chikazumi, 'Physics of Magnetism', 1 ed. (John Wiley & Sons, New York, 1964).
- E. M. Chudnowsky, Gunther, L., Phys. Rev. Lett. 60, 661 (1988 *a*).
- E. M. Chudnowsky, Gunther, L., Phys. Rev. B 37, 9455 (1988 *b*).
- J. M. D. Coey, Phys. Rev. Lett. 27, 17, 1140-42 (1971).
- J. M. Coey, Khalafalla, D., Phys. Stat. Sol. (a) 11, 229 (1972).
- W. T. Coffey, Phys. Rev. B 51, 22, 15947-56 (1995).

- A. Colteu, J. Magn. Magn. Mater. 39, 88 (1983).
- M. D. Cowley, Rosensweig, R.E., J. Fluid Mech. 30, 671 (1967).
- D. M. Cox, Trevor, D.J., Whetten, R.L., Rohlfing, E.A., Kaldor, A., Phys. Rev. B 32, 7290 (1985).
- D. M. Cox, Louderback, J.C., Bloomfield, L.A., Phys. Rev. Lett. 71, 923 (1993).
- B. D. Cullity, 'Introduction to Magnetic Materials', Vol. 1 (Addison-Wesley Publishing Company, Massachusetts, 1972).
- K. J. Davies, Wells, S., Charles, S.W., J. Magn. Magn. Mater. 122, 24-28 (1993).
- W. A. de Heer, Milani, P., Châtelain, A., Phys. Rev. Lett. 65, 488 (1990).
- E. Della Torre, J. Appl. Phys. 36, 2, 518-522 (1965).
- D. P. E. Dickson, Reid, N.M.K., Hunt, C., Williams, H.D., El-Hilo, M., O'Grady, K., J. Magn. Magn. Mater. 125, 345-350 (1993 *a*).
- D. P. Dickson, in Nanophase Materials: synthesis-properties-applications; Vol. 260, edited by G. C. Hadjipanayis and R.W. Siegel, (Kluwer Academic Publishers, Dordrecht / Boston / London, 1993 *b*) p. 729.
- J. L. Dormann, Bessais, L., Fiorani, D., J.Phys.C: Solid State Phys. 21, 2015-2034 (1988).
- J. L. Dormann, D'Orazio, F., Lucari, F., Tronc, E., Prené, P., Jolivet, J.P., Fiorani, D., Cherkaoui, Noguès, M., Phys. Rev. B 53, 21, 14291-14297 (1996).
- J. L. Dormann, Fiorani, D., Tronc, E., in Advances in Chemical Physics; Vol. XCVIII, edited by S. A. R. I. Prigogine (John Wiley & Sons, 1997), p. 283-493.
- J. L. Dormann, Belayachi, A., Maknani, J., Ezzir, A., Cruz, M., Godinho, M., Cherkaoui, R., Noguès, M., J. Magn. Magn. Mater. 185, 1-17 (1998 *a*).
- J. L. Dormann, Cherkaoui, R., Spinu, L., Noguès, M., Lucari, F., D'Orazio, F., Fiorani, D., Garcia, A.,Tronc, E., Jolivet, J.P., J. Magn. Magn. Mater. 187, L139-L144 (1998 *b*).
- J. L. Dormann, Spinu, L., ,Tronc, E., Jolivet, J.P., Lucari, F., D'Orazio, F., Fiorani, D., J. Magn. Magn. Mater. 183, L255-L260 (1998 *c*).

- P. Dova, O'Grady, K., Morales, M.P., Doerner, M. F., J. Appl. Phys. 81, 8, 19 (3949) (1997).
- P. Dugourd, Rayane, D., Labastie, P., Vezin, B., Chevaleyer, J., Broyer, M., in Physics and Chemistry of Finite Systems: from Clusters to Crystals; Vol. 1, edited by P. Jena, D. P. E. B. Dickson, Mössbauer Spectroscopy, Vol. I (Cambridge University Press, 1986).
- P. H. Duvigneaud, Derie, R., J. Sol. State Chem. 34, 323-333 (1980).
- D. Eastham, Quiang, Y., Maddock, T.H., Kraft, J., Schille, J-P, J. Phys.: Condens. Matter. 9, L497-L502 (1997).
- O. Echt, Sattler, K., Recknagel, E., Phys. Rev. Lett. 47, 1121 (1981).
- A. S. Edelstein, Cammarata, R.C., 'Nanomaterials: Synthesis, Properties and Applications', Vol. ISBN-07 503 03 581 (Naval Research Lab., Washington DC, USA, 1996).
- I. Eisenstein, Aharoni, A., Phys. Rev. B 14, 2087 (1976).
- M. El-Hilo, O'Grady, K., Popplewell, J., Chantrell, R.W., Ayoub, N., J. de Physique Colloque C8, Suppl. au no. 12, Tome 49 (1988).
- M. El-Hilo, Ph.D. Thesis, University College of North Wales (1990).
- M. El-Hilo, O'Grady, K., Chantrell, R.W., J. Magn. Magn. Mater. 109, L164-L168 (1992 *a*).
- M. El-Hilo, O'Grady, Chantrell, R.W., J. Magn. Magn. Mater. 114, 295-306 (1992 *b*).
- M. El-Hilo, O'Grady, Chantrell, R.W., J. Magn. Magn. Mater. 114, 307-303 (1992 *c*).
- M. El-Hilo, O'Grady, K., Chantrell, R.W., J. Magn. Magn. Mater. 117, 21-28 (1992 *d*).
- M. El-Hilo, O'Grady, K., Nguyen, T.A., Baumgart, P., Sanders, I.L., IEEE Trans. on Magn. 29, 6, 3724-3726 (1993 *a*).
- M. El-Hilo, O'Grady, K., Chantrell, R.W., Dickson, D.P.E., J. Magn. Magn. Mater. 123, 30-34 (1993 *b*).
- M. El-Hilo, Chantrell, R. W. O'Grady, K., J. Appl. Phys. 84, 9, 5114-122 (1998).
- G. J. Fan, Toupin, R.A., Patent, Vol. 2 (Germany, 1975), p. 120.
- J. D. F. Farges, M.F., Raoult, B., Torchet, G., J. Chem. Phys. 84, 3491 (1986).

- R. W. Farley, Ziemann, P., Castleman, A.W. Jr., Z. Phys. 14, 353 (1989).
- M. Fearon, Chantrell, R.W., J. Magn. Magn. Mater. 86, 197 (1990).
- G. B. Ferguson, Ph.D. Thesis, University of Wales, Bangor (1990).
- D. Fiorani, Dormann, J.L., Tholence, J.L., Bessais, L., Villers, D., J. Magn. Magn. Mater. 54-57, 173-174 (1986 *a*).
- D. Fiorani, Tholence, J.L., Dorman, J.L., J. Phys. C: Solid State Physics 19, 5495 (1986 *b*).
- D. Fiorani, Tholence, J., Dormann, J.L., J. Phys. C: Solid State Phys. 19, 5495-5507 (1986 *c*).
- E. H. Frei, Shtrikman, S., Treves, D., Phys. Rev. 106, 446-455 (1957).
- J. Frenkel, Dorfman, J., Nature 1266, 274-275 (1930).
- F. Galton, Proc. R. Soc. (London) 29, 365 (1879).
- M. Garcia del Muro, Batlle, X., Labarta, A., Gonzalez, J.M., Montero, M.I., J. Appl. Phys. 81, 8 (1997).
- M. Garcia del Muro, Batlle, X., Labarta, A., J. Magn. Magn. Mater. 196-197, 138-139 (1999).
- Granqvist, J. Appl. Phys. 47, 2200-19 (1976).
- P. Gaunt, J. Appl. Phys. 59, 12, 4129-4132 (1986).
- R. Gerber, IEEE Trans. Mag. MAG-18, 812 (1982).
- R. Gerber, Birss, R.R., High Gradient Magnetic Separation (Research Studies Press - New York - Brisbane, New York - Brisbane, 1983).
- J. W. Gibbs (1929) Full reference not known
- J. I. Gittleman, Abeles, B., Bozowski, S., Physical Review B9, 9, 3891-3897 (1974).
- D. Givord, Lu, Q., Rosignol, M.F., in Science and technology of nanostructured materials; Vol. I, edited by G. C. Hadjipanayis, Prinz, G.A. (Plenum Press, New York, 1991), p. 635.
- M. Godinho, Dormann, J.L., Nogués, M., Prené, P., Tronc, E., Jolivet, J.P., J. Magn. Magn. Mater. 140-144, 369-370 (1995).

- H. Gohlich, Lange, T., Bergmann, T., Näher, U., Martin, T.P., in Physics and Chemistry of Finite Systems: from Clusters to Crystals; Vol. 1, edited by P. Jena, S.N. Khanna and B.K. Rao (Deventer: Kluwer, 1992), p. 633.
- A. N. Goldstein, Echer, C.M., Alivisatos, A.P., Science 256, 1425 (1992).
- Granqvist, J. Appl. Phys. 47, 5, p. 2200-19 (1976).
- N. M. Gribanov, Bibik, E.E., Buzunov, O.V., Naumov, V.N., J. Magn. Magn. Mater. 85, 7 (1990).
- A. Guinier, 'Théorie et technique de la radio-cristallographie' (Dunod, Paris, 1964).
- L. Gunther, Phys. World 3, 12, 28 (1990).
- L. Gunther, Barbara, B., Phys. Rev. B 49, 6, 3926-33 (1994).
- G. Hadjipanayis, Sellmyer, D.J., Brandt, B., Phys. Rev. B 23, 7, 3349-54 (1981 *a*).
- G. Hadjipanayis, Sellmyer, D.J., Phys. Rev. B 23, 7, 3355-59 (1981 *b*).
- G. C. Hadjipanayis, Siegel, R.W, Nanophase materials synthesis-Properties-Applications, Vol. 260, 1st ed. (Kluwer Academic Publishers, Dordrecht/Boston/London, 1993).
- H. C. Hamaker, Rec. Trav. Chim. 55, 1015 (1936).
- M. F. Hansen, Bødker, Mørup, S., Lefmann, K., Clausen, K.N., Lindgård, P., Phys. Rev. Lett. 79, 24, 4910-13 (1997).
- M. F. Hansen, Bødker, F., Mørup, S., Djurberg, C., Svedlindh, P., J. Magn. Magn. Mater. 117-181, 928-930 (1998).
- M. Hanson, Johansson, C., Mørup, S., J. Phys. Condens. Matter. 5, 725-732 (1993).
- U. Hartmann, Mende, H.H., J. Magn. Magn. Mater. 45, 409 (1984).
- C. F. Hayes, J. Coll. Int. Sci. 52, 239 (1975).
- C. F. Hayes, Hwang, S.R., J. Coll. Int. Sci. 60, 443 (1977).
- P. V. Hendriksen, Nucl. Instrum. Methods B 76, 1381 (1993).
- P. V. Hendriksen, Bødker, F., Linderoth, S., Wells, S., Mørup, S., J. Phys.: Condens. Matter. 6, 3081-3090 (1994 *a*).

- P. V. Hendriksen, Linderoth, S., Oxborrow, C.A., Mørup, S., J. Phys.: Condens. Matter. 6, 3091-3100 (1994 *b*).
- O. Henkel, Phys. Stat. Sol. 7, 919 (1964).
- J. J. Hermans, in Colloid Science; Vol. 2, edited by H. R. Kruyt (Elsevier, Amsterdam, 1949).
- P. H. Hess, Parker, P.H.Jr., J. Appl. Polym. Science 10, 1915-1927 (1966).
- M. Holmes, O'Grady, K., Popplewell, J., J. Magn. Magn. Mater. 85, 47-50 (1990).
- S. R. Hoon, Ph.D. Thesis, U.C.N.W. (1980).
- R. R. Irani, J. Phys. Chem. 63, 1603 (1959).
- Jackson, Can. Pat. (1965).
- I. S. Jacobs, Bean, C.P., Phys. Rev. 100, 1060-1067 (1955).
- P. Jena, Rao, B.K., Khanna, S.N., Physics and Chemistry of Small Clusters, Vol. NATO-ASI Series 158 (New York: Plenum, 1987).
- P. Jena, Khana, S.N., Rao, B.K., Physics and Chemistry of Finite Systems: from Clusters to Crystals (Deventer: Kluwer, 1992).
- B. Jirgensons, Straumanis, M.E., Colloid Chemistry (Pergamon Press, London, 1954).
- B. F. G. Johnson, Transition Metal Clusters (New York: Wiley, 1980).
- D. H. Jones, Srivastava, K.K.P., J. Magn. Magn. Mater. 78, 320-27 (1989).
- T. Jonsson, Djurberg, C., Khan, F.A., Nordblad, P., Svendlindh, P., Phys. Rev. Lett. 75, 22, 4138-4141 (1995).
- T. Jonsson, Ph.D. Thesis (1998 *a*).
- T. Jonsson, Nordblad, P., Svedlindh, P., Phys. Rev. B 57, 1, 497-504 (1998 *b*).
- J. Jortner, Z. Phys. D 24, 247 (1992).
- P. Jund, Kim. S.G., Tománek, D., Hetherington, J., Phys. Rev. Lett. 74, 15, 3049-3052 (1995 *a*).
- P. Jund, Kim, S.G., Tsallis, C., Phys. Rev. B. 52, 50-53 (1995 *b*).
- J. Phys. Chem. 91, entire issue (1987).

- R. Kaiser, Miskolczy, G., J. Appl. Phys. 41, 3, 1064-1072 (1970).
- R. Kaiser, Mir, L., Curtiss, R.A.; Vol. 3 (U.S. Patents, U.S. America, 1976), p. 784-5.
- D. Kechrakos, Trohidou, K.N., Phys. Rev. B 58, 18, 12169-12177 (1998).
- P. E. Kelly, O'Grady, K., Mayo, P.I., Chantrell, R.W., IEEE Trans. Magn. MAG-25, 3881 (1989).
- S. E. Khalafalla, Reimers, G.W., Sep. Sci. 8, 161 (1973).
- S. E. Khalafalla, Reimers, G.W., IEEE Trans. on Magn. MAG-16, 2, 178- (1980).
- S.N. Khanna, and B.K. Rao (Deventer: Kluwer, 1992), p. 555.
- C. Kittel, Phys. Rev. 70, 965 (1946).
- C. Kittel, Gaunt, J., Solid State Phys. 3, 437 (1956).
- I. Klik, Gunther, L., J. Appl. Phys. 67, 4505 (1990 *a*).
- I. Klik, Gunther, L., J. Statistical Phys. 60, 3-4, 473-84 (1990 *b*).
- E. Kneller, Proc. Int. Conf. on Magn. (Nottingham) 174 (1964).
- H. Knözinger, Fundamental Aspects of Heterogeneous Catalysis Studied by Particle Beams (New York - Plenum, New York, 1991).
- R. H. Kodama, Berkowitz, A.E., McNiff, E.J., Foner, S., Phys. Rev. Lett. 77, 2, 394-97 (1996).
- F. Kottler, J. Franklin Inst. 250, 339 and 419 (1950).
- F. Kottler, J. Franklin Inst. 251, 449 and 617 (1951).
- K. Krop, Korecki, J., Zukrowski, J., Karas, W., Int. J. Magnetism 6, 19-23 (1974).
- D. A. Krueger, J. Appl. Phys. 50, 8169 (1979).
- J. J. Kurkijärvi, Phys. Rev. B. 6, 3, 832-35 (1972).
- A. Labarta, Iglesias, O., Balcells, Ll., Badia, F., Phys. Rev. B 48, 14, 10240-46 (1993).
- S. Labroo, Ebrahimi, Park, J.Y., Yeh, W.J., IEEE Trans. Mag. MAG-28, 1895 (1992).
- K. LaiHing, Wheeler, R.G., Wilson, W.L., Duncan, M.A., J. Chem. Phys. 87, 3401 (1987).

- D. B. Lambrick, Mason, N., Hoon, S.R., Kilner, M., J. Magn. Magn. Mater. 65, 257-260 (1987).
- P. Langevin, Annales de Chemie et de Physique 8, 5, 70-127 (1905).
- R. H. Leary, J. of global optimization 11, 1, 35-53 (1997).
- M. Lederman, Gibson, G.A., Schultz, S., J. Appl. Phys. 73, 10, 6961-63 (1993).
- A. J. Legget, Directions in Condense Matter Physics (World Scientific, Singapore, 1986).
- P. G. Lethbridge, Stace, A.J., J. Chem. Phys. 91, 7685 (1989).
- J. S. Li, Rosenblum, W., Hayashi, H., Sinclair, R., J. Magn. Magn. Magn. 155, 157 (1996).
- S. Linderoth, Balcells, L., Labarta, A., Tejada, J., Hendriksen, P.V., Sehti, S.A., J. Magn. Magn. Mater. 124, 269-276 (1993).
- S. Linderoth, Hendriksen, P.V., Bødker, F., Wells, S., Davies, K., Charles, S.W., Mørup, S., J. Appl. Phys. 75, 10, 6583-85 (1994).
- F. E. Luborsky, Paine, T.O., J. Appl. Phys. 31, 68S (1960).
- F. E. Luborsky, C. R. Morelock, J. Appl. Phys. 35, 2058 (1964).
- W. Luo, Nagel, S.R., Rosenbaum, T.F., Rosensweig, R.E., Phys. Rev. Lett. 67, 2721 (1991).
- A. C. Mackay, Acta Crystallogr. 15, 916 (1962).
- E. L. Mackor, J. Colloid. Sci. 6, 492 (1951).
- G. A. R. Martin, Bradbury, A., Chantrell, R.W., IEEE Trans. on Mag. MAG-22, 1137-1139 (1986).
- G. A. R. Martin, Bradbury, A., Chantrell, R.W., J. Magn. Magn. Mater. 65 (1987).
- G. A. R. Martin, Ph.D. Thesis, University of Wales, Bangor (1992).
- T. P. Martin, Bergmann, T., Gohlich, H., Lange, T., Chem. Phys. Lett. 172, 209 (1990).
- A. Martinet, Rheol. Acta. 13, 260 (1974).
- S. Maruno, Yubakami, K., Soga, M., J. Magn. Magn. Mater. 39, 189 (1983).

- R. Massart, IEEE Trans. Mag. MAG-17, 1247 (1981).
- J. Mattssson, Jonsson, T., Nordblad, P., Aruga Katori, H., Ito, A., Phys. Rev. Lett. 74, 21, 4305-4308 (1995).
- P. I. Mayo, Erkkila, R.M., Bradbury, A., Chantrell, R.W., I.E.E.E. Trans. Magn. 26, 1984 (1990).
- P. I. Mayo, O'Grady, K., Kelly, P.E., Cambridge, J., Sanders, I.L., Yogi, T., Chantrell, R.W., I. E. E. E. Trans. Magn. 18, 800 (1991).
- C. W. Mays, Vermaak, J.S., Kuhlmann-Wilsdorf, D., Surf. Sci. 12, 134 (1968).
- T. K. McNab, Fox, R.A., Boyle, J.F., J. Appl. Phys. 39, 12, 5703-11 (1968).
- C. D. Mee, Daniel, E.D., 1990 magnetic Recording Handbook (New York: Mc-Graw Hill, 1990).
- P. Melinon, Paillard, V., Dupuis, V., Perez, A., Jensen, P., Hoareau, A., Perez, J.P., Tuaillon, J., Broyer, M., Vialle, J.L., Pellarin, M., Baguenard, B., Lerme, J., Int. J. Mod. Phys. B 9, 339 (1995).
- S. Menear, Bradbury, A., Chantrell, R.W., J. Magn. Magn. Mater. 39, 17-20 (1983).
- S. Menear, Bradbury, A., Chantrell, R.W., J. Magn. Magn. Mater. 43, 166 (1984).
- S. v. Molnar, Barbara, B., McGuire, T.R., Gambino, R., J. Appl. Phys. 53, 3, 2350-52 (1982).
- A. H. Morrish, 'The physical principles of magnetism', (John Wiley & Sons Inc., New York-London-Sydney, 1965).
- A. H. Morrish, Haneda, K., Schurer, P.J., J. Physique (Paris) 37, C6, Suppl. au no. 12, 301-05 (1976).
- A. H. Morrish, Haneda, K., J. Magn. Magn. Mater. 35, 105-113 (1983).
- M. D. Morse, Geusic, M.E., Heath, J.R., Smalley, R.E., J. Chem. Phys. 83, 2293 (1985).
- R. Moskowitz, Rosensweig, R.E., Appl. Phys. Lett. 11, 301 (1967).
- M. Moskovitz, Metal Clusters (New York: Wiley, 1986).
- B. M. Moskowitz, Frankel, R.B., Walton, S. A., Dickson, D.P.E., and K. K. W. Wong, Douglas, T, Mann, S., J. of Geophysical Research 102, B10, 671-680 (1997).

- R. Mössbauer, R. L. Z. Physik 151, 124 (1958).
- S. Mørup, Topsøe, H., J. Magn. Magn. Mater. 31-34, 953-954 (1983 *a*).
- S. Mørup, Madsen, M.B., Franck, J., Villadsen, J., Koch, C.J.W., J. Magn. Magn. Mater. 40, 163 (1983 *b*).
- S. Mørup, Europhysics Letters 28, 9, 671-676 (1994).
- S. Mørup, Bødker, F., Hendriksen, P.V., Linderoth, S., Phys. Rev. B 52, 1, 287-293 (1995).
- I. Nakatani, Furubayashi, T., Takahashi, T., Hanaoka, H., J. Magn. Magn. Mater. 65, 261-264 (1987).
- I. Nakatani, Hijikata, M., Ozawa, K., J. Magn. Magn. Mater. 122, 10 (1993).
- J. L. Neuringer, Rosensweig, R.E., Phys. Fluids 7, 1927 (1964).
- L. Néel, C. R. Acad. Sci., Paris 224, 1488-90 (1947 *a*).
- L. Néel, C. R. Acad. Sci., Paris 224, 1550-51 (1947 *b*).
- L. Néel, Ann. Géophys. 5, 99 (1949 *a*).
- L. Néel, C. R. Acad. Sci. (Paris) 228, 664-66 (1949 *b*).
- L. Néel, J. de Phys. et Radium 11, 49-61 (1950).
- L. Néel, J. Phys. Rad. 12, 339 (1951).
- L. Néel, Chapitre XIV, Problèmes de surface, A122, 485-514 (1955).
- J. Nogués, Schuller, Ivan K., J.M.M.M. 192, 203-232 (1999).
- J. A. Northby, J. Chem. Phys. 8, 6166 (1987).
- K. O'Grady, Chantrell, R.W., Popplewell, Charles,, IEEE Trans. Mag. MAG-16, 5, 1077-79 (1980).
- K. O'Grady, Ph.D. Thesis, U.C.N.W. (1982).
- K. O'Grady, R.W., K., Popplewell, Charles, S.W., IEEE Trans. Mag. MAG-17, 6, 2943-45 (1981).
- K. O'Grady, Bradbury, A., J. Magn. Magn. Mater. 39, 91-94 (1983).

- K. O'Grady, Stewardson, H.R., Chantrell, R.W., Fletcher, D., Unwin, D., Parker, M.R., IEEE Trans. Mag. MAG-22, 1134 (1986).
- K. O'Grady, Chantrell, R.W., Studies of Magnetic Properties of Fine Particles and their Relevance to Materials Science; Vol. 1, edited by J. L. Dormann and D. Fiorani (Elsevier Science Publishers, 1992), p. 93-102.
- J. A. Oberteuffer, IEEE Trans. on Magn. MAG-9, 3, 303-30 (1973).
- J. T. G. Overbeek, Colloid Science, Vol. 1 (Elsevier, Amsterdam, 1952).
- Q. A. Pankurst, Pollard, P.J., Phys. Rev. Lett. 67, 2, 248-50 (1991).
- S. S. Papell, US Patent, 3 15 572 (1965).
- F. T. Parker, Foster, M.W., Margulies, D., Berkowitz, A.E., Phys. Rev. B 47, 13,7885-91 (1993).
- M. R. Parker, van Reef, R.P.A.R., Myron, H.W., Wyder, P., J. Magn. Magn. Mater. 27, 250-56 (1982).
- S. S. P. Parkin, More, N., Roche, K.P., Phys. Rev. Lett. 64, 2304 (1990).
- S. S. P. Parkin, Bhadra, R., Roche, K.P., Phys. Rev. Lett. 66, 2152 (1991).
- C. Paulsen, Sampaio, L.C., Barbara, B., Tucoulou-Tachoueres, R., Fruchart, D., Marchand, A., Tholence, J.L., Europhys. Lett. 16, 643 (1992).
- R. Pauthenet, J. Appl. Phys. 53, 11, 2029 (1982).
- R. A. Pelcovitz, Mukamel, D., Phys. Rev.B. 28, 5374 (1983).
- M. Pellarin, Vialle, J.L., Lerme, J., Valadier, F., Baguenard, B., Blanc, J., Broyer, M., Physics and Chemistry of Finite Systems: from Clusters to Crystals, Vol. 1 (Deventer: Kubler, 1992).
- S. J. Peppiatt, Sambles, J.R., Proc. R. Soc. A 345, 387 (1975).
- E. A. Peterson, Krueger, D.A., J. Coll. Int. Sci. 62, 24 (1977).
- F. Petroff, Barthélémy, A., Mosca, D.H., Lottis, D.K., Fert, A., Schroeder, R.A., Pratt, W.P. Jr., Loloee, R., Lequien, S., Phys. Rev. B 44, 5355 (1991).
- H. Pfeiffer, Phys. Stat. Solidi 118 A, 295 (1990 *a*).
- H. Pfeiffer, Phys. Stat. Solidi 118 A, 233 (1990 *b*).

- J. Popplewell, Al-Qenaie, A., Charles, S.W., Moskowitz, R., Raj., K., J. Colloid. Polymer Sci. 260, 333 (1982).
- J. Popplewell, Davies, P., Llewellyn, J.P., J. Magn. Magn. Mater. 65, 235 (1987).
- J. Popplewell, Rosensweig, R.E., Johnston, R.J., J. Magn. Magn. Mater. 54-57, 761 (1990).
- J. J. Prejean, Souletie, J. Phys. (Paris) 41, 1335 (1980).
- P. Prené, Tronc, E., Jolivet, J-P., Livage, J., IEEE Trans. Magn. 29, 2658 (1993).
- P. Prené, Tronc, E., Jolivet, J.P., Livage, J., Cherkaoui, R., Nogués, M., Dormann, J.L., Hyperfine Interactions 93, 1409-1414 d (1994).
- W. H. Press, Flannery,1988 B.P., Teukolsky, S.A., Vetterling, W.T., Numerical Recipes in C, The Art of Scientific Computing, Vol. 1 (Cambridge University Press, New York, 1988).
- R. Rammal, Ph.D. Thesis (1977).
- B. V. Reddy, Khanna, S.N., Dunlap, B.I., Phys. Rev. Lett. 70, 3323 (1993).
- E. L. Resler, Rosensweig, R.E., A. I. A. A. Journal 2, 1418 (1964).
- M. Respaud, Broto, J.M., Rakoto, H., Ousset, J.C., Osuna, J., Ould Ely, T., Amiens, C., Chaudret, B., Askenazy, Physica B 246-247, 432-536 (1998).
- S. Roath, Smith, A.R., Watson, J.H.P., J. Magn. Magn. Mater. 85, 285 (1990).
- C. Rocchiccioli-Deltcheff, Franck, R., Cabuil, V., Massart, R., J. Chem. Research (S), 126 (1987).
- R. E. Rodbell, J. Phys. Soc. Jap. 17, Suppl. B1 (1962).
- M. J. Rosen, Sufactants and Interfacial phenomena (John Wiley & Sons, New York-Chichester-Brisbane, 1978).
- R. E. Rosensweig, Kaiser, R., Miskolczy, G., J. Colloid. Sci. 29, 680 (1969).
- R. E. Rosensweig, Advances in Electronics and Electron Physics 48, 101 (1979).
- R. E. Rosensweig, Scientific American (1982).
- R. E. Rosensweig, Ferrohydrodynamics (Cambridge University Press, 1985).

- R. E. Rosensweig, Popplewell, J., Johnston, R.E., J. Magn. Magn. Mater. 85, 171 (1990).
- R. S. Rósing (1897).
- D. H. Russell (Plenum, New York, 1989).
- L. Sakhini, Popplewell, J., J. Magn. Magn. Mater. 122, 146-149 (1993).
- C. J. Sambuceti, I.E.E.E. Trans. Mag. MAG-16, 364 (1980).
- A. Satoh, Chantrell, R.W., Coverdale, Geoff N., Kamiyama, Shin-Ichi, Journal of Colloid and Interface Science 209, 44-59 (1998).
- M. E. Schabes, Bertram, H.N., J. Appl. Phys. 64, 3, 1347-57 (1988).
- P. C. Scholten, Thermodynamics of Magnetic Fluids (Hesmisphere, 1978).
- P. C. Scholten, I.E.E.E. Trans. Magn. MAG-16, 221 (1980).
- K. E. Schriver, Hahn, M.Y., Persson, J.L., LaVilla, M.E., Whetten, R.L., J. Phys. Chem. 93, 2869 (1989).
- A. J. Schwartz, Soffa, W.A., IEEE Trans. Mag. MAG-26, 5, 1816 (1990).
- M. I. Shliomis, Sov. Phys. JETP. 34, 1291 (1972).
- S. A. Shustrov, ICMF-6 (Paris) Abstracts, 418 (1992).
- A. L. Smith, Dispersions of Powders in Liquids CH3 (Applied Science Publishers Ltd., London, 1969).
- T. W. Smith, U. S. Patent 4252673 (1981).
- F. Söffge, Schmidbauer, E., J. Magn. Magn. Mater. 24, 54-56 (1981).
- F. E. Spada, Parker, F.T., Nakakura, C.Y., Berkowitz, A.E., J. Magn. Magn. Mater. 120, 129 (1993).
- A. Stancu, Bisell, P.R., Chantrell, R.W., J. Magn. Magn. Mater. 000, 000 (1998).
- D. Stauffer, Introduction to percolation theory (Taylor & Francis, London, 1985).
- E. C. Stoner, Phil. Mag., Ser. 7, 36, 263, 803-821 (1945).
- E. C. Stoner, Wohlfarth, E.P., Phil. Trans. Roy. Soc. (London), A240, 599-642 (1948); (Reprint) IEEE Trans. on Mag. 27, 4, 3475-3517.

- R. Street, Woolley, J.C., Proc. Phys. Soc. A 62, 562 (1949).
- R. Street, McCormick, P.G., Estrin, Y., Proc. 10th Intern. Works. on Rare Earth Magnets, Kyoto, Japan 83 (1989).
- S. Sugano, Nishina, Y., Ohnishi, Microclusters (New York: Springer, 1987).
- T. Sugimoto, Matijevic, E., J. Colloid. Int. Sci. 74, 227 (1990).
- M. Takahashi, Shimbo, K., Ohkawa, R., Matsuzaki, M., Inoue, A., ICMF-6 (Paris) Abstracts, 108 (1992).
- Z. X. Tang, Sorensen, C.M., Klabunde, K.J., Hadjipanayis, G.C., J. Appl. Phys. 69, 8, 5279-81 (1991).
- A. Tari, Chantrell, R.W., Charles, S.W. and Popplewell, J., Physica 97B, 57-64 (1979).
- G. Tatara, Fukuyama, H., Phys. Rev. Lett. 72, 772 (1994).
- K. J. Taylor, Pettietle-Hall, C.L., Cheshnovsky, O., Smalley, R.E., J. Chem. Phys. 96, 3319 (1992).
- J. Tejada, Balcells, Ll., Linderoth, S., Perzynski, R., Rigau, B., Barbara, B., Bacri, J.C., J. Appl. Phys. 73, 6952 (1993 *a*).
- J. Tejada, Zhang, X.X., Chudnowsky, E.M., Phys. Rev. B 47, 14977 (1993 *b*).
- J. L. Tholence, Solid State Comm. 35, C4, 229 (1980).
- D. Tománek, Kim. S.G., Jund, P., Borrmann, P., Stamerjohanns, H., Hilf, E.R., Z. Phys. D 40, 539-541 (1997).
- K. N. Trohidou, Blackman, J.A., Phys. Rev. B 51, 17, 11521-526 (1995).
- E. Tronc, Prené, P., Jolivet, J.P., d'Orazio, F., Lucari, F., D. Fiorani, Godinho, M., Cherkaoui, R., Nogués, M., Dormann, J.L., Hyperfine Interactions 95, 129-148 (1995).
- N. Umehara, Kato, K., J. Magn. Magn. Mater. 65, 397 (1987).
- S. Uren, O'Grady, K., Chantrell, R.W., J. de Phys. C8 (12), 1927 (1988).
- H. V. P. Volkenstein, S.B., J.Techn. Phys. (U.S.S.R) 26, 2204 (1956).
- A. Wagendisrtel, Wang, Y., An introduction to Physics & Technology of Thin Films (World Scientific, 1994).

- N. S. Walmsley, Chantrell, R.W., O'Grady, K., J. Magn. Magn. Mater. 193, 420-22 (1999).
- N. S. Walmsley, Chantrell, R.W., To be published in J. Appl. Phys. (2000).
- J. H. P. Watson, J. Appl. Phys. 44, 4209 (1973).
- L. Weil, J. Phys. Radium 12, 437-47 (1951).
- L. Weil, J. Chem. Phys. 51, 715 (1954).
- P. Weiss, J. Phys. 6, 661 (1907).
- L. E. Wenger, Mydosh, J.A., J. Appl. Phys. 55, 6, 1717-1719 (1984).
- W. Wernsdorfer, Hasselbach, K., Mailly, D., Barbara, B., Benoit, A., Thomas, L., Suran, G., J. Magn. Magn. Mater. 145, 33-39 (1995 *a*).
- W. Wernsdorfer, Hasselbach, K., Benoit, A., Cernicchiaro, G., Mailly, D., Barbara, B., Thomas, L., J. Magn. Magn. Mater. 151, 38-34 (1995 *b*).
- W. Wernsdorfer, Hasselbach, K., Benoit, A., Wernsdorfer, W., Barbara, B., Mailly, D., Tuaillon, J., Perez, J.P., Dupuis, V., Dupin, J.P., Guiraud, G., Perex, A., J. Appl. Phys. 78, 7192-95 (1995 *c*).
- W. Wernsdorfer, Doudin, B., Mailly, D., Hasselbach, K., Benoit, A., Meier, Ansermet, J.-Ph., A., Barbara, B., Phys. Rev. Lett. 77, 9, 1873-76 (1996 *a*).
- W. Wernsdorfer, Hasselbach, K., Sulpice, A., Benoit, A., Wegrowe, J.-E., Thomas, L., Barbara, B., Mailly, D., Phys. Rev. B. 53, 3341-47 (1996 *b*).
- W. Wernsdorfer, Bonet Orozco, E., Hasselbach, K., Benoit, A., Barbara, B., Demoncy, N., Loiseau, A., Pascard, H., Mailly, D., Phys. Rev. Lett. 78, 9, 1791-94 (1997).
- R. M. White, J. Magn. Magn. Mater. 88, 165 (1990).
- H. D. Williams, ESF Dissertation, UCNW, Bangor (1990).
- H. D. Williams, Ph.D. Thesis, University of Wales, Bangor (1993 *a*).
- H. D. Williams, O'Grady, K., El-Hilo, M., Chantrell, R.W., J. Magn. Magn. Mater. 122, 129-133 (1993 *b*).
- E. P. Wohlfarth, Proc. Roy. Soc. A 232, 208-207 (1955).
- E. P. Wohlfarth, J. Appl. Phys. 29, 595 (1958).

- E. P. Wohlfarth, Phys. Lett. 70 A, 489-491 (1979).
- E. P. Wohlfarth, J. Phys. F 10, L241 (1980).
- E. P. Wohlfarth, J. Magn. Magn. Mater. 39, 39-44 (1983).
- E. P. Wohlfarth, J. Phys. F: Met. Phys. 14, L155-L159 (1984).
- J. Woltersdorf, Nepijko, A.S., Pippel, E., Surf. Sci. 106, 64 (1981).
- I. Yamada, Inokawa, H., Takagi, T., J. Appl. Phys. 56, 2746 (1984).
- S. Yang, Knickelbein, M.B., J. Chem. Phys. 93, 2319 (1990).
- H. Zhang, Widom, M., J. Magn. Magn. Mater. 122, 119-122 (1993).
- J.-G. Zhu, Bertram, H. Neal, J. Appl. Phys. 63, 8, 3248-3253 (1988).
- G. Zibold, J. Phys. F: Metal Phys. 9, 917 (1979).
- Z. Phys. D. 3, 2-3, entire issue (1986).
- Z. Phys. D. 26, 1-4, entire issue (1993).

" The eagle builds her nest in steep cliffs where neither birds of prey or
the inclemency of the elements can reach.
It is an inaccessible place except for her.
There her chicks are born,
she takes care of them, feeds them, teaches them to fly.
She also teaches them, day by day, which is their role.
In her teachings,
the eagle tells her chicks when is the right moment for the first flight,
and the chicks understand;
and one day, they start flying and honour their role in life"
(from *Bringers of the Dawn*)